THE SHAKING TABLE TESTS COLUMN DATABASE AND EVALUATION OF DRIFT CAPACITY MODELS FOR NON-DUCTILE COLUMNS

by

YAQIONG LI

B.Eng., Tongji University, 2009

A THESIS SUBMITTED IN PARTIAL FULFILLMENT OF

THE REQUIREMENTS FOR THE DEGREE OF

MASTER OF APPLIED SCIENCE

in

THE FACULTY OF GRADUATE STUDIES

(Civil Engineering)

THE UNIVERSITY OF BRITISH COLUMBIA

(Vancouver)

January 2012

Abstract

A Shaking Table Tests Column Database comprised of 59 reinforced concrete columns subjected to shaking table tests is compiled in this research. Key geometrical information, material properties and test data of the columns are provided and used to improve the seismic assessment of old reinforced concrete structures.

Several structural models estimating the column effective stiffness and drift capacities at shear failure and axial-load failure are evaluated. Models based on the design parameters, such as transverse reinforcement ratio and axial load ratio, generally underestimate the column drift at shear failure (loss of 20% of lateral resistant force) in the dynamic test. Empirical plastic drift capacity models for columns subjected to subduction earthquakes and general types of ground motions are proposed. For column drift at axial-load failure, models based on shear-friction mechanism could capture the drift capacity fairly well.

The provisions of the current seismic rehabilitation standard ASCE/SEI 41 Supplement 1 regarding the concrete columns are also evaluated with this dynamic database. It is found that this standard generally overestimates the column effective stiffness and could provide the mean value of the column shear strength. The modeling parameters specified in the standard provide fairly conservative estimate of the column drift capacities and are consistent with the targeted probability of failure. Refinements of the shear strength model and the criteria for column classifications are suggested in this research.

Table of Contents

List of Tables

List of Figures

Acknowledgements

I would like to express my sincerest appreciation for all the guidance, support and help from my supervisor Dr. Kenneth Elwood. I offer my special thanks to Professor Shyh-Jiann Hwang and Professor Chiun-lin Wu, who gave me numerous valuable suggestions and helped me greatly when I was visiting Taipei. I also greatly appreciated the support of Civil Engineering Department of UBC and the generous help from my colleagues, Dr. Yavari and Nazli.

Dedication

To my parents

Chapter 1: Introduction

1.1 Background

1.1.1 Inelastic Seismic Analysis

In seismic regions of Canada and all over the world, many existing structures are old reinforced concrete buildings with structural deficiencies that do not satisfy the requirements specified in current seismic codes. The major vertical supporting components and the lateral resistant systems of these old structures are usually non-ductile columns with inadequate transverse reinforcement detailing, such as large spacing of transverse reinforcing bars and 90-degree hooks.

During a strong earthquake, the lateral demand from the ground shaking may exceed the capacities of these non-ductile columns, causing severe shear degradation and column damage. With reduced lateral strength, the columns may fail to support the vertical load imposed by the gravity load of the structures and additional axial load from the overturning moment. Thus these old structures are very vulnerable to catastrophic collapse and will endanger human lives.

To retrofit these structures economically and efficiently, the capacities of the column components to resistant earthquake load need to be identified. Columns can develop inelastic deformations when subjected to a strong earthquake and tend to suffer shear failure and severe shear degradation after reaching a certain inter-story drift level. With increased horizontal drift, columns may lose the ability to support for gravity load, leading to the collapse of the whole structure.

Unlike the traditional linear structural analysis and design, the inelastic behaviour and drift capacities of the column can be more important than the column strength in seismic

assessment of existing buildings. Thus the focus of research on seismic rehabilitation for old reinforced concrete structures has shifted from strength-based, linear elastic evaluation to deformation-based, non-linear inelastic analysis.

1.1.2 Shaking Table Tests

In current seismic analysis for reinforced concrete structures, column response is often modeled by a force-deformation backbone curve, which is constructed by using several key parameters, such as column effective stiffness, shear strength and the deformation capacity at significant loss of lateral force and at loss of axial load.

Most available models for estimating these key parameters for non-ductile columns in reinforced concrete moment frames are developed based on the data of monotonic static tests or reversed-cyclic tests. These tests were mostly conducted on single columns and often terminated before the axial-load failure of the columns.

More and more shaking table tests have been performed on specimens of simple reinforced concrete moment frames. Compared with other testing methods, shaking table tests can directly simulate earthquake ground motions and better reflect the dynamic effect on structures. Since some of those tests were conducted on frames with multiple columns, axial load redistribution and column interactions within the frame are captured, making the test results for column components more realistic. Since most shaking table tests are conducted on the specimens scaled from the real frames, the input motions need to be compressed and adjusted in the time-domain. Thus the strain rate might be higher than that experienced by real structures in earthquakes.

1.1.3 Column Classifications by Failure Type

Generally speaking, reinforced concrete columns could be classified into three types roughly by their failure modes: flexure-critical columns, flexure-shear-critical columns and shear-critical columns.

Flexure-critical columns usually have well-detailed transverse reinforcement and are expected to demonstrate extended deformation beyond the column yielding when subjected to seismic loads. With adequate shear strength and ductility capacities, shear failure is not likely to occur and these ductile columns often experience failure associated with flexure damage, such as the concrete spalling, buckling of longitudinal reinforcement, crushing of concrete blocks, formation of plastic hinges at column ends, etc. Lateral load-deformation relations for flexure-critical columns are characterized by a plastic plateau after the initial linear response.

Non-ductile columns with inadequate transverse reinforcement are vulnerable to the damage associated with shear failure when subjected to seismic loads, such as diagonal cracks and fracture of transverse reinforcements. If shear failure occurs after the column yielding, these non-ductile columns are often referred to as flexure-shear-critical columns. After the initial linear response in lateral load-deformation relations, flexure-shear-critical columns tend to develop limited inelastic deformation and suffer severe degradation in lateral strength. As shear-damaged plane develops, columns may lose their capacity to sustain gravity loads, eventually leading to the collapse of the whole structural systems.

The non-ductile columns that experience shear failure before column yielding are often classified as shear-critical columns, for example, the short columns with low aspect ratio (a / d) and inadequate transverse reinforcement. Shear-critical columns subjected to seismic

loads tend to develop very limited inelastic deformations and suffer severe lateral force degradation due to the shear distress or diagonal cracking. Those non-ductile columns tend to lose their capacity to support gravity loads shortly after the shear failure and experience very sudden and brittle failure.

1.2 Summary of ASCE/SEI 41 Provisions for Concrete Columns

1.2.1 Introduction

Seismic Rehabilitation of Existing Buildings, known as ASCE/SEI 41-06 supplement 1 (ASCE, 2008), is a national consensus standard in the United States of America and used internationally for seismic assessment and rehabilitation of existing concrete buildings.

To better reflect the observed performance of concrete components from laboratory tests (Elwood et al., 2007), the latest edition of *ASCE/SEI 41/06 supplement 1* updated the concrete provisions from its predecessor Seismic Rehabilitation of Existing Buildings (41/06) (ASCE, 2007). These updates include significant changes to the modeling parameters and acceptance criteria for concrete columns. For brevity, ASCE/SEI 41/06 supplement 1 will be referred to as ASCE/SEI 41 herein.

1.2.2 Generalized Load-Deformation Relation

ASCE/SEI 41 recommends modeling the column behaviors by a generalized load-deformation relation shown in Figure 1.1. The ordinate Q / Q_y represents the normalized lateral force with Q_y = lateral force at the time of flexural yielding. The abscissa is usually taken as the lateral drift ratio calculated by dividing the lateral deformation with column clear height.

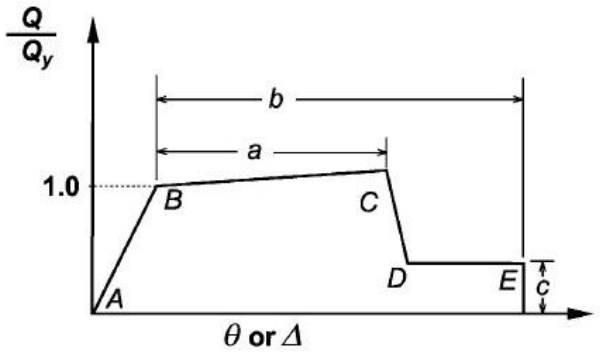

Source: ASCE/SEI 41

Figure 1.1 Generalized force-deformation relations in ASCE/SEI 41

Before the column yielding, the column response is represented by a linear line from unloaded point A to effective yield point B, slope of which equals to lateral stiffness k_{eff}. Then, column behavior is described as linear response at reduced stiffness from point B to point C. The ordinate of point C equals to the column shear strength and the corresponding abscissa shall be taken as the deformation at the time of significant loss of lateral force. It is generally believed that column lateral strength degrades rapidly beyond the point that column loses 20% of its peak lateral resistant force and the corresponding deformation shall be used as the abscissa of point C. The slope from point B to C is usually between zero and 10% of the initial stiffness. Beyond point C, the lateral strength suddenly degrades to point D and then column deforms at the residual shear resistant force until axial load failure point E, at which column fails to sustain gravity load.

The modeling parameter a referring to the portion of deformation from the yield point B to point C, which could be considered as the plastic rotation at shear failure. Similarly, the modeling parameter *b* is used to describe the plastic rotation at the time of axial-load failure. The modeling parameter c represents the percentage of the residual force in terms of the maximum lateral force at the stage between point D and E.

1.2.3 Shear Strength Model

Several models and methods (Priestley et al., 1994; Caltrans, 1995; Kato, Ohnishi, 2002; ACI 318-02) have been developed to estimate the column shear strength. For columns with inadequate transverse reinforcement, ASCE/SEI 41 adopted the shear strength model proposed by Sezen (2004), which was developed based on an assembled database consisting of 51 flexure-shear-critical columns subjected to cyclic lateral loads. According to Sezen (2004), column shear strength V_n could be calculated by summing the contribution from concrete compression block V_c and transverse reinforcement V_s.

$$V_n = kV_0 = k\left(V_c + V_t\right)$$

$$V_c = \lambda\left(\frac{0.5\sqrt{f_c^{'}}}{M/Vd}\sqrt{1+\frac{N_u}{0.5\sqrt{f_c^{'}}A_g}}\right)0.8A_g \quad \text{(MPa)} \qquad \text{Equation 1.1}$$

$$V_s = \frac{A_{st} f_{yt} d}{s}$$

where, A_{st} = cross-sectional area of one layer of transverse reinforcement parallel to the direction of lateral load; f_{yt} = yield stress for transverse reinforcement; s = spacing of transverse reinforcement; $\lambda = 1.0$ for normal weight concrete while $\lambda = 0.75$ for light weight concrete; $f_c^{'}$ = the concrete compressive stress on test day; N_u = axial compression force (=0 for tension force); M/Vd is the largest ratio of moment to shear times column effective depth under design loadings for column, but shall not be taken greater than 4 or less than 2; A_g = gross cross-sectional area of column; d = the effective depth of column section and is permitted to use 80% of column section height.

For columns, the ratio of *M/V* could be taken as shear span a and M/Vd equals to the aspect ratio a/d. For columns in The Database that had fixed-fixed restrained at both ends, a equals to half of the column clear height L.

k is the modifying factor related to the displacement ductility demand μ_δ, which is the ratio of ultimate displacement (ultimate drift) over yield displacement (yield drift). It is generally believed that columns experience shear failure at the point that column lost 20% of its peak lateral load and the corresponding displacement (drift) is considered to be the ultimate displacement (ultimate drift ratio). Yield displacement is taken as the measured yield displacement obtained by TEST Method in section 3.2.4. Research shows that the column shear strength will decrease as the ductility demand increases. As shown in Figure 1.2, when ductility demand μ_δ is greater or equal than 6, its modifying factor $k = 0.7$; when ductility demand is less than or equal to 2, then $k = 1$; when ductility demand is in between these two extremes, *k* is calculated by linear interpolation.

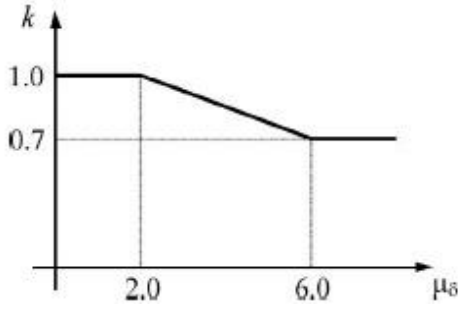

Source: Sezen (2004)

Figure 1.2 Modifying factor k for shear strength model

According to truss models, column shear strength contributed by transverse reinforcement could be defined as $V_s = \alpha A_{st} f_{yt} d / s$. Sezen (2004) compared the quantity $V_{Test} - V_c$ with $\alpha A_{st} f_{yt} d / s$ for all the columns included in the assembled database and found

that $\alpha = 1$ achieved the best match. Therefore, the transverse reinforcement contribution is expressed as $V_s = A_{st} f_{yt} d / s$.

According to ASCE/SEI 41, if spacing of column transverse reinforcement is larger than half of column section effective depth ($s > d/2$) in the direction of shear force, the transverse reinforcement should be taken as no more than 50% effective when resisting shear or torsion and thus $V_s = 0.5 A_v f_y d / s$ .However, if the spacing is larger than the effective depth of the column section ($s > d$), the transverse reinforcement shall be considered ineffective and set $V_s = 0$.

1.2.4 ASCE/SEI 41 Column Classification

According to ASCE/SEI 41, columns are classified into three conditions based on shear strength V_n, plastic shear capacity V_p and transverse reinforcement detailing. Detailed classification criteria can be found in Figure 1.3.

	Transverse Reinforcement Details		
	ACI conforming details with 135° hooks	Closed hoops with 90° hooks	Other (including lap spliced transverse reinforcement)
$V_p/(V_n/k) \leq 0.6$	i*	ii	ii
$1.0 \geq V_p/(V_n/k) > 0.6$	ii	ii	iii
$V_p/(V_n/k) > 1.0$	iii	iii	iii

* To qualify for condition i, a column must have $A_v/b_w s \geq 0.002$ and $s/d \leq 0.5$ within the flexural plastic hinge region. Otherwise, the column shall be assigned to condition ii.

Source: ASCE/SEI 41

Figure 1.3 ASCE/SEI 41 column classification

The plastic shear capacity V_P is the shear demand corresponding to the flexural yielding of plastic hinges and could be calculated by dividing the maximum moment strength obtained from section analysis by shear span *a*. The shear strength V_n is calculated by the

shear strength model ($V_n = kV_0 = k\left(V_c + V_s\right)$) mentioned in section 6.2.3 and the term V_n/k is the shear strength excluding the reduction factor related to ductility demand.

As shown in the first column of Figure 1.3, by comparing plastic shear capacity V_P with $V_0 = V_n / k$, columns with transverse reinforcement including 135-degree hooks are classified into three conditions: condition i, ii and iii, which approximately correspond to the failure modes, namely flexure failure, flexure-shear failure and shear failure respectively.

Past researches have shown that poor transverse reinforcement detailing reduces the column lateral deformation capacity. Therefore, columns with transverse reinforcement including 90-degree hooks or having lap splices are adjusted from condition i to condition ii if $V_p / V_0 \le 0.6$; columns with lap-spliced transverse reinforcement are classified into condition iii instead of condition ii for the case of $0.6 < V_p / V_0 \le 1.0$.

By classifying columns into the aforementioned three conditions roughly by failure modes, ASCE/SEI 41 then provides recommendations on allowed plastic rotations in generalized load-deformation relation for each condition.

1.3 Objective and Scope

The overall objective of this research is to compile a comprehensive database providing the key properties and test data for columns that have been subjected to shaking table tests and use this database to improve the accuracy of the seismic assessments of older concrete buildings with non-ductile columns. Available structural models and provisions of current seismic rehabilitation standards ASCE/SEI 41 regarding concrete column are evaluated with this database. Influence of varying axial load and the dynamic effects will be investigated. Only the large-scale columns in relatively simple moment-frames are intend to be included in

this Shaking Table Tests Column Database. A total of 59 columns from seven shaking table tests programs are selected, of which 36 are non-ductile columns with inadequate transverse reinforcement. The effective lateral force will be obtained from the recorded shear data by correcting the P-delta effect and section analysis will be conducted based on column properties to get several key points, such as yield point and plastic shear demand.

The available models of estimating column effective stiffness, shear strength, drift capacities at shear failure and axial-load failure are evaluated with the test data from the dynamic column database in this research and the results are compared with the evaluation with static cyclic test data.

This research will focus on the provisions of ASCE/SEI 41 regarding the reinforced concrete columns. The test data will be used to assess the accuracy of estimated column stiffness and column shear strength recommended by ASCE/SEI 41. Columns included in the compiled database are classified into three conditions and the level of conservatism of the modeling parameters specified in ASCE/SEI 41 for each condition are being evaluated.

Columns are subjected to varying axial load during the shaking table tests. Especially for outside columns, the difference between axial load in the positive and negative direction could be very significant due to the overturning moment. When evaluating the models for column shear strength and drift capacities, this research will compare the effects of different column axial load on the calculated results.

1.4 Organization

Chapter 2, "Shaking Table Tests Column Database", introduces the dynamic column database compiled in this research. Detailed information and literature review of each shaking table test are presented. Two important static cyclic test column databases are briefly introduced. This chapter also provides the main properties of this dynamic column database, adjustments of the test data (i.e. P-Delta correction) and other key parameters (e.g. the yielding point from section analysis). The number of the cycles that each column went through during the dynamic tests and experimental envelope of the column response are also investigated in this chapter.

Chapter 3, "Column Effective Stiffness", discusses two methods to interpret the measured column effective stiffness EI_{eff} , namely the "PEER Method" and "TEST Method". With the measured effective stiffness, performance of the method proposed by ASCE/SEI 41 and the Three-Component model is evaluated in this chapter.

Chapter 4, "Column Drift at Shear Failure", presents three methods to obtain the measured column drift at shear failure. Four available drift capacity models for non-ductile columns, namely Pujol (1999) model, Kato and Ohnishi (2006), Zhu et al. (2006) and Elwood and Moehle (2005), are evaluated in this chapter. The procedure of each model is introduced and the evaluation with the test data of Shaking Table Tests Column Database is presented along with the comparison of the evaluation with static cyclic test data in past studies to gain better understanding of the dynamic effect on drift capacities.

Chapter 5, "Column Drift at Axial-Load Failure", discusses different ways to define column axial-load failure based on measured column axial load, shear degradation or the column lengthening/shortening. Measured column drifts at axial-load failure are compared

with calculated drifts from Shear-Friction models, Kato and Ohnishi (2006) and Zhu et al. (2006) in this chapter.

Chapter 6, "Evaluation of ASCE/SEI 41-06 Supplement 1", evaluates the performance of current rehabilitation standard (ASCE, 2008) in terms of column classification and estimations of modeling parameters a and b. This chapter also suggests some refinements and changes of this standard based on the test data of Shaking Table Tests Column Database.

Finally, the Chapter 7, "Conclusions and future work", summarizes the main conclusions from each chapter and provides some suggestions for future research.

Chapter 2: Shaking Table Tests Column Database

2.1 Introduction

This chapter introduces the compiled Shaking Table Tests Column Database and detailed information of each shaking table test program is presented. Two important static cyclic tests column databases are briefly introduced. This chapter also provides interpretations of the test data, such as the effective force obtained after P-Delta correction, key parameters (e.g. the yielding point from section analysis) from section analysis. The methods to count the number of the cycles that each column went through and develop experimental envelopes of the column lateral response are also presented in this chapter.

2.2 Static Cyclic Test Column Databases

2.2.1 Introduction to Static Cyclic Test Column Database

Many available models estimating the column shear strength and drift capacities were developed based on the static test data. Two important static test column databases will be introduced in this section, namely the PEER Structural Performance Database and Sezen (2002) column database.

By comparing the evaluation of the available models with both cyclic test data and the shaking table test data, an improved understanding of the column behaviour, dynamic effects, as well as the performance of the column drift capacity models could be gained.

2.2.2 PEER Structural Performance Database

The PEER Structural Performance Database is a comprehensive database compiled by numerous researches for columns tested by static reversed-cyclic lateral load. It includes 253 rectangular reinforced concrete columns and 163 spiral columns. Column geometry, material properties and digitalized data of lateral force-deformation histories are provided for each column in the database. Herein, the PEER Structural Performance Database will be referred to as PEER database for brevity.

A number of studies have been carried out using the column data in PEER database to investigate the column behaviour, evaluate the available structural models and develop new methods. For example Camarillo (2003) evaluated four existing shear-strength models using the PEER database.

Since all the columns included in the compiled dynamic database had rectangular cross section, this research will focus on the rectangular columns included in the PEER database. The main properties of the rectangular columns included in the PEER database are summarized in Table 2.1.

Table 2.1 Properties of PEER database

Parameters	Symbol	Unit	Max	Min	Mean	STD	COV
Aspect Ratio	a/d		3.7	0.5	3.58	1.46	41%
Concrete compressive strength	$f_c^{'}$	*MPa*	118	16	51.7	29.2	56%
Long. Rein. Yield Stress	f_{yl}	*MPa*	587	318	429	75	18%
Long. Rein. Ratio	ρ_l		0.0400	0.0600	0.0240	0.0010	40%
Trans. Rein. Yield Stress	f_{yt}	*MPa*	1424	249	487	221	45%
Trans. Rein. Ratio	ρ_t		0.0600	0.0002	0.0020	0.0010	61%
Axial Load Ratio	$P_{ini}/f_c^{'}A_g$		0.90	0.00	0.27	0.20	74%

2.2.3 Sezen (2002) Column Database

Sezen (2002) compiled a database consisting of 50 flexure-shear-critical columns with light transverse reinforcement ($\rho_t \leq 0.007$) that are subjected to static cyclic lateral load .

Most of the columns included in Sezen (2002) database were large scale specimens representative of the columns commonly used in older reinforced concrete buildings, while around 20% of the columns were one-third scale. These columns were subjected to unidirectional cyclic lateral load and observed to suffer severe degradation of lateral strength and shear failure. The properties of the Sezen (2002) column database are given in Table 2.2.

Table 2.2 Properties of Sezen (2002) database

Parameters	Symbol	Unit	Max	Min	Mean
Aspect Ratio	a/d		4	2	3
Concrete compressive strength	$f_c^{'}$	*MPa*	44.8	13.1	24.8
Long. Rein. Yield Stress	f_{yl}	*MPa*	524.0	324.1	406.8
Long. Rein. Ratio	ρ_l		0.04	0.01	0.023
Trans. Rein. Yield Stress	f_{yt}	*MPa*	648.1	317.2	427.5
Trans. Rein. Ratio	ρ_t		0.0065	0.0010	0.003
Initial Axial Load Ratio	$P_{ini} / f_c^{'} A_g$		0.6	0.0	0.2
Maximum shear stress	$v / \sqrt{f_c^{'}}$	$\sqrt{MPa}$	0.71	0.23	0.46

Most of the column drift models at shear failure and axial-load failure studied in this thesis had been developed from or evaluated with the Sezen (2002) database.

2.3 Properties of Shaking Table Tests Column Database

Similar to PEER database, a Shaking Table Tests Column Database is assembled to provide the geometrical information, material properties and the test data for columns belonging to reinforced concrete frames subjected to shaking table tests. For brevity, The Shaking Table Tests Column Database will be referred to as "The Database" herein.

The Database intends to include only relatively large scale columns in simple two-dimensional frames. As a result, seven shaking table tests programs are included in The Database, three of which were conducted by scholars of UC Berkeley (Ghannoum, 2007, Elwood, 2003, Shin, 2007) and the remaining four were carried out at NCREE (National Center for Research on Earthquake Engineering) of Taiwan. (Yavari, 2011, Su, 2007, Kuo, 2008, Wu et al., 2006) The information of these seven test programs is summarized in Table 2.3 and details of each program will be introduced in section 2.4. Most shaking table tests are conducted up to collapse of the frame specimens.

Table 2.3 Characteristics of specimens in seven shaking table test programs

			Per Specimen				
Test programs		***No. of Specimens***	***No. of Stories***	***No. of Bays***	***No. of Columns***	***No. of Ductile Columns***	***No. of |Non-Ductile Columns***
1	**NCREE 2009**	4	2	2	6	0	6
2	**NCREE 2007**	1	1	2	3	2	1
		1	1	1	2	2	0
		2	1	1	2	0	2
3	**NCREE 2005**	4	1	3	4	2	2
4	**NCREE 2004**	3	1	1	2	0	2
5	**Ghannoum 2006**	1	3	3	12	6	6
6	**Shin 2005**	4	1	1	2	2	0
		4	1	1	2	1	1
		4	1	1	2	0	2
7	**Elwood 2002**	2	1	1	3	2	1
Total		29	N.A.	N.A.	97	34	63

Table 2.4 summarizes the information about the specimens and columns included in The Database. Only first-story columns out of the total 97 columns in these dynamic tests are included in The Database, since the first-storey columns were subjected to the greatest axial load and were considered to be the most vulnerable and critical columns in multiple-story moment-resisting frames Also the test data was more complete for first-story columns, while it was relatively difficult to measure the axial load and shear force for upper-story columns. Some first-story columns were excluded for various reasons. For example, the circular outside columns in Elwood 2002 Tests were neglected as The Database focused on square columns; the ductile columns in specimen S2 of NCREE 2007 were omitted because the test data file is damaged and unreliable.

Among the 59 columns included in the Database, 36 columns are non-ductile columns with light transverse reinforcement ($\rho_t = A_v / bs \leq 0.002$) and poor configurations that were typically used in older reinforced concrete structures and do not satisfy the current seismic code. These columns are expected to demonstrate limited inelastic response during earthquake shaking and experience pure shear or flexure-shear failures. There are 23 ductile columns with adequate transverse reinforcement (i.e. closely spaced transverse reinforcement with 135 degree hooks) in The Database and the column responses are expected to be dominated by flexural behavior.

Appendix A presents the column geometry, material properties and reinforcement details for each column. Some columns were subjected to more than one test series and Appendix B provides the key information for each test series, such as initial axial load ratio and PGA.

Test data including time step, table acceleration, horizontal inter-story drift ratio, shear, axial load and column shortening/lengthening are also available for most of the dynamic tests series.

Table 2.4 Information of the shaking table test programs

			Per Specimen			*Per Column*
Test programs		*No. of Specimens*	*No. of Columns*	*No. of Ductile Columns*	*No. of Non-Ductile Columns*	*No. of Test series**
1	**NCREE 2009**	4	3	3	0	2
2	**NCREE 2007**	1	3	2	1	2
		2	2	0	2	1
3	**NCREE 2005**	2	4	2	2	2
4	**NCREE 2004**	2	2	0	2	1
5	**Ghannoum 2006**	1	4	2	2	4
6	**Shin 2005**	4	2	2	0	1
		4	2	1	1	1
		3	2	0	2	1
7	**Elwood 2002**	2	2	0	2	1
Total		25	59	23	36	88

*: "No. of test series" = the number of tests to which each column is subjected.

Key properties of the Database are summarized in Table 2.5. The "initial axial load P_{ini}" refers to the column axial load obtained before column was subjected to the input motions and could be considered as the gravity load imposed on the column. Initial axial load could be measured by the load cell at the column base, however for most columns the measured gravity load was not reliable and thus was obtained by computed structural model (e.g. the OpenSees model) instead. The "Max Axial Load" P_{max} refers to the maximum axial load that column was subjected to during the shaking table tests. Notice that due to the limit of shaking table capacities, most of the columns are subjected to axial load ratios smaller than 0.2.

Table 2.5 Properties of columns in The Database

Parameters	Symbol	Unit	Max	Min	Mean	Standard Deviation	COV
(a) Non-Ductile Columns							
Aspect Ratio	a/d		4.3	1.5	3.2	0.7	20.9%
Concrete compressive strength	$f_c^{'}$	*MPa*	36.5	23.9	29.9	4.2	13.9%
Long. Rein. Yield Stress	f_{yl}	*MPa*	479	386	442	24	5.5%
Long. Rein. Ratio	$\rho_l = A_{sl}/A_g$		0.0324	0.0143	0.0248	0.0046	18.5%
Trans. Rein. Yield Stress	f_{yt}	*MPa*	689.7	385.9	550.6	78	14%
Trans. Rein. Ratio	$\rho_t = A_{st}/bs$		0.0018	0.0007	0.0014	0.0004	25.4%
Initial Axial Load Ratio	$P_{ini}/A_g f_c^{'}$		0.36	0.03	0.13	0.07	53.4%
Max. Axial Load Ratio	$P_{max}/A_g f_c^{'}$		0.43	0.04	0.19	0.068	42.5%
Normalized shear Stress	$v/\sqrt{f_c^{'}}$	$\sqrt{MPa}$	0.59	0.17	0.35	0.09	25.0%
(b) Ductile Columns							
Aspect Ratio	a/d		3.5	1.5	3.2	0.4	12.1%
Concrete compressive strength	$f_c^{'}$	*MPa*	35.8	24.6	28.5	4.2	14.6%
Long. Rein. Yield Stress	f_{yl}	*MPa*	483	232	413	86	20.8%
Long. Rein. Ratio	$\rho_l = A_{sl}/A_g$		0.0253	0.0109	0.0209	0.0055	26.2%
Trans. Rein. Yield Stress	f_{yt}	*MPa*	662	475	568	59	10.4%
Trans. Rein. Ratio	$\rho_t = A_{st}/bs$		0.0119	0.0030	0.0087	0.0027	31.1%
Initial Axial Load Ratio	$P_{ini}/A_g f_c^{'}$		0.20	0.05	0.12	0.05	43.7%
Max. Axial Load Ratio	$P_{max}/A_g f_c^{'}$		0.43	0.12	0.23	0.10	43.9%
Normalized shear Stress	$v/\sqrt{f_c^{'}}$	$\sqrt{MPa}$	0.44	0.20	0.34	0.07	19.8%

2.4 Information of Shaking Table Tests Programs

2.4.1 Introduction

This section provides important information about each shaking table test program included in The Database. Hysteretic response of each non-ductile column is presented with the key points marked.

The "1st yield" point is defined by following the method discussed in section 3.2.4 (TEST Method). The "Max V_{eff} Veff" point is the point that column achieve maximum effective force and the "80% Max Veff" point is the point that column degrades to 80% of its maximum effective force. The "Axial-load failure" point could be found in section 5.1.3. The "Max achieved drift" point refers to the point that achieves maximum lateral column drift during the tests.

2.4.2 NCREE 2009 Tests

NCREE 2009 Tests include four two-storey, two-bay planar frame specimens subjected to unidirectional seismic loads scaled from the ground motion recorded during 1999 Chi-Chi earthquake. These tests are carried out by scholars from University of British Columbia in Canada and National Center for Research on Earthquake Engineering (NCREE) in Taiwan. The elevation view of test specimens is shown in Figure 2.3.

Specimen names summarized the main characteristics of each setup as follows:

HCFS : High axial load ratio Confined joints Flexure-Shear columns

MCFS : Moderate axial load ratio Confined joints Flexure-Shear columns

MUFS : Moderate axial load ratio Unconfined joints Flexure-Shear columns

MUF : Moderate axial load ratio Unconfined joints Flexure columns

Specimens MCFS and HCFS were identical except that the columns of HCFS is designed to have higher column axial load by placing hydraulic jacks that added prestressing force (designed axial load ratio $P/A_g\ f_c^{'} \approx 0.2$ for middle column in HCFS and 0.1 for that in MCFS). Test data show that the behavior of frame specimen, damage patterns and column failure modes were closely related to the axial load that the columns are subjected to. The gap of inter-story drift ratio between shear failure and axial-load failure for middle in MCFS was larger than that of HCFS. After axial-load failure, column B1 in HCFS also experienced vertical shortening and lateral force degradation more rapidly than MCFS. While in HCFS damage was observed in both stories, MCFS suffered damage concentrated in the bottom of first-story columns.

Specimen MUF consisting of three ductile columns and could be used to observe the beam-column joint behavior when subjected to lateral seismic loads. By comparing the test results of MUF and MUFS, one can observe the interactions among beam, column and beam-column joints and check the influence of column strength on joint demand. Those two specimens are included in this column database, since the data is helpful to investigate the possible effects of joint dealing on column stiffness and drift capacities.

Yavari (2011) observed that there was apparent flexure cracking in first-story beams of HCFS, because the beam to column strength ratio was relatively low for specimen HCFS of which columns were subjected to high axial load ratio (designed axial load ratio equal to 0.24). Therefore the total inter-story drift was larger than the actual column deformation due to the additional deformation contributed by the beam flexibility and the rotation of beam-column joints.

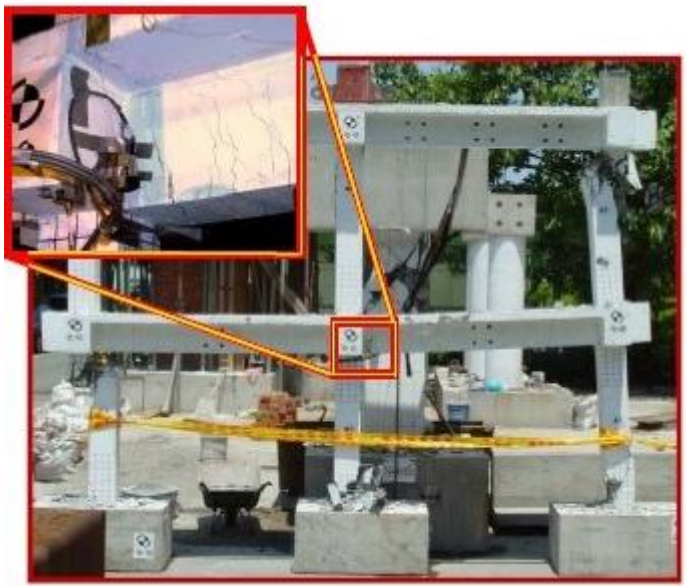

Figure 2.1 Pictures for Specimen HCFS in NCREE 2009 Tests

Yavari (2011) suggest using the chord rotation instead to describe the column behaviour and defined the chord rotation as "the angle between the chord connecting the column ends and the tangent at the member end" (Page 76) as shown in Figure 2.2.

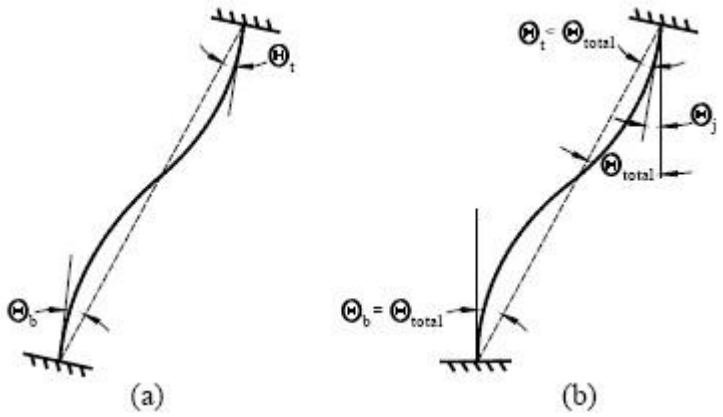

Figure 2.2 Definition of chord rotations; (a) chord rotations at the top and base of the column; (b) comparison of chord rotation with the total rotation

Where θ_{Total} = the total rotation and equal to the inter-story drift ratio; θ_t = chord rotation at the top of the column; θ_b = chord rotation at the base of the column; θ_j = joint rotation.

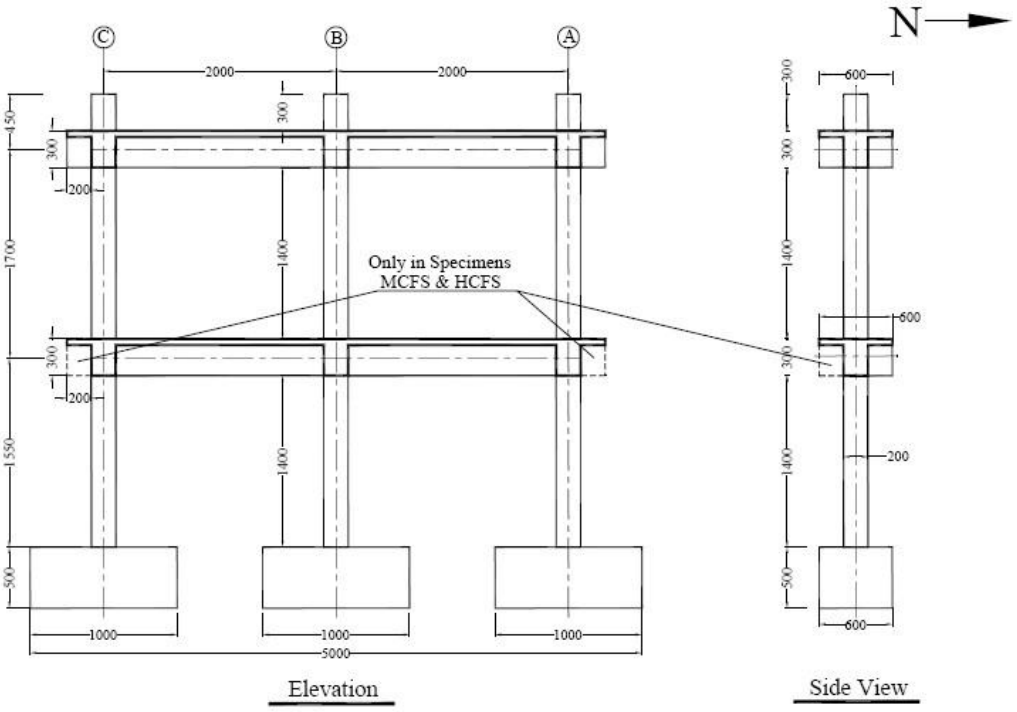

(a) Elevation view of specimens

(b) Column section for MCFS, HCFS and MUFS (c) Column section for MUF

Source: (Yavari, 2011)

Figure 2.3 Information of specimens of NCREE 2009 Tests

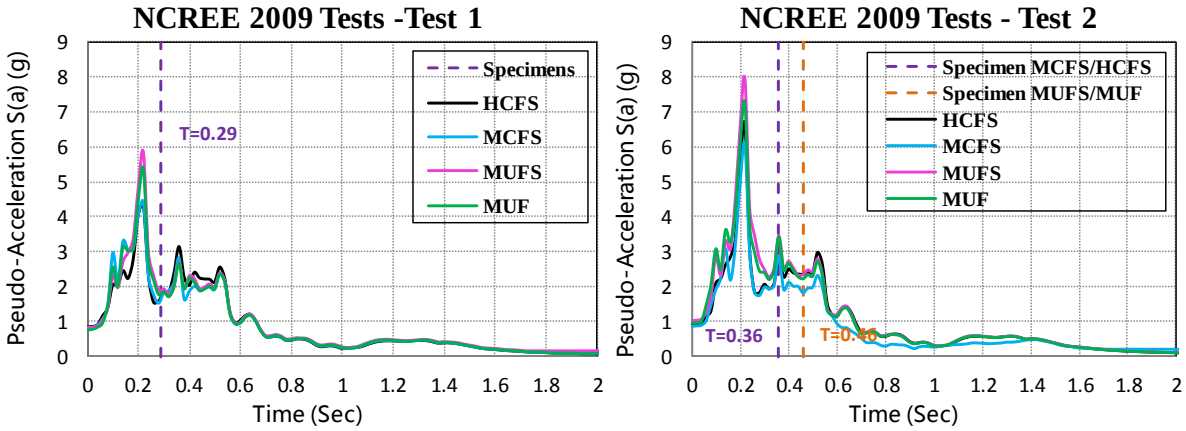

Figure 2.4 Response spectra for NCREE 2009 Tests

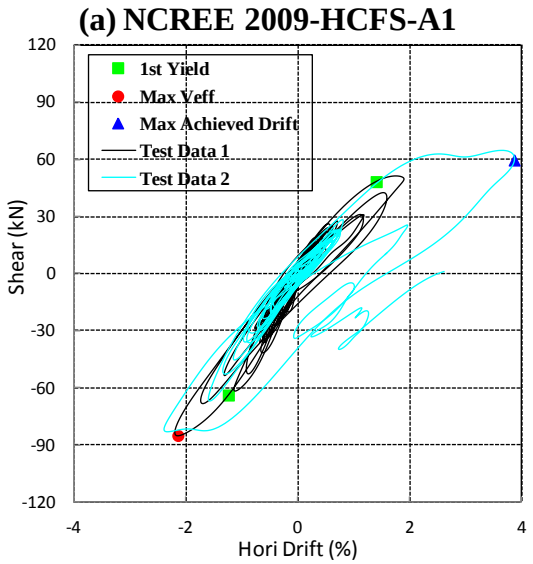
(a) NCREE 2009-HCFS-A1
1st Yield
Max Veff
Max Achieved Drift
Test Data 1
Test Data 2
Shear (kN)
Hori Drift (%)

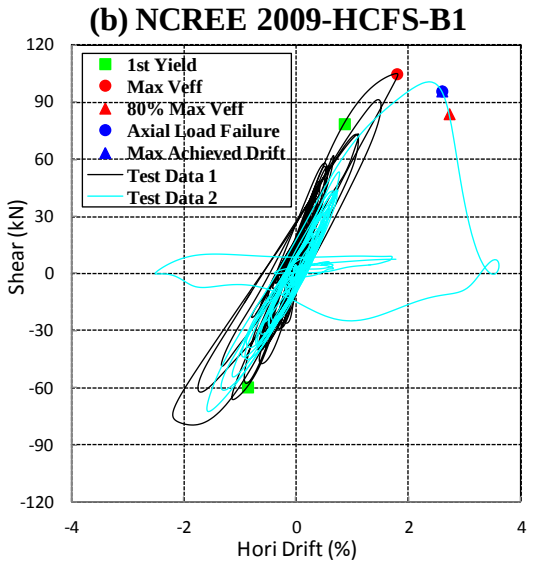
(b) NCREE 2009-HCFS-B1
1st Yield
Max Veff
80% Max Veff
Axial Load Failure
Max Achieved Drift
Test Data 1
Test Data 2
Shear (kN)
Hori Drift (%)

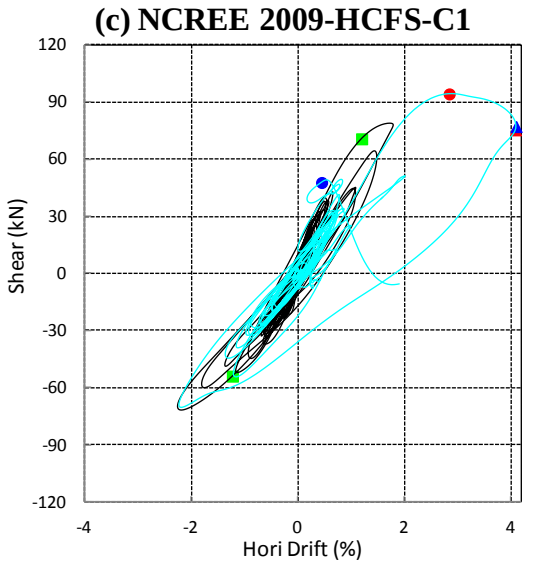
(c) NCREE 2009-HCFS-C1
Shear (kN)
Hori Drift (%)

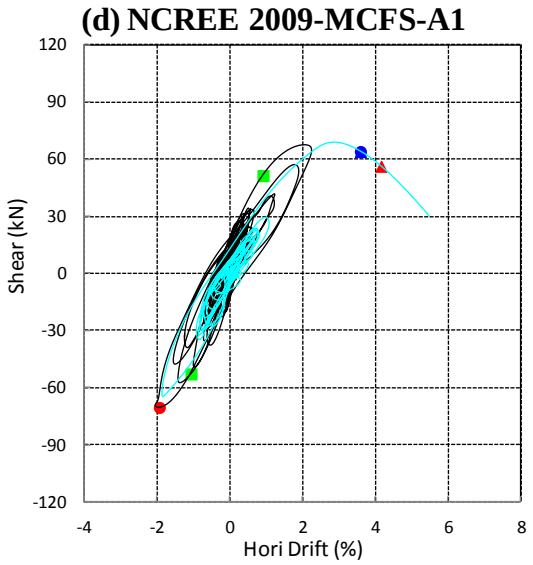
(d) NCREE 2009-MCFS-A1
Shear (kN)
Hori Drift (%)

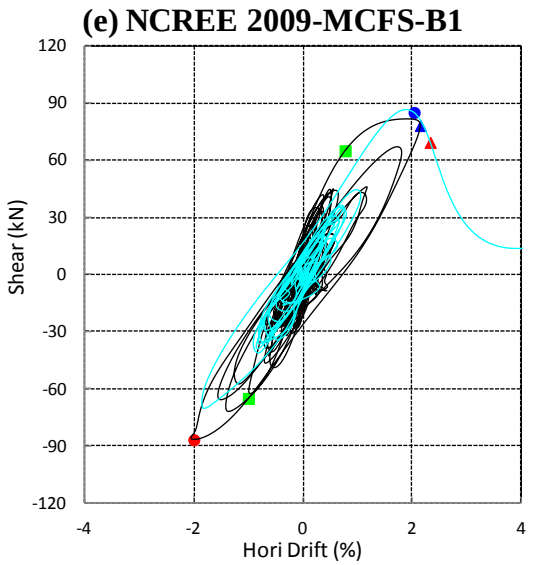
(e) NCREE 2009-MCFS-B1
Shear (kN)
Hori Drift (%)

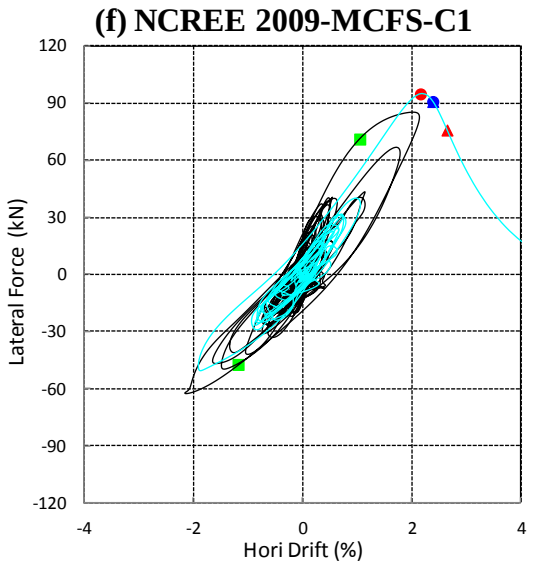
(f) NCREE 2009-MCFS-C1
Lateral Force (kN)
Hori Drift (%)

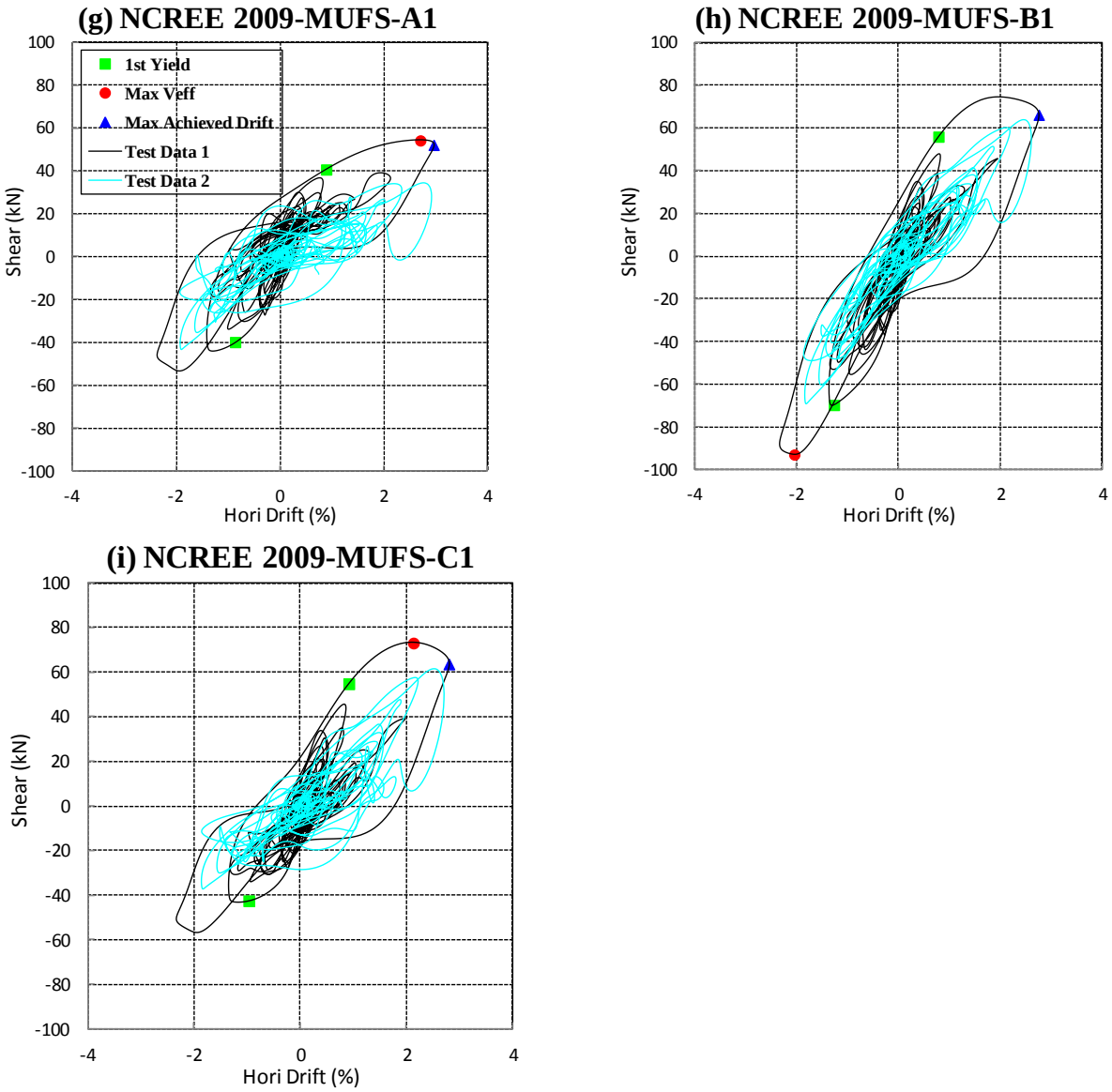

Note: The column is named by the form "Test name-Specimen name-column name". For example, the column "NCREE 2009-MUFS-B1" refers to the column B1 in specimen MUFS in NCREE 2009 Tests. Column B1 is the first-story column in axis B.

Figure 2.5 Hysteretic response of non-ductile columns in NCREE 2009 Tests

2.4.3 NCREE 2007 Tests

Su (2007) performed shaking table tests on four half-scale, single-story reinforced concrete frames. Specimen S1, as shown in Figure 2.7 (a), had one non-ductile column in the middle and two ductile columns outside. Specimen S2, S3 and S4 were portal frames with two columns connected by a rigid beam, as illustrated in Figure 2.7 (b). The test data of specimen S2 consisting of two ductile columns are not available due to the damage of instruments during the tests. Specimen S3 and S4 included two non-ductile columns with column clear height equal to 750mm and 1000mm respectively. Since the ratio of column clear height to column section width (L / D) fell between 3 to 4, these columns are generally regarded as short columns or shear critical columns, which are expected to experience pure shear failures without flexural yielding. Figure 2.7 (c) illustrated the cross-section of the ductile and non-ductile columns.

The dynamic tests were conducted up to collapse of the test frames. It is observed from the tests that shear-critical columns experienced in-cycle or cyclic shear strength degradation and exhibited negative slope in hysteretic response of lateral force soon after column shear failure.

Backbone curves based on the key points estimated by various shear strength models and drift capacity models were also drawn for these short columns and it is found that most backbone curves could predict the column behavior fairly well, yet generally underestimate the column shear strength.

From the hysteretic response of these shear critical columns shown in Figure 2.8 and Figure 2.9, it is observed that the column lateral force was relatively small in the beginning

and then a sudden increase in the lateral force occurred in one cycle followed by the column shear failure and axial-load failure shortly afterwards.

The dynamic test data are compared with the static cyclic test results of full size columns with similar properties. Wu et al. (2007) found that column shear strength in the dynamic test was slightly higher than that of static cyclic test, which probably could be explained by the higher strain rate in dynamic tests, the energy dissipation within reversed cycles in cyclic test and the size effect of column specimens in dynamic test.

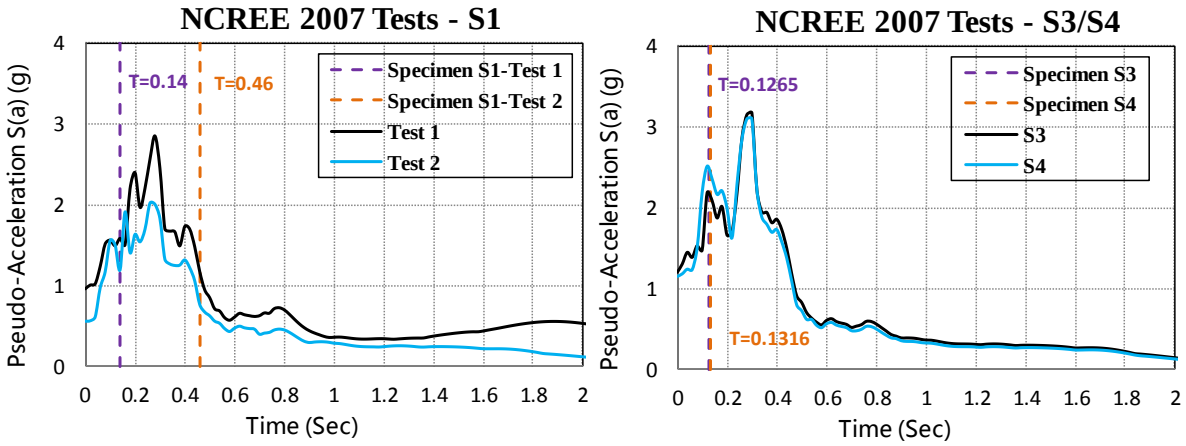

Figure 2.6 Response spectra for NCREE 2007 Tests

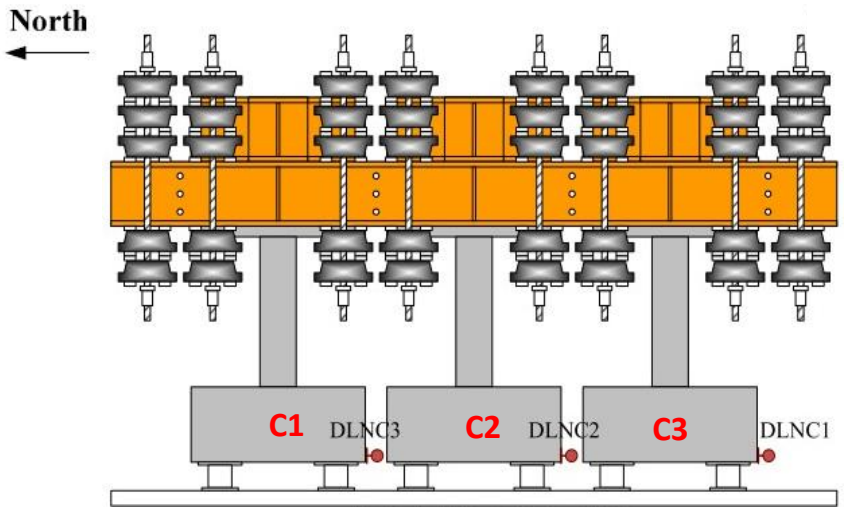

(a) Experimental setup for specimen S1

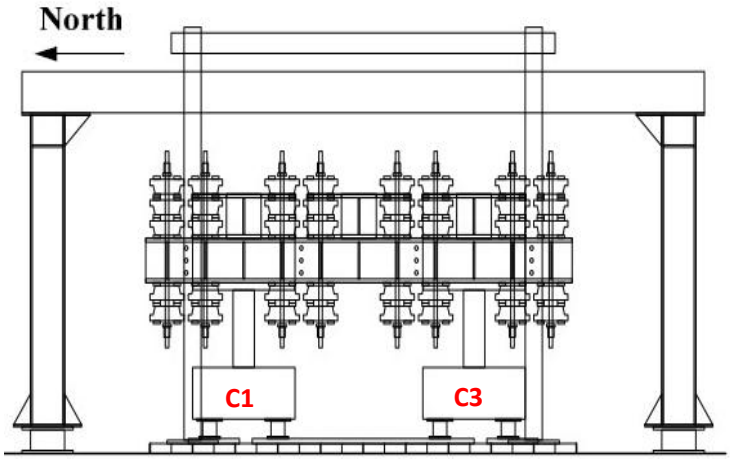

(b) Experimental setup for specimen S2, S3 and S4

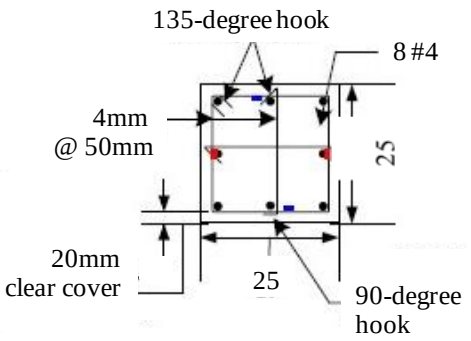

(c) Cross-section for ductile columns

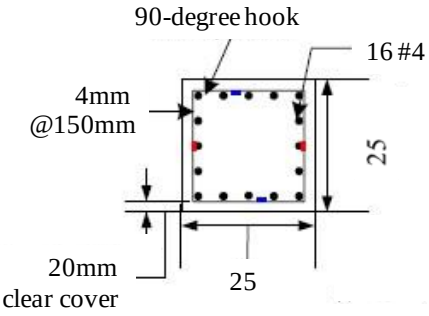

(d) Cross-section for non-ductile columns

Source: Wu et al. (2007)

Figure 2.7 Information of specimens of NCREE 2007 Tests

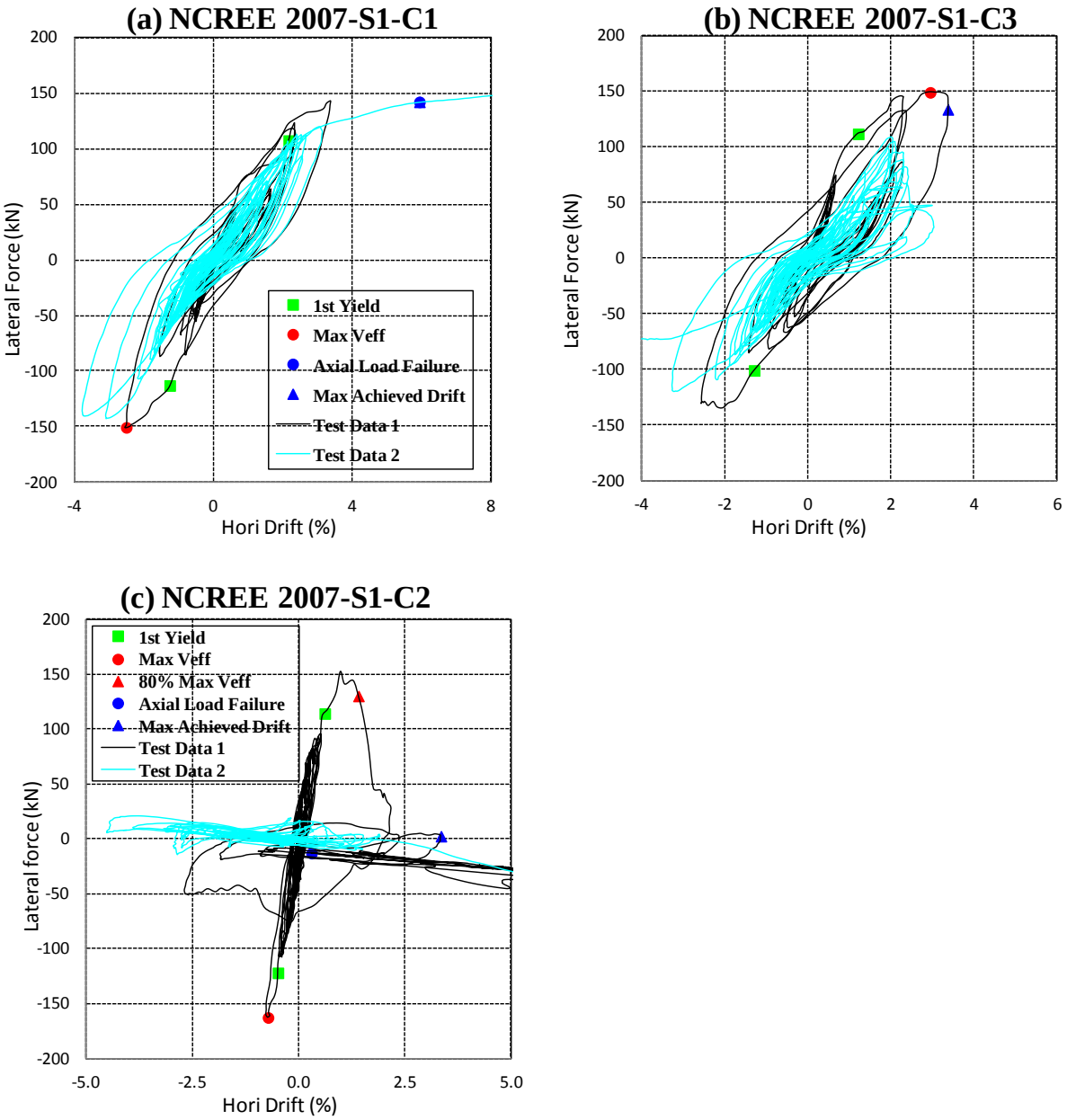

Note: The column is named by the form "Test name-Specimen name-column name". For example, the column "NCREE 2007-S1-C2" refers to the column C2 in Specimen S1 of NCREE 2007 Tests.

Figure 2.8 Hysteretic response of columns in Specimen S1 of NCREE 2007 Tests

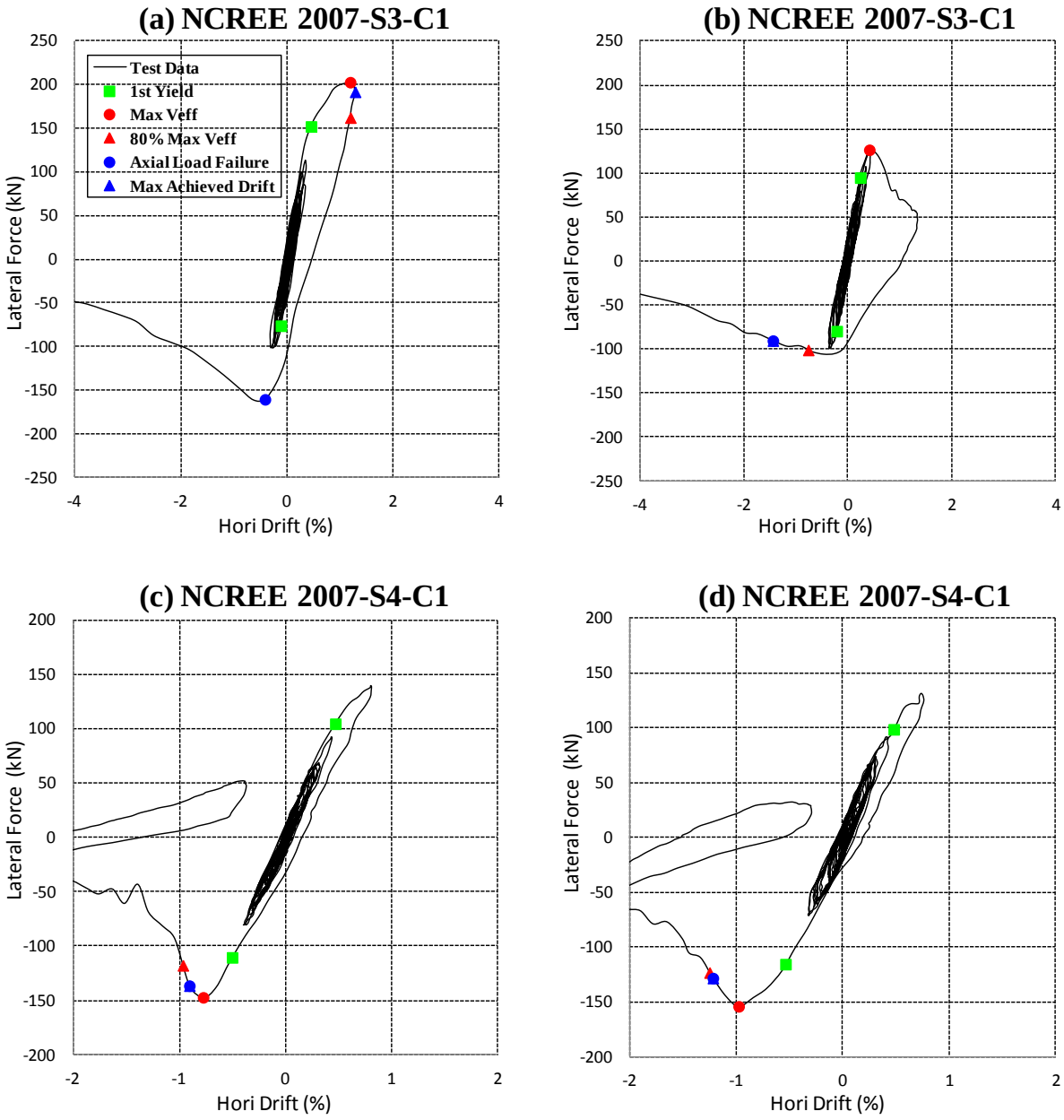

Note: The column is named by the form "Test name-Specimen name-column name". For example, the column "NCREE 2007-S4-C1" refers to the column C1 in Specimen S4 of NCREE 2007 Tests.

Figure 2.9 Hysteretic response for columns in Specimen S3 and S4 of NCREE 2007 Tests

2.4.4 NCREE 2005 Tests

In 2005, Kuo (2008) conducted shaking table tests on four one-third-scale, three-bay by one-story reinforced concrete frames in NCREE. As shown in Figure 2.11, specimens P1 and P2 had four columns, of which two non-ductile columns with inadequate transverse reinforcement were on the north side and two ductile columns were on the south side. Specimen L and W had similar setup as P1 and P2, except that the former had lap-spliced transverse reinforcement in the lower part of non-ductile columns and the latter had additional wing walls on the columns.

The specimens were subjected to seismic load scaled from ground motions recorded in 1999 Chi-Chi earthquake. Specimen P1 was tested in a preliminary experiment to investigate the structural properties (for example, the frame period), check the instrumental system and validate the design methods and specimen W was used to observe the influence of additional wing walls. Thus, only columns from specimens P2 and L are included in the Database.

Dynamic test results of specimen P2 showed that the flexural-shear-critical columns in reinforced concrete frames had fairly large drift capacities when subjected to low axial load ratio, thanks to the axial load redistribution mechanism and column interactions within frames. The non-ductile columns wouldn't experience lateral strength degradation until inter-story drift ratio reached 3.5% to 4% and shear failure usually occurred when inter-story drift ratio reached 4.5% to 5.5%.

For non-ductile columns in specimen L, large vertical splitting cracks were observed and bond splitting failure occurred due to lap splices. Comparing the hysteretic response of non-ductile middle column C2 in specimen P2 and L shown in Figure 2.12, columns with lap-spliced reinforcement experienced larger lateral displacement. However, in the other

direction, the maximum column drift was obviously less than columns without lap splices in P2.

It was noticed that before non-ductile columns C1 and C2 in specimen L reached their maximum drift in the positive direction, large cracks and severe column damage had already been observed. Thus the maximum drift measured during the tests was larger than the actual column drift capacity.

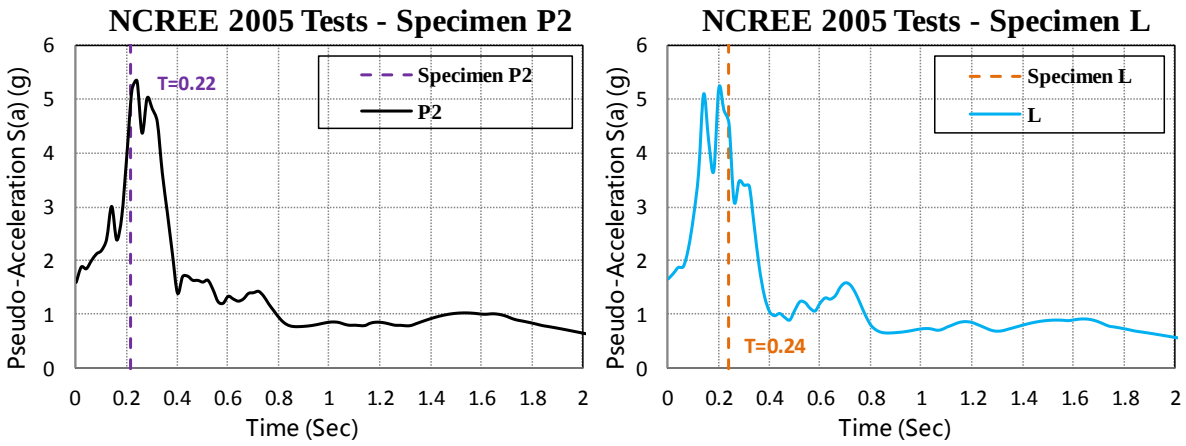

Figure 2.10 Response spectra for NCREE 2005 Tests

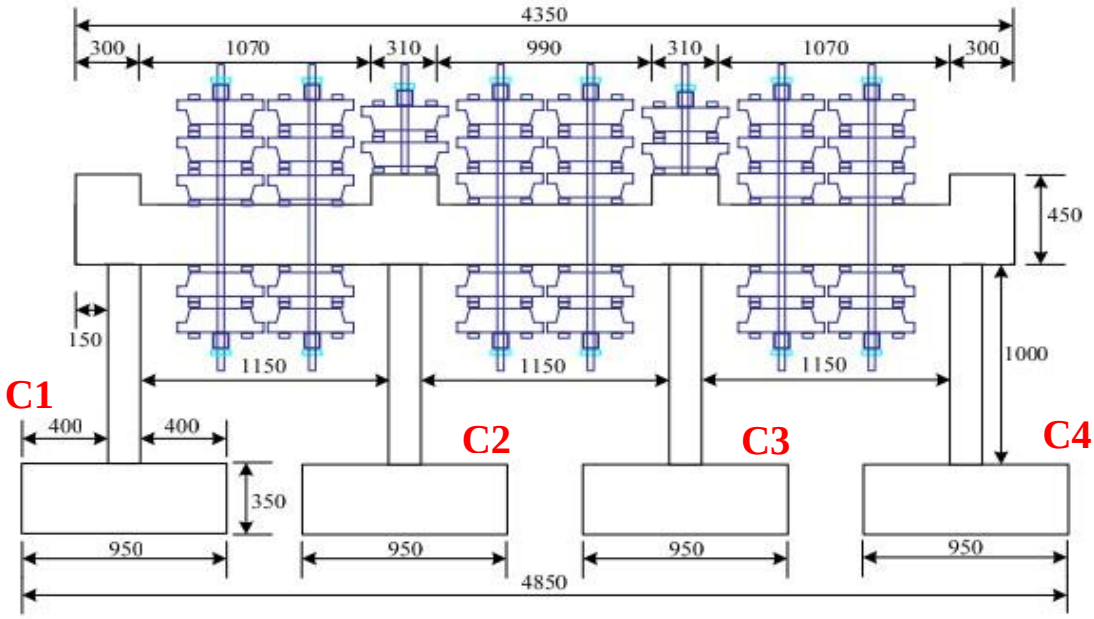

(a) Experimental setup for specimens P2 and L

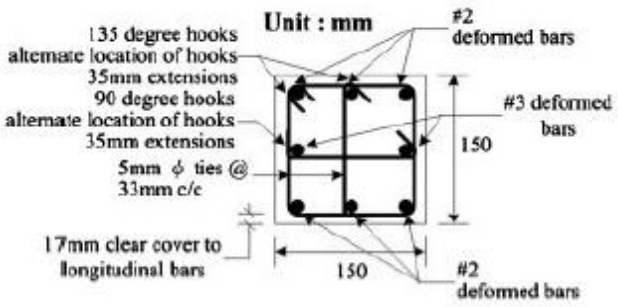

(b) Cross-section for ductile columns (C3, C4)

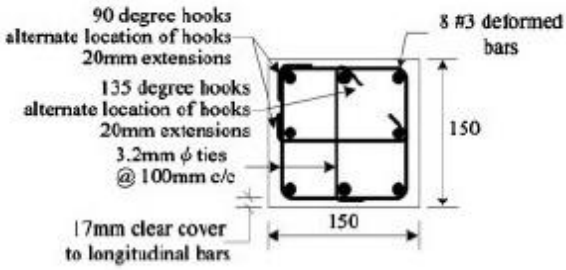

(c) Cross-section for non-ductile columns (C1, C2)

Source: Wu et al. (2009)

Figure 2.11 Information of specimens of NCREE 2005 Tests

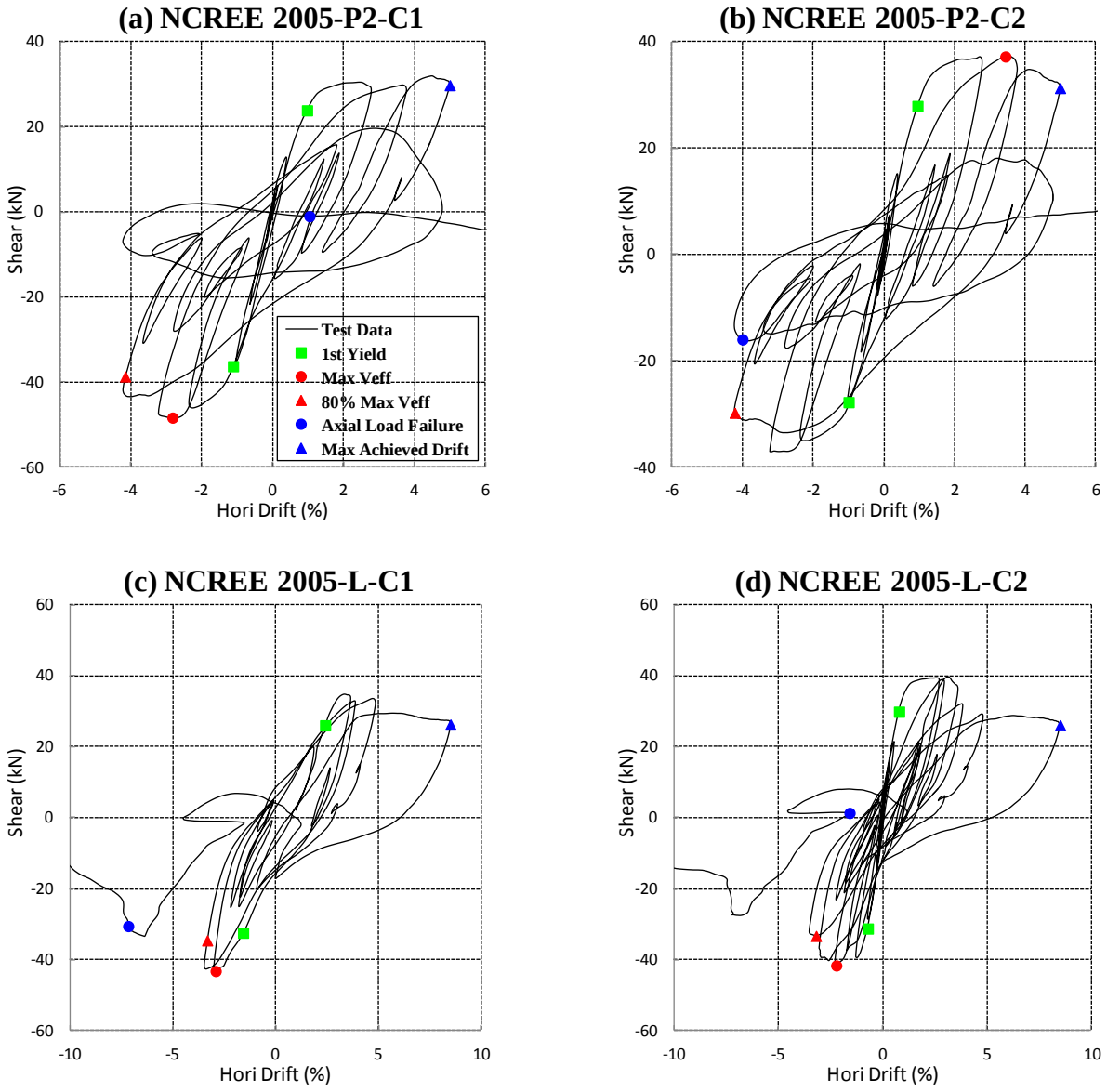

Note: The column is named by the form "Test name-Specimen name-column name". For example, the column "NCREE 2005-L-C1" refers to the column C1 in Specimen L of NCREE 2005 Tests.

Figure 2.12 Hysteretic response of non-ductile columns in NCREE 2005 Tests

2.4.5 NCREE 2004 Tests

In NCREE 2004 Tests, Wu et al. (2006) conducted shaking table tests by on two half-scale, single-story portal frames, specimen S2 and S3. As shown in Figure 2.13, specimens S2 and S3 had two identical non-ductile columns connected by a relatively rigid concrete beam. Since axial load could not be redistributed in two-column system, the system failed simultaneously with the failure of individual columns.

Both Temposonic LDTs and image recorders were installed to record the column displacement history during the tests. Tests showed that image processing technique could interpret data more effectively and accurately, especially when large deformation and structural collapse are expected. Therefore for NCREE 2004 tests, the test data of column horizontal drift provided in the Database were obtained from processing the image data. However, column shortening/lengthening data could not be read reliably through this method and was not provided in the Database.

The identical specimens S2 and S3 are subjected to different input motions with near-fault characteristics and the test results showed that post-peak behavior of columns was strongly dependent on the selected input ground motions. The input motion of S2 was scaled from the ground motion acceleration recorded by TCU076ns station during 1999 Chi-Chi earthquake with PGA as 1.29g and during the test, more flexural deformation was observed. Specimen S3 was subjected to input motions recorded by TCU082ew in Chi-Chi earthquake at two intensity levels with PGA as 0.63g and 1.16g respectively. In S3, shear deformation mainly contributed to the column failure.

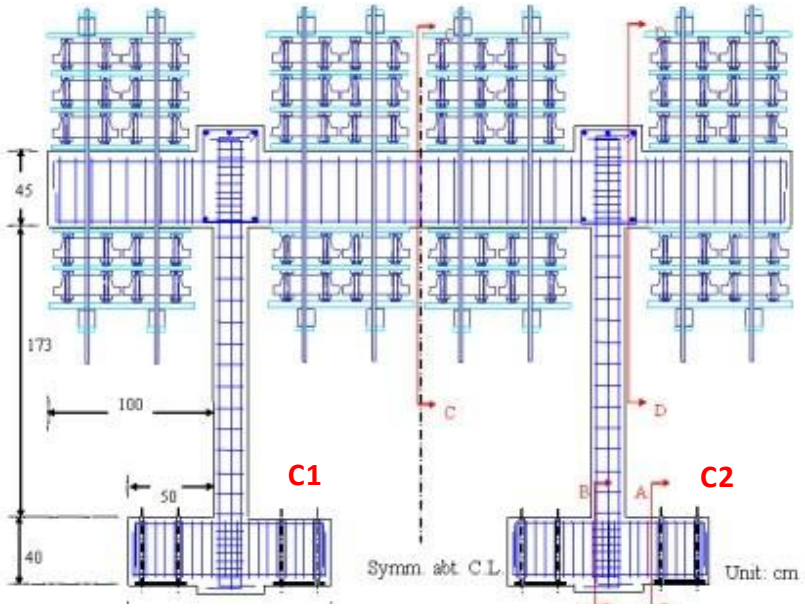

(a) Experimental setup for specimens S2 and S3

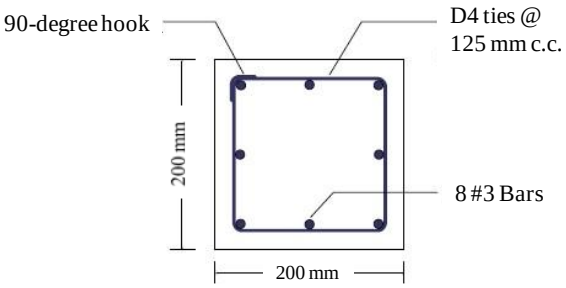

(b) Cross-section for columns in S2 and S3

Source: Wu et al. (2006)

Figure 2.13 Information of Specimen S2 and S3 of NCREE 2004 tests

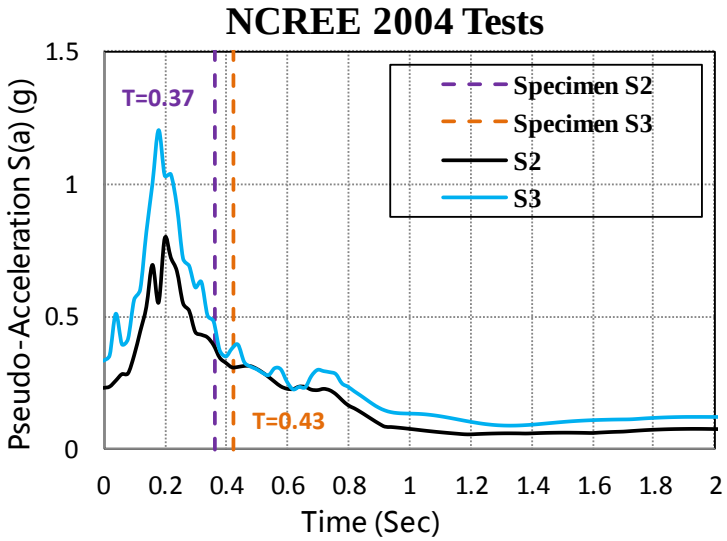

Figure 2.14 Response spectra for NCREE 2004 Tests

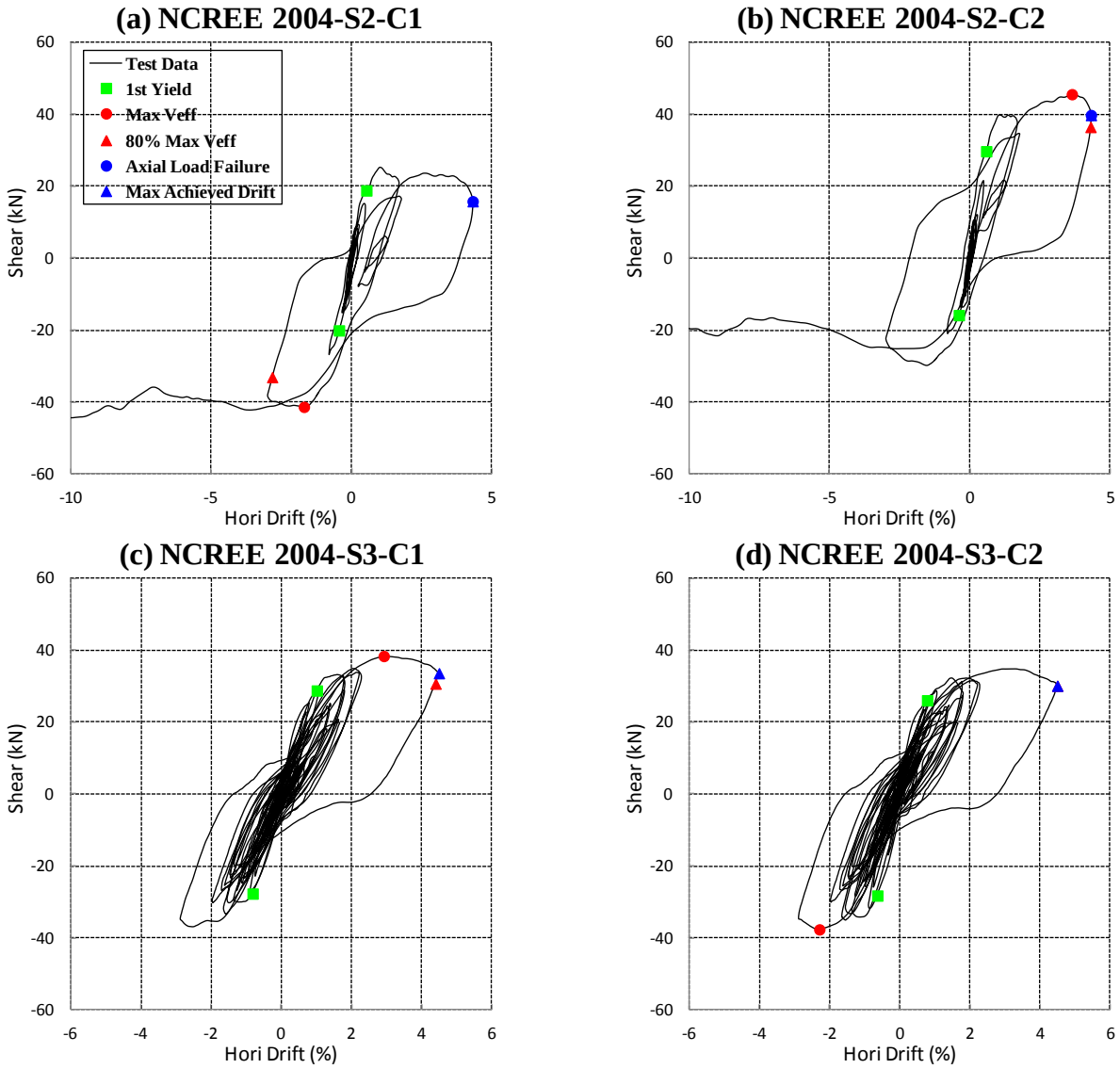

Note: The column is named by the form "Test name-Specimen name-column name". For example, the column "NCREE 2004-S3-C1" refers to the column C1 in Specimen S3 of NCREE 2004 Tests.

Figure 2.15 Hysteretic response of non-ductile columns in NCREE 2004 Tests

2.4.6 Ghannoum 2006 Tests

In 2006, Ghannoum (2007) in UC Berkeley conducted a series of dynamic tests on a three-story, three-bay reinforced concrete frame. The specimen was subjected to uni-directional seismic loading until partial collapse of the frame. The experimental setup of the specimen is shown in Figure 2.16. The specimen had two non-ductile columns in axis A and B on east side and two ductile columns in axis C and D that were introduced to control the failure mode of the frame. The dynamic tests data included in the Database were a half- yield level dynamic test and three high intensity dynamic tests (Dynamic Test 1, 2 and 3).

It is observed from the tests that flexure-shear-critical column B1 (first story, column axis B) suffered significant loss of lateral resistant force and gravity load support in Dynamic Test 1. In Dynamic Test 2, Column B1 continued to lose lateral resistant force. Non-ductile column A1 experienced shear failure as well, but without too much axial load degradation.

In Dynamic Test 3, column A1 gradually lost the axial load support and the whole frame was partially collapsed on the east side.

A shear failure model was also proposed by relating the shear failure to the column rotation measured in region of plastic hinge at the ends of column (assuming the plastic hinge length equal to the column section width).

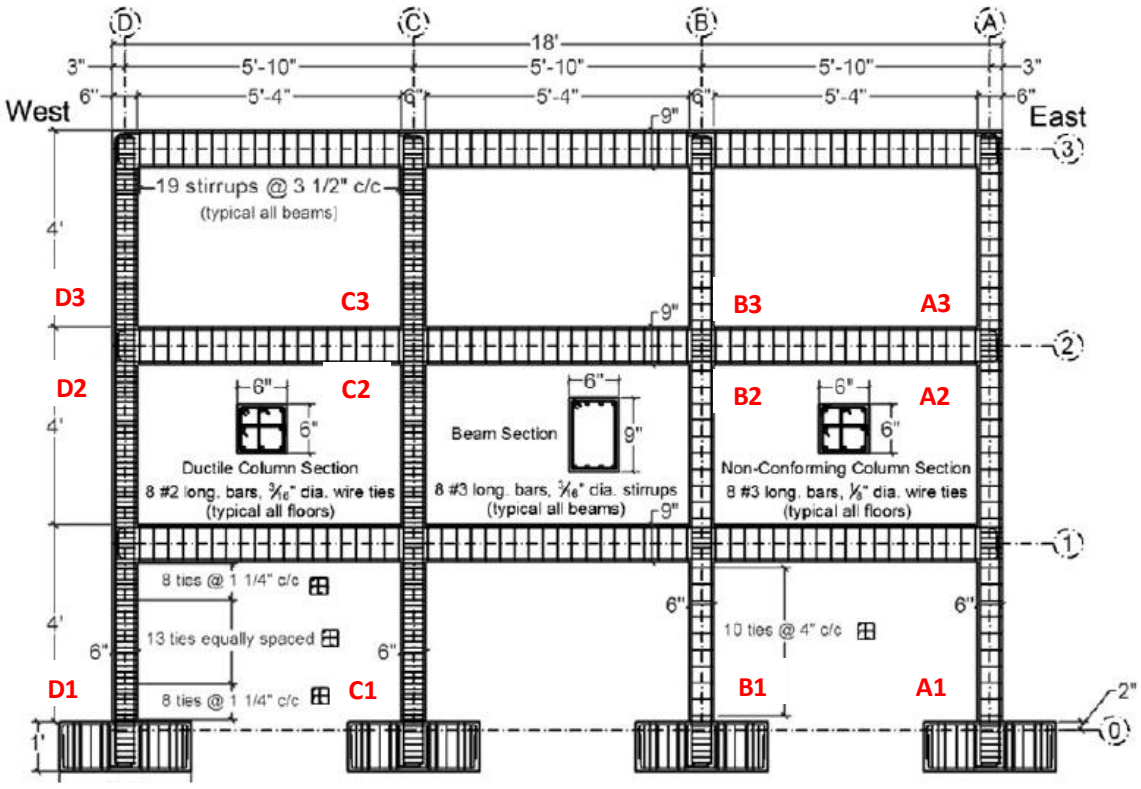

Figure 2.16 Information of specimen of Ghannoum 2006 Tests

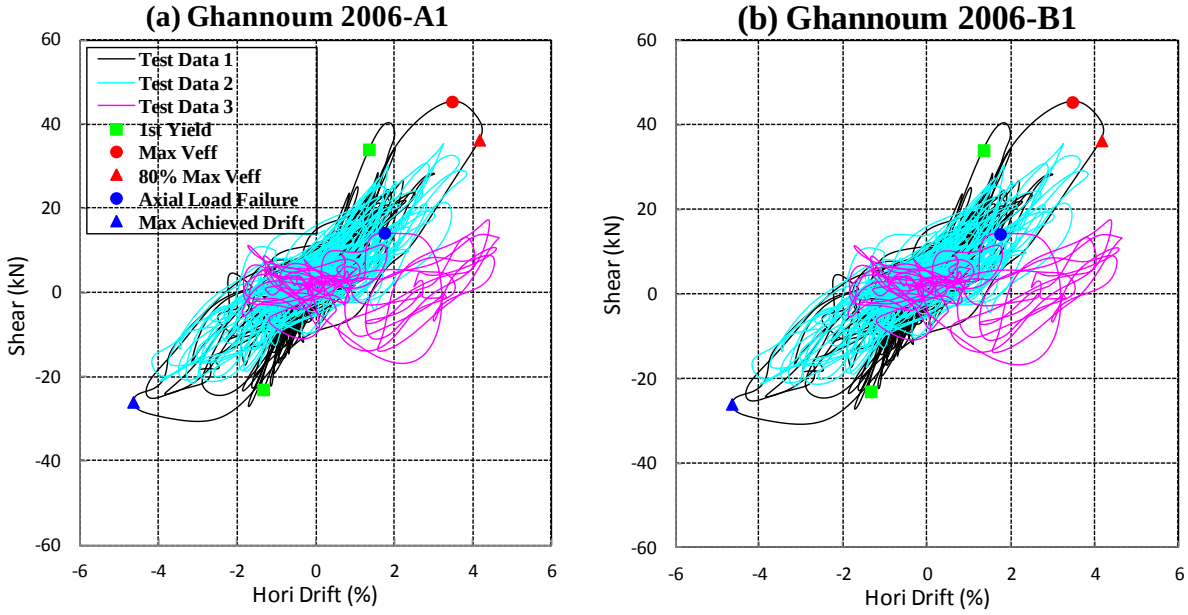

Note: The column is named by the form "Test name- column name". For example, the column "Ghannoum 2006-A1" refers to the column A1 in Ghannoum 2006 Tests. Column A1 is the first story column in axis A.

Figure 2.17 Hysteretic response of non-ductile columns in Ghannoum 2006 Tests

2.4.7 Shin 2005 Tests

Shin (2006) conducted shaking table tests on twelve single-story, single-bay reinforced concrete planar frames that consist of two one-third scale columns connected by a rigid steel beam. There are three kinds of experimental setups, of which specimens with Setup I has two ductile columns, specimens with Setup II includes one ductile on the east side and non-ductile column on the west, and specimens with Setup III consists of two non-ductile columns. The general experimental setup is shown in Figure 2.18.

Four identical specimens were built for each experimental setup and subjected to a pulse-like ground motion with large velocity pulses (Kobe Earthquake) or long-duration motions with low velocity (Chile Earthquake) shown in Figure 2.19.

Experimental results show that frame behaviors was strongly affected by column properties, axial stress level and the input ground motion. Specimens with Setup I exhibited ductile response when subjected to Kobe and Chile input motions for both axial load cases and no shear strength degradation was observed. The non-ductile columns in Setup II specimens experienced shear failure and shear degradation with residual shear strength. Specimens with Setup III collapsed shortly after shear failure of shear-critical columns. Higher axial load ratio also resulted in more rapid shear failure of the columns and the collapse of specimens at lower column drifts.

The columns subjected to Chile input motions tended to experience cyclic shear degradation (lateral resistance decreased from one cycle to the next without negative slope in lateral force-displacement relations), whereas specimens subjected to Kobe input motions more likely had in-cycle shear degradation (lateral resistant force degrades within one cycle, associated with negative slope in the lateral force-displacement relations).

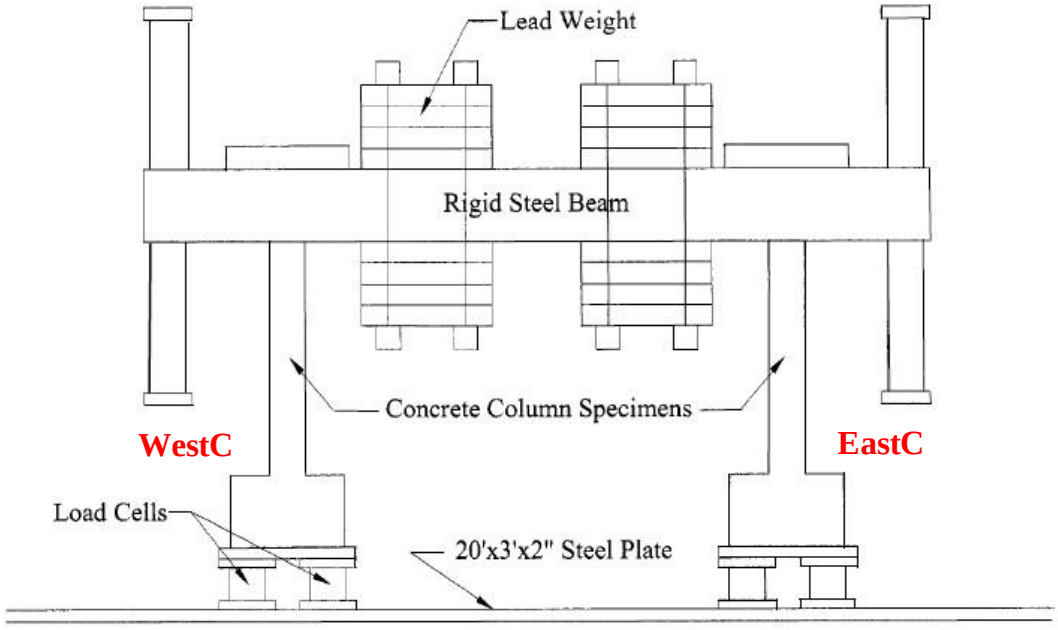

(a) Elevation view of the specimens

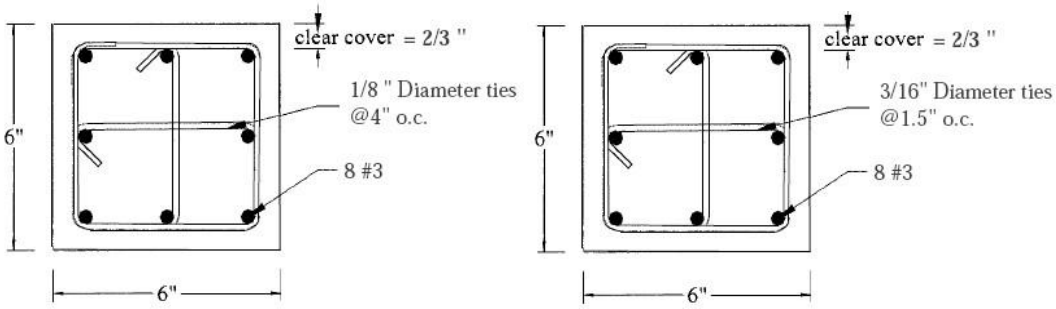

(b) Cross-section for non-ductile columns

(c) Cross-section for ductile columns

Source: Shin (2007)

Figure 2.18 Information of specimens of Shin 2005 Tests

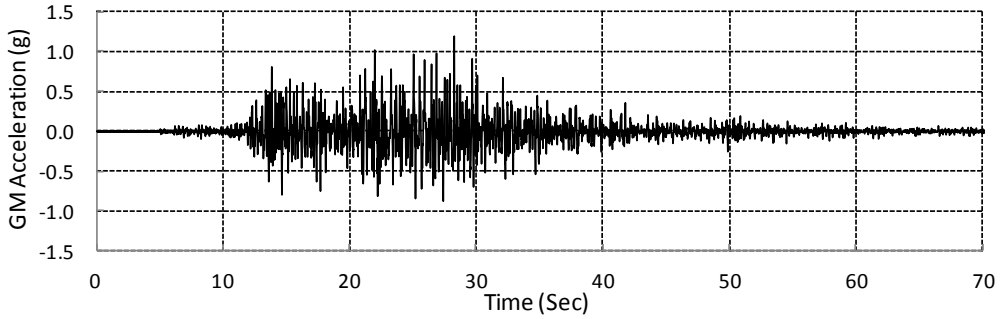

(a) Chile input ground motion

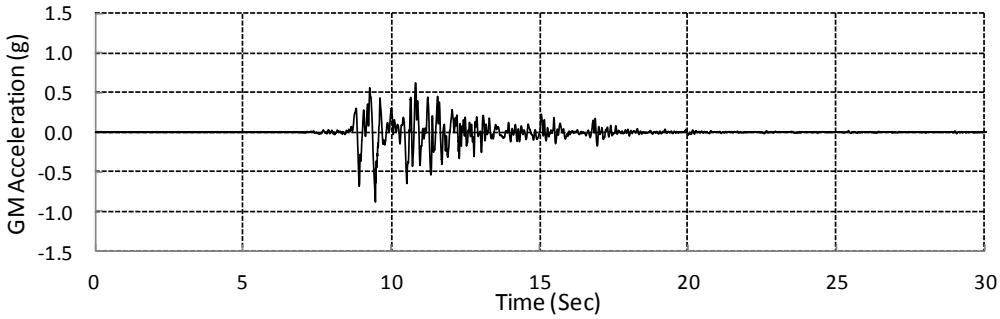

(b) Kobe input ground motion

Figure 2.19 Input ground motions of Shin 2005 Tests

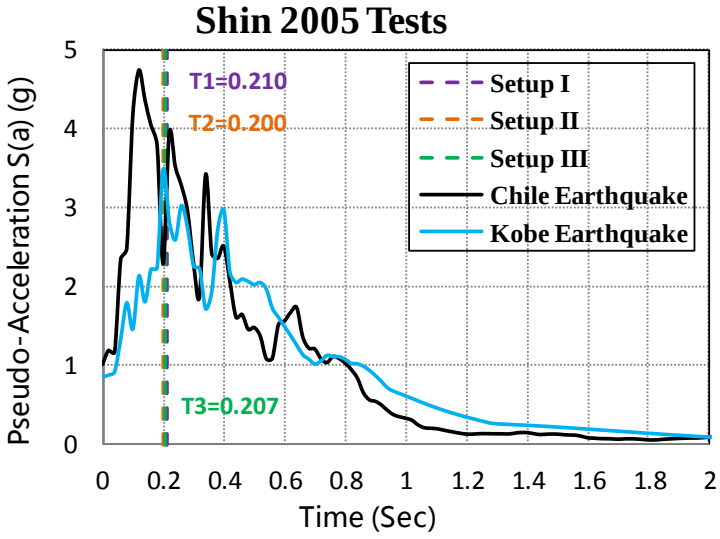

Figure 2.20 Response spectra for Shin 2005 Tests

(a) Shin 2005-II-Test 1-Chile-0.1-WestC

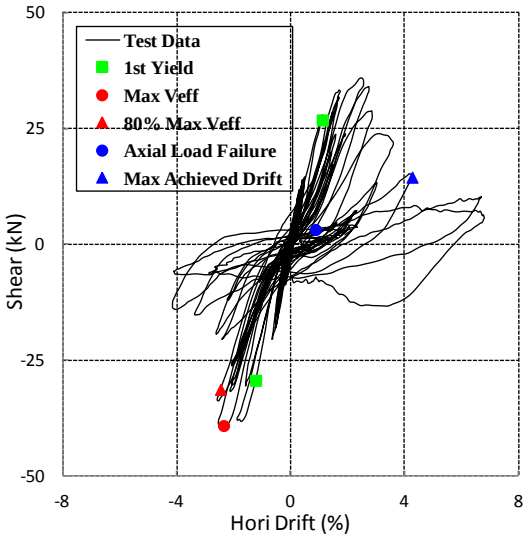

(b) Shin 2005-II-Test 2-Kobe-0.1-WestC

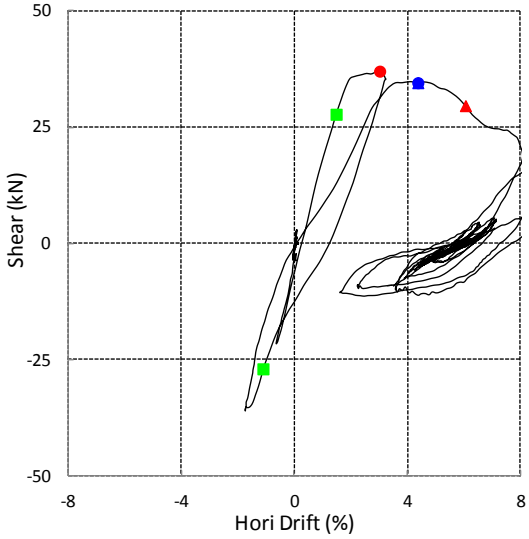

(c) Shin 2005-II-Test 7-Chile-0.24-WestC

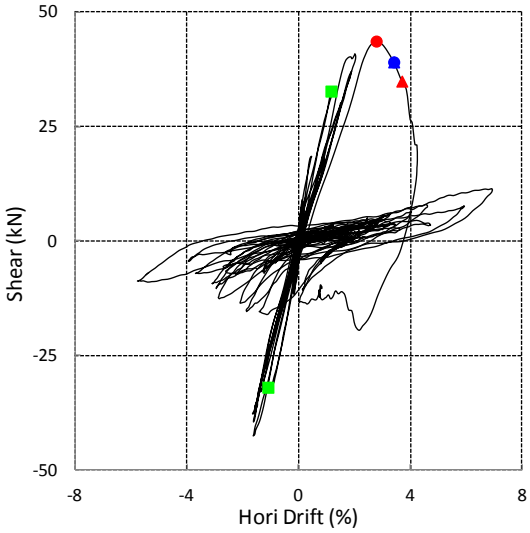

(d) Shin 2005-II-Test 8-Kobe-0.24-WestC

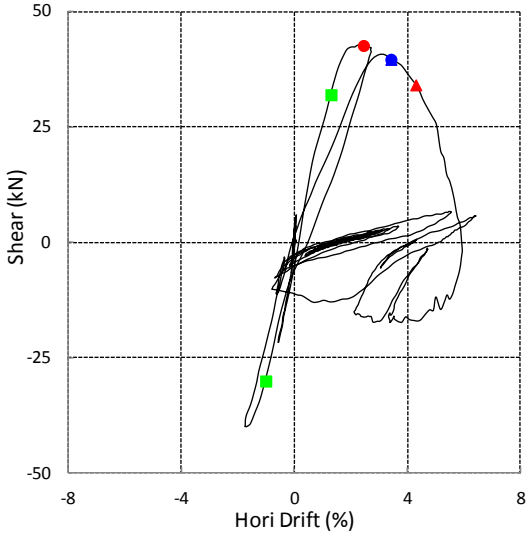

(e) Shin 2005-III-Test 4-Chile-0.1-EastC

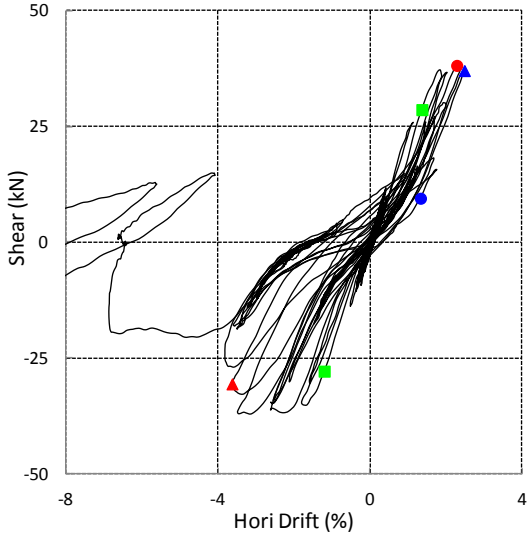

(f) Shin 2005-III-Test 4-Chile-0.1-WestC

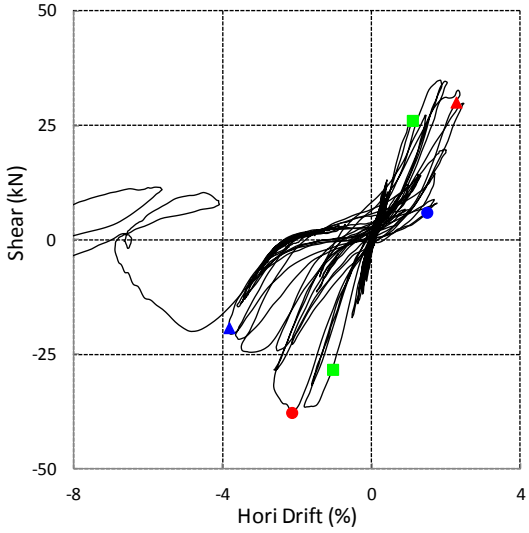

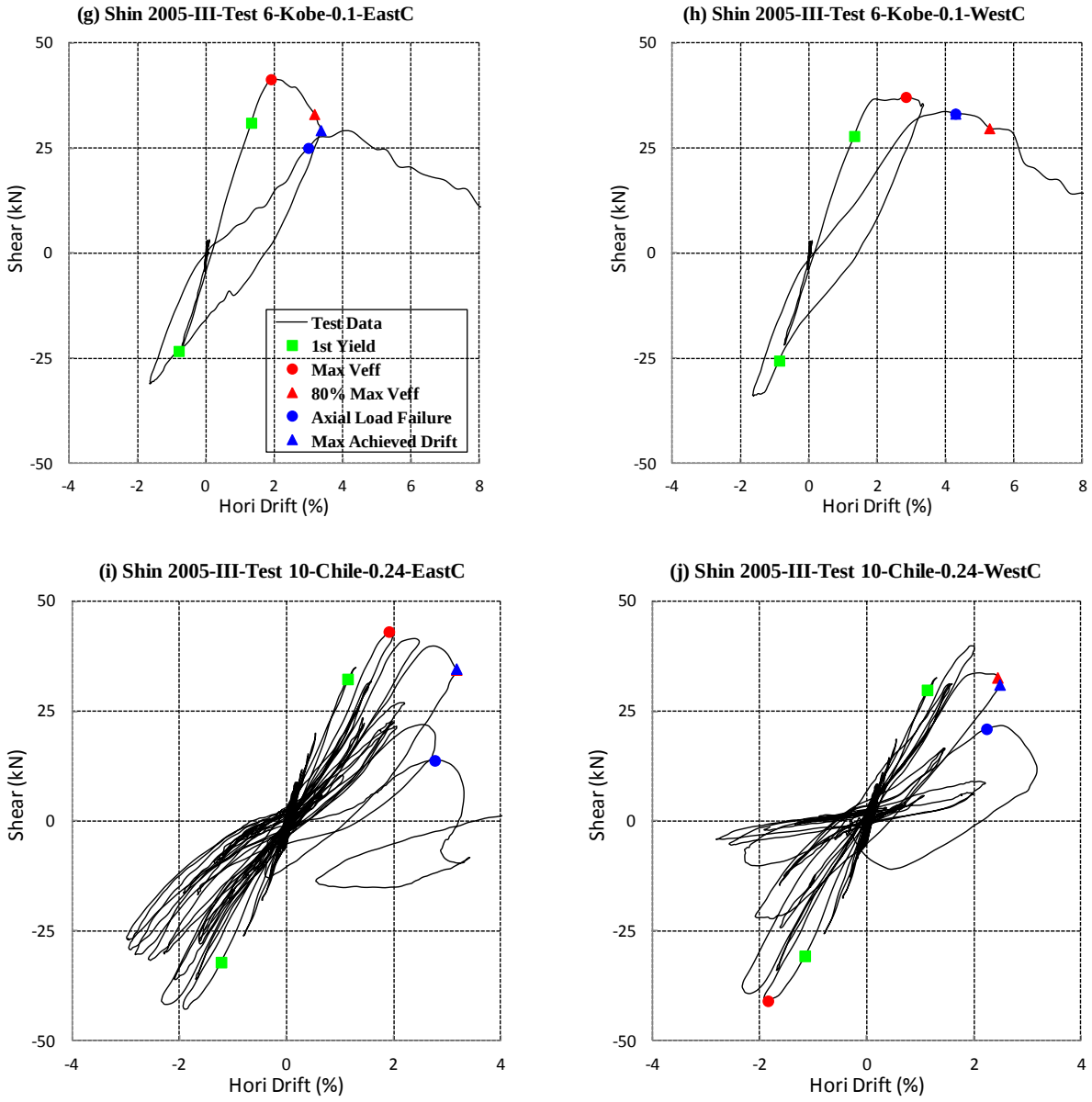

Note: The column is named by the form "Test name-Setup-Test series-Input ground motion-Designed axial load ratio- Column name". For example, the column "Shin 2005-III-Test 10-Chile-0.24-EastC" refers to the eastern column in specimen with type II experimental setup and designed to experience axial load ratio equal to 0.24. It is tested in series Test 10, with Chile earthquake as the input ground motion.

Figure 2.21 Hysteretic response of non-ductile columns in Shin 2005 Tests

2.4.8 Elwood 2002 Tests

Elwood (2002) performed shaking table tests on two one-story, two-bay reinforced concrete frames S1 and S2 to investigate the shear failure and axial load failure of columns that leads to the collapse of frame system during earthquake shaking. Specimens S1 and S2 have identical experimental setups consisting of a non-ductile column in the middle and two circular ductile outside columns, as shown in Figure 2.23. Specimen S2 was subjected to higher axial load ($P/A_g f_c^{'} \simeq 0.2$) compared with that of S1 ($P/A_g f_c^{'} \simeq 0.1$). Only center columns of S1 and S2 are included in the Database since the outside columns are circular ductile columns and should be discussed separately.

Results from specimens S1 and S2 showed that the behavior of frame structures and the column drift capacity are closely related to the axial stress to which the column was subjected. For specimen S1 with moderate axial load on the center column, the column sustained most of its initial axial load after the center column experienced shear failure. For specimen S2 that was subjected to higher axial load, shear failure occurred at a lower drift and was followed shortly by axial-load failure of the center column.

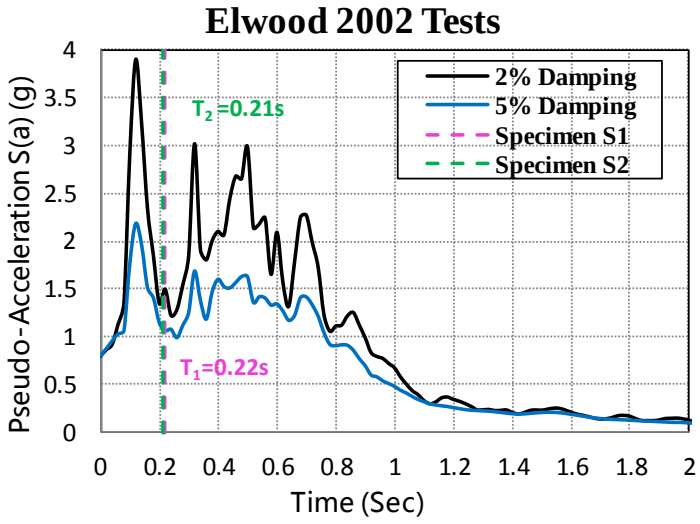

Figure 2.22 Response spectra for Elwood 2002 Tests

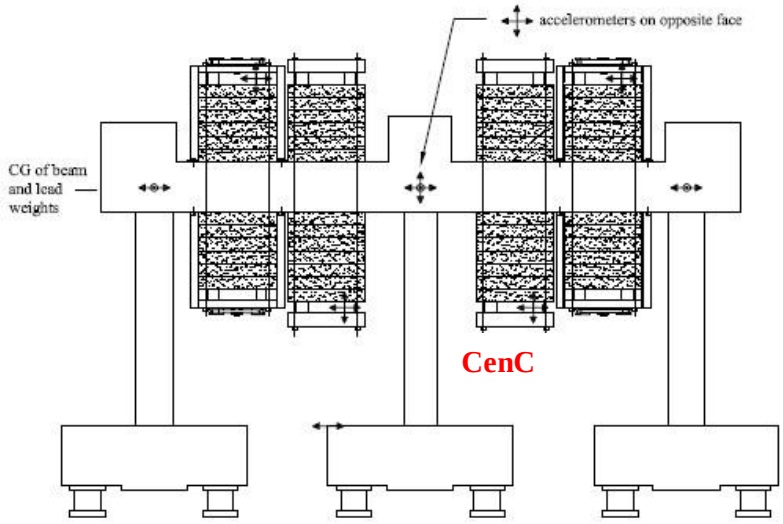

(a) Experimental setup of the specimens S1 and S2

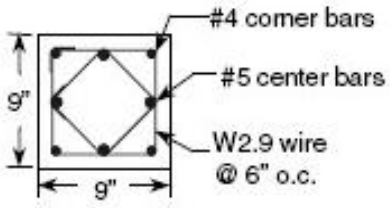

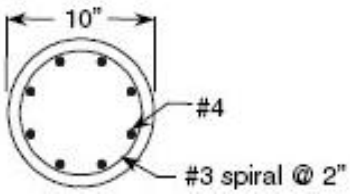

(b) Cross-section for non-ductile columns (c) Cross section for ductile columns

Source: Elwood (2002)

Figure 2.23 Information of specimens of Elwood 2002 Tests

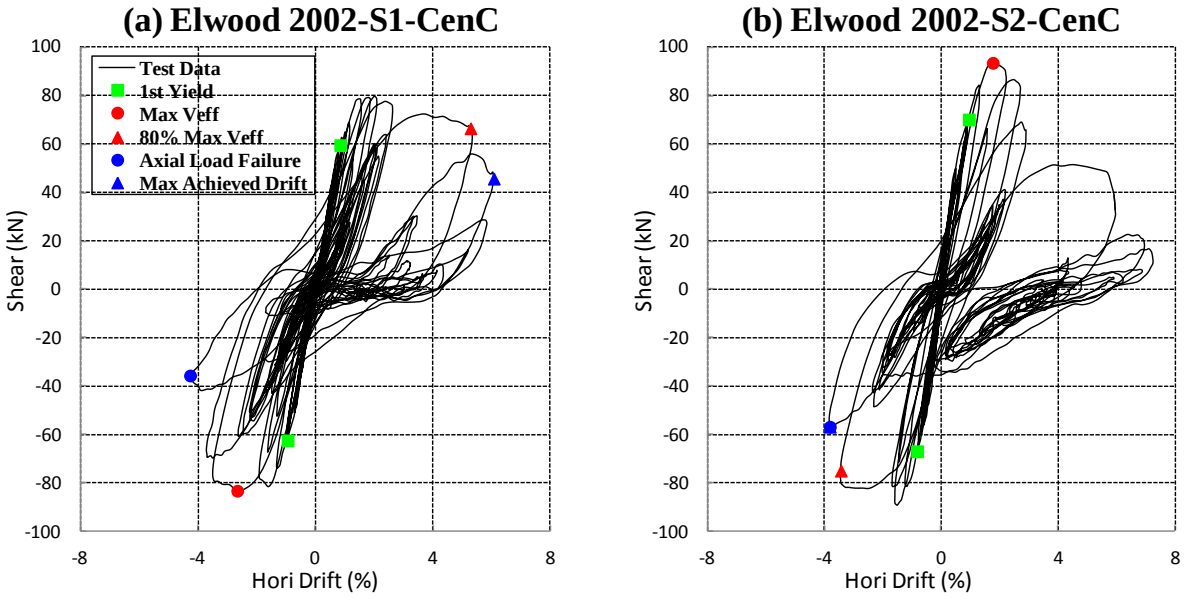

Figure 2.24 Hysteretic response of non-ductile columns in Elwood 2002 Tests

2.5 Test Results Interpretation

2.5.1 P-Delta Correction

The data series "shear" (V) for each column provided in the Database is the column lateral force directly recorded by the force transducers or other instruments during the experiments. As the column lateral deformation Δ increased, axial load P would cause additional moment. Due to this so called P-delta effect, the actual column lateral force, referred to as effective lateral force (V_{eff}), is larger than the recorded shear force. Throughout this research, effective lateral force V_{eff} instead of recorded shear V will be adopted to construct lateral load-deformation relations and evaluate available models, unless specified otherwise. The column effective force could be derived by correcting the P-Delta effect as shown in Figure 2.25.

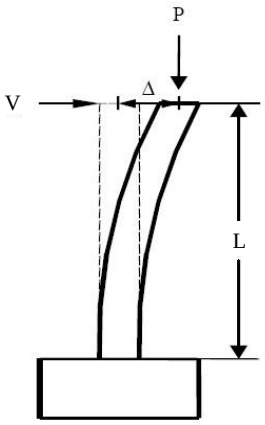

$$V_{eff} = V + \frac{P \times \Delta}{L}$$

Source: PEER Structural Performance Database User's Manual

Figure 2.25 Illustration for correcting P-Delta effect

For most columns included in The Database, there is not much difference in lateral force before and after the P-Delta correction, since the axial load imposed on the columns in The Database is relatively low and the drift achieved by columns, especially non-ductile

columns were very limited. For example, the hysteretic response of recorded shear and effective lateral force for column Elwood 2002-S2-CenC is shown in Figure 2.26(a).

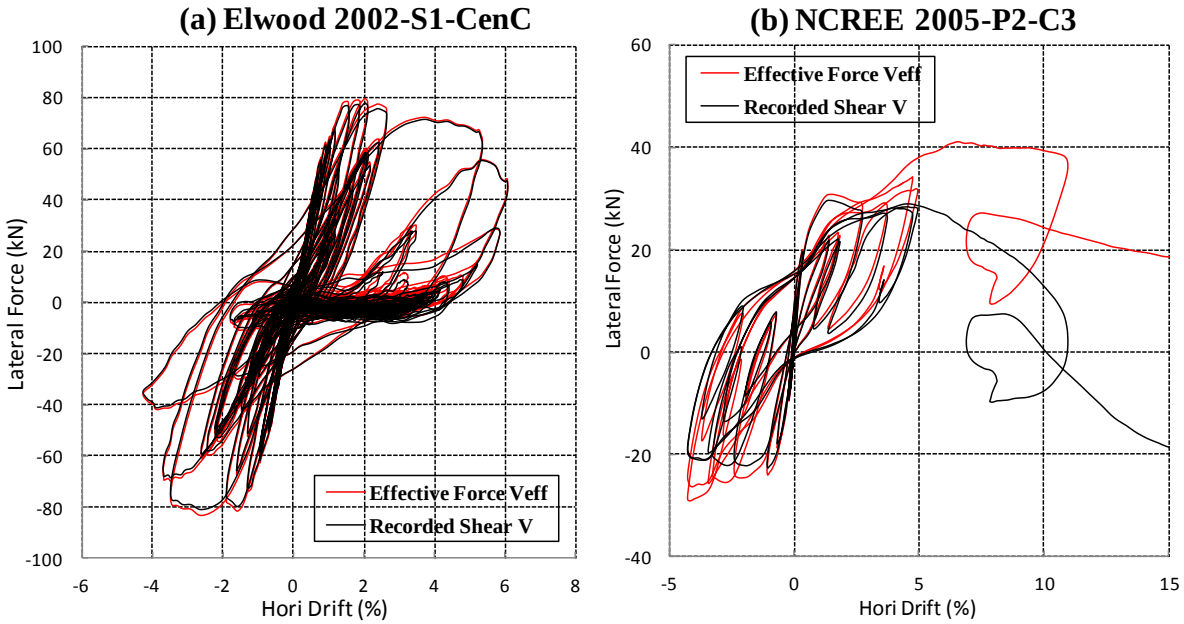

Figure 2.26 P-Delta correction for columns in The Database

However, some ductile columns in concrete frames consisting of multiple columns may experience very high axial load due to the redistribution of gravity load from the non-ductile columns that suffered shear failure. P-Delta effect may greatly influence the lateral force for those ductile columns. For example as shown in Figure 2.26 (b), before the P-Delta correction the ductile column C3 in specimen P2 of NCREE 2005 tests seemed to experience severe shear degradation after the non-ductile center column C2 failed; while after correcting the P-Delta effect, it is found that C3 actually exhibited very ductile behavior and probably went through strain hardening as shown by the increase of shear strength in the last few cycles.

Herein unless otherwise specified, the data of column lateral force will adopt effective lateral force obtained by correcting P-delta effect of recorded shear.

2.5.2 Column Section Analysis

Based on geometric information and material properties of column section, moment-curvature analysis are carried out to obtain the moment-curvature relationships for columns and the key response measures such as first yield point and yield point.

The first yield point is defined as the point that the outermost concrete compressive strain reaches 0.002 or the longitudinal reinforcement yields, whichever comes the first. The corresponding moment and later force are the first yield moment $M_{FirstYield}$ and first yield force $F_{FirstYield}$. The yield point is defined as the point that outermost concrete compressive strain of column reaches 0.004. The moment and lateral force at the yield point are named as ideal moment $M_{0.004}$ and ideal force $F_{0.004}$, respectively.

Simplified method of applying equivalent concrete block is used to calculate the moment-curvature relationship. It assumes that concrete stress could be represented by the equivalent concrete stress block using α_1 and β_1, parameters that can be calculated by Equation 2.1(NBCC, 2005).

$$\alpha_1\beta_1 = \left(\frac{\varepsilon_t}{\varepsilon_c'}\right) - \left(\frac{\varepsilon_t}{\varepsilon_c'}\right)^{2/3}$$
$$\beta_1 = \left[4 - \left(\frac{\varepsilon_t}{\varepsilon_c'}\right)\right] \Big/ \left[6 - 2\left(\frac{\varepsilon_t}{\varepsilon_c'}\right)\right] \qquad \text{Equation 2.1}$$

Where ε_t = concrete strain at the top of the column section; ε_c' = concrete compressive strain.

With different top concrete compressive strain ε_t, the corresponding moment and curvature could be calculated using the force and moment equilibrium principle.

This simplified method could predict the yield point and the ideal moment fairly accurately, yet the data for first yield point is unreliable. For example for the center columns in specimen S1 and S2 of Elwood 2002 Tests shown in Table 2.6, the key points calculated by simplified method are compared with the results from a numerical software such as UC Fyber (Elwood. et al., 2002).

Table 2.6 Results of the section analysis for columns in Elwood 2002 Tests

	Section analysis (UC Fyber)				**Simplified Method**				**comparison**			
	$M_{FirstYield}$ kN m	$\varphi_{FirstYield}$ 1/km	$M_{0.004}$ kN m	$\varphi_{0.004}$ 1/km	$M_{FirstYield}$ kN m	$\varphi_{FirstYield}$ 1/km	$M_{0.004}$ kN m	$\varphi_{0.004}$ 1/km	$M_{FirstYield}$ kN m	$\varphi_{FirstYield}$ rads/km	$M_{0.004}$ kN m	$\varphi_{0.004}$ 1/km
S1	49.7	21	57.9	55.4	46.4	22.8	53.8	50.7	6.6%	8.6%	7.1%	8.5%
S2	59.2	24.7	61.4	45.4	45.4	19.9	56.4	40.7	23.3%	19.4%	8.1%	10.4%

2.6 The Number of Cycles at Key Points

2.6.1 Procedure to Count the Number of Cycles at Key Points

For columns subjected to seismic load, the number of lateral-force cycles that a column experiences is a good indicator of the energy dissipation and column damage.

The number of cycles is counted through an automatic algorithm developed in MATLAB. Using column Shin 2005-II-Test 1-Chile-0.1-WestC (west column in specimen setup II with Chile input ground motion and design axial load ratio as 0.1 in Shin 2005 Tests) as an example, the procedure is described as follows:

- Define the semi-cycles by selecting the semi-cycle points at which the lateral force changes direction, as shown in Figure 2.27. Record the position of each semi-cycle point in the data series. For example, the position of the first semi-cycle point (SemiCycleID=1) is 259 (SemiCyclePos=259). The algorithm starts to select the points when effective force exceeds 30% of peak lateral force for the first time.

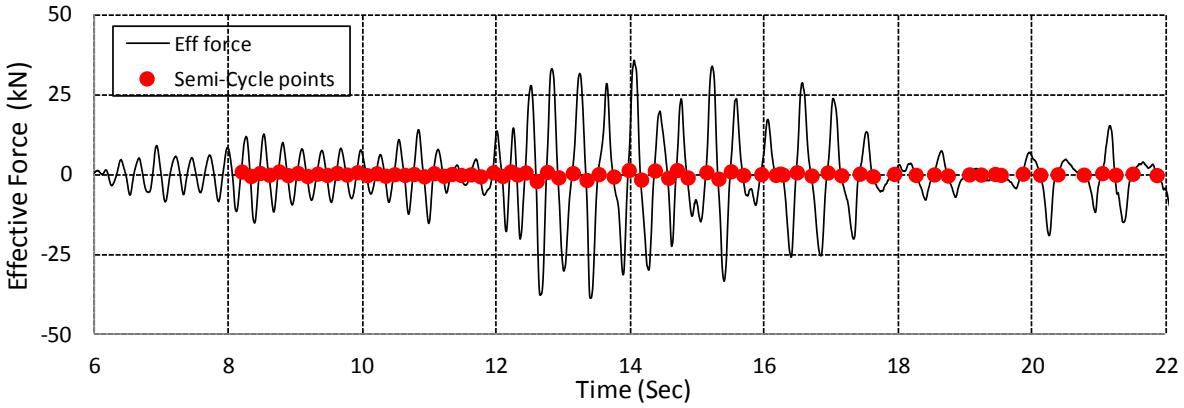

Figure 2.27 Semi-cycle points for column Shin 2005-II-Test 1-Chile-0.1-WestC

- Define the cycles. Three adjacent semi-cycle points are grouped as the key points of one cycle. For example, the first semi-cycle point is considered as the start point of cycle 1 (CycleID=1) and the third semi-cycle point is the end point of cycle 1; The third semi-cycle point is also the start point of cycle 2 (CycleID=2) and the fifth semi-cycle point is the end point of cycle 2, and so on. Group the data between the start point and end point of each cycle and record the maximum drift and lateral force in both positive and negative directions for each cycle, as shown in Figure 2.28.

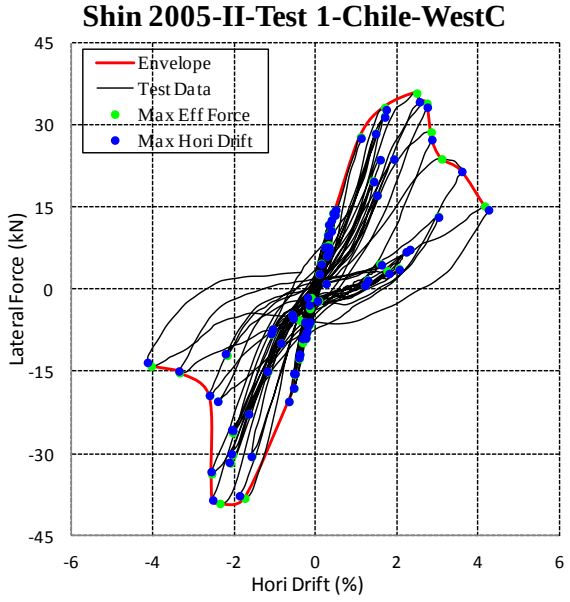

Figure 2.28 The maximum lateral force and drift points in each cycle

- Find the position of the key points and count the number of the cycles that columns have been through. For example, it is found that the key point "80% Max Veff" occurred in cycle 23 (CycleID=23).
- Criteria for counting the number of cycles. To exclude the effect of the small oscillation of lateral force and better reflect the energy dissipation and column damage, insignificant cycles whose maximum lateral force is less than 30% Max Veff are neglected. Thus columns have been through 15 cycles before reaching the key point "80% Max Veff".

Figure 2.29 plots the relations between total number of cycles that column went through before the axial load failure with the maximum column axial load ratio measured during the tests. Results show that while the axial load varied greatly, the number of cycles did not change much and was not directly correlated with the axial load ratio. .

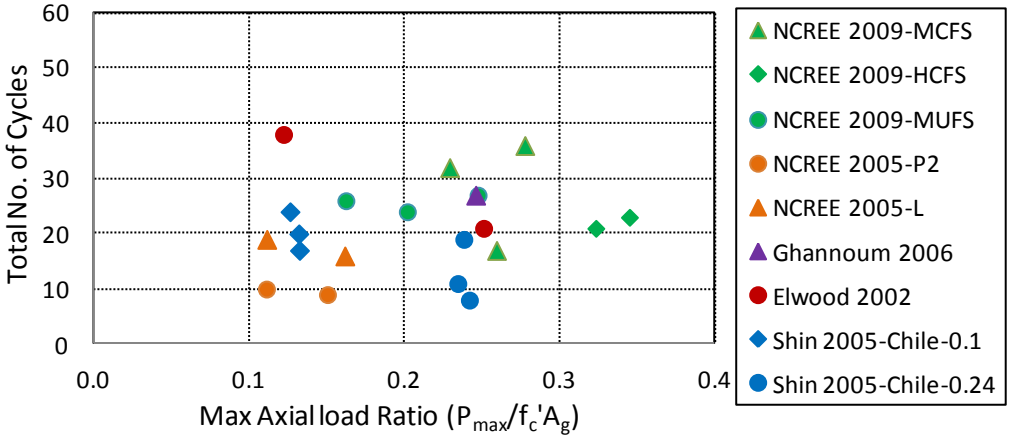

Figure 2.29 Number of cycles with column axial load ratio

2.6.2 Number of Cycles for Columns in Shin 2005 Tests

Table 2.7 summarizes number of cycles that columns in Shin 2005 Tests went through up to the first yield point (column achieved 75% of maximum lateral force), the point column reached maximum lateral force, shear failure point and the axial load failure point.

Table 2.7 Number of cycles for columns in Shin 2005 Tests

(a) Columns in Shin 2005 Tests subjected to Chile earthquake load

Test	**Shin 2005 Tests (Chile Earthquake)**											
Column Type	Ductile columns						Non-ductile columns					
Column ID	38	39	42	43	46	50	47	54	55	51	58	59
Setup	I	I	I	I	II	II	II	III	III	II	III	III
Column	EastC	WestC	EastC	WestC	EastC	EastC	WestC	EastC	WestC	WestC	EastC	WestC
Ground Motion	Chile	Chile	Chile	Chile	Chile	Chile	Chile	Chile	Chile	Chile	Chile	Chile
Designed Axial Load Ratio	0.085	0.083	0.201	0.201	0.090	0.201	0.086	0.087	0.092	0.202	0.192	0.198
0-Δ_{yield}	7	7	3	4	13	2	13	15	18	9	9	8
0-Max V_{eff}	19	27	24	6	32	8	15	19	21	16	10	9
0-80%Max V_{eff}	N.A.	N.A.	N.A.	N.A.	N.A.	N.A.	81	25	22	16	16	12
0-axial failure	81	83	86	84	55	70	30	34	36	16	29	15

(b) Columns in Shin 2005 Tests subjected to Kobe earthquake load

Test	**Shin 2005 Tests (Kobe Earthquake)**									
Column Type	Ductile columns						Non-ductile columns			
Column ID	40	41	44	45	48	52	49	53	56	57
Setup	I	I	I	I	II	II	II	II	III	III
Column	EastC	WestC	EastC	WestC	EastC	EastC	WestC	WestC	EastC	WestC
Ground Motion	Kobe	Kobe	Kobe	Kobe	Kobe	Kobe	Kobe	Kobe	Kobe	Kobe
Initial axial load ratio	0.189	0.191	0.083	0.087	0.086	0.085	0.092	0.088	0.192	0.198
0-Δ_{yield}	1	1	1	1	1	1	1	1	1	1
0-Max V_{eff}	2	2	1	2	2	1	2	2	2	2
0-80%Max V_{eff}	N.A.	N.A.	N.A.	N.A.	N.A.	N.A.	2	2	2	2
0-axial failure	16	18	16	17	17	16	2	2	2	2

From Table 2.7 (a) for columns subjected to the Chile earthquake load, it is observed that increasing axial load could greatly reduce the numbers of cycles that non-ductile columns went through for each key point, by comparing the results of column 51, 58 and 59

with column 47, 54 and 55; while for ductile columns, no significant effect of axial load could be found, except that increasing axial load may cause the column to achieve maximum effective force in fewer cycles.

Results in Table 2.7 (b) show that columns subjected to Kobe earthquake achieved almost all the key points in first two cycles. The ductile columns went through several cycles, yet the number was significantly lower than the identical columns that were subjected to Chile earthquake. It is observed during the test with Kobe ground motion that the lateral force of the non-ductile columns was relatively small (less than 20% of maximum lateral force) initially. Then a sudden increase in lateral force occurred within one cycle and was followed by the column shear failure shortly.

Figure 2.30 compared the number of cycles that non-ductile columns went through with column stiffness k_{eff} and column drift capacities at shear failure and axial load failure.

Non-ductile columns in Shin 2005 Tests were tested in specimens with Setup II (had one ductile and one non-ductile column connected by a rigid beam) and III (consisting two non-ductile columns). One should be cautious when comparing the number of cycles for columns in different specimens, since the cycles might be affected by the structural properties of the specimens, such as frame period and stiffness. The data of non-ductile columns in specimens with setup II was highlighted in a black circle.

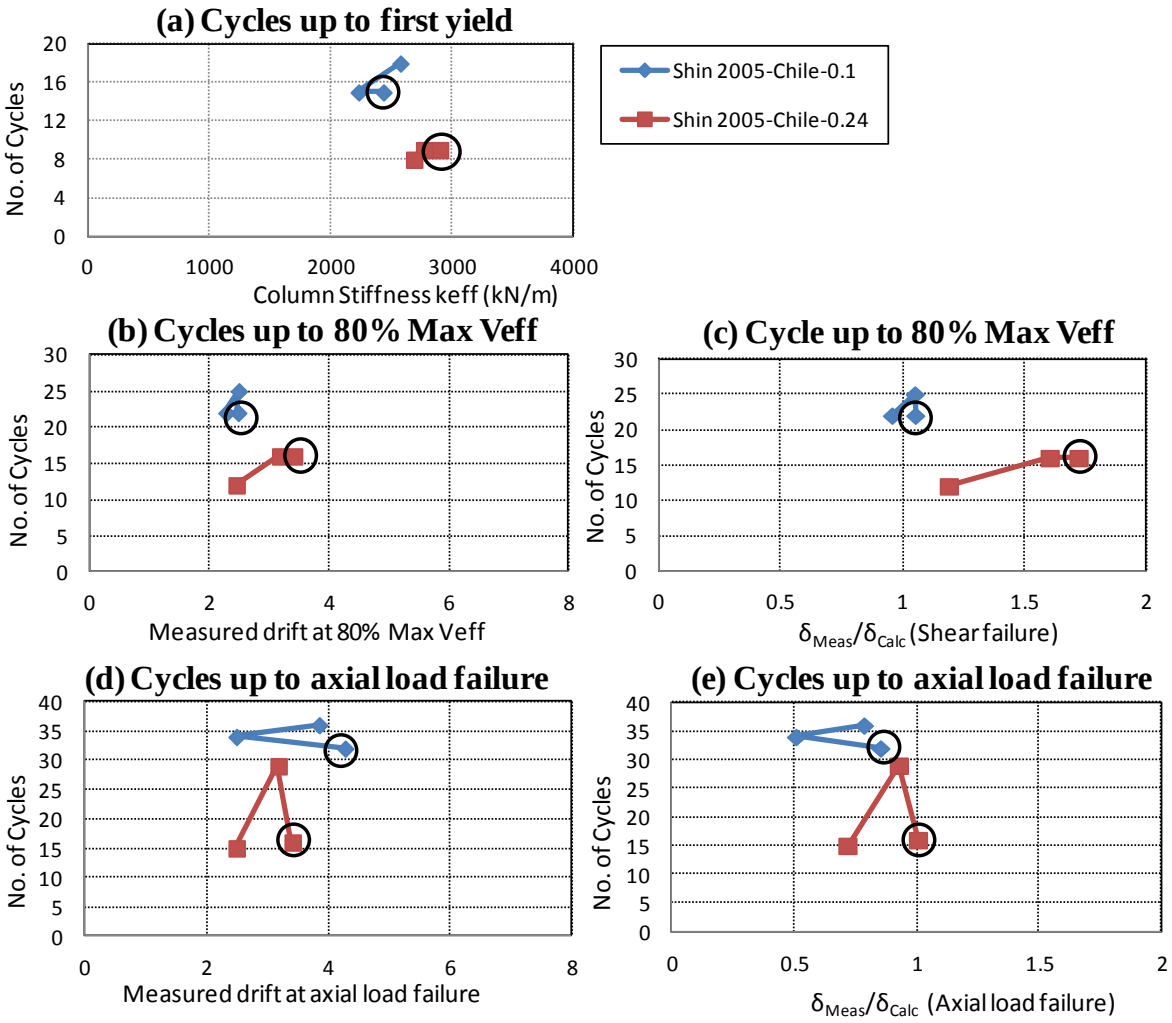

Figure 2.30 Number of cycles for columns in Shin 2005 Tests

2.7 Experimental Envelope of Lateral Force-Drift Relations

To assess the generalized load-deformation relationships recommended by ASCE/SEI 41 and better understand the column response, an experimental envelope is developed by picking the outermost data from the cycles in hysteretic response of lateral force for each column in The Database. The information about each cycle for columns in the Database could be found by following the procedures discussed in section 2.6.1. An example of the experimental envelope is shown in Figure 2.31 for the column Shin 2005-II-Test 1-Chile-0.1-

WestC, with (a) The experimental envelope with hysteretic response of column lateral force; (b) The normalized envelope curve.

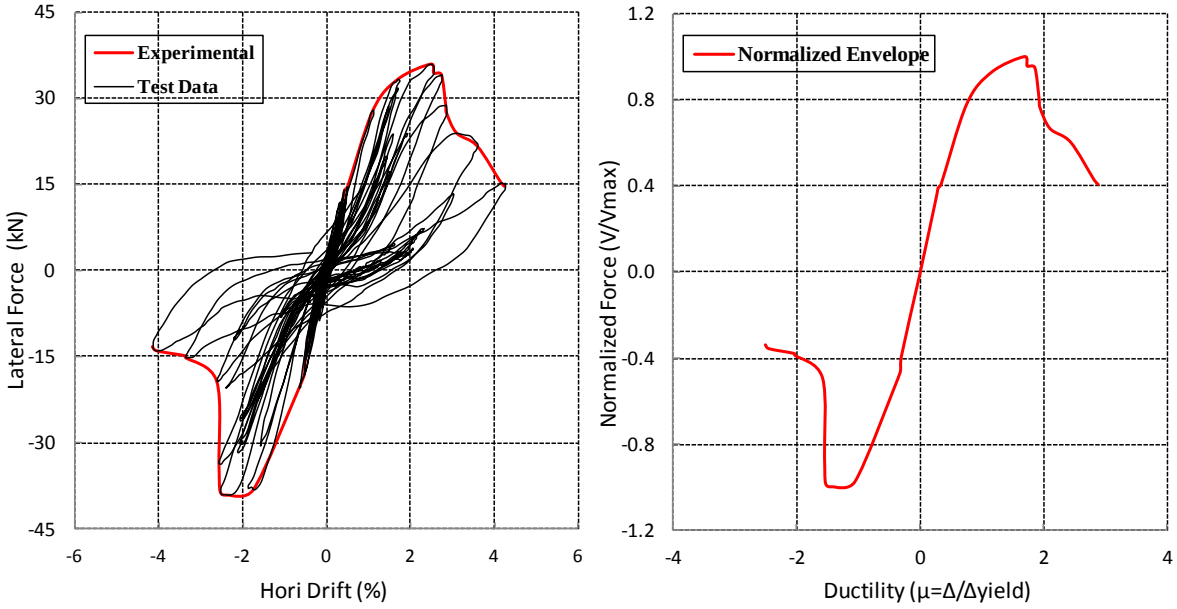

(a) Experimental envelope with test data (b) Normalized envelope

Figure 2.31 Experimental envelope for column Shin 2005-II-Test 1-Chile-0.1-WestC

A normalized envelope is also constructed by dividing the horizontal drift with the yield drift δ_y (defined in section 3.2.5) and the lateral force by the maximum lateral load achieved in each direction. For example, the normalized envelope for Shin 2005-II-Test 1-Chile-0.1-WestC is shown in Figure 2.31 (b).

In the normalized experimental envelopes for columns, the x-coordinate is the ductility demand and the y-coordinate is the non-dimensional effective force ratio related to the maximum lateral force achieved in each direction during the tests. Thus comparing the normalized experimental envelope for different columns will provide a better understanding of column behavior during the dynamic tests.

The observations from the experimental envelope are discussed in section 6.5.1.

Chapter 3: Column Effective Stiffness

3.1 Introduction

In this chapter, two methods to interpret the measured column effective stiffness EI_{eff} are presented, namely the "PEER Method" and "TEST Method". With the obtained measured effective stiffness, performances of the method proposed by ASCE/SEI 41 and the Three-Component model are evaluated and the effect of number of cycles is investigated.

3.2 Measured Column Effective Stiffness

3.2.1 Introduction

For majority structural models predicting the behavior of reinforced concrete frames subjected to earthquake shaking, lateral force-deformation relations need to be established for column components. The column effective stiffness dominates the column behavior in the initial stage and casts a significant influence on the yield displacement and ductility demand of structures. In linear analysis, column effective stiffness controls the prediction of structural period and lateral load distribution. The assumptions made about the column effective stiffness significantly affect the accuracy of structural models.

For most columns in the single-storey specimens, the top connecting beam and the column footings are relatively stiff and the column could be considered as fixed against rotation at both ends. Assuming a linear variation of curvature over the height of the column, the measured effective modulus of rigidity EI_{Meas}, herein referred to as effective stiffness for simplicity, could be derived for columns with double curvature:

$$EI_{Meas} = \frac{2a^3}{3} k_{eff} = \frac{2a^3}{3} \frac{V_y}{\Delta_y} = \frac{2a^2}{3} \frac{V_y}{\delta_y} \qquad \text{Equation 3.1}$$

Where V_y = lateral force at yielding point, which could be taken as the measured maximum effective force V_{Max} or the ideal force $F_{0.004}$ from section analysis discussed in section 2.5.2; Δ_y = measured yield displacement and will be discussed further in following chapters; δ_y = measured yield drift; a = column shear span or equivalent cantilever length, which could be taken as half of the column clear height for fixed-fixed columns; k_{eff} = column lateral stiffness, the slope of the initial linear line from the lateral force-deformation relations, as shown in Figure 3.1. Ideally the area S1 should equal to S2.

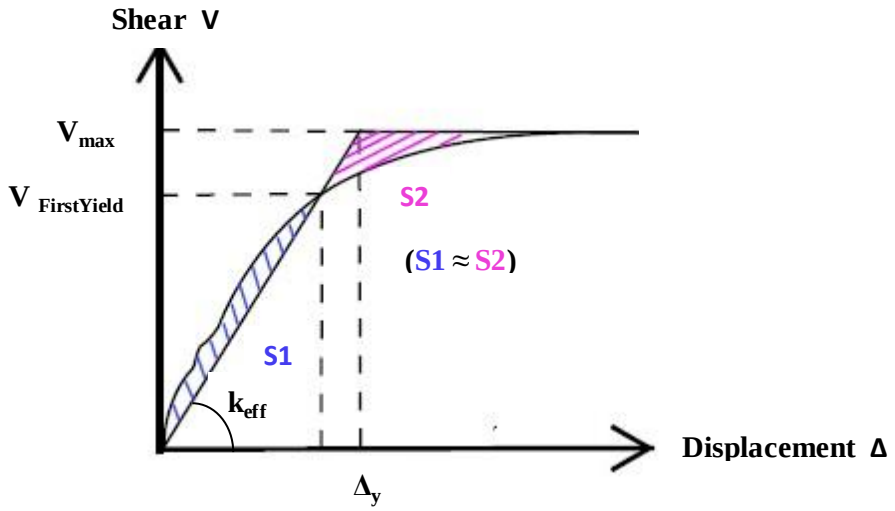

Figure 3.1 Column lateral stiffness k_{eff} from lateral load-deformation relations

The measured effective stiffness is often expressed as a fraction of the gross-section stiffness EI_g . The modulus of elasticity E is estimated by $E = 4500\sqrt{f_c'}$ (MPa) and I_g is the moment of inertia (mm^4). The ratio of EI_{eff} / EI_g will be referred to as effective stiffness ratio herein.

In order to assess the performance of available effective stiffness models with the column data from the Database, consistent methods need to be defined to interpret the lateral

force-deformation data. There are two methods that have been widely used in past research, namely PEER method (Camerillo, 2003) and TEST method (Yavari, 2011).

Both methods are applied to the test data from first test series if columns are subjected to more than one test, so there is no prior cracking from last dynamic test and could represent the initial behavior of the column.

3.2.2 Effect of Column Axial Load

Since the columns included in The Database were subjected to seismic loads, the axial load varied greatly in the positive and negative direction, especially for outside columns in multi-column frame subjected to overturning moment. For example, from the hysteretic response of lateral load and axial load shown in Figure 3.2 for outside non-ductile column C1 in specimen HCFS of NCREE 2009 Tests, it is observed that the column axial load varied from 150kN in negative direction to 420kN in positive direction and column C1 was much stiffer in positive direction due to the higher axial load.

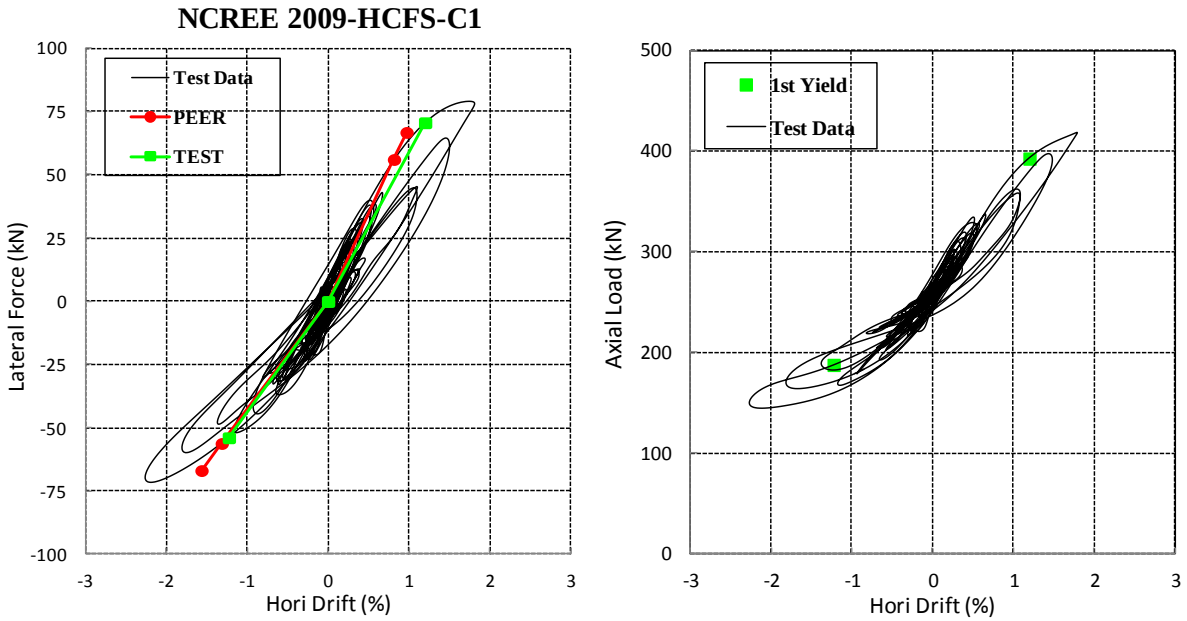

Figure 3.2 Influence of varying column axial load on column effective stiffness

The greatly varying axial load, and the resulting distinct column stiffness, indicates that the measured column effective stiffness should be interpreted separately in positive and negative direction for each column in The Database, instead of averaging the results in both directions. As a result, there will be $59 \times 2 = 118$ data points with regard to the measured of column effective stiffness.

3.2.3 PEER Method

Camarillo (2003) proposed to determine the column effective stiffness from lateral force-deformation relations based on the effective force at first yield point and the yield point (obtained from the section analysis defined in section 2.5.2). This method is adopted to obtain the yield displacement and initial column stiffness for the columns included in PEER database and thus referred to here as "PEER" method.

From the column lateral force-deformation response, the initial stiffness k_{PEER} is determined by linear straight line for the origin to the point at which the lateral force equal to first yield force $F_{FirstYield}$, as shown in Figure 3.3 (a). The line with slope equal to initial stiffness k_{PEER} is extended to the point that column effective force reaches the ideal force k_{PEER} and the corresponding drift is considered yield drift δ_{y-PEER}.

As shown in Figure 3.3(b), for columns whose strength did not exceed the ideal force (not at least 7% higher), for instance the shear critical columns that experienced shear failure before the flexural yielding, the above method was no longer valid and the first yield point is adjusted as the point at which the lateral force reaches 95% of maximum lateral force ($V = F_{FirstYield} = 0.95V_{Max}$).

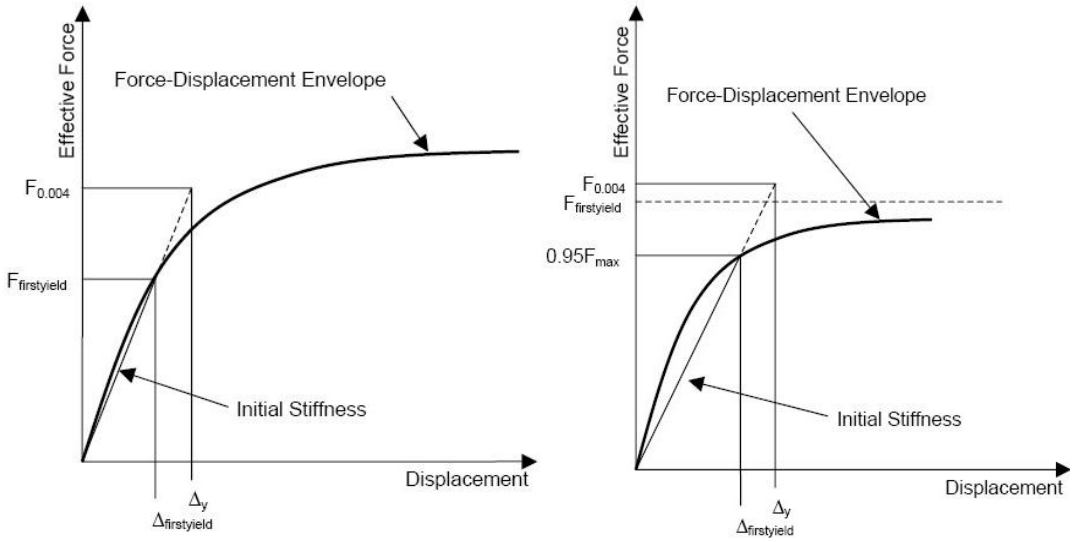

(a) if $F_{Max} \geq 1.07F_{FirstYield}$ (b) if $F_{Max} < 1.07F_{FirstYield}$

Source: Camarillo (2003)

Figure 3.3 Interpretation of column effective stiffness by PEER method

From the initial stiffness k_{PEER} interpreted by PEER method, the column effective stiffness ratio could be calculated by Equation 3.2

$$EI_{PEER}/EI_g = \frac{2a^3}{3} k_{PEER} / EI_g \qquad \text{Equation 3.2}$$

Results of column effective stiffness ratio EI_{PEER}/EI_g interpreted by PEER method are plotted in Figure 3.4 and the data was grouped by the shaking table tests they belong to.

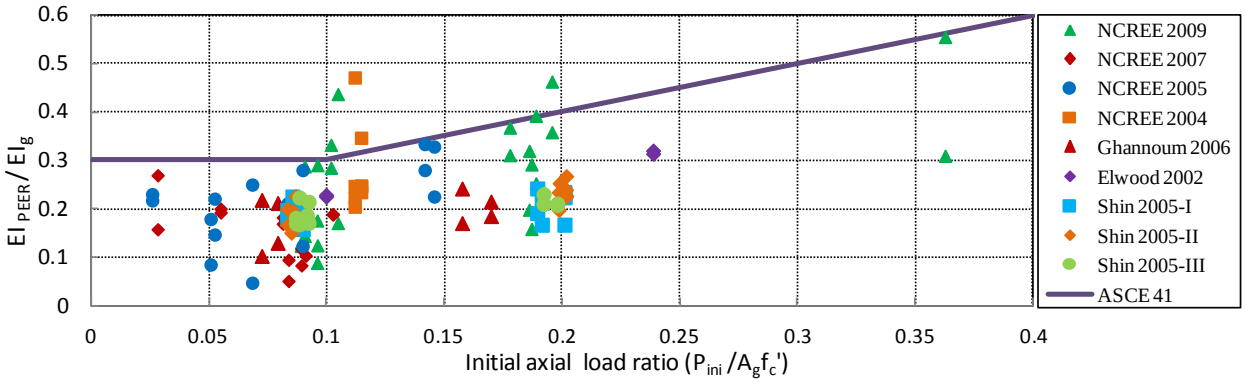

Figure 3.4 Column effective stiffness ratio of PEER method

Most columns included in The Database were subjected to low initial axial load ratio ($P_{ini}/A_g\ f_c^{'} < 0.25$) and the effective stiffness ratio EI_{PEER}/EI_g for most columns were below 0.3. The column effective stiffness increases slightly with the increase of axial load ratio.

3.2.4 TEST Method

Another method commonly used by researchers (e.g. Yavari, 2011) to interpret the column effective stiffness is to define the initial stiffness as shown in Figure 3.5(a) based on 75% of the maximum lateral force (considering the point of $75\%V_{Max}$ as first yield point) and corresponding drift on the measured lateral force-deformation relation,. This method is named as "TEST Method" since it is based on the lateral force-deformation test data.

Figure 3.5 shows an example of interoperating column stiffness by TEST Method. From initial stiffness k_{TEST}, column effective stiffness ratio is calculated by Equation 3.3.

$$EI_{TEST}/EI_g = \frac{2a^3}{3} k_{TEST} \Big/ EI_g \qquad \text{Equation 3.3}$$

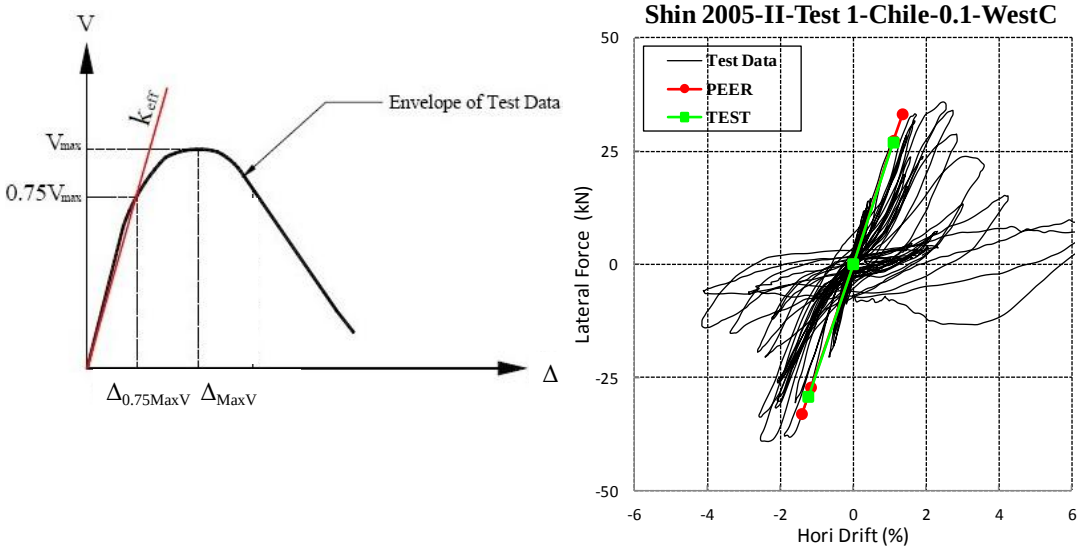

(a) Test Method (b) Effective stiffness for column in Shin 2005 Tests

Source: (a) is adapted from Yavari (2011)

Figure 3.5 Interpretation of column effective stiffness by TEST method

Similar to PEER method, Fig 3.6 shows the effective stiffness ratio derived by TEST method. Most columns included in the Database were subjected to low initial axial load ratio ($P_{ini}/A_g\ f_c^{'} < 0.4$) and the effective stiffness ratio EI_{TEST}/EI_g for most columns were below 0.3. The column effective stiffness increases slightly with the increase of axial load ratio.

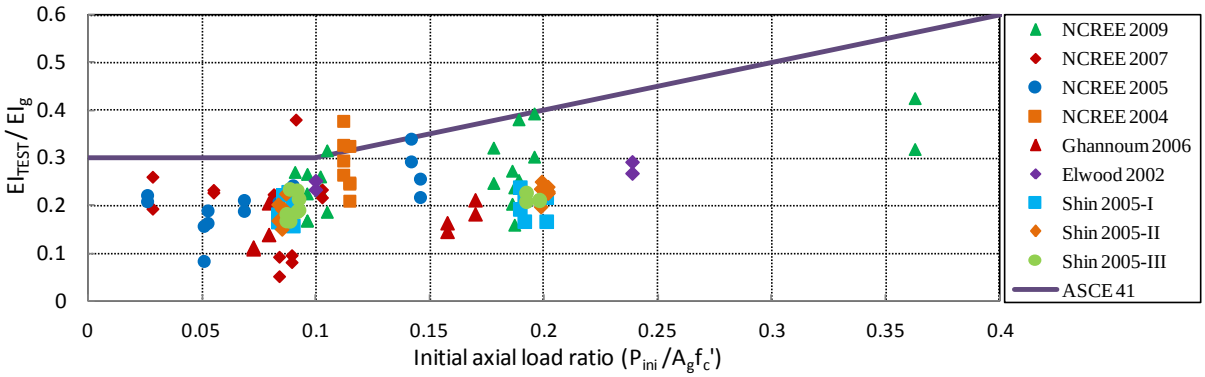

Figure 3.6 Column effective stiffness ratio from TEST method

3.2.5 Measured Column Effective Stiffness

The effective stiffness interpreted by PEER method and TEST method is compared in Figure 3.7. Results show that for most columns, there is not much difference in the effective stiffness from these two methods. The effective stiffness EI_{TEST} from TEST method seems to represent the mean value of the EI_{PEER} from PEER method.

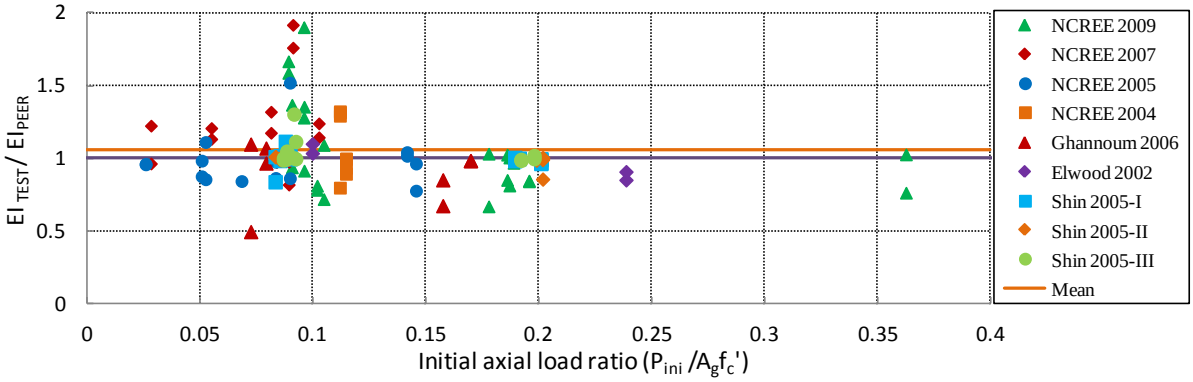

Figure 3.7 Comparison of column effective stiffness from PEER method and TEST method

The effective stiffness interpreted by both methods for the column C1 in NCREE 2009 Tests and Elwood 2002 Tests is very similar as shown in Figure 3.8.

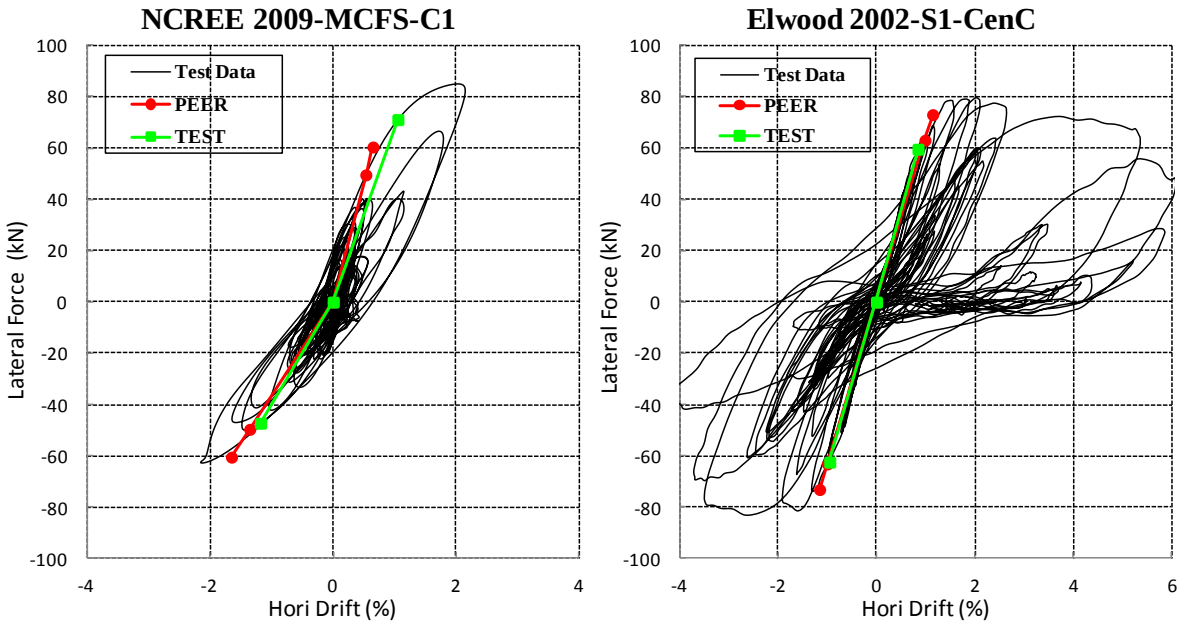

Figure 3.8 Examples of column effective stiffness from PEER method and TEST method

However, for some columns there are large discrepancies in the results of effective stiffness from these two methods, especially in the case for columns had maximum lateral force V_{Max} less than the first yield force $F_{FirstYield}$ obtained from the moment curvature analysis. According to PEER method, the first yield point should be taken as the point that achieved 95% of V_{Max} instead. For example, the maximum lateral force of the shear critical column NCREE 2007-S4-C3 in Figure 3.9 (a) was less than the calculated first yield force and due to the effect that the lateral force increased suddenly in the failure cycle, the first yield point could only be selected in the failure cycle and was quite close to the point with maximum force in negative direction, resulted in a much lower stiffness k_{PEER} than that from TEST method.

Similarly, the column NCREE 2005-L-C4 in Figure 3.9(b) had relatively low lateral force and the maximum lateral force V_{Max} in first few cycles happened to be slightly lower than $0.95V_{Max}$. Thus according to PEER method, the first yield point had to be selected among the data after the column had clearly yielded, resulting in an erroneous interpretation of column initial response.

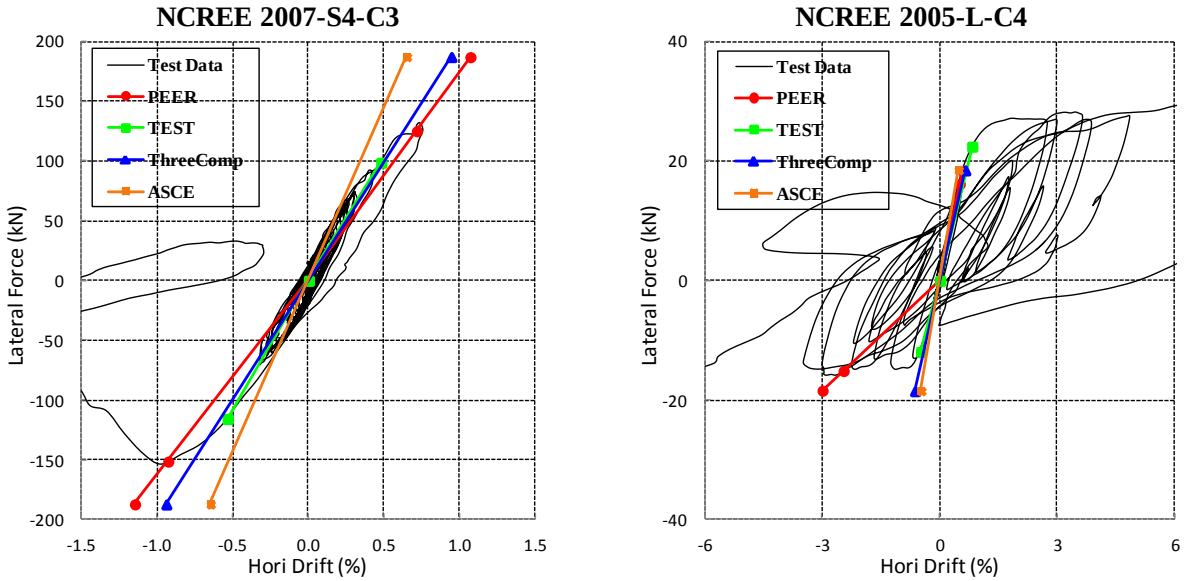

Figure 3.9 Large discrepancies in effective stiffness from PEER method and TEST method

By interpolating the lateral stiffness based on the first yield point from section analysis, the PEER method seems to provide the estimation of column effective stiffness with certain physical meaning. However, the PEER Method can be unreliable and erroneous due to several reasons. Firstly, either initial axial load or maximum axial load was used to carry out the moment curvature analysis for simplicity, while some of the columns were actually subjected to greatly varying axial load during the dynamic tests. Thus it was difficult to get the "true" first yield point of columns and the corresponding lateral force. Secondly, for most columns that had maximum lateral force less than the idea force $F_{0.004}$, the column usually achieved $0.95V_{max}$ at rather later stage and even quite closed to the failure point. The effective

stiffness based on the selected first yield point failed to represent the initial behavior of the columns.

On the other hand, the TEST method generally represented the column behavior fairly well, since the initial response of columns up to $75\%V_{Max}$ was relatively linear for most columns. This method could also be considered as a simplified way to achieve equal energy up to the maximum lateral effective force in most cases ($S_1 = S_2$ as shown in Figure 3.1).

In conclusion, the measured effective stiffness for columns included in The Database will be obtained by following TEST method. Notice that the column stiffness in positive and negative directions is discussed separately in this chapter, while in the following chapters, the measured stiffness and yield drift for columns is obtained by averaging the results in both directions, i.e. $EI_{eff} = \left(EI_{TEST-Post} + EI_{TEST-Nega}\right)/2$, $k_{eff} = \left(k_{TEST-Post} + k_{TEST-Nega}\right)/2$ and $\delta_y = \left(\delta_{y-TEST-Post} + \delta_{y-TEST-Nega}\right)/2$.

3.3 Effect of Key Parameters on Measured Column Effective Stiffness

The measured column effective stiffness ratio EI_{Meas}/EI_g is plotted with key parameters in Figure 3.10 for the columns included in The Database.

The key parameters considered include: (a) Initial axial load ratio $P_{ini}/A_g\ f_c^{'}$; (b) Longitudinal reinforcement ratio ρ_l; (c) Aspect ratio a/D; (d) Ratio of longitudinal reinforcement diameter to the depth of column section d_b/D; (e) Concrete compressive strength on test day $f_c^{'}$; (f) Ratio of yield stress of longitudinal reinforcement to concrete compressive strength $f_{yl}/f_c^{'}$;

In this chapter, the test data is grouped by the column failure type classified by ASCE/SEI 41(discussed in section 6.3). The data series "Shear" in orange triangular marker represents the shear critical columns in The Database (corresponding to the Condition iii in ASCE/SEI 41). The data series "Flex-Shear" (corresponding to Condition ii) in red diamond marker and data series "Flexure" (corresponding to Condition i) in green round marker refer to the flexure-shear critical columns and flexure critical columns respectively. These two data series are from columns that are connected with a rigid beam and hence lateral drifts can be attributed entirely to column deformations. The data series "Flex-Shear (Beam)" in purple diamond marker and data series "Flexure (Beam)" in blue round marker represent the flexure-shear critical columns and flexure critical columns that were connected with flexible beam that may introduce additional flexibility to the total response, and hence, are expected to be softer than that estimated based on column stiffness alone.

Results in Figure 3.10 show that effective stiffness ratio tends to increase consistently with axial load ratio. Increasing ratio of yield strength of longitudinal reinforcement to concrete compressive strength $f_{yl} / f_c^{'}$ also results in a slight increase in column effective stiffness ratio. Other parameters, such as longitudinal reinforcement ratio ρ_l and concrete compressive strength $f_c^{'}$, are not strongly correlated with column effective stiffness ratio.

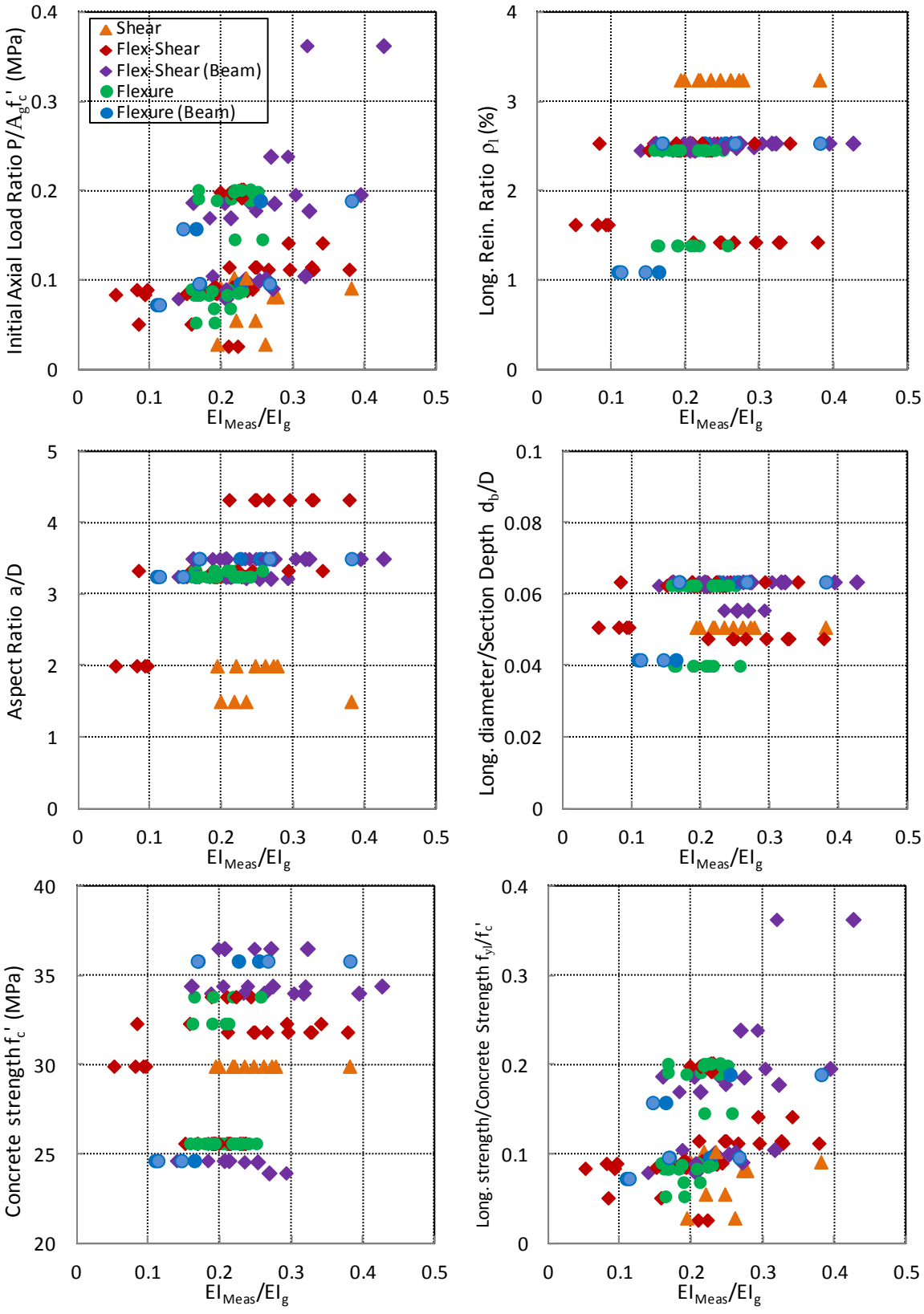

Figure 3.10 The measured effective stiffness with key parameters

3.4 Evaluation of ASCE/SEI 41 Procedure

The current seismic rehabilitation standard ASCE/SEI 41 recommends to estimate the effective stiffness ratio based on the column axial load level. Similar procedures are adopted in the other code and standards, such as American Concrete code, ACI 318-08 and commentary to the New Zealand concrete code, NZS 3101-06(NZS 2006).

According to ASCE/SEI 41 procedure shown in Figure 3.11, the effective stiffness equals to $0.3EI_g$ when columns are subjected to axial load ratio less than 0.1, while for columns have axial load ratio higher than 0.5, the effective stiffness shall be taken as $0.7EI_g$. Linear interpolation of the effective stiffness ratio is required for columns subjected to axial load ratio in between ($0.1 < P/A_g\ f_c^{'} \le 0.7$).

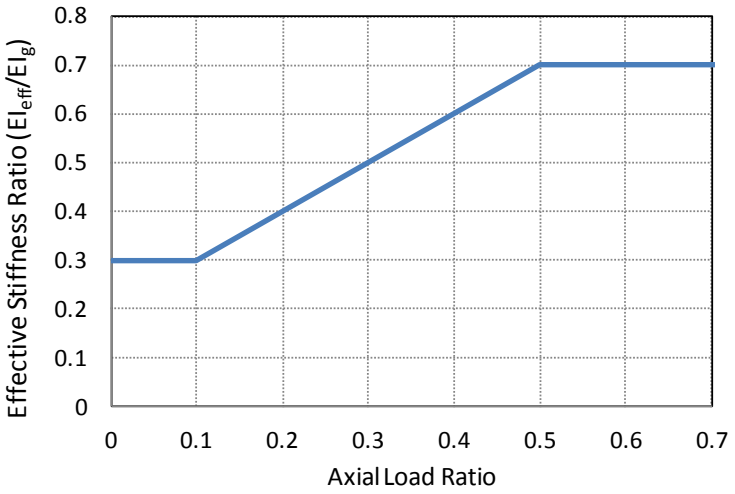

Figure 3.11 Column effective stiffness ratio estimated by ASCE/SEI 41 procedure

Figure 3.12 plots the ratio of measured column effective stiffness EI_{Meas} to calculated results EI_{ASCE} from ASCE/SEI 41 procedures.

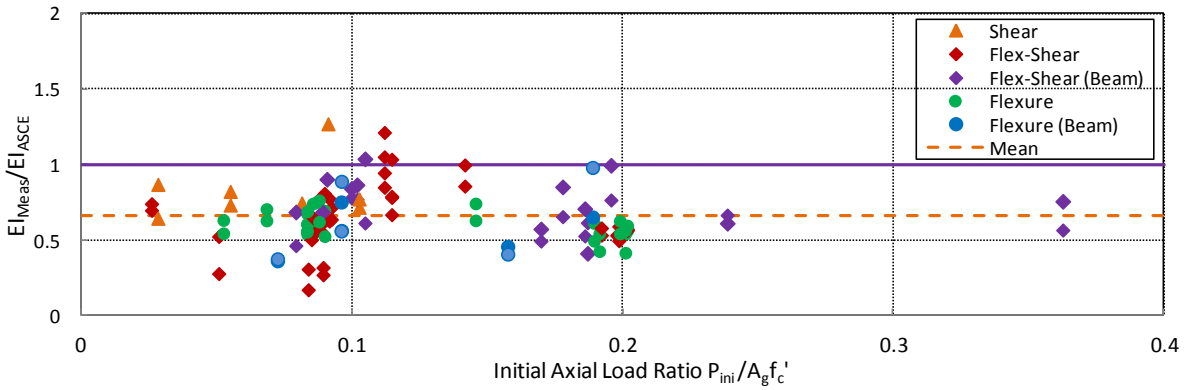

Figure 3.12 Evaluation of column effective stiffness estimated by ASCE/SEI 41 procedure

It is observed in Figure 3.12 that the majority data of EI_{Meas}/EI_{ASCE} falls below unity representing the case that estimated effective stiffness matches exactly with the measured column stiffness. ASCE/SEI 41 procedure generally overestimates the column effective stiffness for all types of columns.

3.5 Evaluation of Three-component Model

Elwood and Eberhard (2009) proposed a three-component model to estimate the column yield deformation by explicitly taking into account the deformation due to the flexure behavior Δ_{flex}, shear response Δ_{shear} and bar-slip effect Δ_{slip}, by Equation 3.4.

$$\Delta_{y-ThreeComp} = \Delta_{flex} + \Delta_{shear} + \Delta_{slip}$$

$$\Delta_{flex} = \frac{2a^2}{3}\phi_y$$

$$\Delta_{shear} = \frac{M_{0.004}}{A_v G_{eff}} \qquad \text{Equation 3.4}$$

$$\Delta_{slip} = \frac{a d_b f_s \phi_y}{8u}$$

Where ϕ_y =the curvature at the yield point (the extreme concrete compressive strain reaches 0.004) obtained from the moment curvature analysis.

A_v = effective shear area, usually taken as 5/6 of the gross-section area for rectangular columns; $G_{eff} = \frac{1}{2}G = \frac{1}{2} \cdot \frac{E_c}{2.4}$, the effective shear modulus is reduced to be half of the elastic shear modulus G due to crack in concrete blocks.

d_b = nominal diameter of longitudinal reinforcement. f_s =stress in the tension rebar at the yield point of the column, usually taken as the yield strength of longitudinal reinforcement f_{yl}. The bond stress u for elastic analysis is ranged from $u = 0.5\sqrt{f_c'}$ to $u = 1.0\sqrt{f_c'}$ (MPa) and here taken as $0.8\sqrt{f_c'}$ (MPa).

Figure 3.13 plots the ratio of measured contributions from each of the deformation components (Δ_{flex}, Δ_{shear} and Δ_{slip}) for the columns included in The Database, for (a) flexure-shear critical columns, (b) flexure critical columns and (c) shear critical columns.

It is observed from Figure 3.13 that for most columns, around half of the column deformations up to the yielding point are attributed to the column flexure behavior. The deformations due to bar slip effect could account for more than 50% of total yield displacement. While the shear response caused less than 5% deformations for shear critical columns, the contribution of shear component was negligible for flexure-shear critical columns and flexure critical columns.

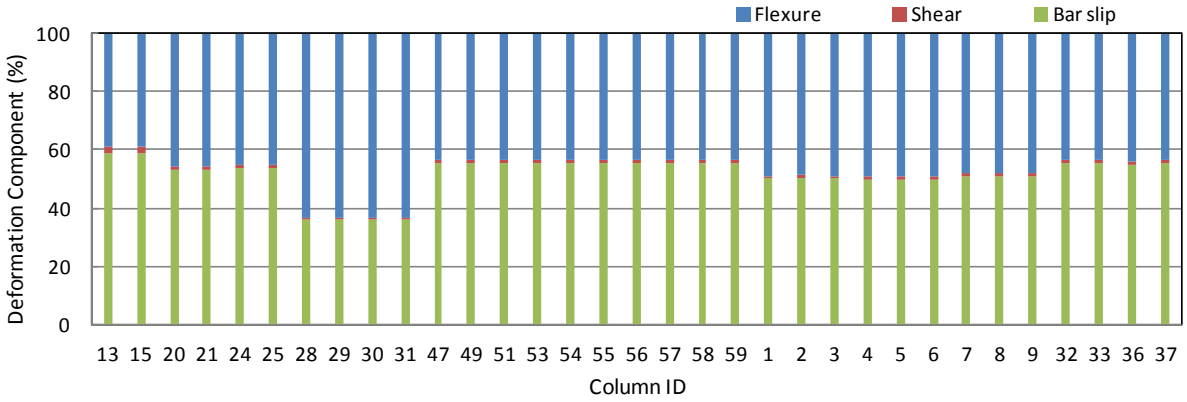

(a) Flexure-shear critical columns

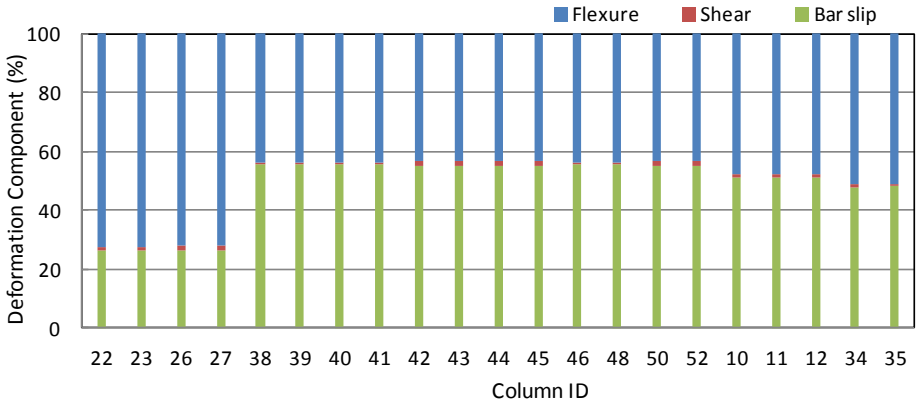

(b) Flexure critical columns

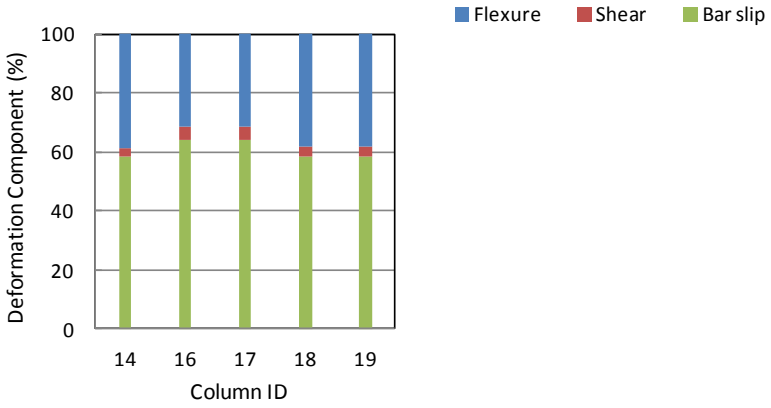

(c) Shear critical columns

Figure 3.13 Deformation components from three-component model

With the column yield drift calculated by three-component model, the column effective stiffness could be estimated by Equation 3.5.

$$EI_{ThreeComp} = \frac{2F_{0.004}a^3}{3\Delta_{y\_ThreeComp}} \qquad \text{Equation 3.5}$$

The ratio of measured column effective stiffness EI_{Meas} to calculated effective stiffness $EI_{ThreeComp}$ from Three-component model is plotted in Figure 3.14.

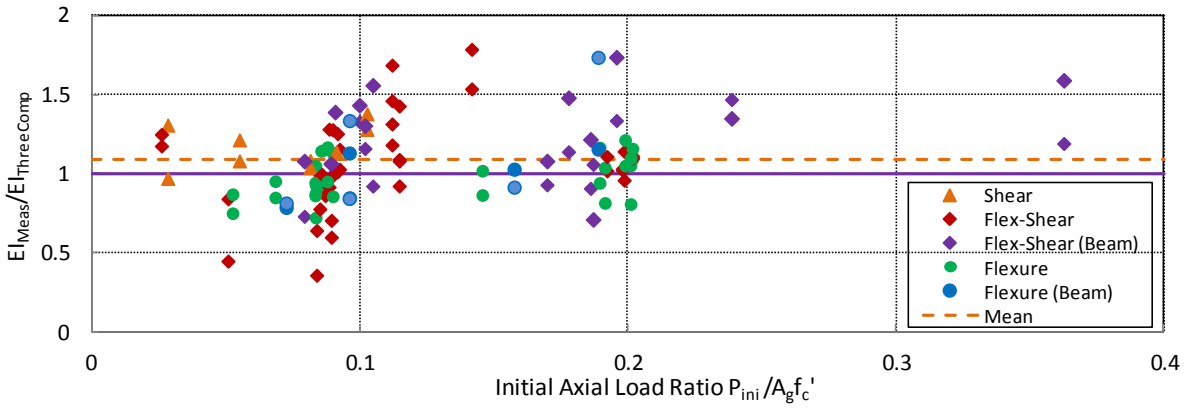

Figure 3.14 Evaluation of column effective stiffness estimated by three-component model

In order to facilitate engineers to estimate the column effective stiffness in preliminary design stage, Elwood and Eberhard (2009) recommended a simplified model to calculate the effective stiffness ratio based on the Three-component model.

$$0.2 \le \frac{EI_{SimpThreeComp}}{EI_g} = \frac{0.45 + 2.5P / A_g f_c^{'}}{1 + 110\left(\frac{d_b}{D}\right)\left(\frac{D}{a}\right)} \le 1.0 \qquad \text{Equation 3.6}$$

The calculated effective stiffness $EI_{SimpThreeComp}$ and the results of from three-component model, $EI_{ThreeComp}$, are compared in Figure 3.16. Results show that other than shear-critical columns in the database that had small aspect ratio a/d, effective stiffness $EI_{Simp-ThreeComp}$ tends to be slightly larger than $EI_{ThreeComp}$ from three-component model for most columns.

Since there is no significant difference between the calculated $EI_{ThreeComp}$ and $EI_{SimpThreeComp}$, it is appropriate to estimate column effective stiffness by applying the simplified three-component model in preliminary analysis.

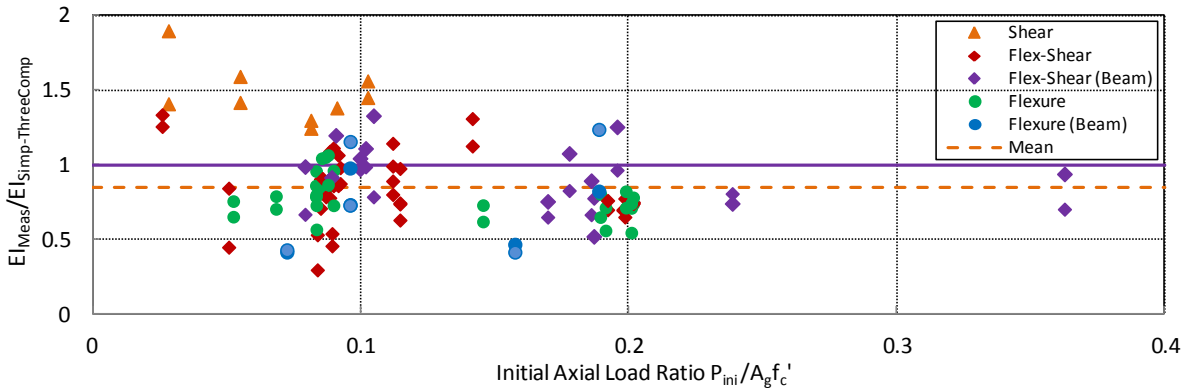

Figure 3.15 Evaluation of column effective stiffness estimated by simplified three-component model

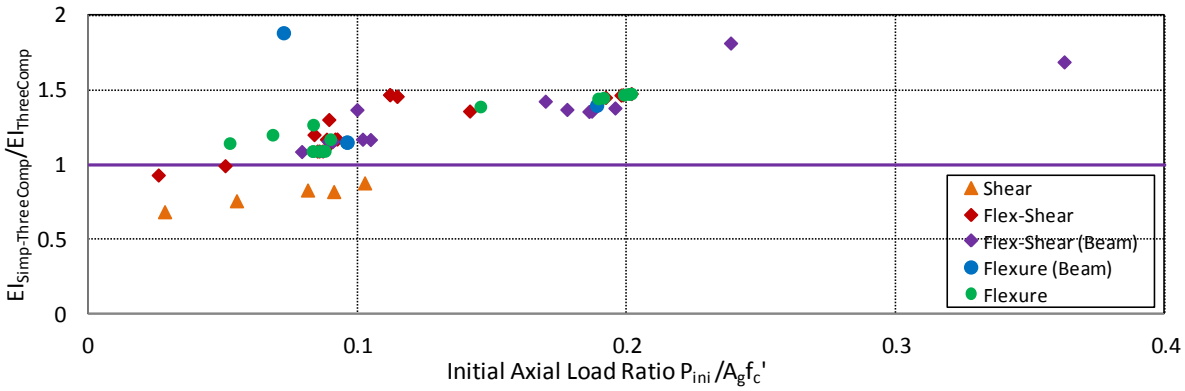

Figure 3.16 Comparison of effective stiffness from three-component model and simplified model

3.6 Comparison with the Static Cyclic Tests Data

While the ASCE/SEI 41 procedure tends to predict stiffer column initial response than that observed, both three-component model and its simplified version could either overestimate or underestimate the column effective stiffness. The calculated effective stiffness $EI_{ThreeComp}$ (discussed in section 3.5) is more likely to represent the mean value of the measured effective stiffness. Table 3.1 summarizes the statistical results of the effective stiffness models for columns included in The Database.

Table 3.1 Statistical results of column effective stiffness ratio for columns in The Database

	Min	Max	Mean	Median	Standard Deviation	COV (%)
(a) Flexure-critical columns						
EI_{TEST}/EI_{ASCE}	0.17	0.98	0.57	0.57	0.15	26.9
$EI_{TEST}/EI_{ThreeComp}$	0.36	1.74	0.97	0.95	0.22	22.6
$EI_{TEST}/EI_{SimpThreeComp}$	0.30	1.24	0.74	0.73	0.20	27.1
(b) Flexure -shear-critical columns						
EI_{TEST}/EI_{ASCE}	0.28	1.21	0.70	0.66	0.17	24.9
$EI_{TEST}/EI_{ThreeComp}$	0.45	1.79	1.15	1.10	0.26	22.4
$EI_{TEST}/EI_{SimpThreeComp}$	0.45	1.34	0.89	0.87	0.20	22.1
(c) Shear-critical columns						
EI_{TEST}/EI_{ASCE}	0.65	1.27	0.80	0.74	0.18	22.6
$EI_{TEST}/EI_{ThreeComp}$	0.97	2.19	1.27	1.18	0.35	27.4
$EI_{TEST}/EI_{SimpThreeComp}$	1.25	2.66	1.59	1.44	0.42	26.1

Elwood and Eberhard (2009) selected 221 rectangular columns from the PEER database and use the static cyclic test data for those columns to evaluate the aforementioned effective stiffness models. The main properties of the dataset compiled by Elwood and Eberhard (2009) are summarized in Table 3.2.

Table 3.2 Properties of the dataset in Elwood and Eberhard (2009)

Parameters	Symbol	Unit	Min	Max	Mean	Median
Aspect Ratio	a/d		1.5	7.6	3.6	3.2
Concrete compressive strength	$f_c^{'}$	*MPa*	21.0	118.0	52.3	36.5
Long. Rein. Yield Stress	f_{yl}	*MPa*	318	587	456	453
Long. Rein. Ratio	ρ_l		0.010	0.060	0.024	0.021
Ratio of depth of section to long. rein. diameter	D/d_b		12	32	18	16
Axial Load Ratio	$P/f_c^{'}A_g$		0.00	0.63	0.23	0.2
Normalized Shear stress	$v/\sqrt{f_c^{'}}$		0.09	0.71	0.32	0.3

Table 3.3 compared the evaluation of the effective stiffness models by the static cyclic test data and dynamic test data.

Table 3.3 Evaluation of column effective stiffness models with dynamic and static cyclic test data

	Min	Max	Mean	Median	COV (%)
(a) Columns in The Database					
EI_{TEST}/EI_{ASCE}	0.17	1.27	0.66	0.63	27.5
$EI_{TEST}/EI_{ThreeComp}$	0.36	2.19	1.09	1.07	24.8
$EI_{TEST}/EI_{SimpThreeComp}$	0.30	2.66	0.89	0.83	35.4
(b) Columns in the static cyclic test dataset					
EI_{TEST}/EI_{ASCE}	0.27	1.95	0.82	0.83	36.0
$EI_{TEST}/EI_{ThreeComp}$	0.45	1.84	0.97	0.92	26.6
$EI_{TEST}/EI_{SimpThreeComp}$	0.46	1.63	0.95	0.94	25.5

3.7 Effects of Number of Cycles

Figure 3.17 plots the number of cycles that columns go through before achieving 75% of maximum lateral effective force (the first yield point specified in TEST method discussed in section 3.2.4) with the measured column effective stiffness k_{eff} for some non-ductile columns included in The Database.

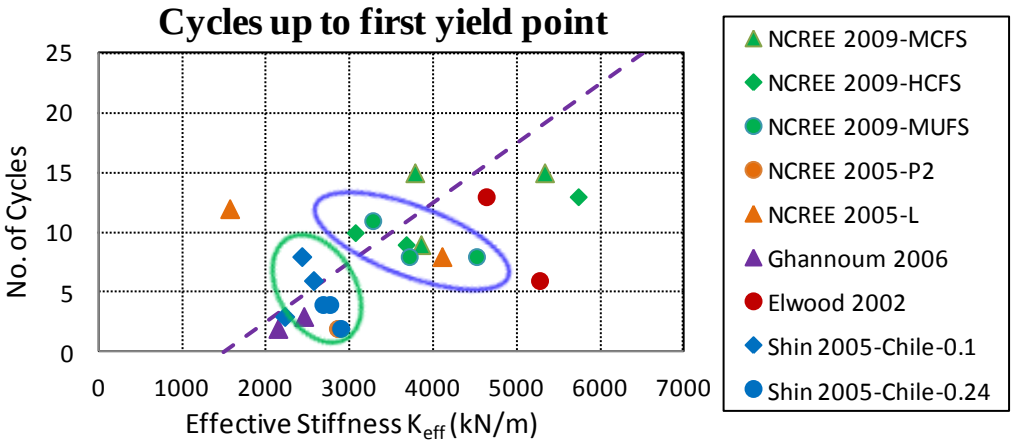

(a) Number of cycles with effective stiffness k_{eff}

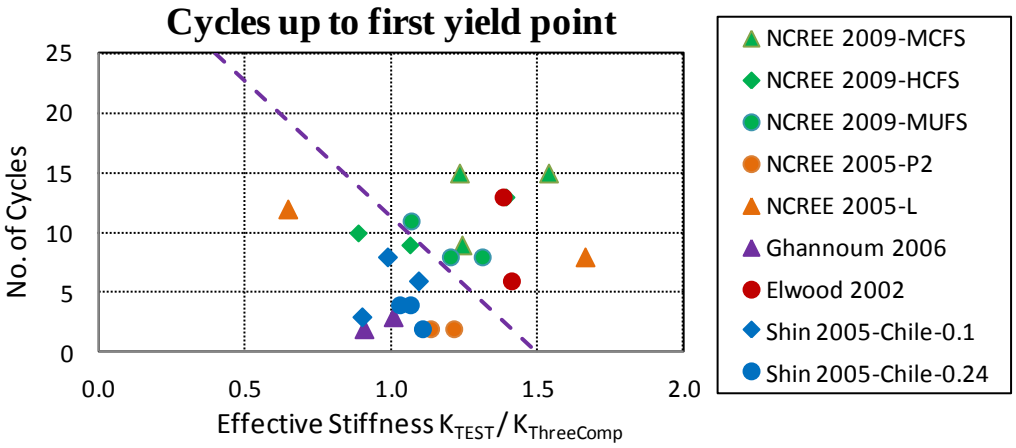

(b) Number of cycles with normalized effective stiffness k_{eff}

Figure 3.17 Number of cycles with column effective stiffness k_{eff}

It is observed from Figure 3.17 (a) that k_{eff} seems to increase slightly as number of the cycles increase. However it is not appropriate to compare the results for all the columns

together, since the lateral stiffness k_{eff} determined by the section properties and column length varied greatly for columns in different test programs.

If grouping the columns into different clusters as shown in Figure 3.17 (a) and only comparing the columns with similar properties experimental setups, the lateral stiffness k_{eff} increased slightly as columns went through less number of cycles for most columns. This negative trend between the lateral stiffness and number of cycles is understandable, since less reversed cycles in the initial stage indicates less flexural cracks and column damage, making the columns stiffer.

The negative correlation between the number of cycles and lateral column stiffness could be observed more obviously in Figure 3.17 (b), which plots the relations between the normalized effective stiffness ($k_{Meas} / k_{ThreeComp}$) and number of cycles up to the first yield point. Similar trend could be found in the relations between the number of cycles and effective stiffness ratio EI_{eff} / EI_g as shown in Figure 3.18.

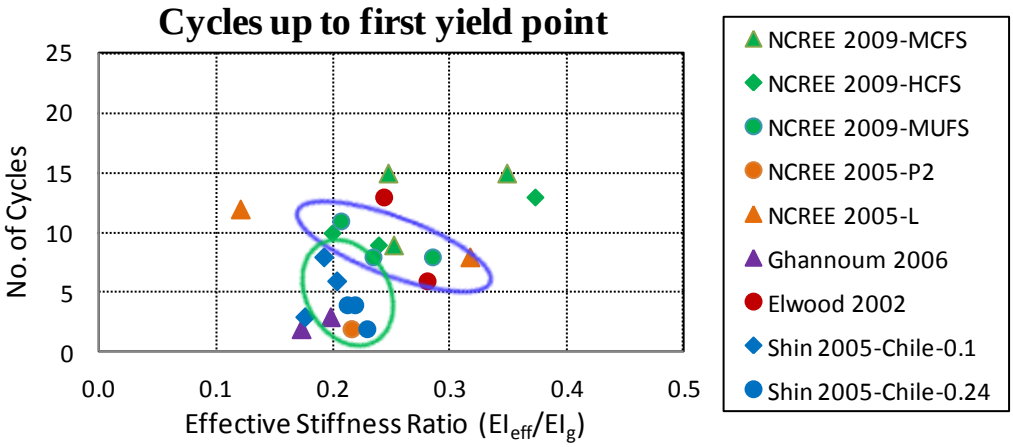

(a) Number of cycles with effective stiffness ratio EI_{eff}/EI_g

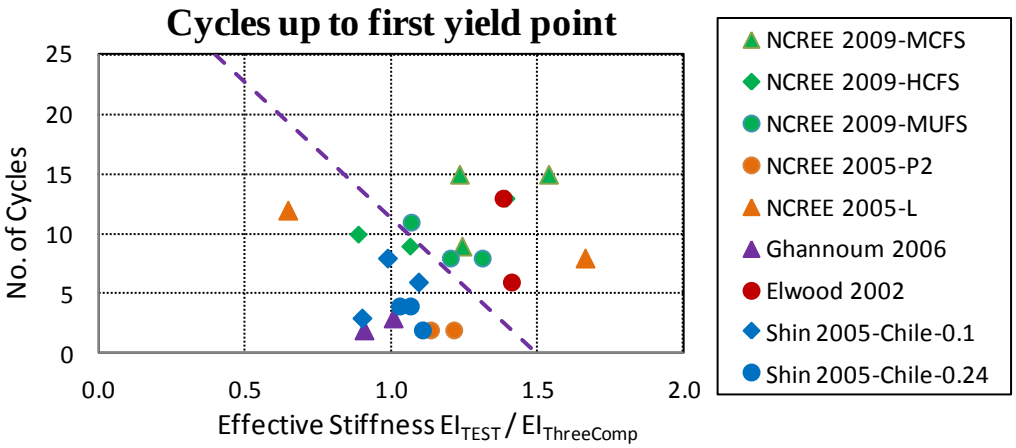

(a) Number of cycles with normalized effective stiffness ratio EI_{eff}/EI_g

Figure 3.18 Number of cycles with effective stiffness ratio EI_{eff}/EI_g

Chapter 4: Column Drift at Shear Failure

4.1 Definition of Column Drift at Shear Failure

Non-ductile columns with light transverse reinforcement are vulnerable to shear failure. As the shear damaged plane develops, the column could lose support for gravity load, leading to the collapse of the whole structure. Several models have been developed to estimate the column drift capacity at shear failure. In order to evaluate the performance of available models with The Database, measured drift at shear failure for each column needs to be interpreted in a consistent way. Based on the observations of column damage during the experiment and the lateral force-deformation (drift) data, there are generally three methods to define the column drift at shear failure:

- Drift at peak shear force. This method suggests that the shear failure occurred when column achieves the maximum shear force recorded during the experiments. Drift at peak shear force could be easily obtained from the data of shear force and horizontal inter-story drift and will be referred to as $(\delta_s)_{MaxV}$ (drift at Max V).
- Drift at peak effective force. According to this definition, column experienced shear failure when it achieved maximum lateral effective force. Effective lateral force could be obtained by correcting the P-delta effect of recorded shear-deformation relations. Drift at peak effective force is usually the same as or slightly higher than the drift at Max Shear and will be referred to as $(\delta_s)_{MaxVeff}$ (drift at Max V_{eff}).
- Drift at 80% peak effective force. This method defines that shear failure occurs when column losses 20% of its peak lateral force. The corresponding drift will be referred to as $(\delta_s)_{80\%MaxVeff}$ (drift at 80% Max V_{eff}). Most drift capacity models are developed

to provide estimations of the column drift at 80% Max V_{eff}. Compared with the column drift $(\delta_s)_{MaxVeff}$ that was very sensitive to the experimental conditions (input ground motion, column axial load ratio etc.), $(\delta_s)_{80\%MaxVeff}$ was more stable and better reflected the strength degradation as well as the drift capacity of columns. The drift obtained from this method is usually much larger than the drift from previous definitions, especially for flexure-critical and flexure-shear-critical columns.

Some columns may experience axial-load failure before loss of 20% peak lateral strength, for example the column C1 in NCREE 2009 Tests shown in Figure 4.1. In this case the $(\delta_s)_{80\%MaxVeff}$ will instead be taken as the maximum column drift achieved before axial-load failure.

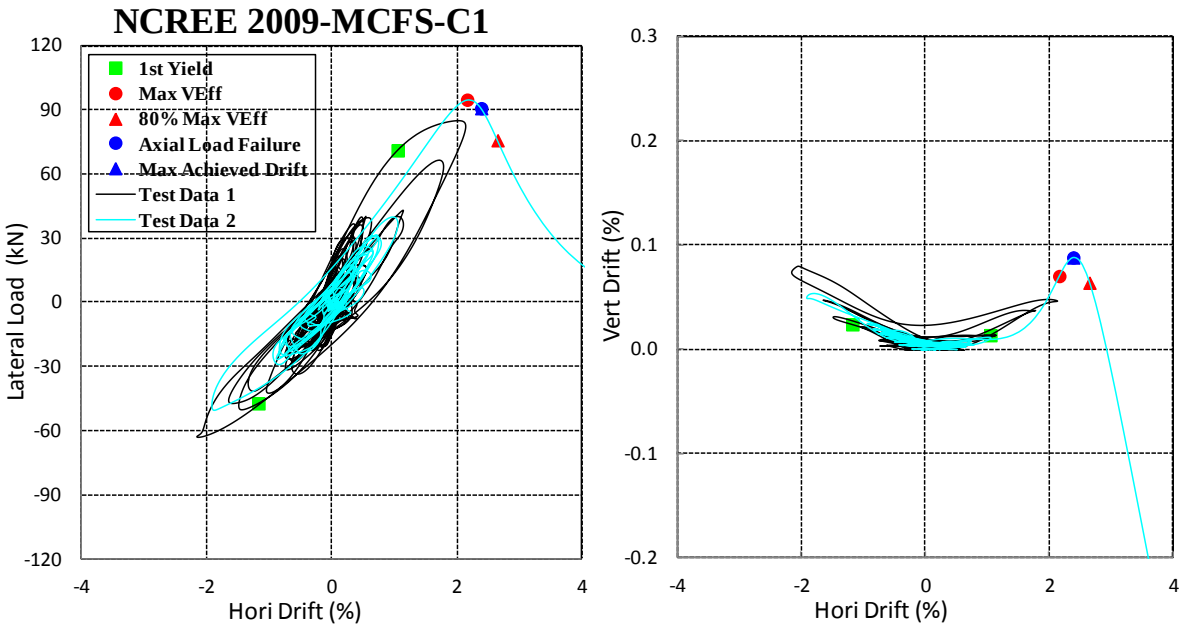

Note: The definition of the axial-load failure could be found in section 5.1.4

Figure 4.1 Axial-load failure occurred before 20% loss of its lateral load

4.2 Effect of key Parameters on Measured Drift at Shear Failure

The measured column drift $(\delta_s)_{MaxVeff}$ and $(\delta_s)_{80\%MaxVeff}$ for non-ductile columns are plotted with key parameters in Figure 4.2 and Figure 4.3 respectively.

The column plastic drift at 80% Max V_{eff} with key parameters are plotted in Figure 4.4. The column plastic drift could be obtained by subtracting the yield drift measured during the tests δ_y (obtained from TEST method in section 3.2.5) from the $(\delta_s)_{80\%MaxVeff}$. The key parameters considered include: (a) maximum normalized shear stress $v/\sqrt{f_c'}$; (b) maximum axial load ratio $P_{max}/A_g f_c'$, where P_{max} is the initial axial load that column is subjected to, A_g is the area of column gross section; (c) transverse reinforcement ratio ρ_t; (d) transverse reinforcement indicator $\rho_t f_{yt} / f_c'$; (e) ratio of transverse reinforcement spacing to depth s/d, where s is spacing of transverse reinforcement, d is effective depth of column cross-section; (f) aspect ratio a/d, where a is column shear span and could be taken as half of column clear height L.

The measured column drift $(\delta_s)_{MaxVeff}$ and $(\delta_s)_{80\%MaxVeff}$ are plotted with key dynamic parameters in Figure 4.5. The dynamic parameters considered include:

(a) the number of cycles that the column went through and the method to count the cycles could be found in section 2.6.1;

(b) the relative strength factor $R = S(a) \cdot W/V_y$, where $S_a(T_1)$ = pseudo acceleration for the fundamental structural period T_1 calculated from the response spectrum (g), the data of the fundamental period T_1 are available for most test frames in The Database; W = the weight of structure and could be calculated by adding the initial axial load of all columns in the

frame and V_y = the yield strength of the specimen and could be calculated by adding the plastic shear demand of all columns.

(c) the bracket duration of input ground motions t_b (sec), defined as time between when the input motion exceeds the certain acceleration threshold for the first and last time. The acceleration threshold is selected as $0.1g$ in this research.

The parameter bracket duration t_b represents one of the main characteristics of the input motions. The number of cycles and relative strength factor R describes the interactions of the structures and input motions, which are unique in dynamic tests.

In this chapter, the test data is grouped by the column failure type classified by ASCE/SEI 41 (discussed in section 6.3). The data series "Shear" (corresponding to the Condition iii in ASCE/SEI 41) in green triangular marker represents the shear critical columns included in The Database. The data series "Flex-Shear" (corresponding to the Condition ii in ASCE/SEI 41) in red diamond marker represents the flexure-shear critical columns that were connected to a rigid beam on the upper end. The data series "Flex-Shear (Beam)" in purple diamond marker represents the flexure-shear-critical columns in the frame connected with flexure beam on the upper end and the data of measured drift may be higher than the actual column drift capacity due to the additional flexibility contributed by the beam. The "Flex-Shear (Lower)" in hollow red diamond marker represents the flexure-shear critical columns that did not fail during the tests and the drift data could be considered as the lower bound of the column drift capacity. The "Flex-Shear (Flex)" in blue diamond marker represents the columns that experienced flexure failure during the test, yet were misclassified by ASCE/SEI 41 as flexure-shear-critical columns.

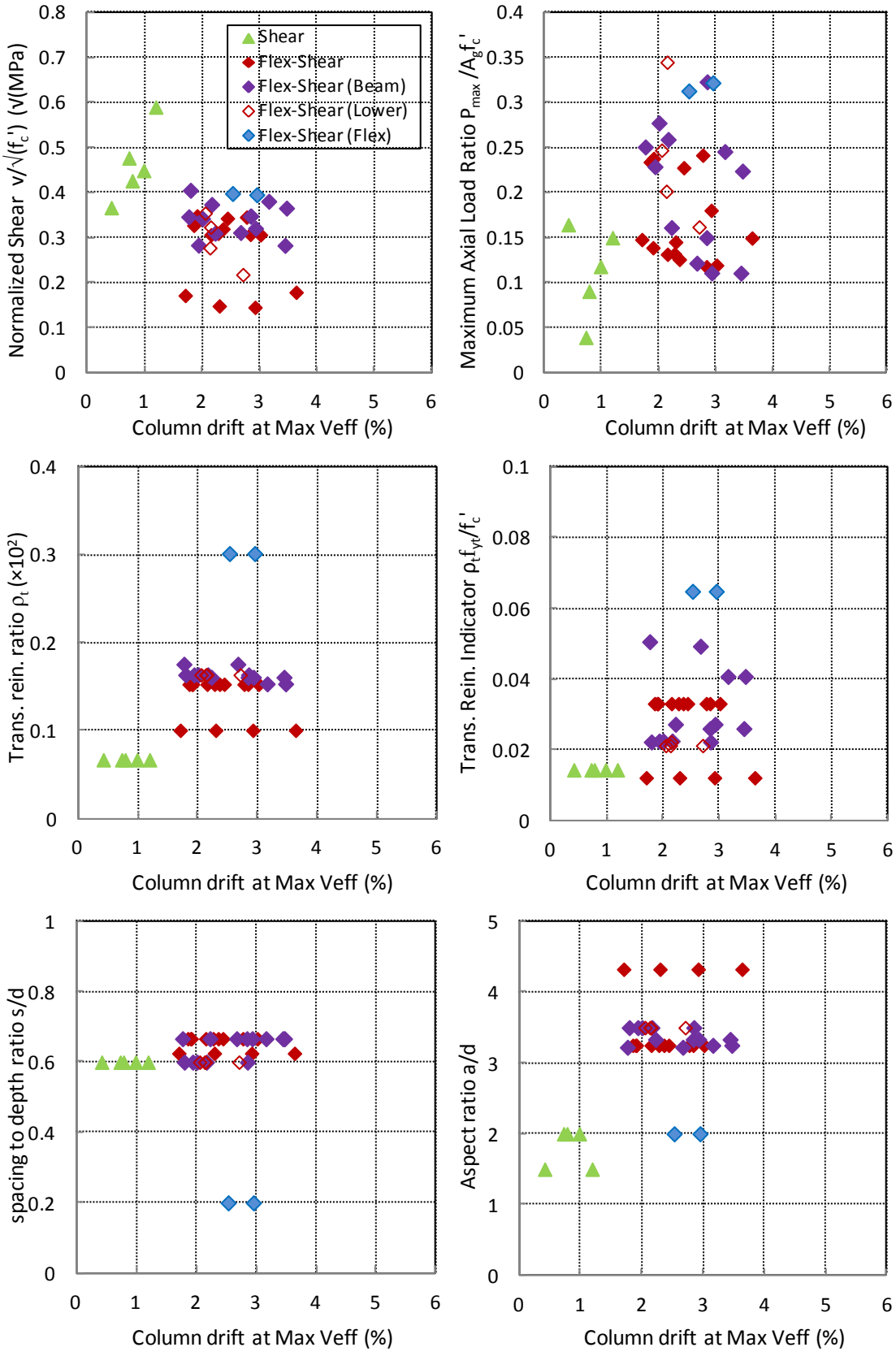

Figure 4.2 Measure column drift at Max V_{eff} with key parameters

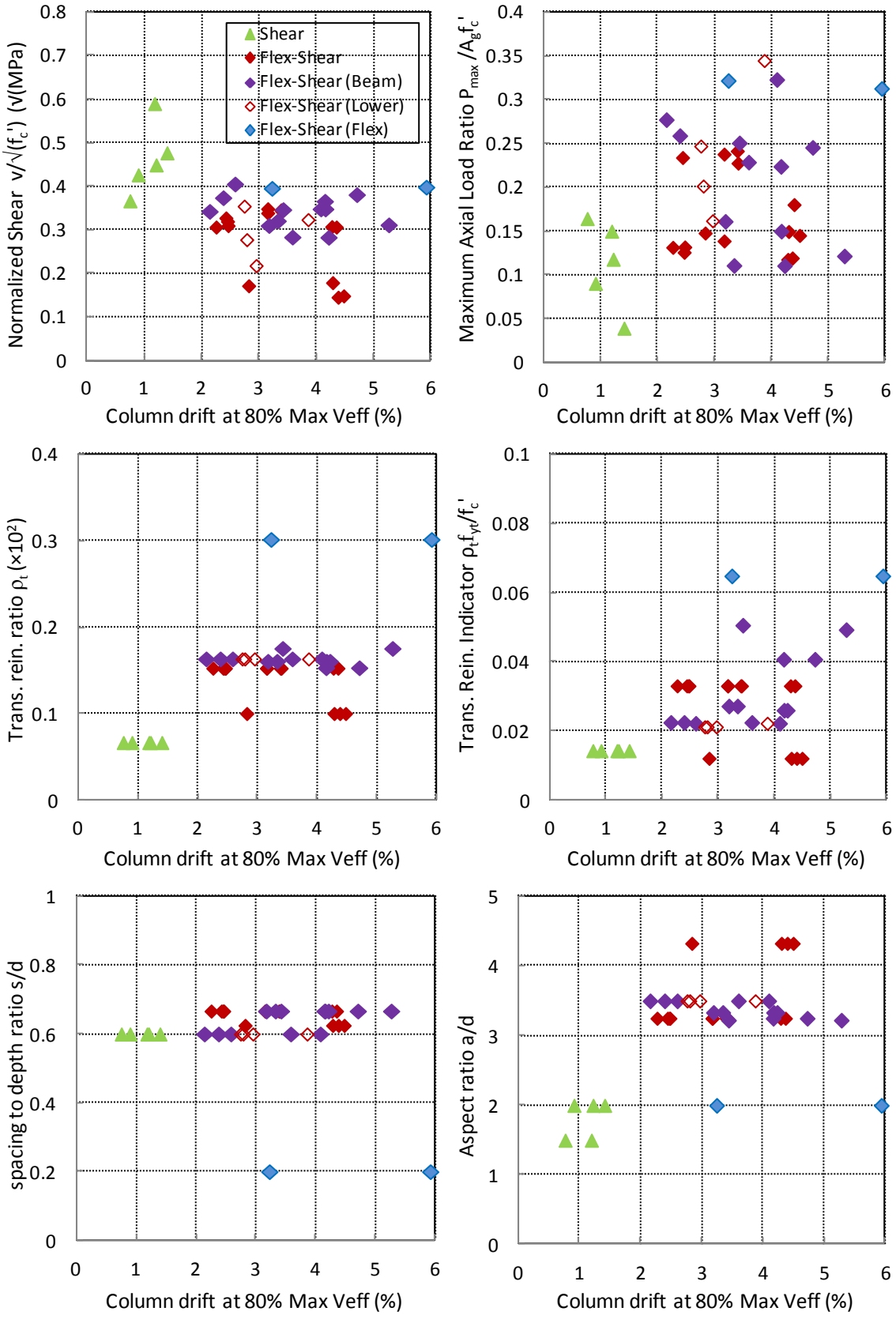

Figure 4.3 Measured column drift at 80% Max V_{eff} with key parameters

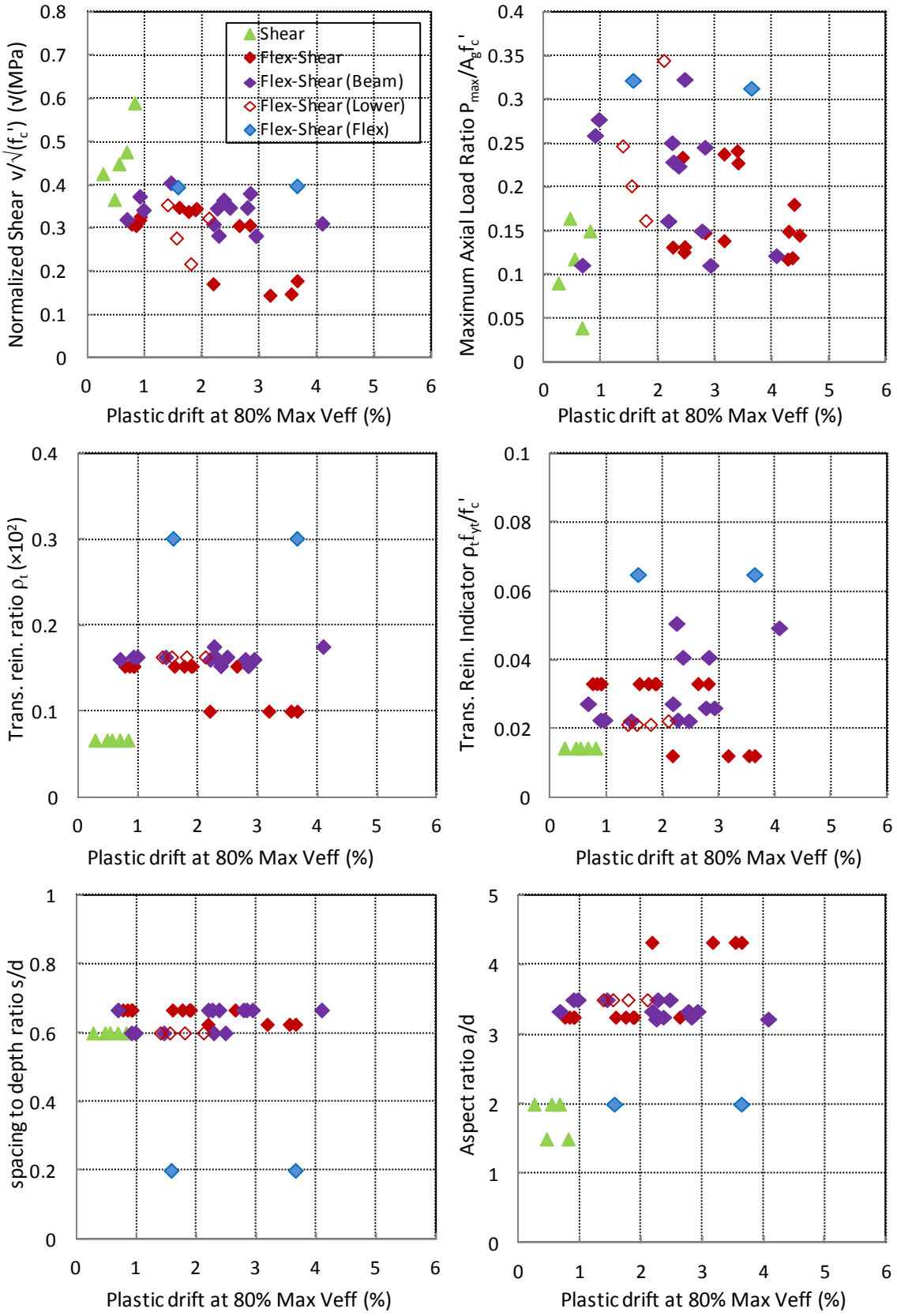

Figure 4.4 Measured column plastic drift at 80% Max V_{eff} with key parameters

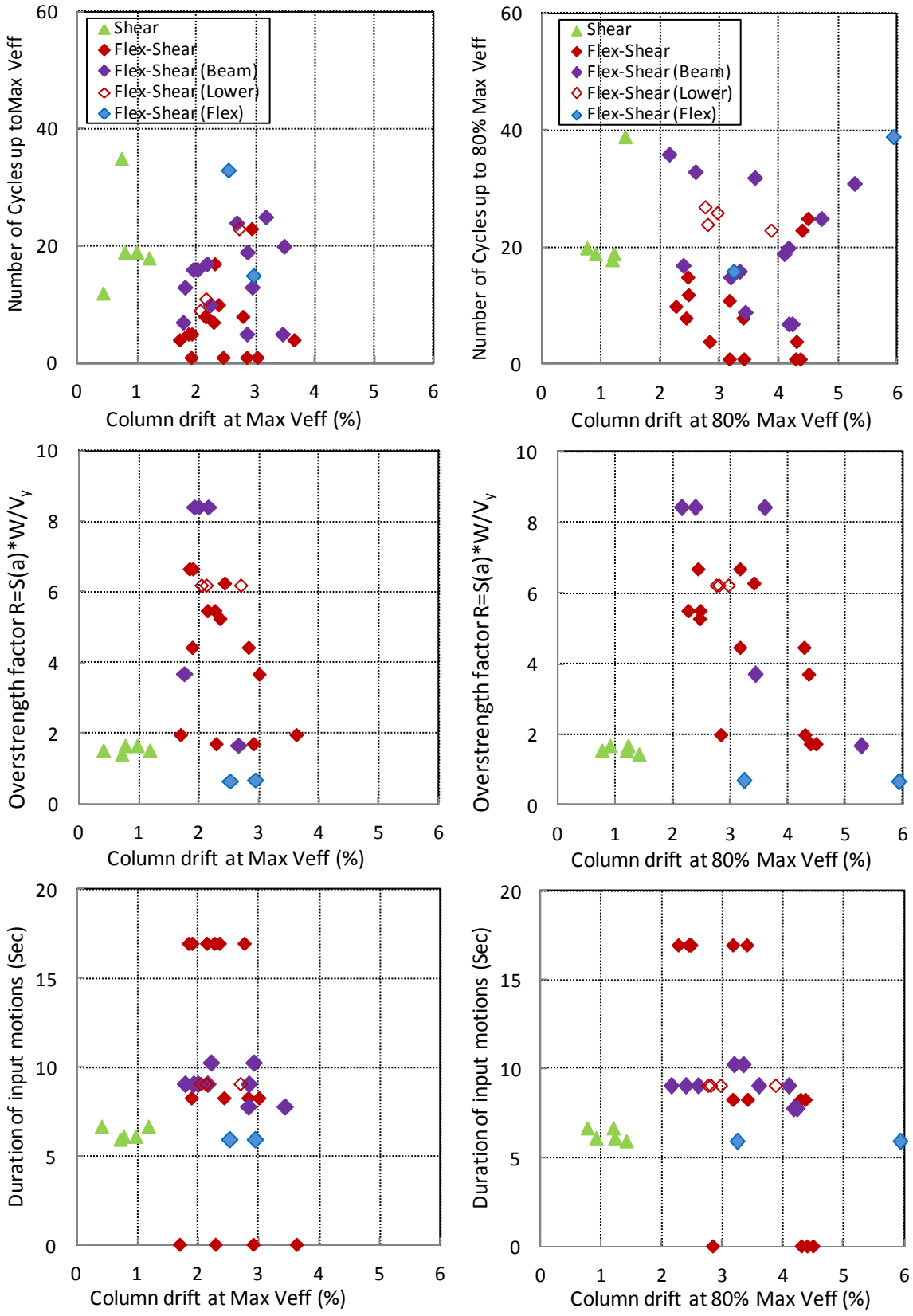

Figure 4.5 Measured column drift with key dynamic parameters

Figure 4.2 and Figure 4.3 show that column drifts at Max V_{eff} and 80% Max V_{eff} are inversely correlated with the maximum axial load ratio. The column drifts also seem to decrease with increasing transverse reinforcement indicator. Other parameters are not strongly related to the column drifts at shear failure.

Since several columns included in The Database had very similar column detailing and experimental setups, the column drift data at shear failure is "banded" at certain parameters, such as transverse reinforcement ratio ρ_t and aspect ratio a/d. Therefore the column data from The Database could be used to evaluate the available drift capacity models, but one must be cautious in developing new models based on this limited data set.

Results in Figure 4.2 show that column drifts at shear failure, especially the 80% Max V_{eff}, tends to decrease with increasing relative strength factor R and more number of cycles. The longer duration of the input motions t_b also slightly decrease the column drift, yet the trend is not very obvious and the data is pretty "banded" (the columns in the same frame have same t_b but different column drift at shear failure).

None of the three dynamic parameters seems to be directly related to column drift at Max V_{eff}, suggesting more randomness and uncertainties are existed and it is better to use column drift at 80% Max V_{eff} as the indicator of the column shear failure.

4.3 Evaluation of Pujol et al. (1999) Model

4.3.1 Procedure

Based on test data of 92 columns in 15 cyclic test series, Pujol et al. (1999) observed that the ratio of maximum column drift at shear failure to the column aspect ratio a/d

tended to be positively correlated with transverse reinforcement index $\rho_t f_{yt} / v$. An empirical model was proposed to provide conservative estimate of the maximum column drift at shear failure by Equation 4.1.

$$(\delta_s)_{Max} = \frac{1}{100} \frac{\rho_t f_{yt}}{v} \frac{a}{d} \leq \begin{Bmatrix} \frac{a}{d} \\ 4 \end{Bmatrix} \qquad \text{Equation 4.1}$$

Where ρ_t = transverse reinforcement ratio; f_{yt} = yield stress of transverse reinforcement (MPa); a = column shear span and for columns have fixed-fixed end conditions, a could be calculated as half of column clear height ($a = L/2$); d = effective depth of column section and could be taken as 80% of column depth D; v = maximum shear stress (MPa).

The properties of the database used by Pujol et al. (1999) could be found in Table 4.1.

Table 4.1 Properties of column database in Pujol et al. (1999)

Parameters	Symbol	Unit	Max	Min
Aspect Ratio	a / d		5	1.3
Concrete compressive strength	$f_c^{'}$	MPa	86.2	20.7
Long. Rein. Ratio	ρ_l		0.005	0.0051
Trans. Rein. Ratio	ρ_t		0.0164	0.0
Axial Load Ratio	$P/f_c^{'}A_g$		0.2	0.0
Maximum shear stress	$v/\sqrt{f_c^{'}}$	$\sqrt{MPa}$	N.A.	0.167

4.3.2 Evaluation with The Database

According to Pujol et al. (1999) model, the column drift at shear failure is inversely related to the column shear stress v. For non-ductile columns vulnerable to shear failure, the calculated shear strength and the measured maximum lateral force should be ideally same.

Yet in fact the shear strength V_0' calculated by ASCE/SEI 41 model (introduced in section 6.2.3) could either underestimate or overestimate the column shear strength. Both the calculated shear strength V_0' and the measured maximum effective force V_{Max} are considered in the assessment of the Pujol et al. (1999) model. The calculated column drift is plotted with the measured column drift $(\delta_s)_{MaxVeff}$ and $(\delta_s)_{80\%MaxVeff}$ in Figure 4.7 and Figure 4.6 respectively, with (a) calculated column drift based on shear strength V_0' from ASCE/SEI 41; (b) calculated drift based on maximum effective force V_{Max}.

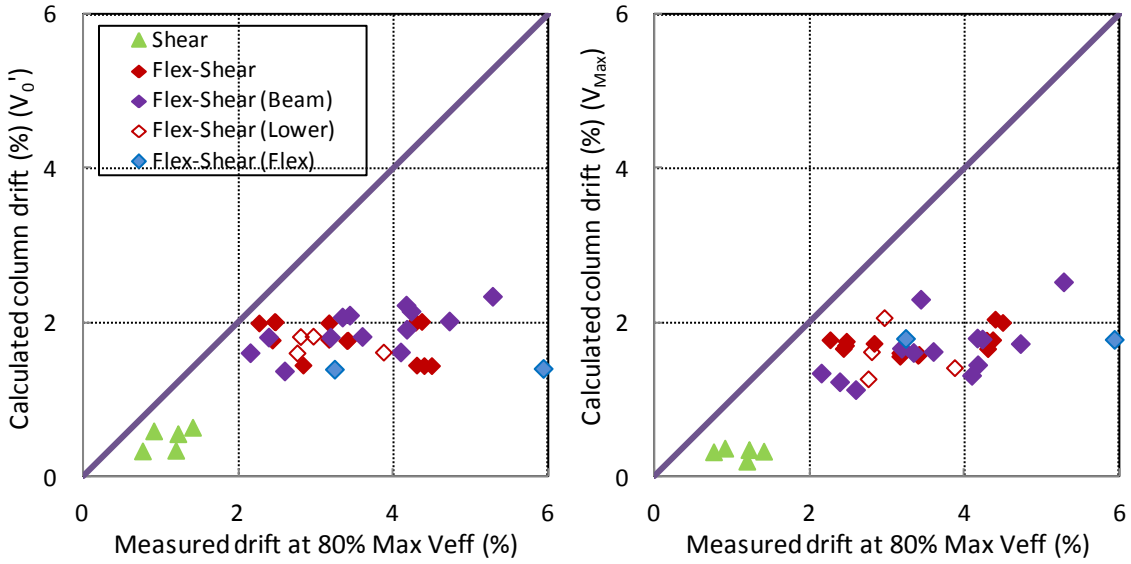

(a) Based on shear strength V_0' (b) Based on maximum effective force V_{Max}.

Figure 4.6 Calculated drift by Pujol et al. (1999) model with measured drift at 80% Max V_{eff}

Results in Figure 4.6 are consistent with the intent of the model to provide conservative estimate of "the maximum column drift at shear failure", since the measured drift at 80% Max V_{eff} exceeded the calculated drift capacity based on either V_0' or V_{Max} for all non-ductile columns in The Database.

As shown in Figure 4.7, Pujol et al. (1999) model also underestimate the column drift at Max V_{eff} for most of the columns.

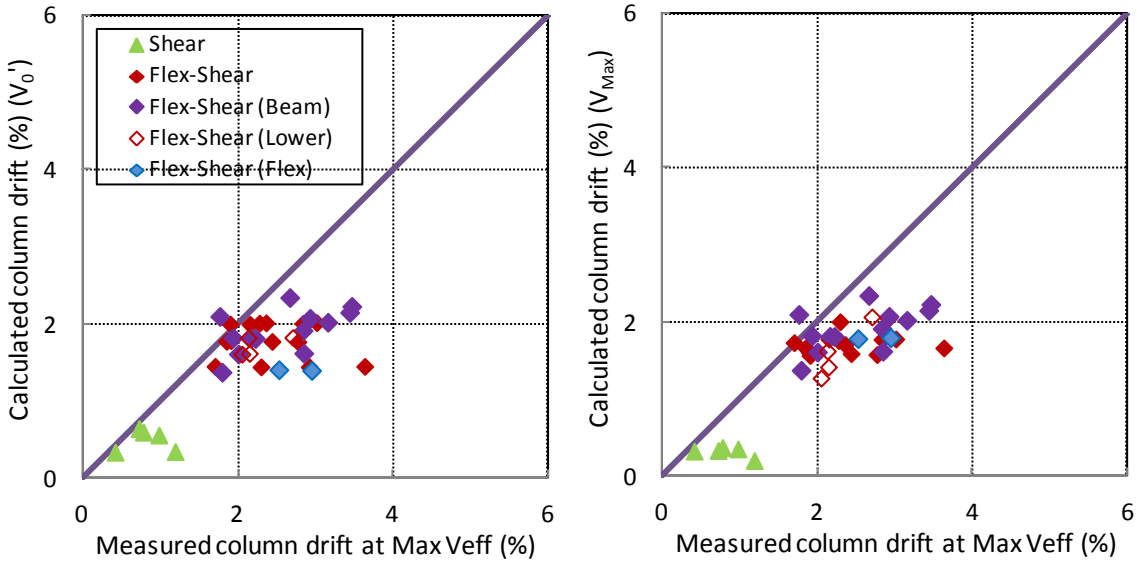

(a) Based on shear strength V_0'

(b) Based on maximum effective force V_{Max}

Figure 4.7 Calculated drift by Pujol et al. (1999) with measured drift at Max V_{eff}

Figure 4.8 plots the ratio ($(\delta_s)_{80\%MaxVeff} / \delta_{Cal}$) of measured drift at 80% Max V_{eff} to the calculated column drifts. The horizontal line "Mean" shows the mean value of the data for flexure-shear-critical columns.

It is observed that Pujol et al. (1999) model underestimated column drift capacity for flexure-shear-critical columns and tended to be more conservative for shear-critical columns with low aspect ratio. The statistical results of the evaluation are reported in Table 4.2.

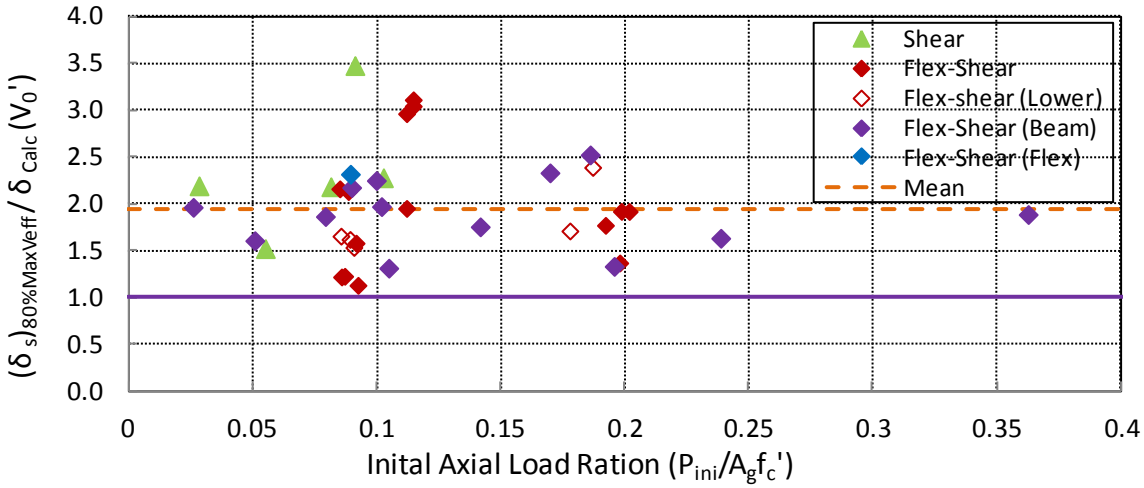

(a) The ratio of measured drift at 80% Max V_{eff} to calculated drift with V_0'

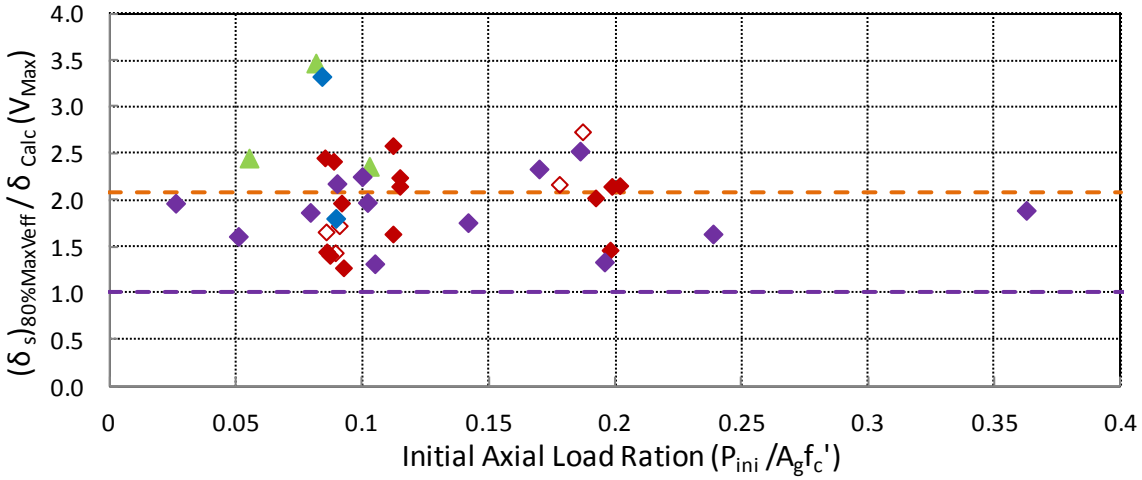

(b) The ratio of measured drift at 80% Max V_{eff} to calculated drift with V_{Max}

Figure 4.8 Evaluation of Pujol et al. (1999) model

Figure 4.8(b) ignores the test data for shear-critical columns NCREE 2007-S1-C2 and NCREE 2007-S3-C1, which had exceptional high ratio $(\delta_s)_{80\%MaxVeff} / \delta_{Cal}$ equal to 4.25 and 5.94 respectively. The measured maximum lateral force V_{Max} is almost two times of the calculated shear strength V_0' for those two columns as shown in Figure 6.4. Thus the calculated column drift δ_{Cal} based on V_{Meas} was significantly lower than the measured column drift and resulted in rather high ratio of $(\delta_s)_{80\%MaxVeff} / \delta_{Cal}$.

Table 4.2 Statistical results of Pujol et al. (1999) model

	Min	Max	Mean	Median	Standard Deviation	COV (%)
$(\delta_s)_{80\%MaxVeff}$ / δ_{Cal} (V_0')	1.13	3.12	1.93	1.92	0.54	27.8
$(\delta_s)_{80\%MaxVeff}$ / δ_{Cal} (V_{Max})	1.27	3.11	2.09	2.15	0.46	22.2
$(\delta_s)_{MaxVeff}$ / δ_{Cal} (V_0')	0.84	2.51	1.37	1.31	0.35	25.7
$(\delta_s)_{MaxVeff}$ / δ_{Cal} (V_{Max})	0.76	2.19	1.50	1.49	0.37	24.8

4.3.3 Comparison with the Evaluation with Sezen (2002) Database

In Elwood and Moehle (2003), Pujol et al. (1999) model was evaluated with the cyclic test data of columns included Sezen (2002) database. Figure 4.9 plots the calculated drift at 80% Max V_{eff} by Pujol et al. (1999) model for (a) columns in the Database, (b) columns included in Sezen (2002) database.

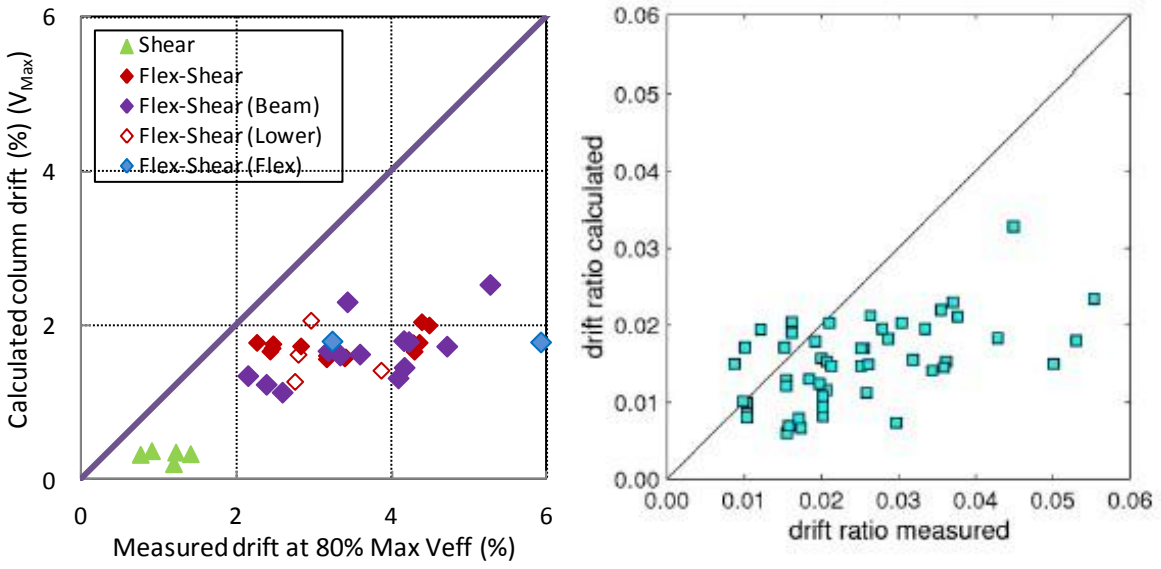

(a) Columns in the Database (b) Columns in Sezen (2002) database

Figure 4.9 Evaluation of Pujol et al. (1999) model with columns in The Database and Sezen (2002) database

While overestimating the drift capacity for six columns in Sezen (2002) database, Pujol et al. (1999) provided conservative estimate of the drift capacity at 80% Max V_{eff} for all the columns subjected to the dynamic tests.

The mean value and coefficient of variation of $(\delta_s)_{80\%MaxVeff} / \delta_{Calc}$ for columns in Sezen (2002) database are 1.71 and 42%. The mean value of ratio $(\delta_s)_{80\%MaxVeff} / \delta_{Calc}$ for columns in The Database was higher (2.09), suggesting that the dynamic nature of the shaking table tests could have resulted in an increased the measured column drift at shear failure. There was also less variability in the dynamic test data, with coefficient of variation less than 30%.

4.4 Evaluation of Kato and Ohnishi (2002) Model

4.4.1 Procedure

Kato and Ohnishi (2002) proposed a model to calculate the column plastic drift at loss of 20% peak lateral force by taking into account the maximum edge strain in concrete core and axial load ratio. The total drift at 80% Max V_{eff} could be estimated by summing drift at column yielding (Δ_y / L) and the calculated plastic drift (Δ_P / L) shown in Equation 4.2.

$$\frac{\Delta_s}{L} = \frac{\Delta_y}{L} + \frac{\Delta_P}{L}$$

$$\frac{\Delta_P}{L} = \begin{Bmatrix} D\left(\frac{m\varepsilon_{cp}}{j_e}\right)\left(\frac{2}{3e_n}\right) \leftarrow \left(0 < e_n < 1/3\right) \\ D\left(\frac{m\varepsilon_{cp}}{j_e}\right)\left(\frac{2}{3\left(5e_n - \frac{4}{3}\right)}\right) \leftarrow \left(1/3 \le e_n < 2/3\right) \end{Bmatrix} \quad \text{Equation 4.2}$$

Where ε_{cp} =maximum edge strain in the core concrete. For non-ductile columns with large-spaced transverse reinforcement in the Database, the concrete core was considered to be unconfined and thus set ε_{cp} equal to 0.002; e_n =equivalent axial load ratio; D =depth of column cross-section; j_e =depth of concrete core and shall be taken as the distance between the tension and compression reinforcement.

m = coefficient selected to achieve good agreement between the proposed model and the test dada. Based on the data of 36 columns subjected to cyclic pseudo-static tests, Kato and Ohnishi (2002) recommended $m = 2.4$ for estimating column drift at shear failure.

e_n = equivalent axial load ratio could be found in Figure 4.10 or calculated by Equation 4.3:

$$e_n = \begin{cases} \eta_p \leftarrow 0 < \eta_p \le 1/3 \\ \eta_p/5 + 4/15 - \eta_s\,(>0.33) \leftarrow 1/3 < \eta_p < 2/3(1+\gamma) \\ (3+2\gamma)/5 \cdot \eta_p - \eta_s\,(>0.33) \leftarrow 2/3(1+\gamma) \le \eta_p \le 2/3 \end{cases} \qquad \text{Equation 4.3}$$

$$\eta_s = A_s \sigma_y / (j_e \cdot j_e \cdot \sigma_s)$$

where γ =min. axial load/max. axial load; η_p =maximum axial load ratio, $P_{Max}/A_g f_c^{'}$; A_s =area of longitudinal reinforcement located at the center of the section; σ_y =yield stress of longitudinal reinforcement; σ_s = stress of longitudinal reinforcement.

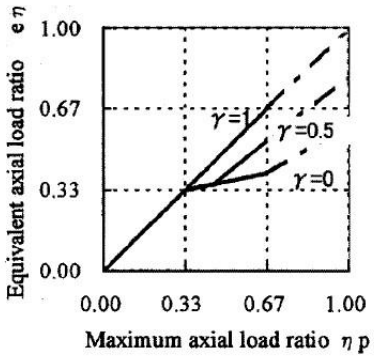

Source: Ghannoum (2007)

Figure 4.10 Equivalent axial load ratio from Kato and Ohnishi (2002) Model

From the Figure 4.10, we can see that for columns subjected to low axial load ratio (less than 0.33), e_n equals to the maximum axial load ratio.

4.4.2 Evaluation with The Database

The calculated column drift at shear failure are compared with the measured drift at 80% Max V_{eff} in Figure 4.11, with (a) calculated column drift based on the measured yield drift δ_y; (b) calculated column drift based on the yield drift $\delta_{y-ThreeComp}$ calculated from three-component model (introduced in section 3.5).

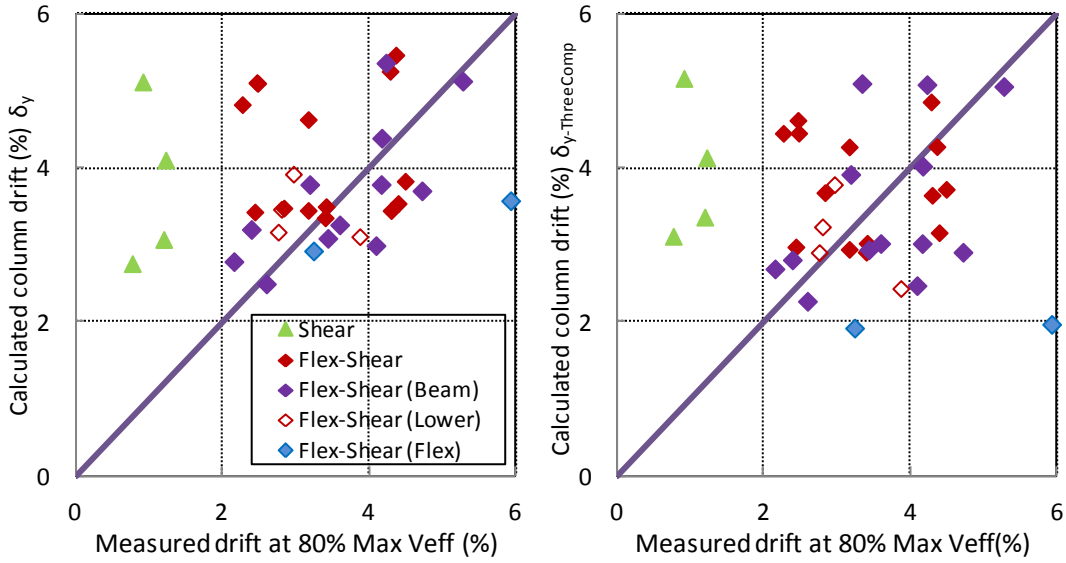

(a) Based on the measured yield drift δ_y (b) Based on the yield drift $\delta_{y-ThreeComp}$

Figure 4.11 Calculated column drift at 80% Max Veff by Kato and Ohnishi (2002) model

There is large scatter existing in the calculated column drift by Kato and Ohnishi (2002) model, especially when applying calculated yield drift from three-components model.

The ratio of measured drift at Max V_{eff} to calculated column drift by Kato and Ohnishi (2002) model is plotted in Figure 4.12. The horizontal line "Mean" shows the mean value of the data for flexure-shear-critical columns.

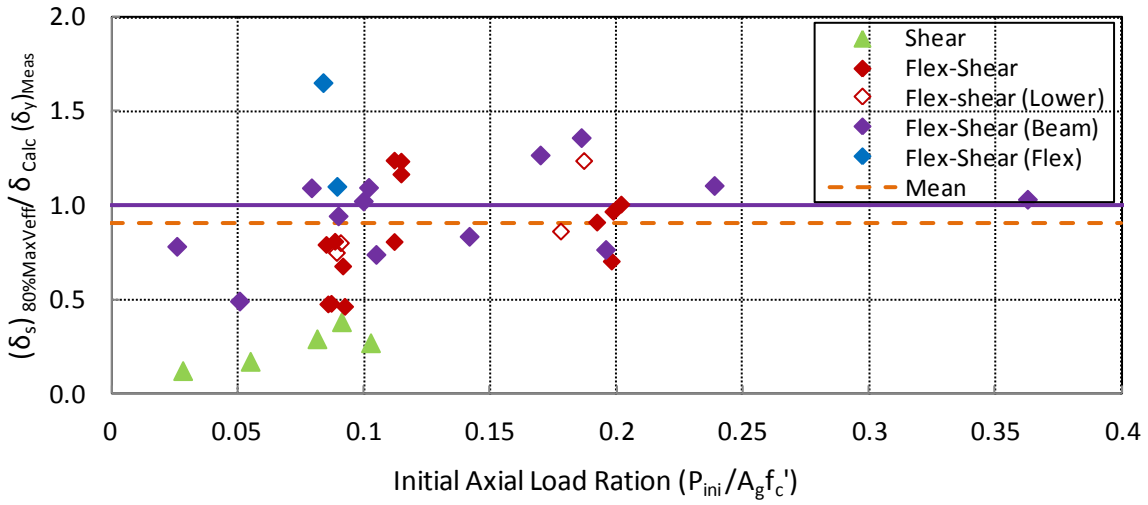

(a) The ratio of measured drift to calculated drift with measured yield drift

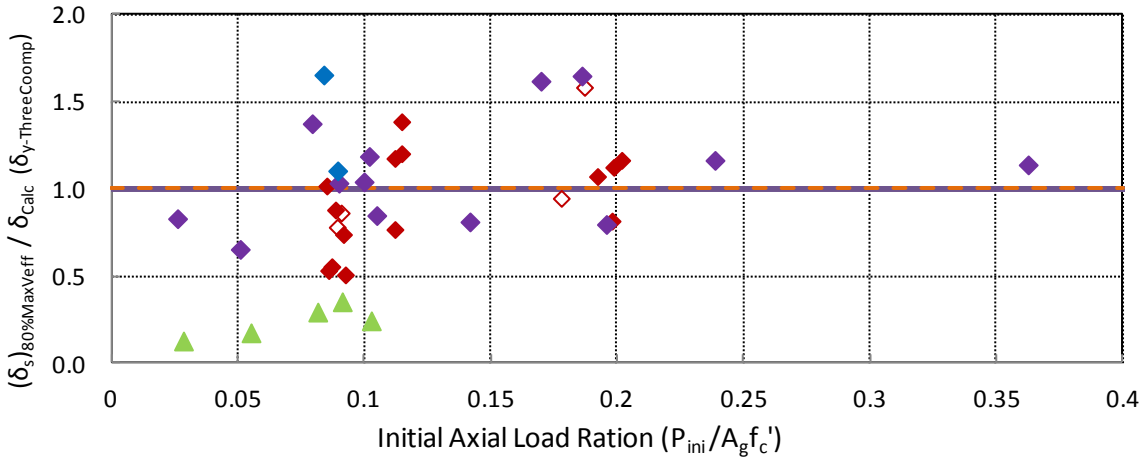

(b) The ratio of measured drift to calculated drift with yield drift from three-component model

Figure 4.12 Evaluation of Kato and Ohnishi (2002) model

Results in Figure 4.12 show that Kato and Ohnishi (2002) model could either underestimate or overestimate the column drift at 80% Max V_{eff} and seems to represent the mean value of the test results. The model is developed to estimate the column drift for flexure-shear-critical columns and turned out to be very unconservative for shear-critical columns.

The statistical results of ratio $(\delta_s)_{80\%MaxVeff} / \delta_{Calc}$ for Kato and Ohnishi (2002) model for flexure-shear-critical columns are summarized in Table 4.3.

Table 4.3 Statistical results of Kato and Ohnishi (2002) model

	Min	Max	Mean	Median	Standard Deviation	COV (%)
$(\delta_s)_{80\%MaxVeff}$ / δ_{Calc} (δ_y)	0.28	1.36	0.88	0.92	0.28	31.9
$(\delta_s)_{80\%MaxVeff}$ / δ_{Calc} ($\delta_{y\text{-}ThreeComp}$)	0.31	1.65	0.98	1.03	0.33	33.6

4.4.3 Comparison with the Evaluation with Sezen (2002) Database

The accuracy of the Kato and Ohnishi (2002) model largely depends on the accuracy of estimated column yield drift. To avoid introducing additional uncertainties and errors, the calculated drift at shear failure was based on the measured yield drift when evaluating the model with the Sezen (2002) database. Results are plotted in Figure 4.13 for (a) columns in the Database (with calculated drift based on measured yield drift δ_y), and (b) columns included in Sezen (2002) database. The shaded data points in Figure 4.13 (b) denoted the column with high axial load ratio ($P/A_g f_c^{'} \leq 0.25$).

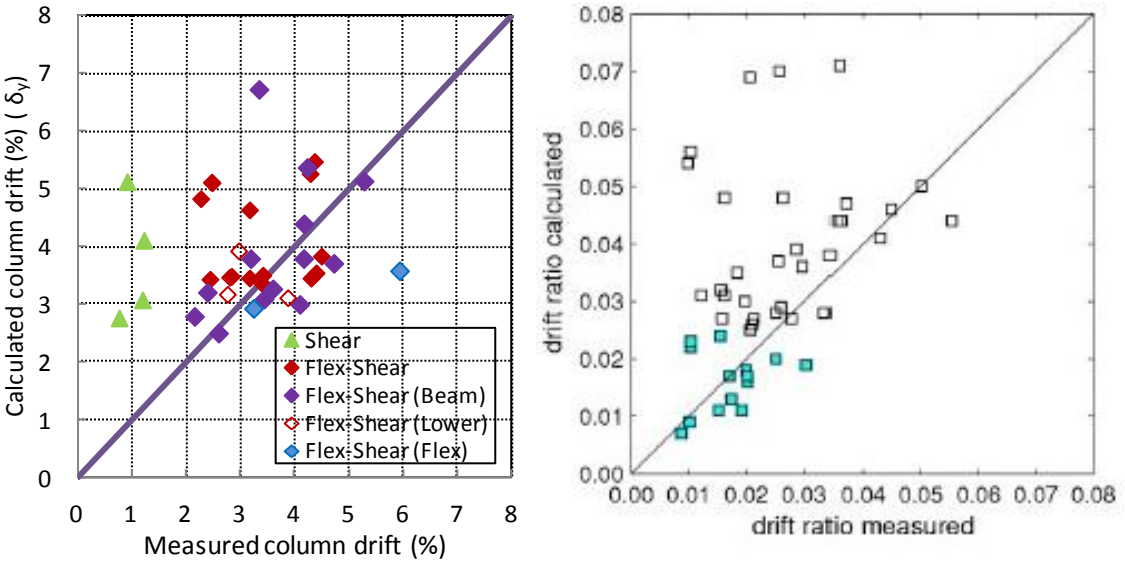

(a) Columns in The Database (b) Columns in Sezen (2002) database

Figure 4.13 Evaluation of Kato and Ohnishi (2002) model with dynamic and cyclic test data

Compared with the columns in Sezen (2002) database, the data of columns subjected to seismic load seems to be shifted closer to the unit line, indicating that the model was less unconservative for most columns. However, it is noticed that most data beneath the unit line in Figure 4.13 (a) belong to the columns connected with flexible beam (in purple diamond markers). The actual column drift capacity might be lower than the measured drift for those columns and data points may as well scattered in the upper triangular area of the plot similar to that in Figure 4.13 (b).

The ratio of $(\delta_s)_{80\%MaxVeff} / \delta_{Calc}$ had slightly lower mean value and higher coefficient of variation (equal to 0.84 and 44% respectively) for columns in Sezen (2002) database.

4.5 Evaluation of Zhu et al. (2006) Model

4.5.1 Procedure

In Zhu et al. (2006), 125 columns with detailing and properties typically found in old reinforced concrete structures were selected from the PEER database and used to develop a probabilistic model to estimate the median column drift at loss of 20% its peak lateral strength. The properties of the column database used are summarized in Table 4.4.

According to Zhu et al. (2006), columns were first classified into two zones: Zone F (flexure-dominated columns) and Zone S (shear-dominated columns). Generally, the columns included in Zone F have adequate transverse reinforcements and are expected to experience column failure associated with flexure damage, while the columns in Zone S are non-ductile columns that are vulnerable to shear failure. The rules of classifying columns in Zone F and Zone S can be found in Zhu et al. (2006). For simplicity this research will

classify the flexure-critical columns (columns in Condition i according to ASCE/SEI 41) into Zone F and non-ductile columns (Columns in Condition ii and Condition iii) into Zone S.

Then the median drift at shear failure for columns in each zone could be calculated as:

Zone S: $$(\delta_s)_{median} = 2.02\rho_t - 0.025\frac{s}{d} + 0.013\frac{a}{d} - 0.031\frac{P}{A_g f_c^{'}}$$ Equation 4.4

Zone F: $$(\delta_s)_{median} = 0.049 + 0.716\rho_l + 0.120\frac{\rho_t f_{yt}}{f_c^{'}} - 0.042\frac{s}{d} - 0.070\frac{P}{A_g f_c^{'}}$$

Table 4.4 Properties of the column database used in Zhu et al. (2006)

Parameters	Symbol	Unit	Max	Min
Aspect Ratio	a/d		7	1.2
Hoop spacing to depth ratio	s/d		1.2	0.1
Concrete compressive strength	$f_c^{'}$	*MPa*	56.2	16
Long. Rein. Yield Stress	f_{yl}	*MPa*	587	318
Long. Rein. Ratio	ρ_l		0.033	0.012
Trans. Rein. Yield Stress	f_{yt}	*MPa*	616	249
Trans. Rein. Ratio	ρ_t		0.022	0.0006
Axial Load Ratio	$P_{ini} / f_c^{'} A_g$		0.8	0
Normalized shear stress	$v / \left(\sqrt{f_c^{'}}/6 + \rho_{st} f_{st}\right)$	$\sqrt{MPa}$	3.1	0.2

4.5.2 Evaluation with The Database

The calculated column drift at shear failure are compared with the measured drift at 80% Max V_{eff} in Figure 4.14, with (a) calculated column drift based on the initial axial load P_{ini}; (b) calculated column drift based on the maximum axial load P_{max}.

The ratio of measured drift at Max V_{eff} to calculated column drift by Zhu et al. (2006) model is plotted in Figure 4.15.

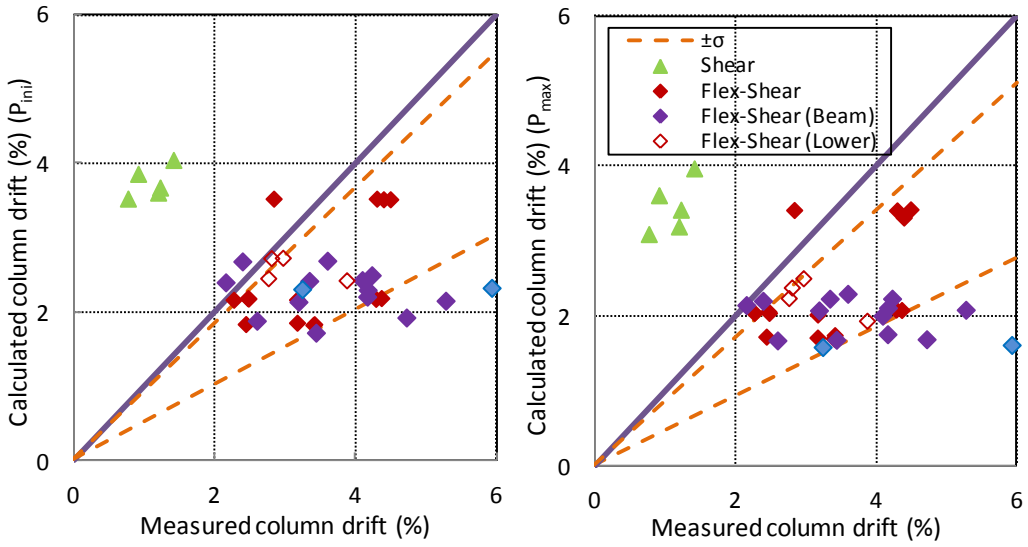

(a) Calculated drift based on P_{ini} (b) Calculated drift based on P_{max}

Figure 4.14 Calculated column drift by Zhu et al. (2006) model

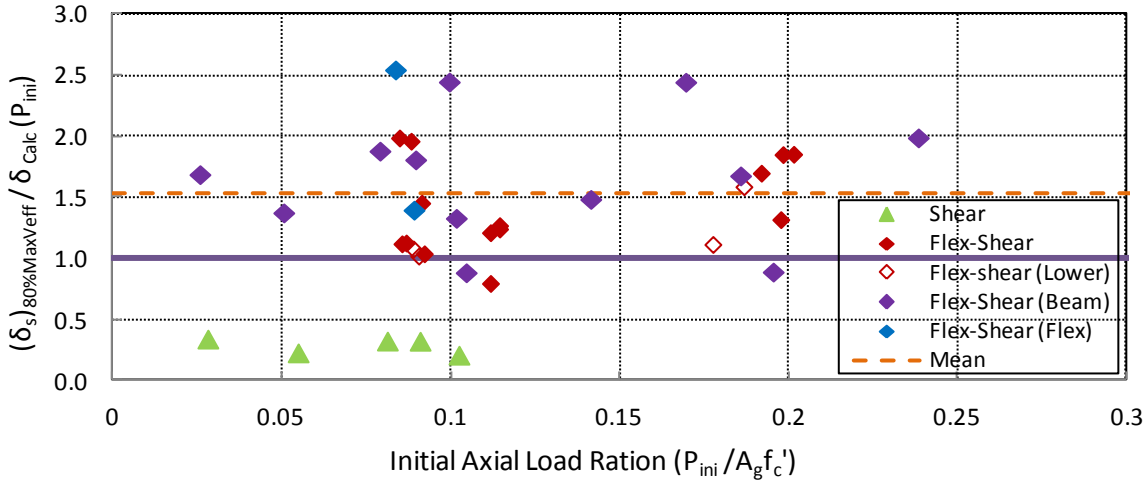

(a) The ratio of measured drift to calculated drift with initial axial load P_{ini}

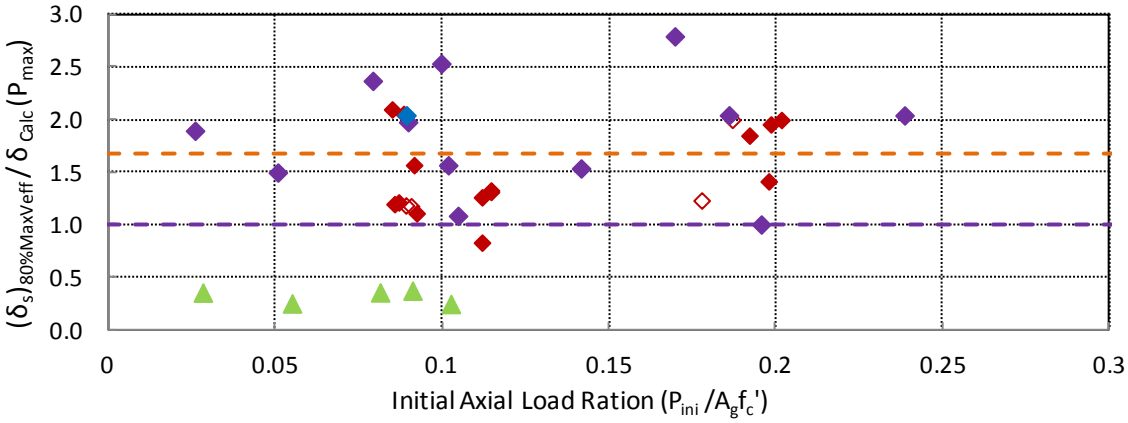

(b) The ratio of measured drift to calculated drift with maximum axial load P_{max}

Figure 4.15 Evaluation of Zhu et al. (2006) model

Zhu et al. (2006) model was intend to represent the median value of the column drift capacity at shear failure, yet the results in Figure 4.15 show that the calculated column drift generally underestimate the drift capacity at 80% Max V_{eff} for most flexure-shear-critical columns. On the other hand, the model can be very unconservative for shear-critical columns. The statistical results of ratio $(\delta_s)_{80\%MaxVeff} / \delta_{Cal}$ are reported in Table 4.5.

Table 4.5 Statistical results of Zhu et al. (2006) model

	Min	Max	Mean	Median	Standard Deviation	COV (%)
$(\delta_s)_{80\%MaxVeff}$ / δ_{Cal} (P_{ini})	0.80	2.45	1.53	1.46	0.44	28.9
$(\delta_s)_{80\%MaxVeff}$ / δ_{Cal} (P_{max})	0.83	2.79	1.67	1.57	0.49	29.4

4.5.3 Comparison with the Evaluation with Cyclic Test Data

The calculated column drift by Zhu et al. (2006) are plotted in Figure 4.16 for (a) columns in The Database (with calculated drift based on maximum axial load), (b) columns in the database used to develop the probability model.

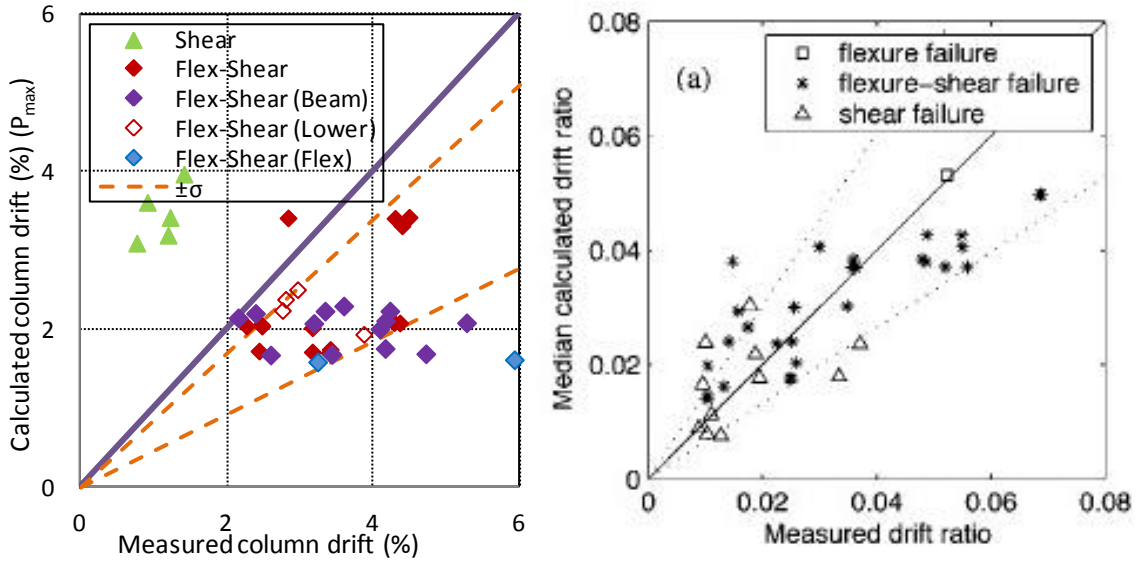

(a) Columns in The Database (b) Columns subjected to static cyclic tests

Figure 4.16 Evaluation of Zhu et al. (2006) model with dynamic and cyclic tests data

Since Zhu et al. (2006) greatly underestimate the column drift capacity as discussed before, the mean value of the ratio $(\delta_s)_{80\%MaxVeff} / \delta_{Cal}$ for flexure-shear-critical columns in The Database is more than 1.5 and the data in Figure 4.16(a) is greatly shifted towards the lower triangle area, while the data for the flexure-shear-critical columns (data series in the "*" marker) was more evenly distributed around the diagonal unit line.

4.6 Evaluation of Elwood and Moehle (2003, 2005) Model

4.6.1 Procedure

Based on the test data of 50 flexure-shear-critical columns in Sezen (2002) database, Elwood and Moehle (2003) proposed an empirical linear model to estimate the column drift at 80% Max V_{eff} :

$$\delta_s = \frac{1}{30} + 5\rho_t - \frac{1}{20}\frac{v}{\sqrt{f_c^{'}}} \geq \frac{1}{100} \qquad \text{Equation 4.5}$$

Where ρ_t = transverse reinforcement ratio; $f_c^{'}$ = concrete compressive stress on test day (MPa); v = maximum shear stress (MPa).

Elwood and Moehle (2005) observed that the column drift at shear failure seems to be inversely related to the axial load ratio for columns with low transverse reinforcement ratio $(\rho_t \leq 0.004)$. Therefore, a variation of the linear model taking into account the influence of column axial load ratio was proposed:

$$\delta_s = \frac{3}{100} + 4\rho_t - \frac{1}{40}\frac{v}{\sqrt{f_c^{'}}} - \frac{1}{40}\frac{P}{A_g f_c^{'}} \geq \frac{1}{100} \qquad \text{Equation 4.6}$$

Where ρ_t =transverse reinforcement ratio; $f_c^{'}$ =concrete compressive stress on test day (MPa); v = maximum shear stress (MPa); P =column axial load; A_g =area of column gross section.

4.6.2 Evaluation with The Database

The calculated column drift at shear failure by the above linear models are compared with the measured drift at 80% Max V_{eff} in Figure 4.17, with: (a) calculated drift by Elwood and Moehle (2003) model based on ASCE/SEI 41 shear strength V_0'; (b) calculated drift by Elwood and Moehle (2003) model based on measured maximum effective force V_{Max}; (c) calculated drift by Elwood and Moehle (2005) model based on ASCE/SEI 41 shear strength V_0'and initial axial load P_{ini}; (d) calculated drift by Elwood and Moehle (2005) model based on the measured maximum effective force V_{Max} and maximum axial load P_{max}.

It is noticed that the calculated column drift of both linear models is largely controlled by the reinforcement ratio ρ_t. Since most of the non-ductile columns in The Database had relatively low transverse reinforcement ratio ($\rho_t = \{0.0010 \sim 0.0016\}$), the calculated column drift tends to fall between 1.5 and 3. As a result, the data of calculated drift in Figure 4.17 was concentrated at a flat banded area instead of being scattered around the diagonal unit line, indicating that some other critical factors might be missing or the importance of the key parameters included in the models need to be re-weighed for columns subjected to low axial load.

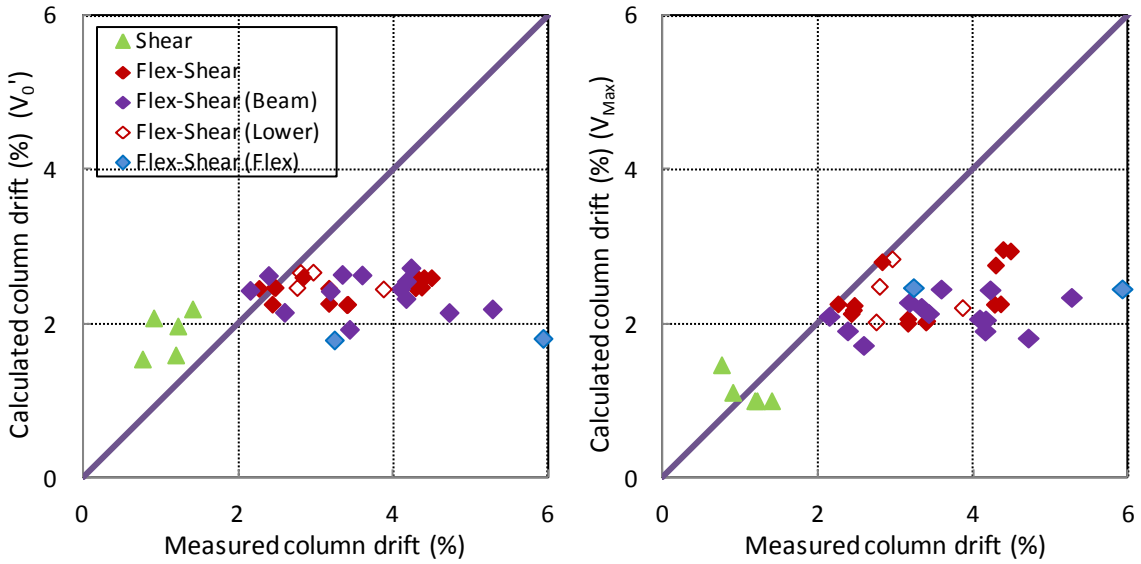

(a) Elwood and Moehle (2003) with V_0'

(b) Elwood and Moehle (2003) with V_{Max}

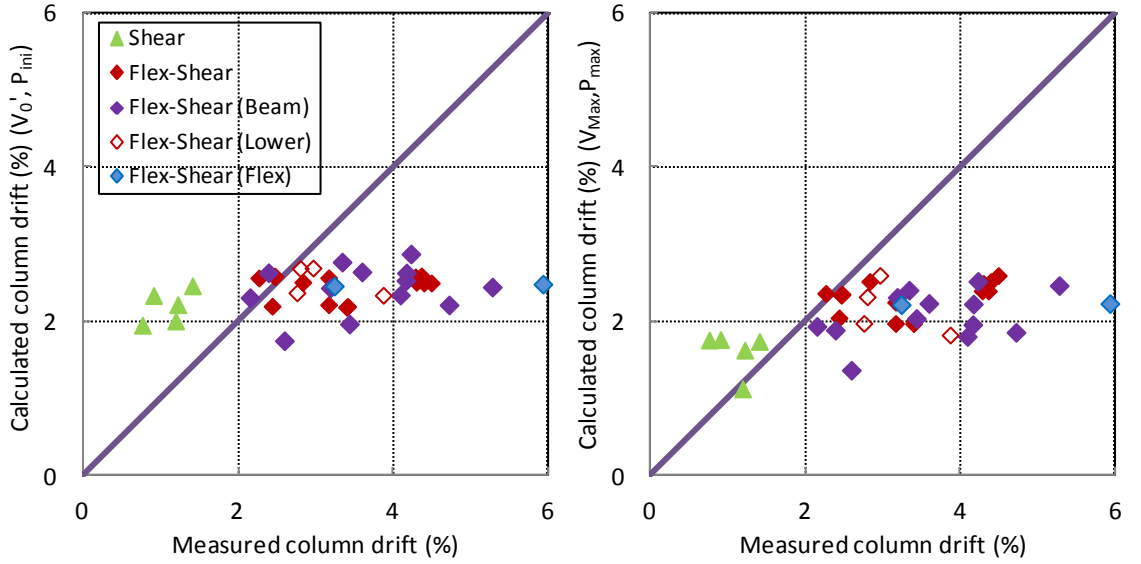

(c) Elwood and Moehle (2005) with V_0' and P_{ini}

(d) Elwood and Moehle (2005) with V_{Max} and P_{max}

Figure 4.17 Calculated column drift by Elwood and Moehle (2003, 2005) models

Comparing Figure 4.17 (a) with (b) and (c) with (d), it is observed that the calculated drift did not change much with the different options of column axial load ratio and shear stress applied in both linear models.

Figure 4.18 plots the ratio of measured column drift over calculated drift $(\delta_s)_{80\%MaxVeff} / \delta_{Cal}$ with: (a) calculated drift from Elwood and Moehle (2003) model based on V_0'; (b) calculated drift from Elwood and Moehle (2005) model based on V_0' and P_{ini}

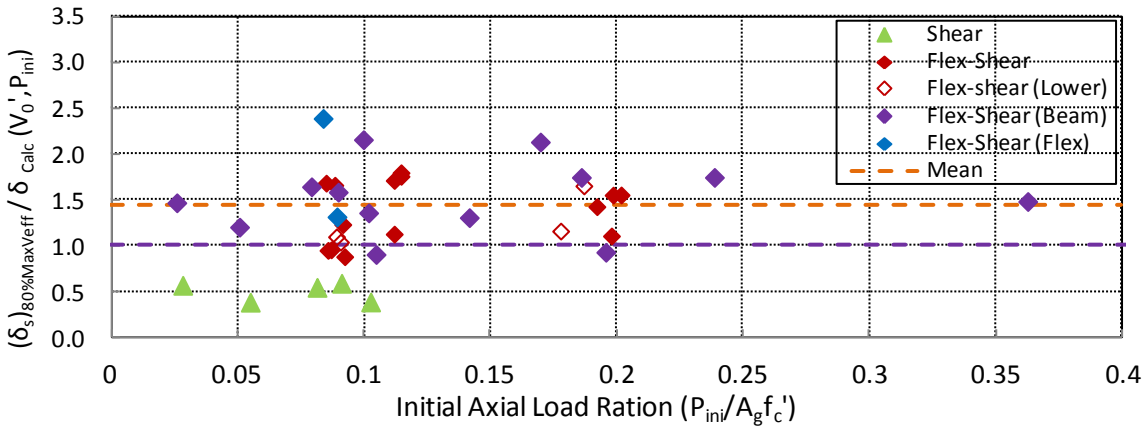

(a) The ratio of measured drift to calculated drift for Elwood and Moehle (2003) model

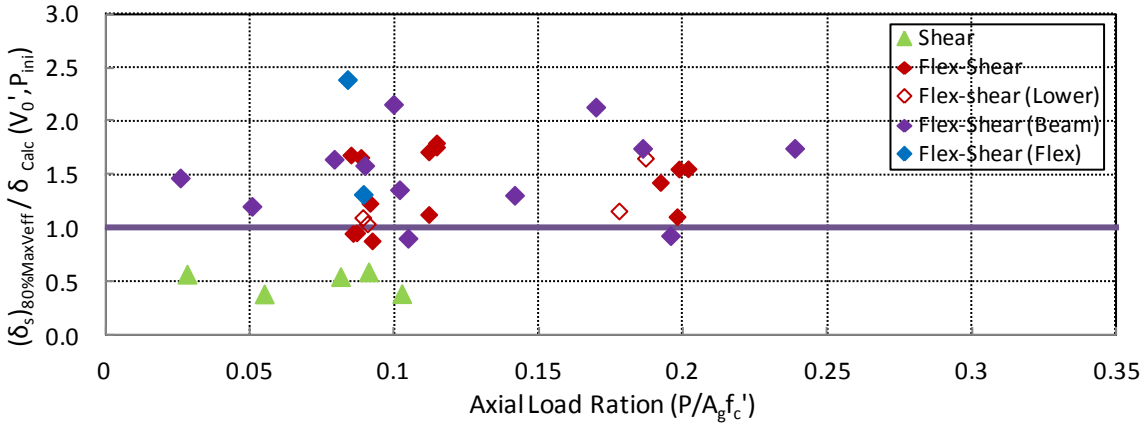

(b) The ratio of measured drift to calculated drift for Elwood and Moehle (2005) model

Figure 4.18 Evaluation of Elwood and Moehle (2003, 2005) models

The statistical results of the linear models for flexure-shear critical columns are reported in Table 4.6.

Table 4.6 Statistical results of Elwood and Moehle (2003, 2005) models

	Min	Max	Mean	Median	Standard Deviation	COV (%)
(a) Elwood and Moehle (2003) model						
$(\delta_s)_{80\%MaxVeff}$ / δ_{Cal} (V_0')	0.88	2.41	1.45	1.51	0.38	26.5
$(\delta_s)_{80\%MaxVeff}$ / δ_{Cal} (V_{Max})	1.00	2.60	1.59	1.53	0.40	25.5
(b) Elwood and Moehle (2005) model						
$(\delta_s)_{80\%MaxVeff}$ / δ_{Cal} (V_0',P_{ini})	0.88	2.16	1.45	1.48	0.36	24.7
$(\delta_s)_{80\%MaxVeff}$ / δ_{Cal} (V_{Max},P_{max})	0.96	2.54	1.61	1.69	0.40	24.7

4.6.3 Comparison with the Evaluation with Sezen (2002) Database

Elwood and Moehle (2005) model was developed based on the cyclic test data of columns in Sezen (2002) database. Figure 4.19 plots the calculated drift at 80% Max V_{eff} by Elwood and Moehle (2005) model for (a) columns in the Database, (b) columns included in Sezen (2002) database.

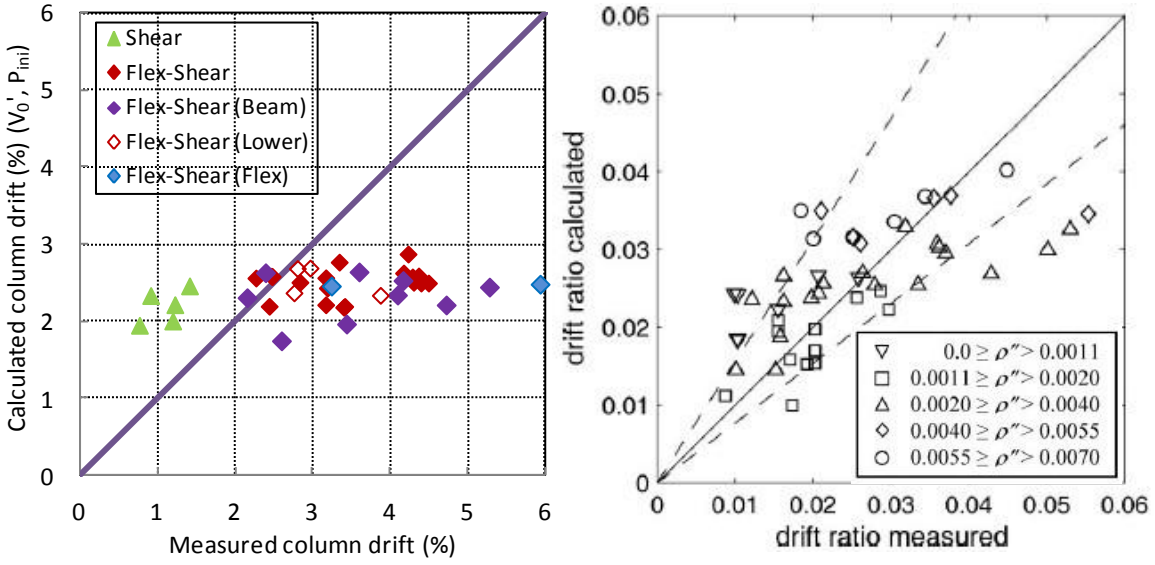

(a) Columns in The Database (b) Columns included in Sezen (2002) database

Figure 4.19 Evaluation of Elwood and Moehle (2005) model with The Database and Sezen (2002) database

Since the transverse reinforcement ratio ρ_t for most flexure-shear-critical columns in the Database is around 0.0010 to 0.0020, the dynamic column data in Figure 4.19 (a) should be compared with the data series in square makers in Figure 4.19 (b).

It is observed that while the data from cyclic tests scattered around the diagonal unit line in Figure 4.19 (b), the dynamic test data is more flat and seemed to be shifted towards the lower triangular area, indicating that the models underestimate column drift capacity.

The performance of shear strength models and drift capacity models is compared in Figure 4.20 for (a) columns in The Database and (b) columns in the Sezen (2002) database. Results showed that shear strength could be estimated more accurately than the column drift capacity at shear failure.

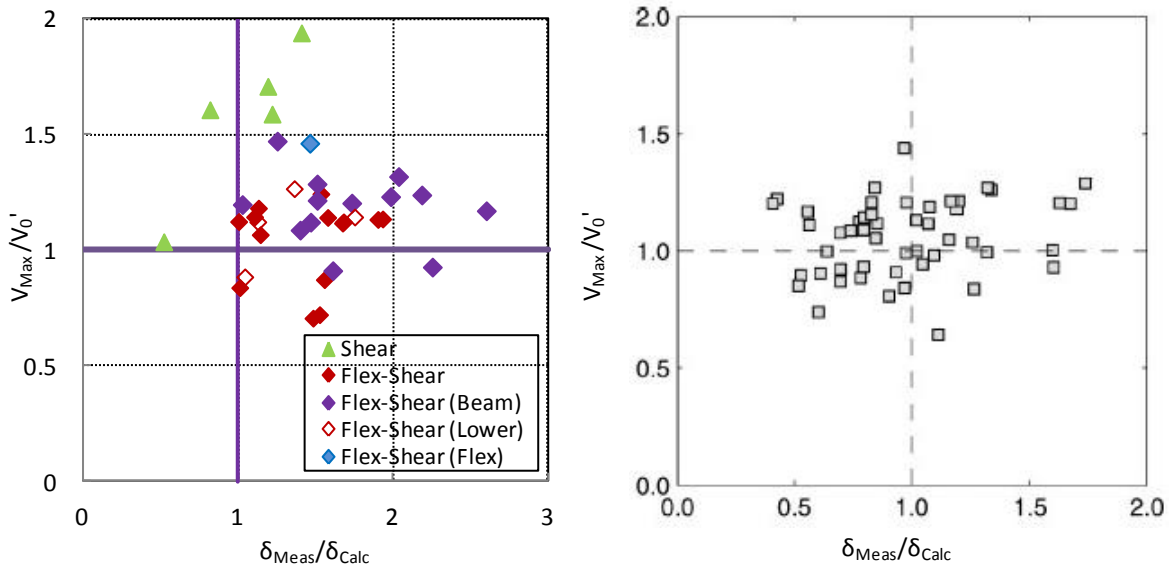

(a) Columns in The Database (b) Columns in Sezen (2002) database

Figure 4.20 Measure shear strength versus measured drift normalized by the calculated shear strength and calculated column drift

The evenly distributed data around the point (1.0, 1.0) in Figure 4.20 (b) indicated that for columns subjected to cyclic lateral load, underestimating or overestimating of the shear strength did not necessary result in underestimation or overestimation the column drift

capacity at shear failure. On the other hand, the data in Figure 4.20 (a) is observed to be concentrated in the upper right part, suggesting current models tend to underestimate the column shear strength and the drift capacity at shear failure.

4.6.4 Column Plastic Drift at Shear Failure

Figure 4.21 compares the plastic drift calculated from linear models with measured plastic drift, which is obtained by deducting the measured yield drift from total drift.

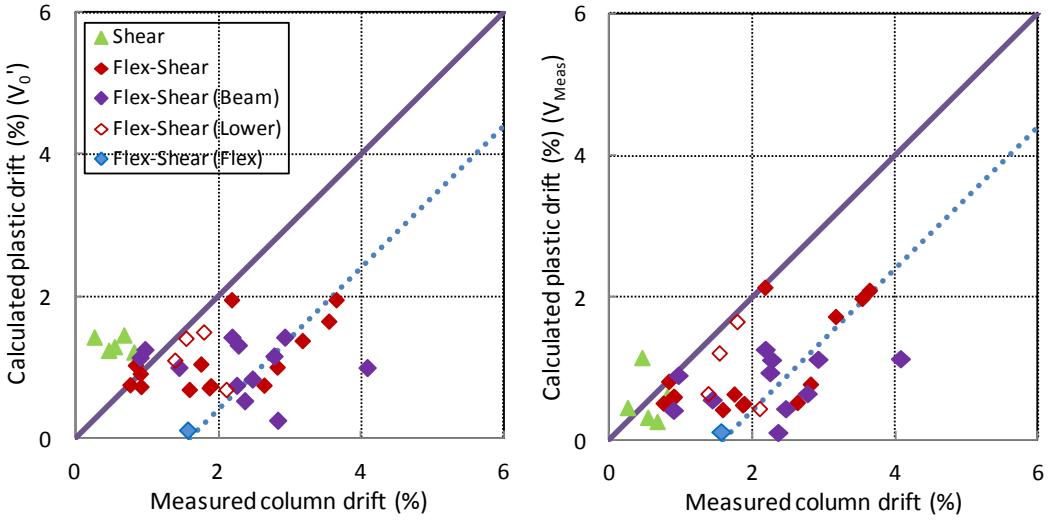

(a) Elwood and Moehle (2003) with V_0' (b) Elwood and Moehle (2003) with V_{Max}

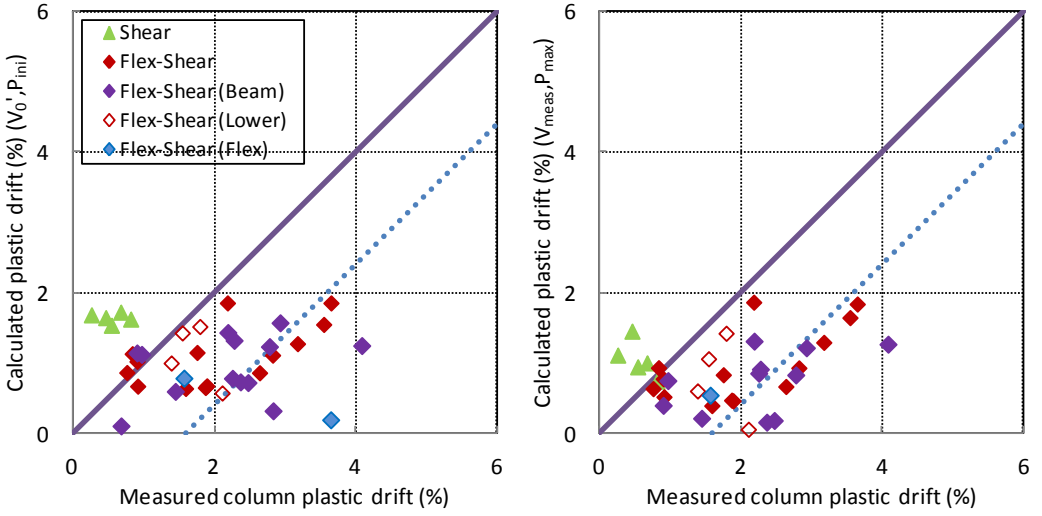

(c) Elwood and Moehle (2005) with V_0' and P_{ini} (d) Elwood and Moehle (2005) with V_{Max} and P_{max}

Figure 4.21 Plastic drift calculated by Elwood and Moehle (2003, 2005) model

The data of calculated plastic drift for shear-critical columns in Figure 4.21 seems to scatter around a dashed line parallel to the unit line. The shift of the data indicates that compared with cyclic test data, the plastic drift capacity at shear failure in shaking table tests increased, possibly due to the dynamic effect.

Recall that no obvious trend could be found for calculated total column drift from linear models in Figure 4.17. Given the trends seen in Fig 4.20 considering plastic drift rather than total, models for estimating of the plastic drift at shear failure probably should be considered instead.

Plastic column drift model has several advantages over the total drift model:

(a) The plastic drift is essential to develop plastic hinge models. Columns in existing reinforced concrete structures usually have different detailing and connections (e.g. splices) with the beam (or column base) at the upper end and the bottom end. Plastic hinge model could capture the column damage and shear failure more appropriately than the model based on the behaviour of entire column.

(b) Plastic drift is a good indicator of column damage and could better reflect the column drift capacity at shear failure. For example, a relatively flexible column may experience extended deformation before the column yielding. Thus at the point that the total column drift reaches the calculated drift from linear models, the column plastic deformation might be very small and it would be inappropriate to define it as shear failure point.

Several columns in Shin 2005 Tests and Elwood 2002 Tests are subjected to input motions scaled from the ground motions recorded in a subduction earthquake (Chile 1985

earthquake). It is noticed in Figure 4.22 (a) that the plastic drifts calculated from Elwood and Moehle (2005) model for those columns (subjected to Chile ground motions) are not as conservative as that for other columns.

If excluding the columns subjected to subduction earthquake and using least-square fit of the test data for those columns subjected to general type of ground motions (e.g. Chi-Chi Earthquake), a new empirical plastic drift model at 80% Max V_{eff} for flexure-shear-critical columns is proposed based on maximum axial load P_{max} and measured maximum effective force V_{Max}. The plastic drift model for columns subjected to subduction earthquake is scaled from the proposed model to achieve best match of the test data, taking into account the ideas that: (a) as column goes through more significant cycles when subjected to subduction earthquake, the effectiveness of transverse reinforcement should be reduced due to the bond degradation; (b) the negative impact of shear stress should be amplified, since the column subjected to subduction earthquake is likely to experience high shear stress level more times; (c) the overall plastic drift is found to be lower than that for similar columns subjected to general type of ground motions.

The proposed empirical plastic drift capacity models are presented in Equation 4.7

General Earthquake: $(\delta_s)_{Subduction} = 0.049 + 0.60\rho_t - 0.05\frac{P}{A_g f_c^{'}} - 0.049\frac{v}{\sqrt{f_c^{'}}}$ Equation 4.7

Subduction Earthquake: $(\delta_s)_{General} = 0.045 + 0.50\rho_t - 0.05\frac{P}{A_g f_c^{'}} - 0.062\frac{v}{\sqrt{f_c^{'}}}$

The calculated plastic drifts at 80% Max V_{eff} from the proposed empirical models are plotted in Figure 4.22 (b). The statistical results of the proposed models and Elwood and Moehle (2005) model are summarized in Table 4.7.

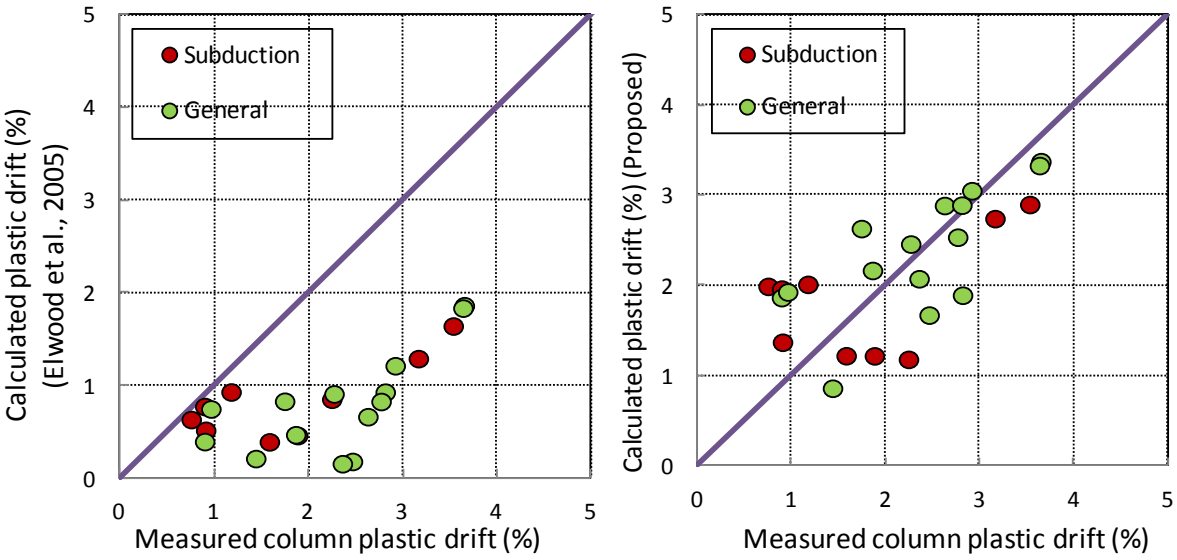

Figure 4.22 Proposed empirical plastic drift model for flexure-shear-critical columns

Results in Figure 4.22 show that the proposed empirical models improves the estimation of column plastic drift capacities compared with Elwood and Moehle (2005) model and could reflect the trends of the column plastic drift capacity at shear failure fairly well. Table 4.7 shows that the model tends to represent the mean value of the column drift capacity, but large varieties still existed in the data.

Table 4.7 Statistical results of proposed plastic drift models

	Min	Max	Mean	Median	Standard Deviation	COV (%)
(a) Proposed plastic drift model						
$(\delta_s)_{Meas} / (\delta_s)_{Subduction}$	0.38	1.94	1.03	1.13	0.54	52
$(\delta_s)_{Meas} / (\delta_s)_{General}$	0.48	1.67	1.02	0.97	0.34	33
$(\delta_s)_{Meas} / (\delta_s)_{Cal}$	0.38	1.94	1.02	1.03	0.41	40
(b) Elwood and Moehle (2005) model						
$(\delta_s)_{Meas} / (\delta_s)_{Subduction}$	0.40	1.65	0.84	0.78	0.41	49
$(\delta_s)_{Meas} / (\delta_s)_{General}$	0.00	1.87	0.75	0.75	0.57	76
$(\delta_s)_{Meas} / (\delta_s)_{Cal}$	0.00	1.87	0.80	0.78	0.51	63

The large variation (coefficient of variation) existed in the data of the ratio of measured plastic drift to calculated plastic drift from proposed model could be greatly reduced if the

coefficient of the axial load ratio term is positive, yet this contradict to the fact that higher axial load tends to reduce the column drift capacity.

The quantity of the columns subjected to subduction earthquake included in The Database is also very limited. It is noted that most flexure-shear-critical columns used for developing this model achieved greatly varied plastic drift at 80% Max V_{eff}, yet had very similar transverse reinforcement ratio (ρ_t is around 0.0016) and were subjected to relatively low axial load ratio ($P/A_g f_c^{'}$ is between 0.08 and 0.25) and shear stress ($v/\sqrt{f_c^{'}}$ is around 0.3). Some other parameters that could better represent the characteristics of subduction input ground motions might be missing.

With more shaking table tests with subduction earthquakes and other types of earthquakes as input ground motions conducted on columns covering larger property range, a more reliable plastic drift capacity model could be developed.

4.7 Effect of Number of Cycles

Figure 4.23 plots the number of cycles that columns went through up to the shear failure point with the column drift at 80% Max V_{eff}.

The ordinate of Figure 4.23(b) is the normalized column drifts obtained from dividing the measured column drift by the calculated drift. The calculated drift at shear failure was obtained from Elwood and Moehle (2005) model (discussed in section 4.6.1) based on the maximum axial load P_{Max} and measured maximum effective force V_{Max}. Using the normalized column drifts could roughly take into account the effect of axial load ratio and shear stress

level and gain a better idea of the relations between number of cycles and column drift capacity.

Results in Figure 4.23 (a) show that there is no strong correlation between the number of cycles that columns went through and the drift capacity at 80% Max V_{eff} .

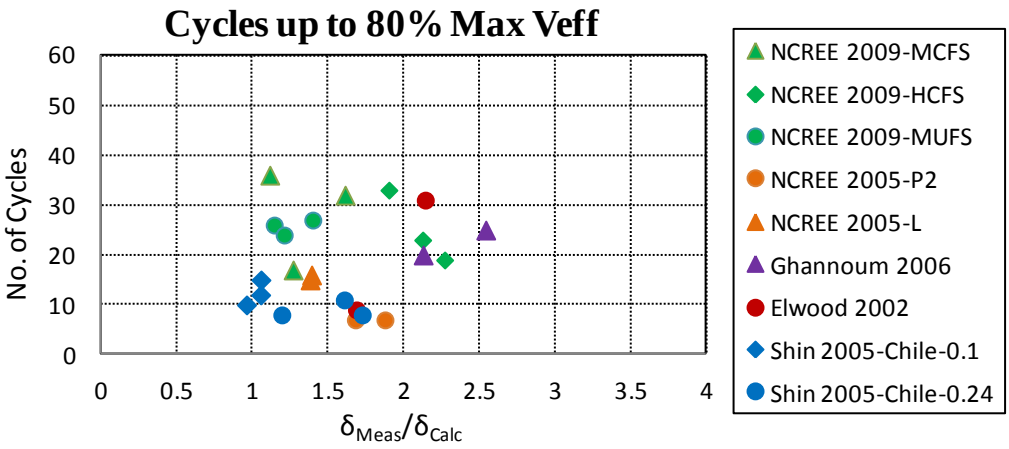

(a) Number of cycles with normalized column drift at 80% Max Veff

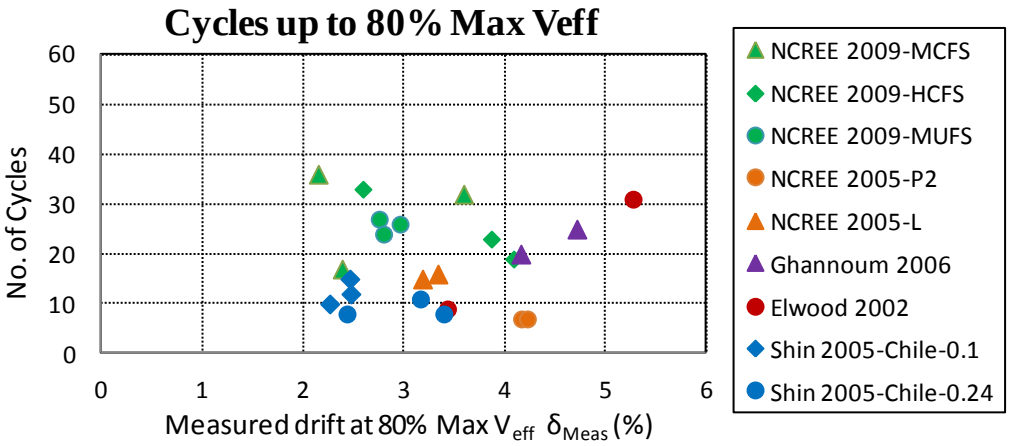

(b) Number of cycles with column drift at 80% Max Veff

Figure 4.23 Number of cycles with normalized column drift at shear failure

Chapter 5: Column Drift Capacity at Axial-Load Failure

5.1 Definition of Axial-Load Failure

The behaviour of ductile columns with adequate transverse reinforcement is dominated by flexure response. The failure mechanisms of these flexure-critical columns are often assumed to be either reaching the ultimate curvature that the column section could withstand or suffering structural instability due to P-Delta effect.

Most available models estimating ultimate column drift capacity are based on the ultimate concrete and steel strains with consideration of P-Delta effect. These models are not applicable to shear-dominated columns that have light transverse reinforcement. As the shear failure plane develops, non-ductile columns may experience axial-load failure and lose gravity load support after shear failure, potentially leading to the collapse of the structures.

There is lack of consensus on the definition of column axial-load failure, since loss of axial load support is closely related to many factors, such as column axial load response, lateral strength degradation and the column lengthening/shortening. In order to evaluate the performance of models proposed to estimate column drift capacity at axial-load failure, a consistent method needs to be adopted to define the axial-load failure point and the measured column drift at axial-load failure.

5.1.1 Definition Based on Hysteretic Response of Axial Load

Since axial-load failure occurs when columns lose support for gravity load, it is intuitive to associate axial-load failure with the sudden change of column axial load response. Using the west column in Shin 2005 Tests as an example (Figure 5.1), axial-load failure

could be defined as the point at which axial load suddenly dropped (point in blue diamond marker). It is observed that lateral force degraded to almost zero at this point too.

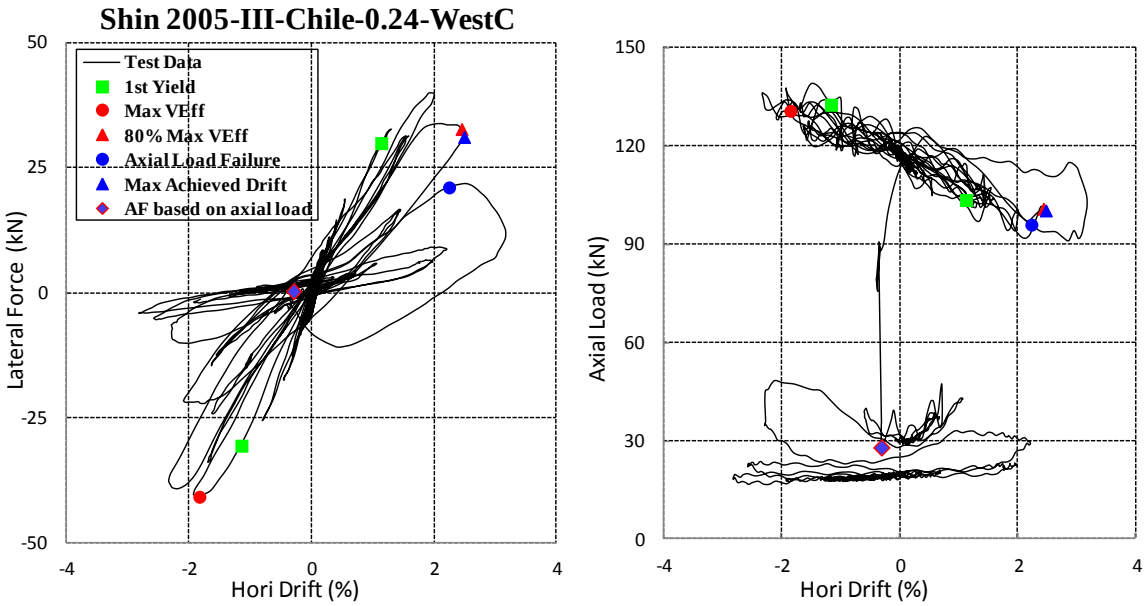

Figure 5.1 Axial-load failure based on axial load response for column in Shin 2005 Tests

The sudden change of the column axial load may also be accompanied by the abrupt change in slope of the column lengthening/shortening-horizontal drift response, as shown in Figure 5.2 for column C3 in NCREE 2007 Tests.

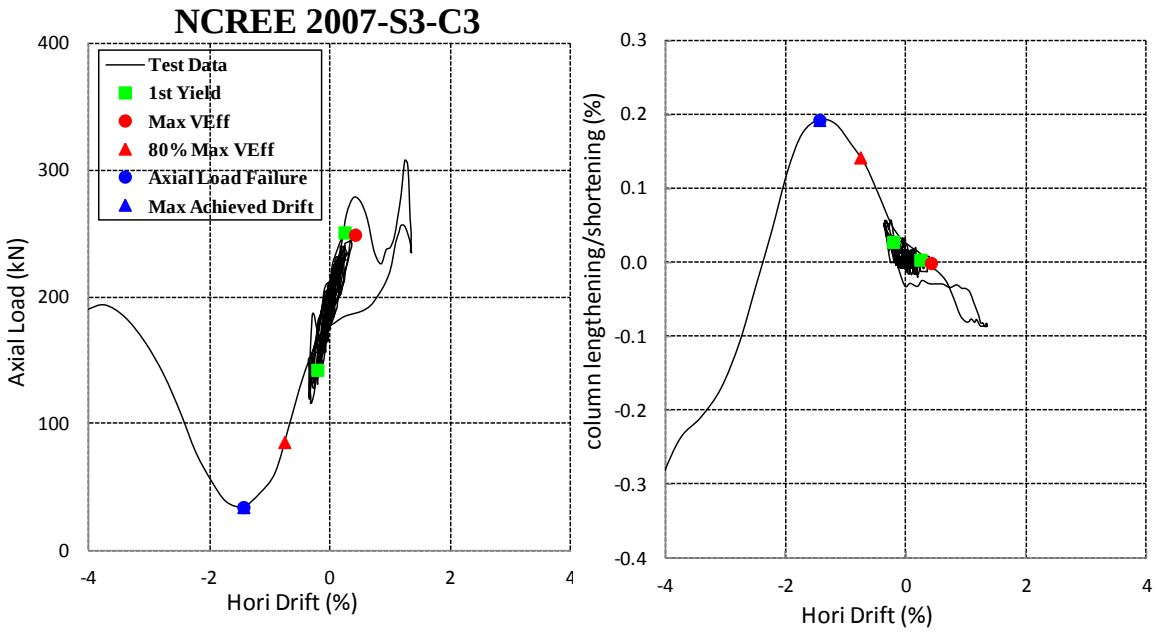

Figure 5.2 Axial-load failure based on axial load response for column in NCREE 2007 Tests

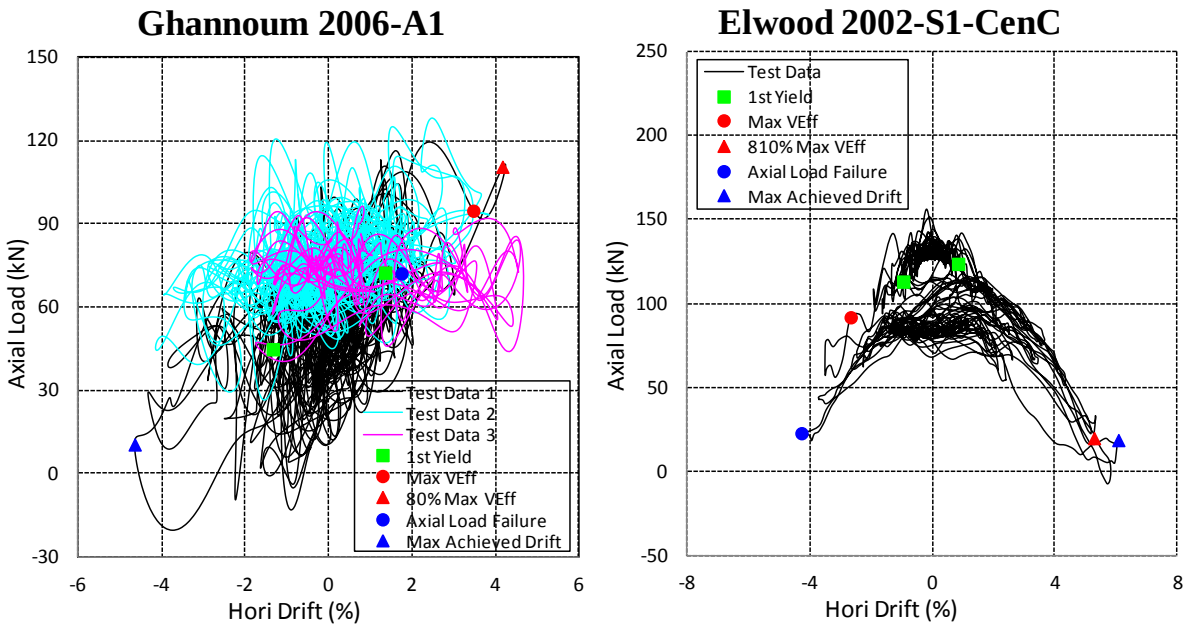

Figure 5.3 Axial-load failure definitions for columns without sudden change in axial load response

However, for some columns that experienced axial-load failure, there was no obvious change in the axial load response. For example, the column A1 in Ghannoum 2006 Tests and the center columns in specimen S1 of Elwood 2002 Tests lost the gravity load support in the later stage of the test (axial-load failure could be considered occurred at the point shown in blue round marker), yet there seemed to be no significant change in the axial load response in Figure 5.3. It would be difficult to identify the axial-load failure point solely based on axial load hysteretic response for these columns.

The axial load response is also affected by the type of the frames. For columns in specimens with multiple columns, such as specimens in NCREE 2005 Tests, axial load redistribution within the frame is allowed after the column axial-load failure; while in specimens with only two columns, such as specimens in Shin 2005 Tests, no axial load redistribution is allowed and the specimen tends to collapse after the column failed.

5.1.2 Definition Based on Degradation of Lateral Resistance

Past studies (Kabeyasawa. et al. 2002) show that columns tend to lose support for gravity load when column lateral resistance degrades to zero. Using column C1 in specimen P2 of NCREE 2005 Tests shown in Figure 5.4 as an example, the axial-load failure point could be defined based on the degradation of lateral resistance.

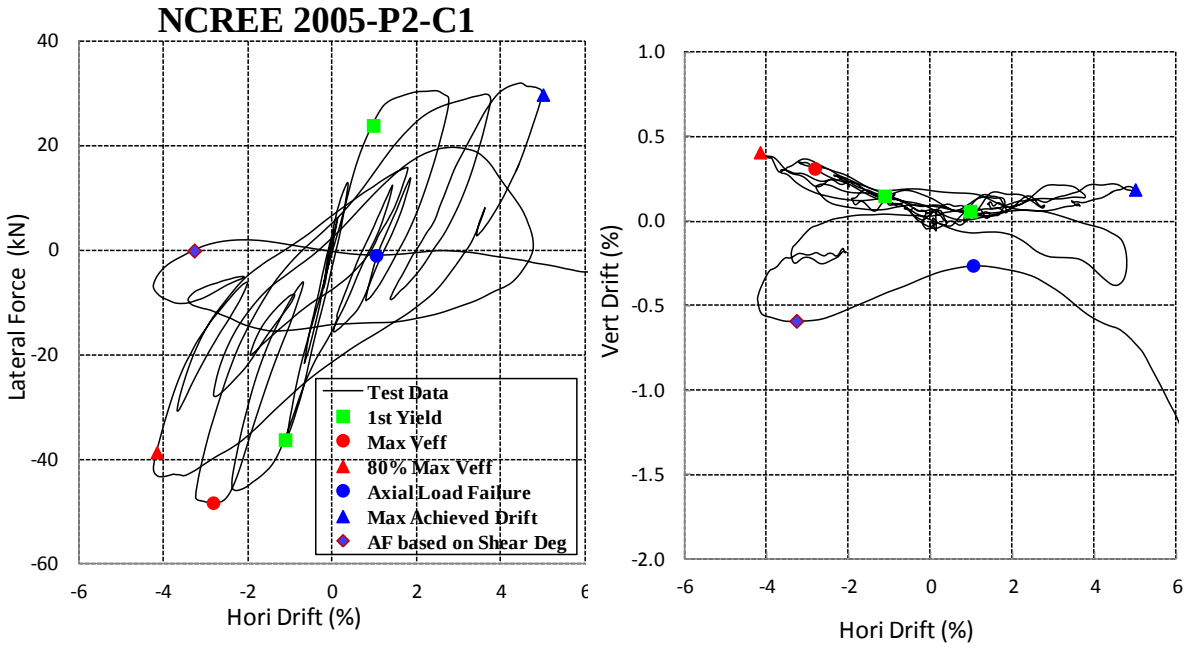

Figure 5.4 Axial-load failure based on shear degradation

However for some non-ductile columns, the lateral strength did not suffer severe shear degradation (the residual shear is not less than 10% of its peak strength) prior to the loss of axial load support. For example as shown in Figure 5.5(a), it would be inappropriate to apply this definition for column A1 in specimen MCFS of NCREE 2009 Tests whose lateral resistance did not degrade to zero during the tests.

What's more, in the case of column C3 of NCREE 2007 Tests shown in Figure 5.5 (b), the lateral force degraded to almost zero at the very end of the test, yet the column was severely damaged before this point and the horizontal drift data was not reliable (the upper

part of the columns slid away along the shear damaged plane). Drift at the point with zero lateral resistance was exceptional high for those columns and defining the axial-load failure at this point might result in a very unconservative interpretation of the column drift capacity at loss of axial load support.

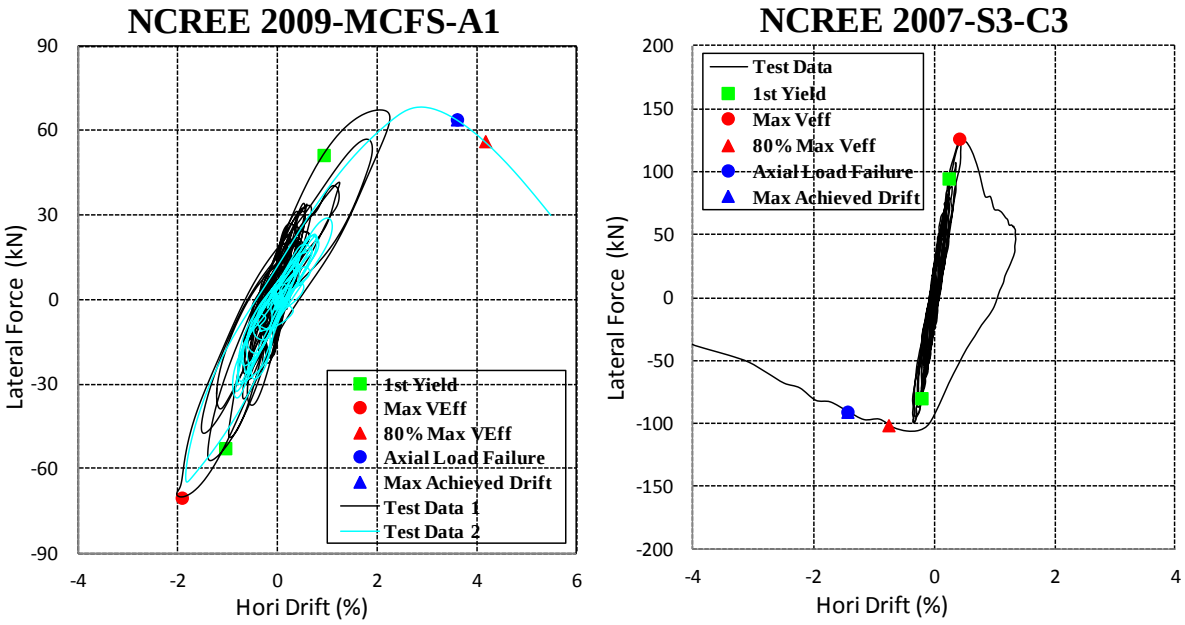

Figure 5.5 Inappropriate to define the column axial-load failure based on shear degradation

5.1.3 Definition Based on Column Shortening/Lengthening

The axial-load failure of non-ductile columns with light transverse reinforcement is usually induced by the development of a diagonal failure plane after column shear failure. The column may fail to transfer axial load with the sliding of columns along the critical diagonal crack, indicating that the change in vertical deformation response might be a good indicator of column axial-load failure.

Yavari (2011) defined the onset of column axial-load failure as "the point at which the peak vertical displacement due to column lengthening is recorded followed by a sudden shortening of the column" (Yavari, 2011, p. 59). The axial-load failure points for columns in

NCREE 2009 Tests and NCREE 2007 Tests interpreted by this definition are shown in Figure 5.6.

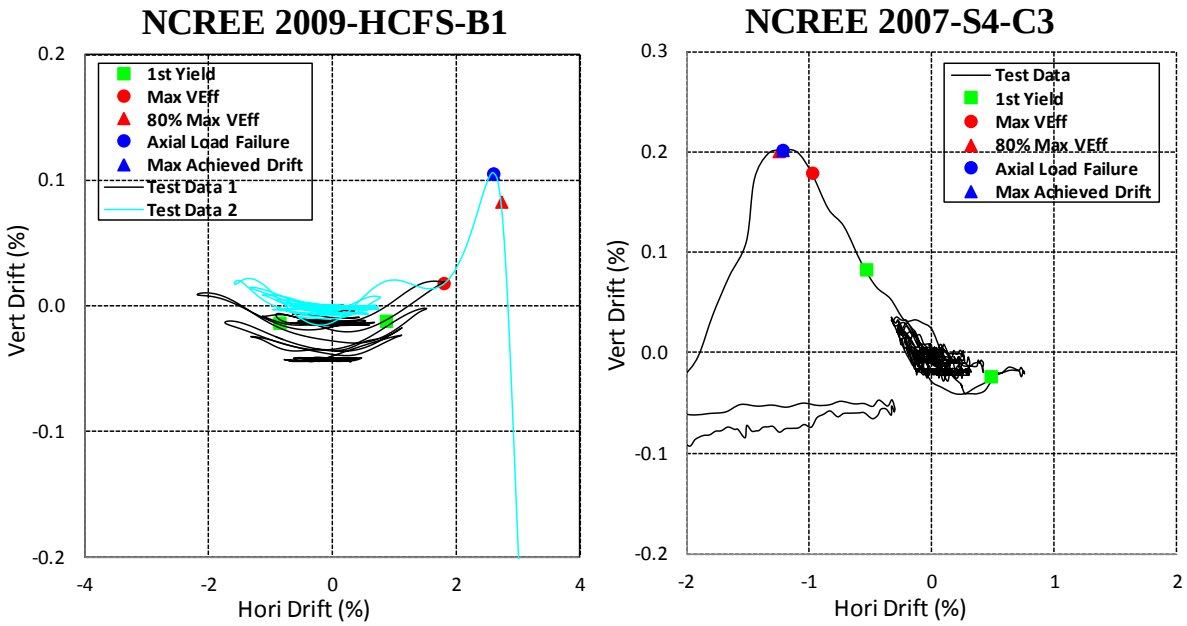

Figure 5.6 Axial-load failure based on column lengthening/shortening

5.1.4 Measured Column Drift at Axial-Load Failure

For a majority of non-ductile columns in The Database, the point with sudden change in the sign of the slope of the column shortening/lengthening-horizontal drift relations is in accordance with the change of axial load. This point is also able to reflect the shear degradation fairly well. Therefore the column axial-load failure point in this research will be defined based on the column shortening/lengthening data (derived from the vertical deformation).

However based on this definition, the column drift at the axial-load failure point might be very small for some columns; for example, column C3 in specimen MCFS in NCREE 2009 Tests as shown in Figure 5.7.

Since this chapter focuses on estimating the drift capacity up to the point that column losses gravity load support, the measured column drift at axial-load failure δ_a shall be taken as the maximum drift that the column achieved before the axial-load failure point as defined above. The measured plastic drift at axial-load failure could be calculated by subtracting the measured yield drift δ_y (obtained from TEST method discussed in section 3.2.4) from the total column drift at axial-load failure.

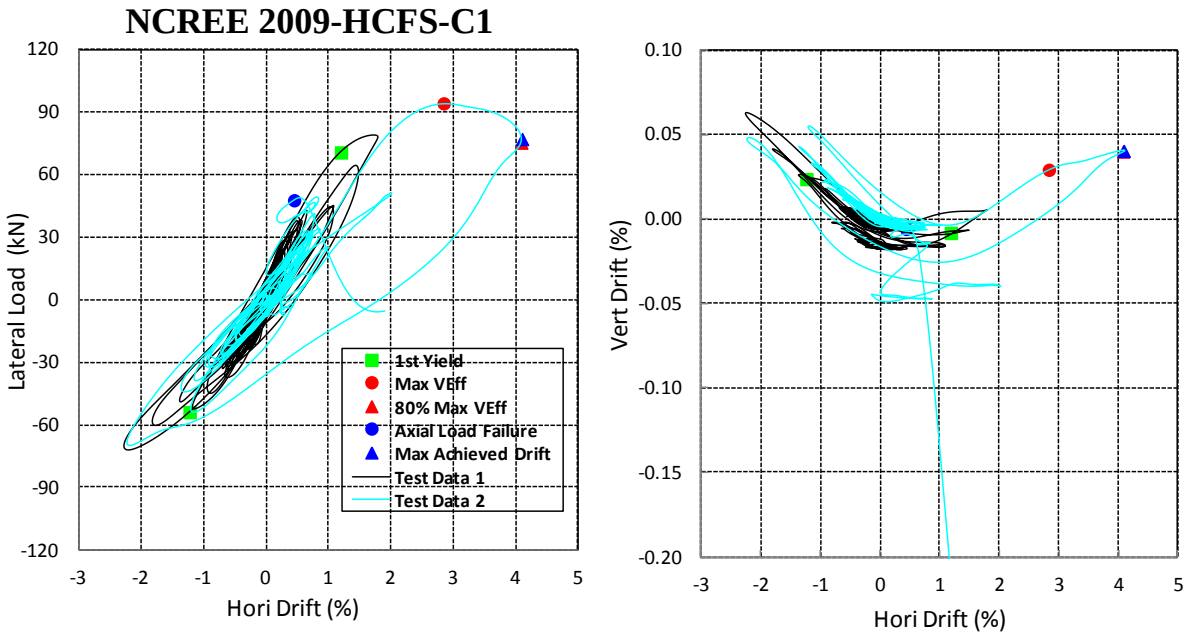

Figure 5.7 Axial-load failure at low lateral drift for column in NCREE 2009 Tests

5.2 Effect of Key Parameters on Measured Drift at Axial-Load Failure

Figure 5.8 plots the measured column drifts at axial-load failure for non-ductile with several key parameters. The plastic drift at axial-load failure is plotted in Figure 5.9. The key parameters considered and the columns that each data series represents are similar to that for column drift at shear failure in section 4.2 of this thesis.

It is observed from Figure 5.8 that the column drift tends to decrease with increasing axial load ratio and normalized shear stress. Increasing transverse reinforcement indicator

also appears to increase the column drift at axial-load failure. Other parameters are not strongly correlated with either the column drift or plastic drift capacities.

Results in Figure 5.10 show that column drift at axial-load failure tends to decrease with increasing relative strength factor R, possibly could be explained by the fact that weaker structure system is more likely to incur dynamic instability and the resulted dynamic excitations (or the inertia forces) caused the column to experience axial-load failure at lower drift. Going through more number of cycles slightly increase the column drift capacity for most non-ductile columns. The relation between the bracket duration and the column drift is not very obvious and the data is pretty "banded" (the columns in the same frame have same t_b but different column drift at axial-load failure).

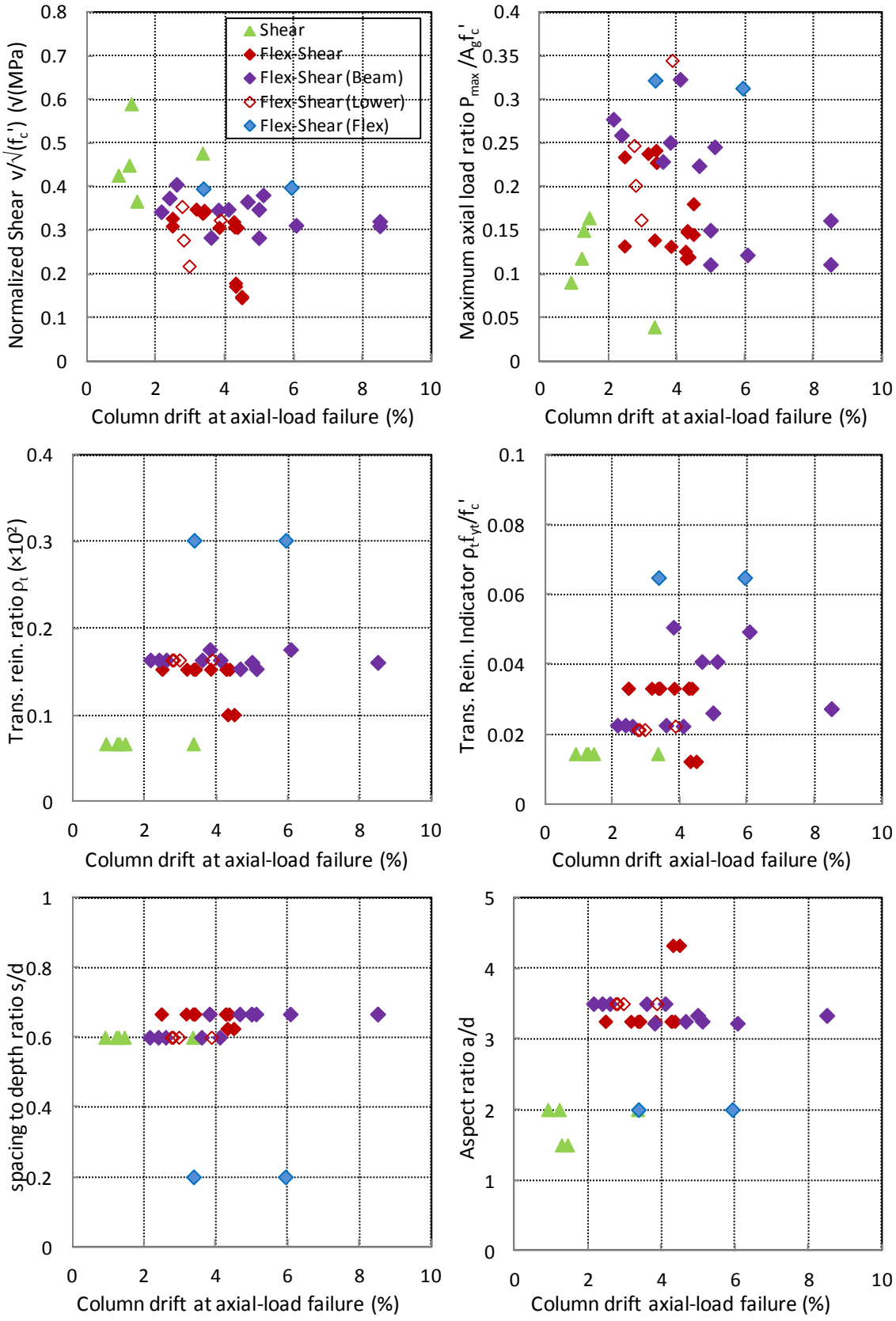

Figure 5.8 Measured drift at axial-load failure with key parameters

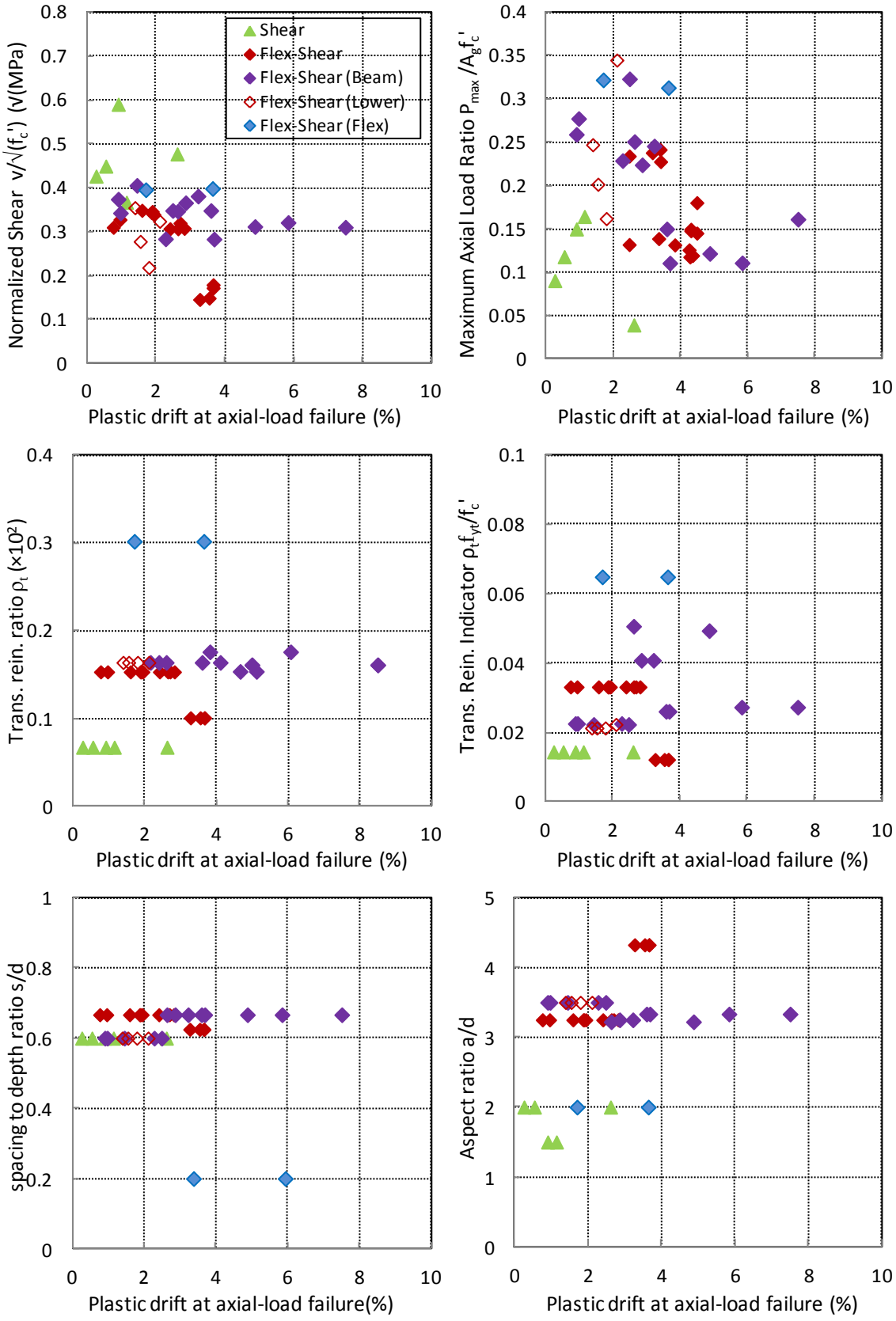

Figure 5.9 Measured plastic drift at axial-load failure with key parameters

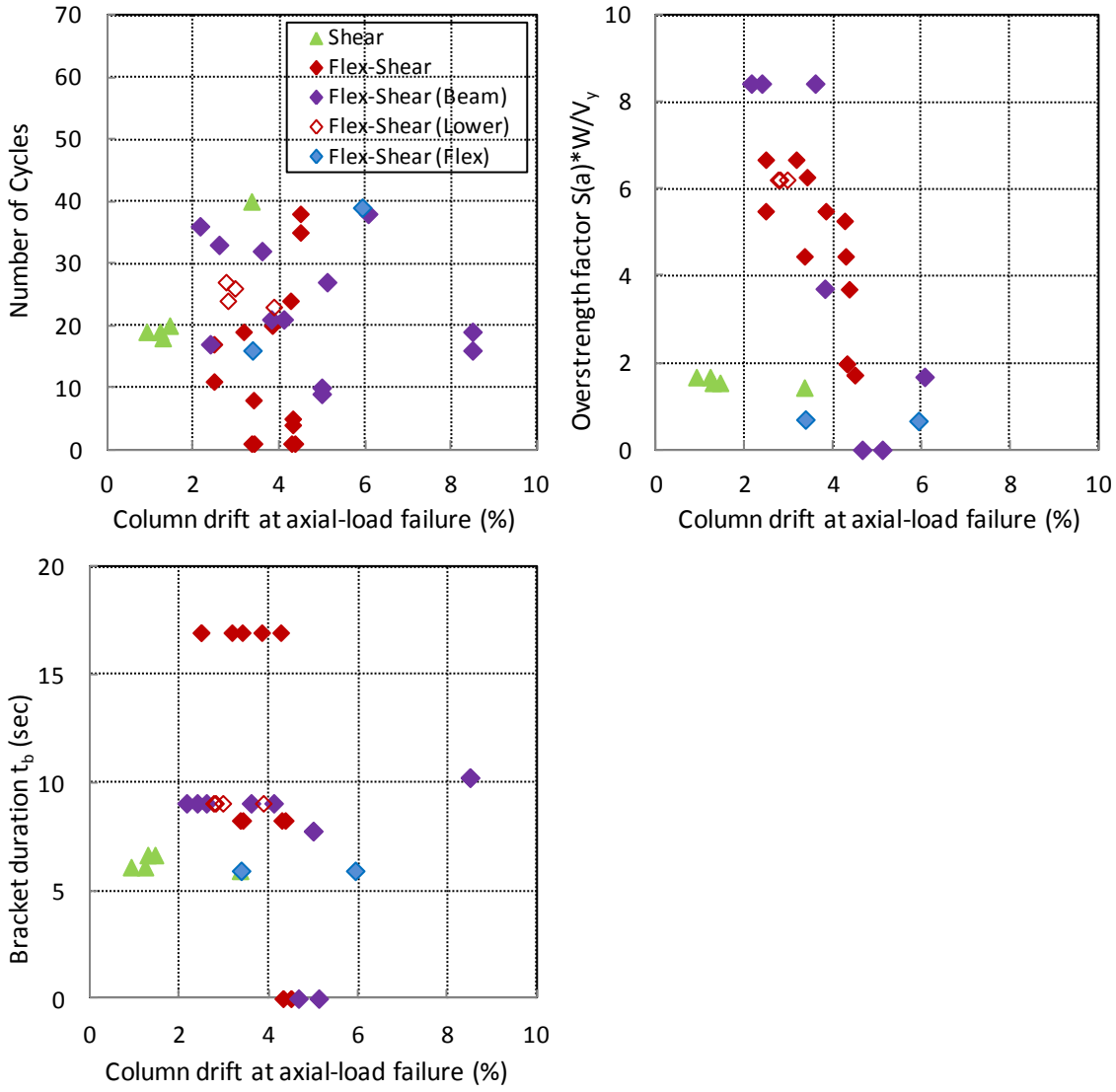

Figure 5.10 Measured drift at axial-load failure with dynamic parameters

5.3 Evaluation of Shear-Friction Model

5.3.1 Procedure

According to Elwood and Moehle (2003), axial load has to be transferred across the shear failure plane to be supported after column suffers shear failure. This mechanism is known as shear friction. The classic shear-friction model related the shear V_{sf} transferred across the shear-failure plane (i.e. the main crack) with the normal stress N (perpendicular to the cracking surface) by an effective coefficient of friction μ.

$$V_{sf} = \mu N \qquad \text{Equation 5.1}$$

By drawing a free-body diagram across the shear damaged plane and ignoring the contribution from longitudinal reinforcement, the effective coefficient of friction μ for non-ductile columns with light transverse reinforcement could be expressed as:

$$\mu = \frac{\frac{P}{A_{st} f_{st} d_c / s} - 1}{\frac{P}{A_{st} f_{st} d_c / s} \frac{1}{\tan\theta} + \tan\theta} \qquad \text{Equation 5.2}$$

Where P = column axial load; A_{st} = area of transverse reinforcement; f_{st} = yield strength of transverse reinforcement; d_c = distance between the center line of longitudinal reinforcement in tension and compression; θ = critical crack angle and is assumed to be 65°.

Elwood and Moehle (2003) plotted the calculated coefficient of friction μ with the measured drift at loss of gravity load support for 12 full scale flexure-shear-critical columns tested by Lynn (2001) and Sezen (2002). A trend was observed and approximated by a linear line:

$$\mu = \tan\theta - \frac{100}{4}\delta_{Axial} \geq 0 \qquad \text{Equation 5.3}$$

Combining the aforementioned two equations, Elwood and Moehle (2003) proposed a Shear-Friction model to estimate the column drift capacity at axial load failure for non-ductile columns:

$$\delta_{Axial} = \frac{4}{100} \frac{1+(\tan\theta)^2}{\tan\theta + \frac{P}{A_{st} f_{st} d_c / s} \frac{1}{\tan\theta}} \qquad \text{Equation 5.4}$$

5.3.2 Evaluation of Shear-Friction Model with The Database

The calculated column drift by Shear-Friction model are compared with the measured column drift at axial-load failure in Figure 5.11. The ratio of calculated column drift to measured drift δ_a / δ_{Cal} is plotted in Figure 5.12, with (a) calculated drift based on initial axial load P_{ini} ; (b) calculated drift based on maximum axial load P_{max} .

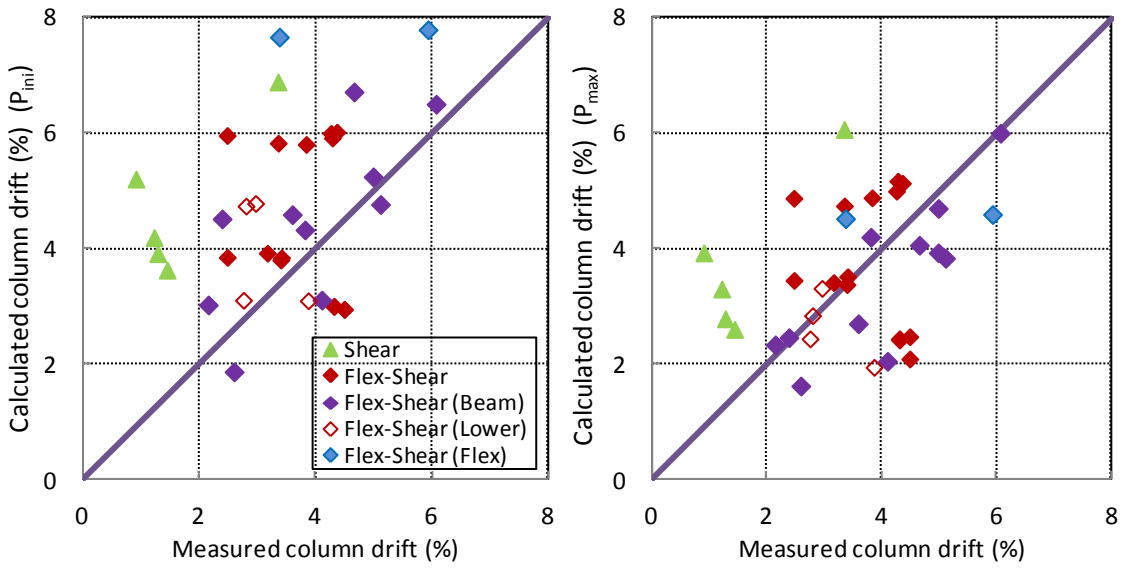

(a) Calculated drift based on P_{ini} (b) Calculated drift based on P_{max}

Figure 5.11 Calculated column drift at axial-load failure of shear-friction model

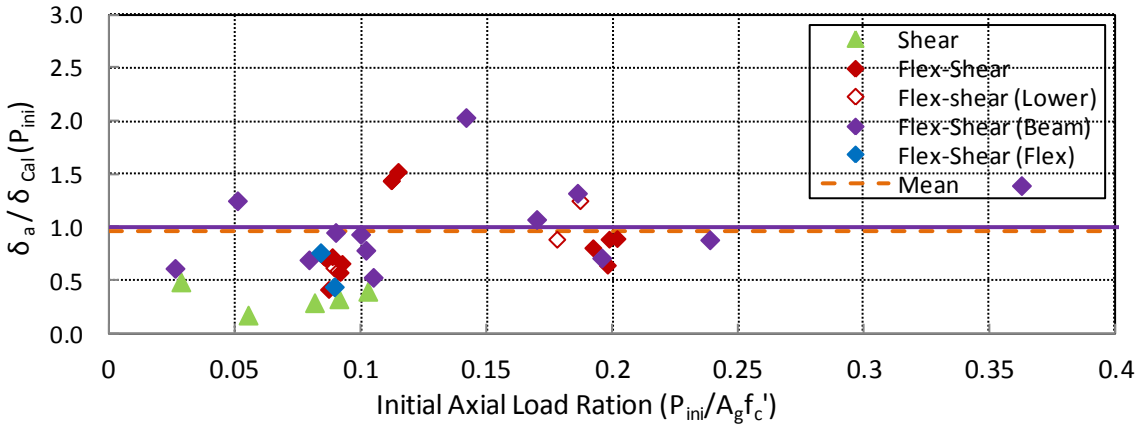

(a) Calculated column drift at axial-load failure with initial axial load P_{ini}

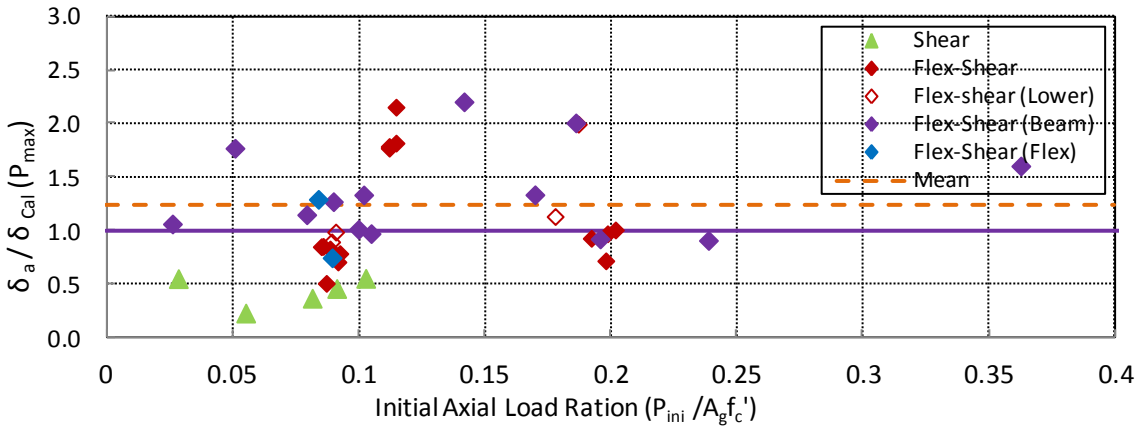

(b) Calculated column drift at axial-load failure with maximum axial load P_{max}

Figure 5.12 Evaluation of shear-friction model

Results in Figure 5.12(a) show that calculated drift based on initial axial load P_{ini} tends to overestimate the column drift capacity at axial-load failure for most flexure-shear-critical columns. With more accurate estimation of the column axial load level (the maximum axial load in this case), the calculated drift seems to represent the mean value of the drift capacity at axial-load failure, though with large variability existed in the data.

Table 5.1 Statistical results of shear-friction model

	Min	Max	Mean	Median	Standard Deviation	COV (%)
$\delta_a / \delta_{Cal} (P_{ini})$	0.42	2.03	0.97	0.88	0.39	40.4
$\delta_a / \delta_{Cal} (P_{max})$	0.51	2.20	1.23	1.01	0.48	39.2

5.3.3 Comparison with the Cyclic Test Data

Elwood and Moehle (2003) suggested that effective coefficient of friction μ calculated based on axial load P and critical crack angle θ could be related to the column drift at axial-load failure. Figure 5.13 plots the calculated coefficient of friction μ with the measured drift at axial-load failure for columns in The Database, with (a) coefficient μ calculated based on initial axial load P_{ini}; (b) coefficient μ calculated based on maximum axial load P_{max}. The purple solid line represents the Equation 5.3 recommended by Elwood and Moehle (2003).

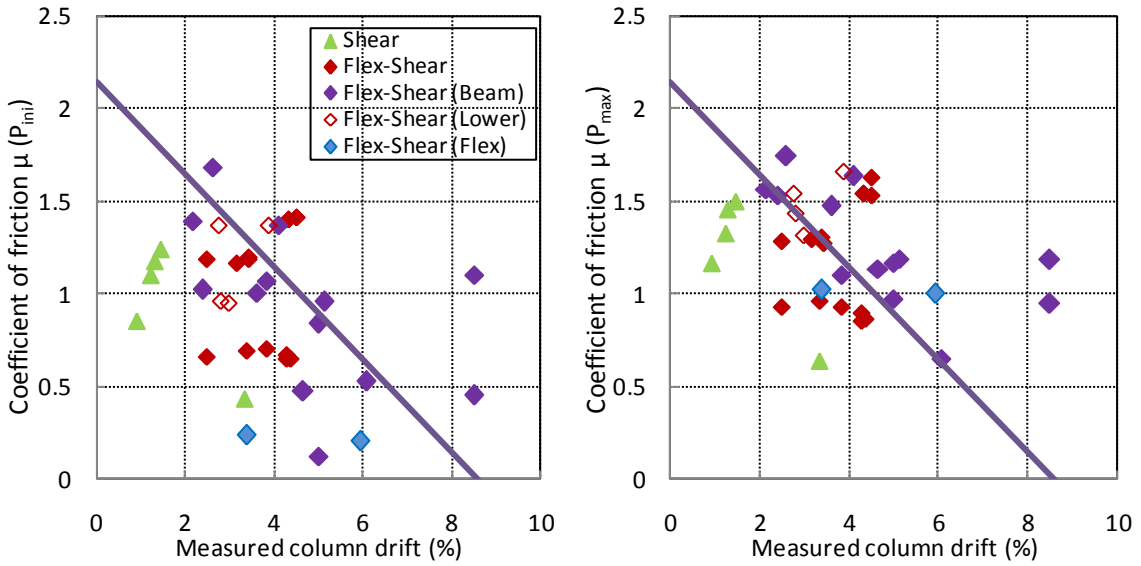

(a) Calculated drift based on P_{ini} (b) Calculated drift based on P_{max}

Figure 5.13 Relation between effective coefficient of friction μ and column drift at axial-load failure

Results in Figure 5.13 show that if calculating the coefficient of friction μ based on maximum axial load P_{max} for shear-critical columns, the measured drift is evenly distributed around the solid purple line. If calculating the μ based on initial axial load P_{ini}, the data is likely to be shifted towards left and become more scattered. While columns were subjected to varying axial load during shaking table tests, it is believed that maximum axial load

P_{max} represented the column axial load stress level at axial-load failure better than the designed axial load P_{ini}. Results in Figure 5.13(b) indicate that the column drift at axial-load failure during the dynamic tests follows a similar trend to that observed from the cyclic test data.

For shear-critical columns, no such trend was observed and the coefficient of friction μ seemed to be positively correlated to the column drift at axial-load failure. However, no reliable conclusion could be drawn due to the limited number of test data.

Figure 5.14 plots the Shear-Friction model with the measured drift at axial-load failure with (a) columns in the Database; and (b) columns from Lynn (2001) tests and Sezen (2002) Tests.

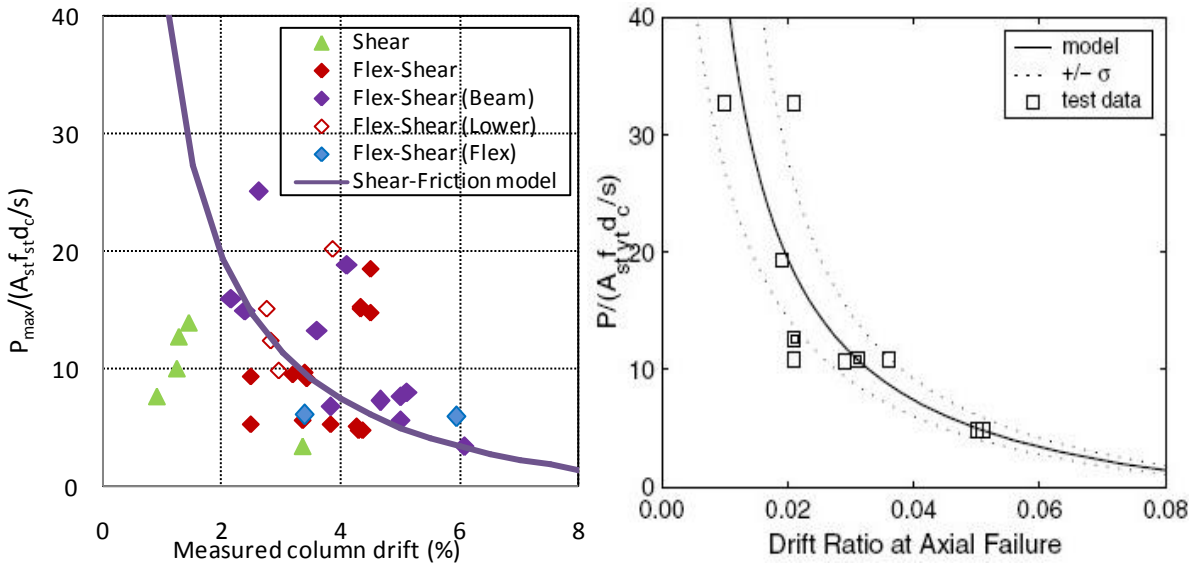

(a) Columns in The Database (b) Columns in static cyclic tests

Figure 5.14 Evaluation of shear-friction model by dynamic and cyclic test data

The concave curve in Figure 5.14 indicated that the Shear-Friction model is very sensitive to the axial load factor and transverse reinforcement details. Especially for columns subjected to relatively low axial load, a small change in axial load level may result in a significant difference in the predicted column drift capacity.

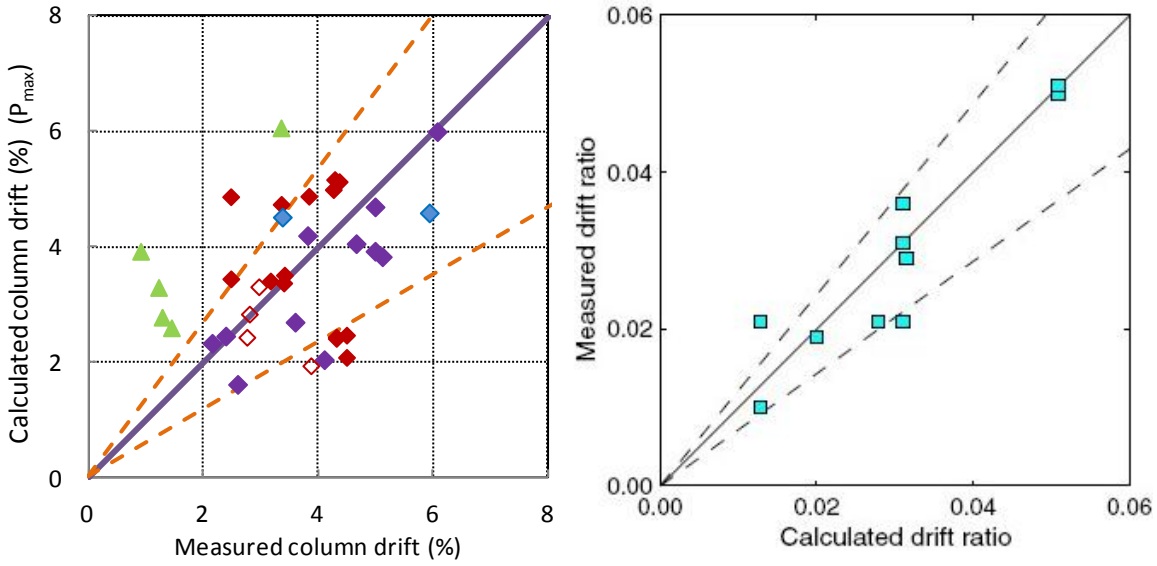

(a) Columns in The Database (b) Columns in static cyclic tests

Figure 5.15 Evaluation of shear-friction model by dynamic and cyclic tests data

5.4 Evaluation of Kato and Ohnishi (2002) Model

5.4.1 Procedure

The drift capacity model proposed by Kato and Ohnishi (2002) discussed in section 4.4 could also be applied to estimate the column drift at axial load failure δ_a by using $m = 3.6$:

$$\frac{\Delta_a}{L} = \frac{\Delta_y}{L} + \frac{\Delta_P}{L}$$

$$\frac{\Delta_P}{L} = \begin{cases} D\left(\frac{m\varepsilon_{cp}}{j_e}\right)\left(\frac{2}{3e_n}\right) \leftarrow \left(0 < e_n < 1/3\right) \\ D\left(\frac{m\varepsilon_{cp}}{j_e}\right)\left(\frac{2}{3\left(5e_n - \frac{4}{3}\right)}\right) \leftarrow \left(1/3 \le e_n < 2/3\right) \end{cases}$$

Equation 5.5

5.4.2 Evaluation with The Database

The calculated plastic column drift is compared with the measured plastic drift at axial-load failure in Figure 5.16. Results show that Kato and Ohnishi (2002) model generally overestimate the plastic column drift at axial-load failure.

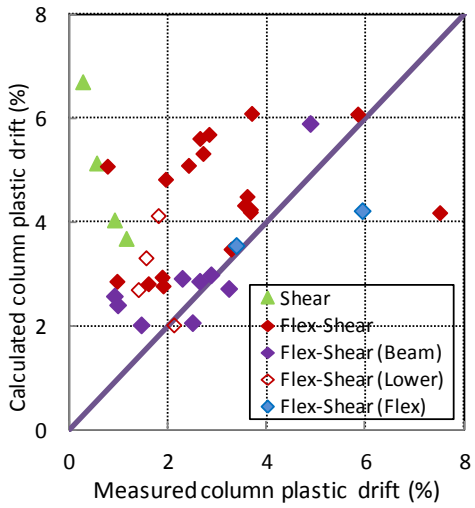

Figure 5.16 Calculated column plastic drift at axial-load failure by Kato and Ohnishi (2002) model

The accuracy of the Kato and Ohnishi (2002) model largely depends on the accuracy of estimated column yield drift. The calculated column drift at shear failure are compared with the measured drift at axial-load failure in Figure 5.17.

The test data seems to be scattered around a dashed line parallel to the diagonal unit line in Figure 5.17, indicating the coefficient m selected as 3.6 based on the cyclic test data might be too large when estimating the drift capacity at axial-load failure for columns subjected to earthquake load.

The ratio of measured drift at axial-load failure to calculated column drift is plotted in Figure 5.18. Results show that Kato and Ohnishi (2002) model overestimates the column drift capacity for most of the flexure-shear-critical columns.

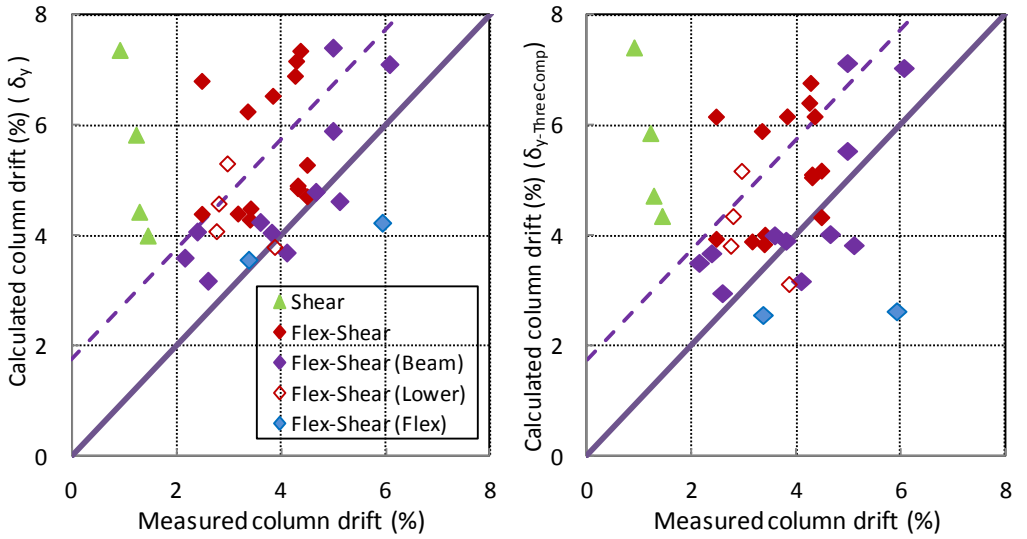

(a) Calculated drift based on δ_y (b) Calculated drift based on $\delta_{y-ThreeComp}$

Figure 5.17 Calculated column drift at axial-load failure by Kato and Ohnishi (2002) model

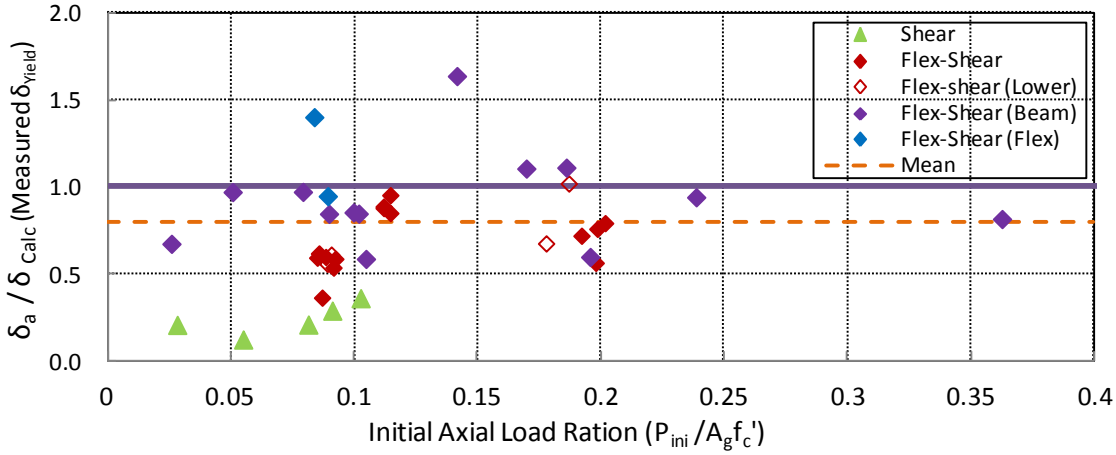

(a) The ratio of measured drift to calculated drift with measured yield drift δ_y

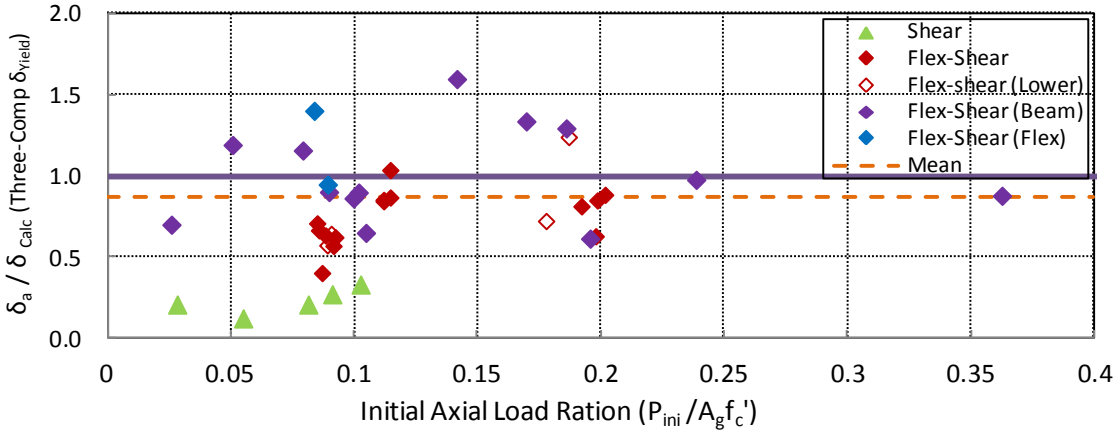

(b) The ratio of measured drift to calculated drift with yield drift from three-components $\delta_{y-ThreeComp}$

Figure 5.18 Evaluation of Kato and Ohnishi (2002) model

Table 5.2 Statistical results of Kato and Ohnishi (2002) model

	Min	Max	Mean	Median	Standard Deviation	COV (%)
δ_a / δ_{Cal} ($\delta_{y\text{-}Meas}$)	0.36	1.64	0.80	0.82	0.25	31.0
δ_a / δ_{Cal} ($\delta_{y\text{-}ThreeComp}$)	0.40	1.60	0.87	0.85	0.27	30.8

5.5 Evaluation of Zhu et al. (2006) Model

5.5.1 Procedure

Based on a database consisting 28 columns that experienced axial load loss during unidirectional pseudo-static tests, Zhu et al. (2006) proposed a probability model to give the median prediction of the column drift at axial-load failure for flexure-shear-critical columns that experience yielding before shear failure.

According to the classic shear-friction model proposed by Elwood and Mohele (2005), the coefficient of friction μ could be expressed by Equation 5.2:

$$\mu = \frac{\frac{P}{A_{st} f_{st} d_c / s} - 1}{\frac{P}{A_{st} f_{st} d_c / s}\frac{1}{\tan\theta} + \tan\theta}$$

Subsequently, Zhu et al. (2006) related the coefficient μ with the drift capacity at axial-load failure for the 28 columns and proposed to estimate the median drift capacity by:

$$\left(\delta_{Axial}\right)_{median} = 0.184\exp\left(-1.45\mu\right) \qquad \text{Equation 5.6}$$

5.5.2 Evaluation of Zhu et al. (2006) Model

Figure 5.19 plots the calculated column drift by Zhu et al. (2006) model with the measured drift at axial-load failure with (a) calculated column drift based initial axial load P_{ini}; (b) calculated column drift based maximum axial load $P_{\max}$.

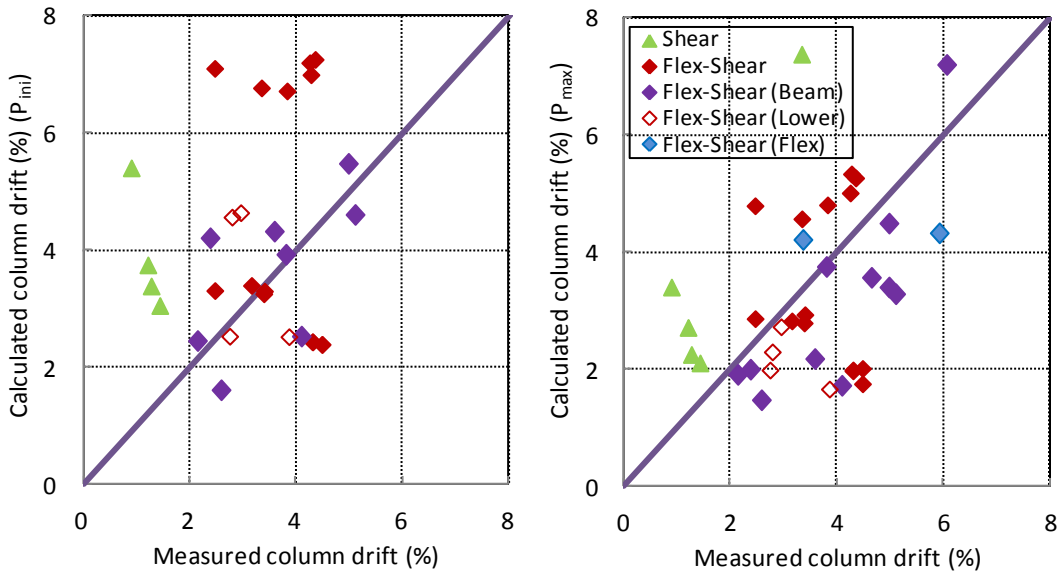

(a) Calculated drift based on P_{ini} (b) Calculated drift based on P_{max}

Figure 5.19 Calculated column drift at axial-load failure by Zhu et al. (2006) model

Notice that this probability model is a deterministic model developed independent of the shear capacity of the columns. Therefore, if the calculated drift at axial-load failure is lower than the column drift at shear failure by Zhu et al. (2006) model introduced in section 4.5, the axial-load failure should be considered occurred simultaneously with the shear failure and the drift capacity at shear failure should be used instead. Considering the above assumptions, the calculated column drift by Zhu et al. (2006) model is adjusted and plotted in Figure 5.20.

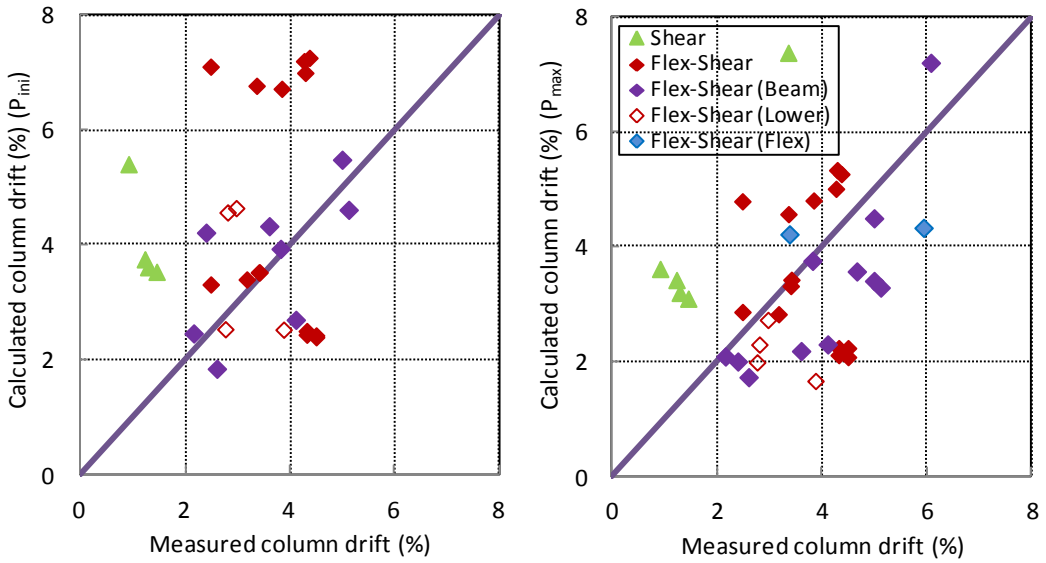

(a) Calculated drift based on P_{ini} (b) Calculated drift based on P_{max}

Figure 5.20 Adjusted calculated column drift at axial-load failure by Zhu et al. (2006) model

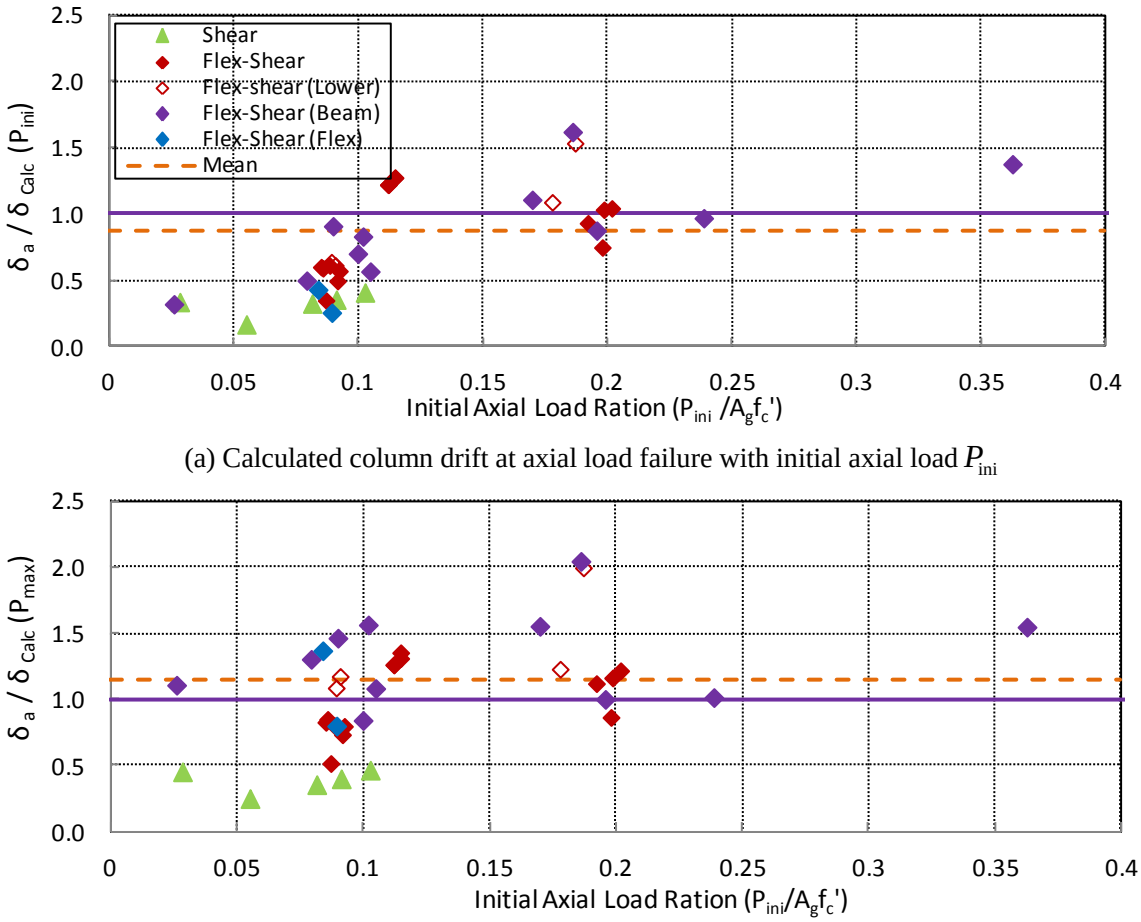

(a) Calculated column drift at axial load failure with initial axial load P_{ini}

(b) Calculated column drift at axial load failure with maximum axial load P_{max}

Figure 5.21 Evaluation of Zhu et al. (2006) model

The ratio of measured column drift to calculated drift δ_a / δ_{Cal} is plotted in Figure 5.21. Results in Figure 5.20(a) and Figure 5.21(a) show that the calculated column drift based on initial axial load P_{ini} tends to overestimate the column capacity at axial-load failure for most flexure-shear-critical columns.

The data in Figure 5.20 (b) is distributed more evenly along the diagonal unit line, indicating that with relatively accurate estimation of column axial load level (maximum axial load P_{max} in this case), Zhu et al. (2006) model tends to represent the mean value of the column drift capacity fairly well.

Table 5.3 Statistical results of Zhu et al. (2006) model

	Min	Max	Mean	Median	Standard Deviation	COV (%)
δ_a / δ_{Cal} (P_{ini})	0.32	1.62	0.87	0.88	0.34	39.4
δ_a / δ_{Cal} (P_{max})	0.52	2.05	1.15	1.12	0.34	29.6

5.5.3 Comparison with Static Cyclic Test Data

The Zhu et al. (2006) probability model was developed based on the test data of 28 columns subjected to cyclic lateral load. The calculated column drift for these columns is plotted in Figure 5.22 (b).

Results in Figure 5.22 show that Zhu et al. (2006) could capture the mean value of column drift at axial-load failure for columns in both the dynamic tests and cyclic tests fairly well.

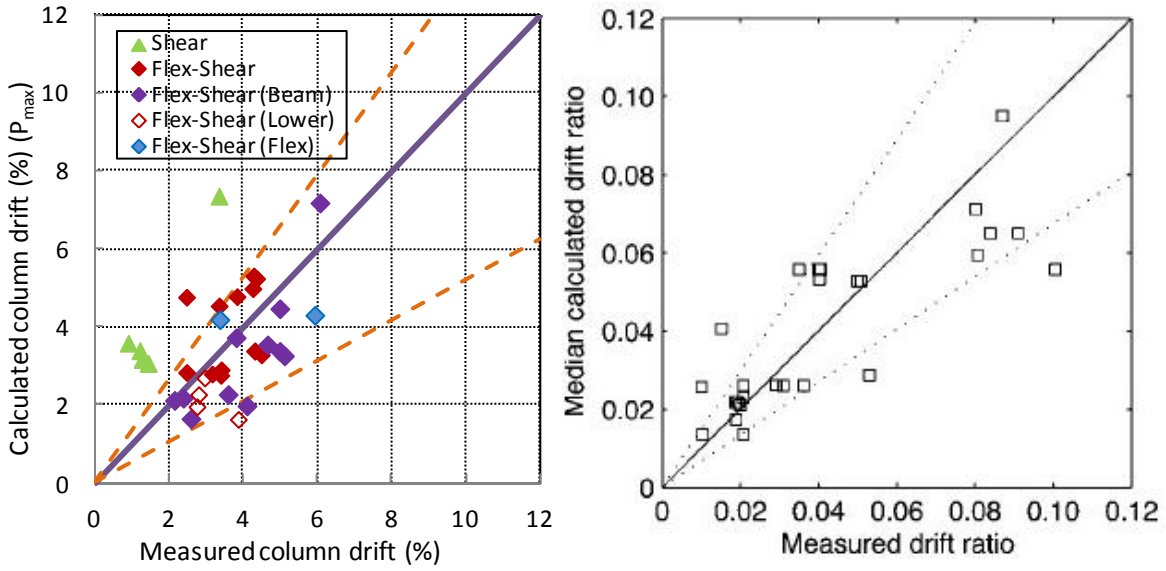

(a) Columns in The Database (b) Columns in static cyclic tests

Figure 5.22 Evaluation of Zhu et al. (2006) model with the dynamic and cyclic test data

5.6 Effect of Number of Cycles

Figure 4.23 plots the number of cycles that columns went through up to the axial-load failure with the normalized measured column drift.

The ordinate of Figure 4.23 is the normalized column drifts obtained from dividing the measured column drift by the calculated drift. The calculated drift at axial-load failure was obtained from Shear-Friction model (discussed in section 5.3.1) based on the maximum axial load ratio and measured shear strength. Using the normalized column drifts could roughly take into account the effect of axial load ratio and shear stress level and gain a better idea of the relations between number of cycles and column drift capacity.

In Figure 5.23 (a), there is a positive correlation between the number of cycles and normalized column drift at axial-load failure. This could be explained by the fact that the cracks in one direction would be closed when column deformed to the opposite direction and

the column damage was more evenly distributed as the column went through more reverse cycles.

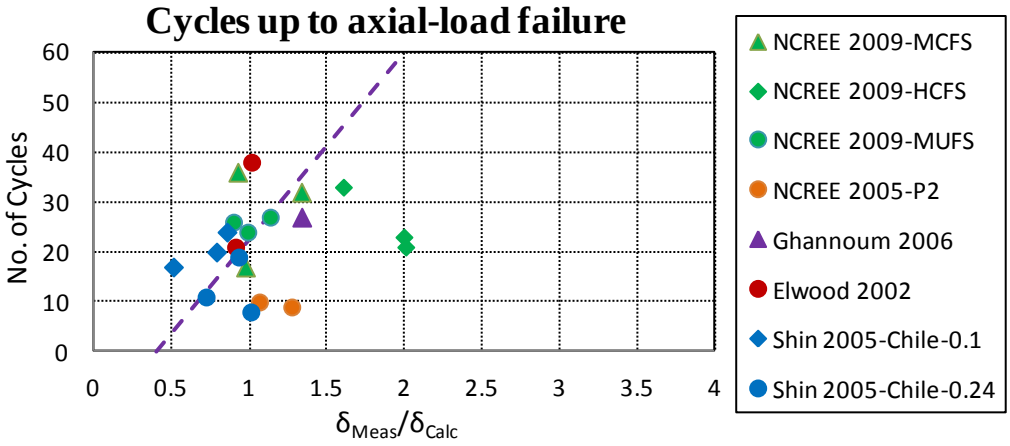

(a) Number of cycles with normalized column drift at axial-load failure

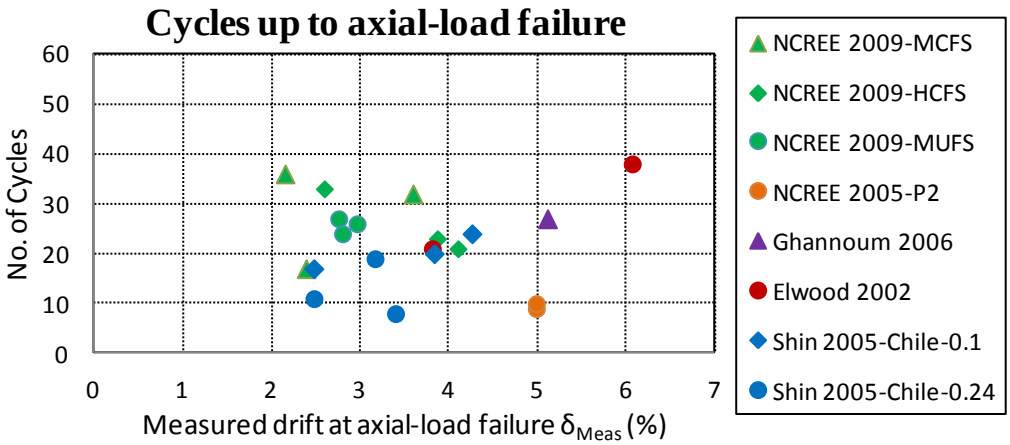

(b) Number of cycles with column drift at axial-load failure

Figure 5.23 Number of cycles with column drift capacity at axial-load failure

Chapter 6: Evaluation of ACSE/SEI 41-06 Supplement

6.1 Introduction

This chapter focuses on using The Database to evaluate the provisions of the current seismic rehabilitation standard ASCE/SEI 41 regarding reinforced concrete columns, such as column shear strength, column classification and level of conservertism for modeling parameters. Some refinements and changes of this standard are provided based on the test data from The Database.

6.2 Column Shear Strength

6.2.1 Evaluation of Shear Strength Ratio V_{Max}/V_n

For columns with inadequate transverse reinforcement, ASCE/SEI 41 adopted the shear strength model proposed by Sezen (2004) .According to ASCE/SEI 41, column shear strength V_n could be calculated by Equation 6.1.

$$V_n = kV_0 = k\left(V_c + V_t\right)$$

$$V_c = \lambda\left(\frac{0.5\sqrt{f_c'}}{M/Vd}\sqrt{1+\frac{N_u}{0.5\sqrt{f_c'}A_g}}\right)0.8A_g \qquad \text{Equation 6.1}$$

$$V_t = \begin{Bmatrix} \frac{A_v f_y d}{s} \leftarrow \left(s/d\right) \le 0.5 \\ 0.5\frac{A_v f_y d}{s} \leftarrow 0.5 < \left(s/d\right) \le 1.0 \\ 0 \leftarrow \left(s/d\right) > 1.0 \end{Bmatrix}$$

The definition of each parameter could be found in Sezen (2004) model introduced in section 1.2.3 of this thesis. It is recommended by ASCE/SEI 41 that if spacing of column transverse reinforcement is larger than half of the effective depth of column section

($s > d/2$) in the direction of applied shear force, the transverse reinforcement should be taken as no more than 50% effective when resisting shear or torsion, and thus $V_s = 0.5A_v f_y d / s$ .Moreover, if the spacing is larger than the effective depth of the column section ($s > d$), the transverse reinforcement shall be considered ineffective and set $V_s = 0$.

In order to evaluate the accuracy of column shear strengths estimated by ASCE/SEI 41, the shear strength ratio is calculated by dividing measured maximum lateral force V_{Max} by calculated shear strength V_n. The results are plotted in Figure 6.1 and grouped by the failure types of columns (discussed in section 1.1.3). The dashed line represents the mean value of the shear strength ratio for flexure-shear-critical columns.

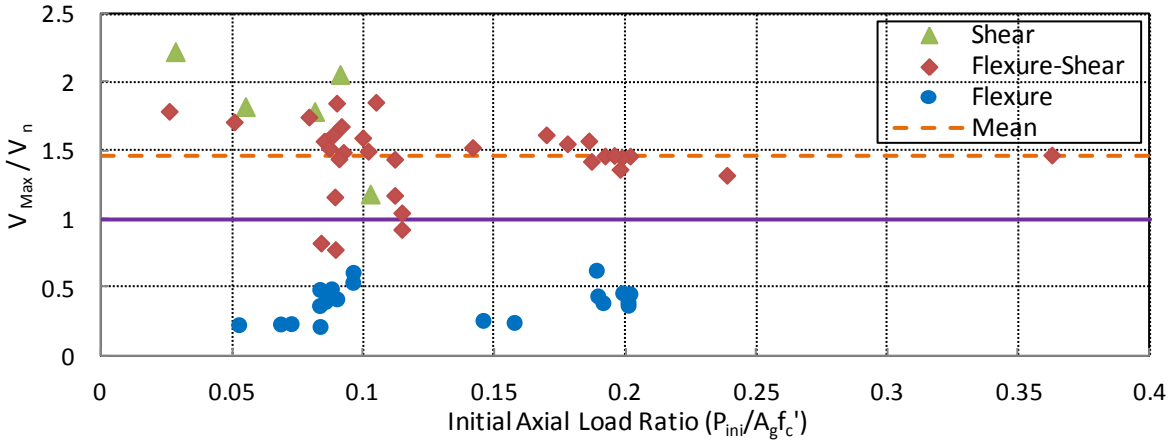

Figure 6.1 Evaluation of shear strength ratio (V_{Max}/V_n)

For flexure-shear-critical and shear-critical columns, the shear strength ratio data are well above the horizontal line representing the case that measured shear strength exactly matches the calculated value, indicating the ASCE/SEI 41 generally underestimates the shear strength for non-ductile columns. The mean value of V_{Max}/V_n is 1.45 for flexure-shear columns with a coefficient of variation of 18.3%.

Since the ASCE/SEI 41 shear strength model is mainly proposed to calculate the shear strength of non-ductile columns, it provides a poor estimation for shear resistance of ductile columns. This may be attributed to the fact that the plastic demand was much smaller than the shear strength for flexure-critical columns and those ductile columns encountered flexure yielding before achieving the shear strength.

6.2.2 Evaluation of Shear Strength Ratio V_{Max}/V_0

When estimating column shear strength by ASCE/SEI 41, modifier factor *k* is applied to account for the reduction of column drift capacity due to high ductility demand. If the modifier factor *k* is removed, shear strength could be estimated as $V_0 = V_n / k = V_c + V_s$.

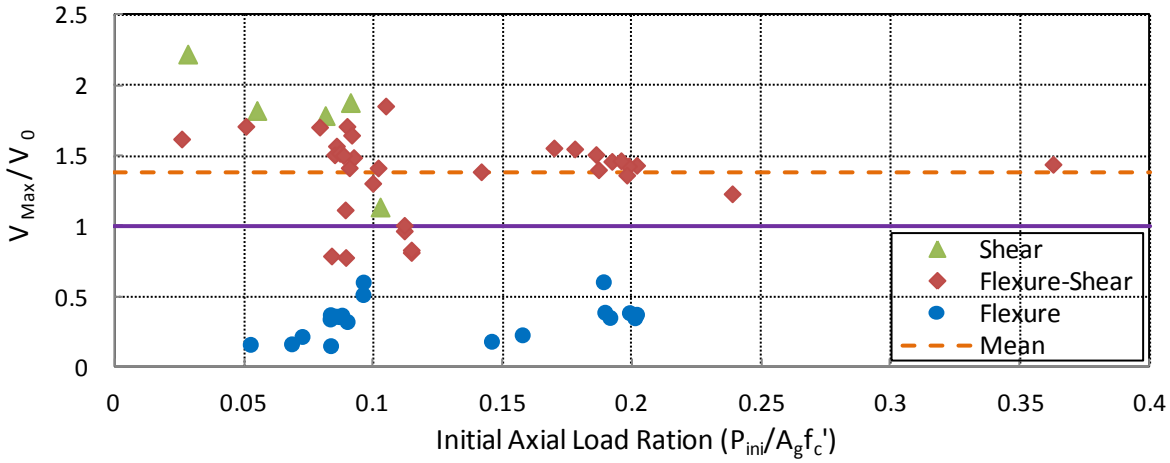

Figure 6.2 Evaluation of shear strength ratio (V_{Max}/V_0)

Figure 6.2 plots the shear strength ratio V_{Max}/V_0. For flexure-shear-critical columns, ignoring the reduction due to ductility demand brings the data closer to the unit horizontal line. The statistical results in Table 6.1 also indicate that the calculated V_0 provides a better estimation of column shear strength (the mean value decreased from 1.45 to 1.38). V_0 still underestimated the shear strength for shear critical columns.

6.2.3 Evaluation of Shear Strength Ratio V_{Max}/V_0'

Further, if reduction on transverse reinforcement contribution is ignored for columns with widely spaced ties ($s/d > 0.5$ or $s/d > 1.0$), the shear strength could be calculated as V_0' by Equation 6.2.

$$V_0' = V_n'/k = V_c + V_s'$$
$$V_c = \lambda \left(\frac{0.5\sqrt{f_c'}}{M/Vd} \sqrt{1 + \frac{N_u}{0.5\sqrt{f_c'} A_g}} \right) 0.8A_g \qquad \text{Equation 6.2}$$
$$V_s' = \frac{A_v f_y d}{s}$$

The resulting shear strength ratio V_{Max}/V_0' is evaluated in Figure 6.3.

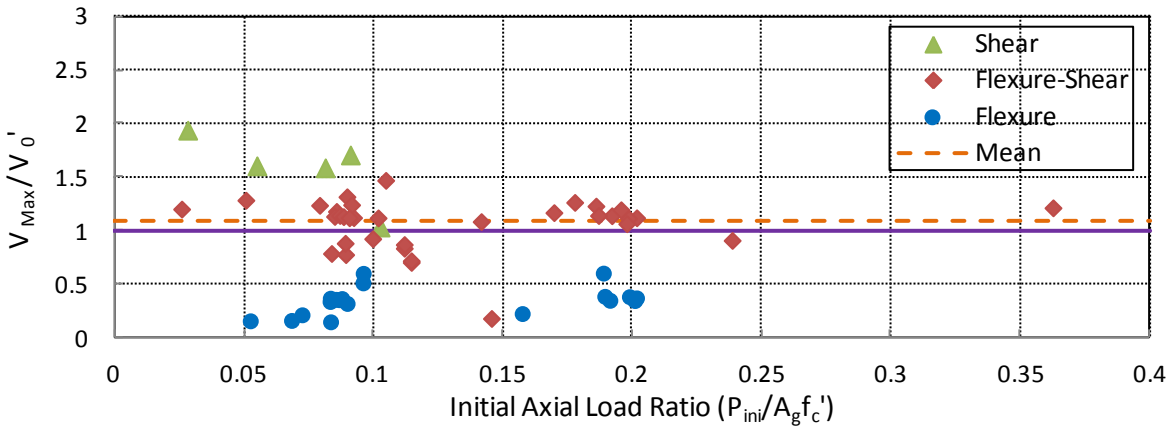

Figure 6.3 Evaluation of shear strength ratio (V_{Max}/V_0')

Results show that for flexure-shear-critical columns, calculated shear strength V_0' tends to represent the mean value of column shear strength. The resulted shear strength ratio has a coefficient of variation of 17.0% and mean value of 1.09.

It is observed that V_0' underestimates the shear strength of shear-critical columns compared to that of flexure-shear-critical columns. It is observed that a sudden increase in lateral force occurred in the cycle of shear failure for shear-critical columns, as shown in Figure 6.4.

The shear-critical columns in NCREE 2007 Tests have low aspect ratio a/d (around 1.5 for columns in specimen S3 and 2. 0 for columns in S4) that exceeded the property range of the Sezen (2002) database ($2<a/d<4$) that the shear strength model was developed based on. The columns have relative heavy longitudinal reinforcement ($\rho_l = 3.24\%$) and very light transverse reinforcement ($\rho_t = 0.067\%$). The behaviour of 90-degree hooks of the transverse reinforcement could not be estimated reliably. Scaled from full size columns, some shear-critical columns may experience higher strain rate during the dynamic tests, which contributed to the increase in column lateral resistances.

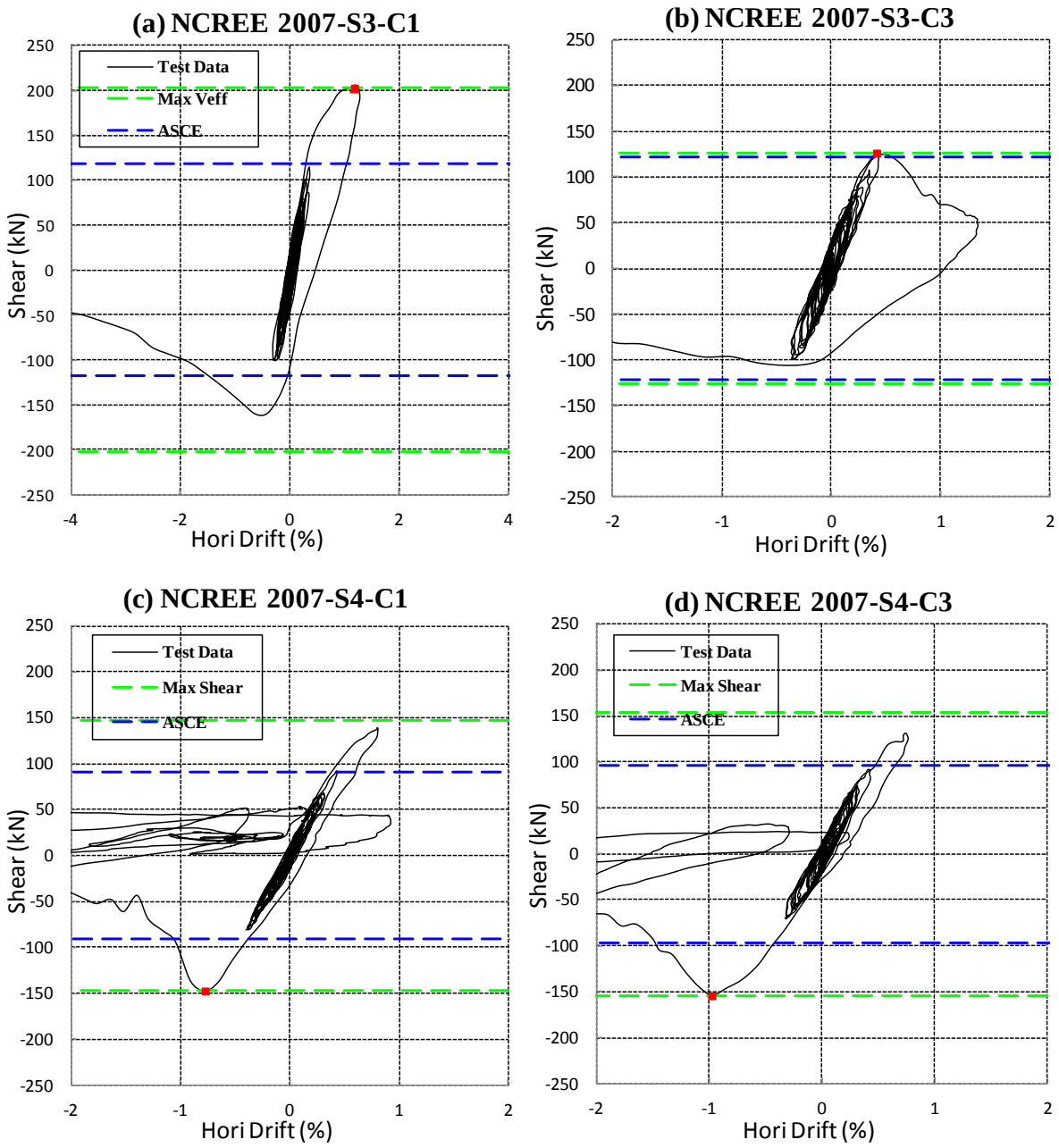

Figure 6.4 Sudden increase in lateral resistance for columns in NCREE 2007 Tests

6.2.4 Influence of Axial Load Ratio

In the above evaluation of column shear strength, initial axial load ratio was used to estimate the shear strength. However, columns subjected to dynamic loads would experience varying axial loads due to the overturning moment. Other axial loads measured during the tests, such as maximum axial load P_{max} and the axial load $P_{MaxVeff}$ at the time that columns achieved maximum effective force, could also be applied in the shear strength model. The corresponding shear strength ratio is plotted in Figure 6.5. Results show that shear strength ratio is not very sensitive to the selected axial load ratio. Shear strength V_0' calculated by following ASCE/SEI 41 procedure could represent the mean value of column shear strengths fairly well and is not very sensitive to the applied axial load ratio.

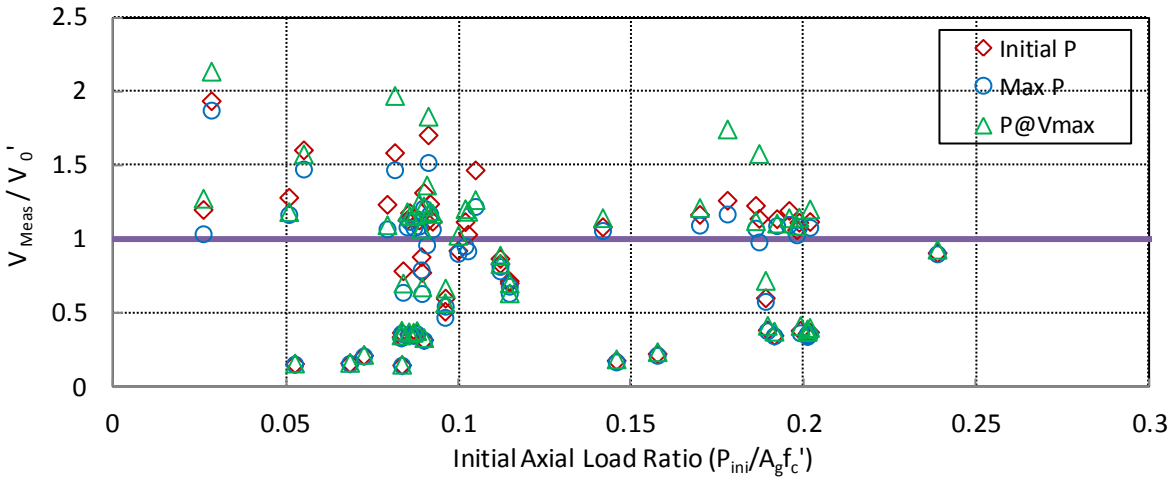

Figure 6.5 Shear strength ratio calculated with different axial load ratio

Table 6.1 summarizes the statistical characteristics for the aforementioned methods of estimating column shear strength.

Table 6.1 Evaluation of ASCE/SEI 41 shear strength model

Method	Min	Max	Mean	Median	Standard Deviation	COV (%)
(a)flexure-shear-critical columns						
$V_n = kV_0 = k\left(V_c + V_s\right)$	0.78	1.85	1.45	1.48	0.26	18.3
$V_n' = kV_0' = k\left(V_c + V_s'\right)$	0.78	1.85	1.38	1.44	0.29	20.7
$V_0' = V_c + V_s'$	0.70	1.47	1.09	1.13	0.18	16.9
$V_0' = V_c + V_s'$ (w. P_{max})	0.63	1.22	1.00	1.07	0.17	17.2
$V_0' = V_c + V_s'$ (w. P@V_{Max})	0.64	1.24	1.03	1.08	0.17	16.9
(b)shear-critical columns						
$V_n = kV_0 = k\left(V_c + V_s\right)$	1.18	2.22	1.82	1.82	0.40	21.7
$V_n' = kV_0' = k\left(V_c + V_s'\right)$	1.14	2.22	1.77	1.72	0.39	22.3
$V_0' = V_c + V_s'$	1.04	1.94	1.58	1.61	0.33	21.1
$V_0' = V_c + V_s'$ (w. P_{max})	0.92	1.88	1.45	1.48	0.34	23.5
$V_0' = V_c + V_s'$ (w. P@V_{Max})	0.97	2.14	1.65	1.80	0.45	27.0

6.3 Column Classification

6.3.1 ASCE/SEI 41 Column Classification

According to ASCE/SEI 41, columns are classified into three conditions based on shear strength V_n, plastic shear capacity V_p and transverse reinforcement detailing. As illustrated in Figure 1.3 in section 1.2.4, columns in Condition i roughly correspond to flexure-critical columns, while columns in Condition ii and iii generally referred to flexure-shear-critical columns and shear-critical columns respectively.

The accuracy of the ASCE/SEI 41 classification method could be evaluated by the matrix shown in Table 6.2. The diagonal data in the blue zone indicates the number of columns that are classified properly, for example, "5" indicates that there were 5 columns failed in shear during the tests and were also classified as shear-critical columns by ASCE/SEI 41. The column data that falls in the green zone provides a "safer" estimation of

the column failure type in terms of column drift capacity, for example "23" indicates that there were 23 columns that are classified as shear-critical columns, yet were observed to have experienced flexure-shear failure during the tests. On the other hand, we would prefer to avoid classifying the column into the red zone.

When evaluating the performance of column classification method recommended by ASCE/SEI 41, only columns that were observed to experience failure during the tests are included in the Table 6.2, ensuring sure that the "observed failure type" is fairly reliable.

Table 6.2 Evaluation of ASCE/SEI 41 column classification method

$1.0 \geq V_p / V_0 > 0.6$ $\rightarrow$ *Flexure – Shear*		ASCE/SEI 41 Classification			
		Flexure (Condition i)	**Flexure-Shear (Condition ii)**	**Shear (condition iii)**	**Total**
Observed Failure Type	**Flexure**	0	2	0	2
	Flexure-Shear	0	4	23	27
	Shear	0	0	5	5
	Total	0	6	28	34

Table 6.2 shows that five columns that were observed to experience pure shear failure are classified properly by ASCE/SEI 41.

In NCREE 2007 tests, two ductile outside columns C1 and C3 were observed to experience flexure failure, yet were classified as condition ii columns. ASCE/SEI 41 adopts $V_p \leq 0.6V_0$ as the criteria for the condition i and those two flexural-critical columns had ratio of V_p / V_0 slightly above 0.6 (0.66 and 0.68 respectively). This conservatism is appropriate since ASCE/SEI 41 intends to avoid the case that flexure-shear-critical columns are unconservatively classified as flexure-critical columns in condition i.

Most flexure-shear-critical columns were misclassified under condition iii. According to ASCE/SEI 41, shear failure occurs at zero plastic rotation for columns in condition iii,

which is way too conservative for most non-ductile columns since these columns usually developed certain deformation prior to the shear failure. Misclassifying flexure-shear-critical columns into condition iii would greatly underestimate the drift capacities of columns.

As discussed in section 6.2.3, column shear strength V_n calculated by ASCE/SEI 41 is generally much lower than measured column shear capacity. It is intuitive that column classification procedure should use the 'real' shear strength to classify columns, instead of being conservative as is commonly done in strength based assessments.

Therefore, it is better to ignore the reduction due to large-spacing transverse reinforcement as specified in ASCE/SEI 41 and use $V_0^{'} = V_n^{'} / k = V_c + V_s^{'}$ when estimating shear strength. Table 6.3 summarized the results of this variation of the ASCE/SEI 41 classification method. Most of the flexure-shear-critical columns are classified properly.

Table 6.3 Evaluation of variation of ASCE/SEI 41 classification method

$1.0 \geq V_p / V_0^{'} > 0.6$ $\rightarrow$ *Flexure – Shear*		ASCE/SEI 41 Classification			
		Flexure (Condition i)	**Flexure-Shear (Condition ii)**	**Shear (Condition iii)**	**Total**
Observed Failure Type	**Flexure**	0	2	0	2
	Flexure-Shear	0	14	13	27
	Shear	0	0	5	5
	Total	0	16	18	34

It is noticed that for most flexure-shear-critical columns that are misclassified as Condition iii, the ratio of plastic shear capacity V_p over shear strength $\left(V_n^{'}/k\right)$ is just slightly above 1.0 and it is too conservative to classify these columns as shear-critical columns.

If the criterion for flexure-shear columns is changed to $1.1 \geq V_p / \left(V_n^{'}/k\right) > 0.6$ instead of $1.0 \geq V_p / \left(V_n^{'}/k\right) > 0.6$, the results of modified ASCE/SEI 41 classification method are summarized in Table 6.4.

Table 6.4 Evaluation of modified ASCE/SEI 41 classification method

$1.1 \geq V_p / \left(V_n^{'}/k\right) > 0.6$ $\rightarrow$ *Flexure – Shear*		ASCE/SEI 41 Classification			
		Flexure (Condition i)	**Flexure-Shear (Condition ii)**	**Shear (Condition iii)**	**Total**
Observed Failure Type	**Flexure**	0	2	0	2
	Flexure-Shear	0	27	0	27
	Shear	0	0	5	5
	Total	0	29	5	34

Results in Table 6.4 shows that by using non-reduced column shear strength ($V_0' = V_n'/k$) and the modified classification criteria, all flexure-shear-critical columns are classified properly by failure type and thus the resulting load-deformation relation will be more accurate and result in a more economical retrofit solution. In the following sections, columns are classified based on the modified ASCE/SEI classification method.

6.4 Modeling Parameters of Generalized Load-Deformation Relation

6.4.1 Measured Plastic Rotations

During seismic response of older concrete frames, plastic rotations are generally concentrated at the ends of concrete columns. In Ghaunnoum 2006 tests, column rotations are measured over a plastic hinge with length equal to the depth of column section. However, there is lack of consensus on the plastic hinge length. Also it is very difficult to measure column rotations at the ends directly for most shaking table tests. Therefore, column rotation

is taken as the inter-story drift ratio, which assumes that the plastic hinge length equals to column clear height *L*.

The yield rotation θ_y equals to the column drift at column yielding and plastic rotation at shear failure and axial-load failure can be calculated by Equation 6.3.

$$\theta_y = \frac{\Delta_y}{L} = \frac{a}{3}\frac{M_p}{EI_{ASCE}} \qquad \text{Equation 6.3}$$

Where *L* = the column clear height, *a* = the shear span that equals to *L/2* for fixed-fixed columns. M_p = the moment strength obtained from section analysis; EI_{ASCE} = the effective column stiffness recommended by ASCE/SEI 41 (discussed in section 3.4).

According to ASCE/SEI 41, plastic rotation at shear failure and axial-load failure is calculated by subtracting the yield rotation θ_y from total rotation. The total column rotation θ_l and θ_a is taken as the measured column drift at shear failure and axial-load failure. The method to obtain the plastic rotation is consistent with the definition used to construct the table of recommended modeling parameters in Elwood et al. (2007).

For the purpose of evaluating the modeling parameters a and b, the plastic rotation ratio are defined as the ratio of measured plastic rotation to the corresponding modeling parameters.

Plastic Rotation Ratio (PRR) at shear failure = $\left(\theta_l - \theta_y\right)\big/a$ Equation 6.4

Plastic Rotation Ratio (PRR) at axial-load failure = $\left(\theta_a - \theta_y\right)\big/b$ Equation 6.5

Where θ_l = the total rotation at shear failure; θ_a = the total rotation at axial-load failure; θ_y = the yield rotation.

6.4.2 Influence of Varying Column Axial Load

The recommended values of modeling parameters a and b for columns can be found in ASCE/SEI 41 (*Table 6-8 Modeling parameters and numerical acceptance criteria for nonlinear procedures-reinforced concrete columns*). For columns in condition i and iii, plastic rotations a and b are based on axial load ratio $P / A_g f_c^{'}$ and transverse reinforcement ratio $\rho_t = A_v / b_w s$; linear interpolation between values is required to achieve best estimation. For condition ii, modeling parameters a and b are obtained based on axial load ratio $P / A_g f_c^{'}$, transverse reinforcement ratio ρ_t and normalized shear stress $V / b_w d \sqrt{f_c^{'}}$; linear interpolation among these three variables can be done in any order.

Due to the overturning moment demands during the dynamic tests, outside columns in frame system are usually subjected to axial load (e.g. the maximum axial load P_{max}) larger than the initial axial load P_{ini}. Some middle columns in the frame were subjected to additional axial load imposed by prestressed force and the movement of the actuator during the shaking table tests caused varying axial load on columns. Also the calculated shear strength $V_0{}'$ for non-ductile columns may be different from the measured shear strength V_{Max}.

Since the modeling parameters a and b represent the plastic rotations at significant loss of lateral strength and loss of axial load support, a and b are compared with the measured plastic rotation at shear and axial-load failure for The Database in Figure 6.6 and Figure 6.7, respectively.

Similar to the evaluation in Chapter 4 and Chapter 5, the test data is grouped by the column failure type that generally corresponds to the ASCE/SEI 41 classification. The data series "Shear" (corresponding to the Condition iii in ASCE/SEI 41) in green triangular

marker represents the shear-critical columns included in the Database. The data series "Flex-Shear" (corresponding to the Condition ii in ASCE/SEI 41) in red diamond marker represents the flexure-shear-critical columns that were connected to a rigid beam on the upper end. The data series "Flex-Shear (Beam)" in purple diamond marker represents the flexure-shear-critical columns in the frame connected with flexure beam on the upper end and the data of measured drift may be higher than the actual column drift capacity due to the additional flexibility contributed by the beam. The "Flex-Shear (Lower)" in hollow red diamond marker represents the flexure-shear-critical columns that did not fail during the tests and the drift data could be considered as the lower bound of the column drift capacity. The "Flex-Shear (Flex)" in blue diamond marker represents the columns that experienced flexure failure during the test, yet were misclassified by ASCE/SEI 41 as flexure-shear-critical columns.

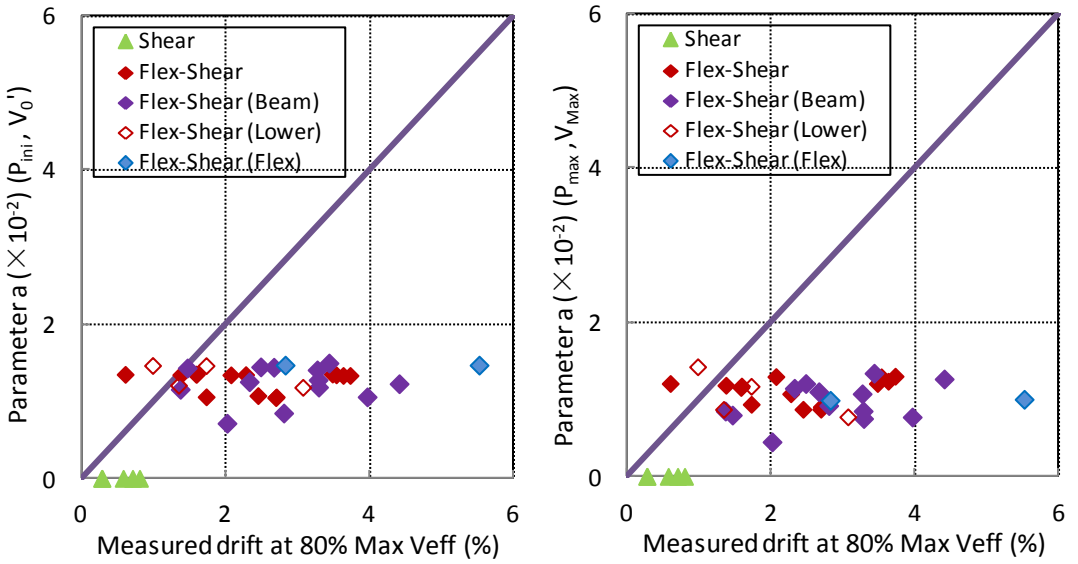

(a) Parameter a based on P_{ini} and V_0' (b) Parameter a based on P_{max} and V_{Max}

Figure 6.6 Evaluation of modeling parameter *a* for non-ductile columns

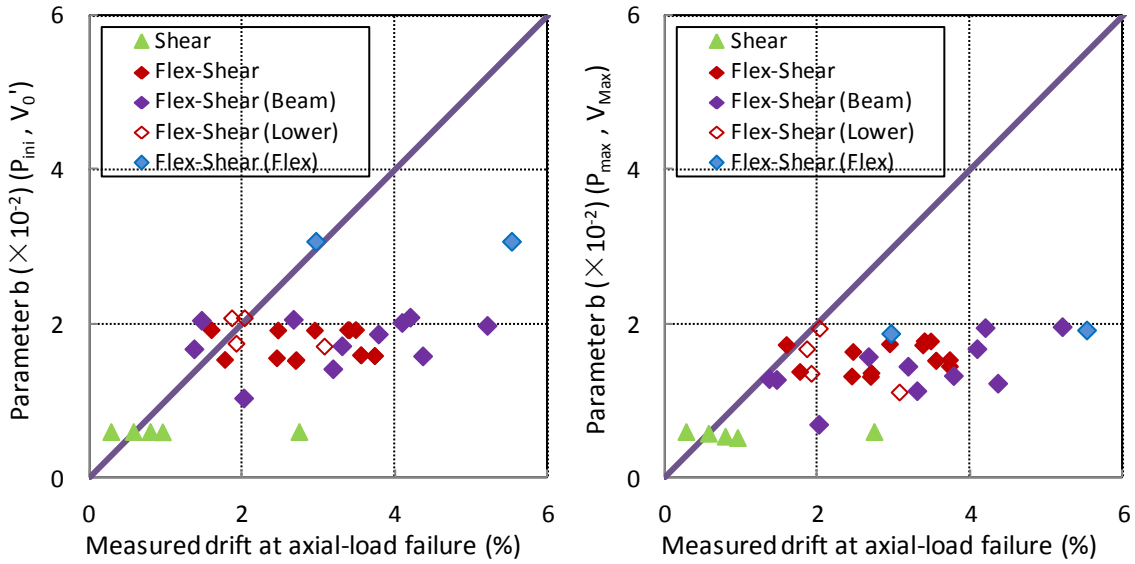

(a) Parameter b based on P_{ini} and V_0' (b) Parameter b based on P_{max} and V_{Max}

Figure 6.7 Evaluation of modeling parameter *b* for non-ductile columns

Results in Figure 6.6 and Figure 6.7 show that the modeling parameters a and b based on initial axial load P_{ini} and calculated shear strength V_0' are slightly higher than the results interpolated based on maximum axial load ratio P_{max} and measured shear strength V_{meas}. Yet the difference between the modeling parameter is less than 10% for most columns based on different column axial load and shear strength.

Also in structural design stage, engineer could only estimate the column plastic rotation at loss of lateral load based on the calculated shear strength and designed axial load level which could be represented by initial axial load ratio. Therefore for the assessment of level of conservatism provided by ASCE/SEI 41, modeling parameters a and b are interpolated based on initial axial load P_{ini} and calculated shear strength V_0' in the following sections.

6.4.3 Assessment of ASCE/SEI 41 Modeling Parameter a

6.4.3.1 Plastic Rotation Ratio at Loss of Lateral Resistance

As shown in Figure 1.1, modeling parameter *a* represents the column plastic rotation at significant loss of lateral resistant force. It is generally assumed that column shear failure occurred when the lateral force degrades to 80% of its peak strength and the lateral resistance would degrade rapidly afterwards.

Figure 6.8 plots results of the assessment of parameter *a* for columns in the database.

The data in solid markers in Figure 6.8 is PRR (plastic rotation ratio) for columns that actually failed during the test, while the hollow marker represents the PRR based on maximum drift ratio for columns that did not fail in tests and could be considered as lower bound of PRR.

The red solid diamond marker (Condition ii) represents the PRR for flexure-shear critical columns that were connected by rigid beam in reinforced concrete frame, while the PRR of non-ductile columns that were connected by a flexible beam are represented by purple solid diamond marker, namely Condition ii (Beam). Influenced by the deflection of the flexible beam, the measured column rotation may include significant rigid body rotation at the ends of columns. The PRR represented by purple solid diamond marker might be higher than the actual value and should be evaluated with caution. The horizontal line at 1.0 represents the case where test results exactly match the plastic rotation limit in ASCE/SEI 41.

Two ductile outside columns C1 and C3 in specimen S1 of NCREE 2007 tests were observed to experience flexure failure, yet classified as columns in condition ii. The yellow diamond marker, namely Condition ii (Flex-shear), represents the PRR for those two columns by following the procedure of interpolating table value *a* for columns in Condition

ii. Since these two columns demonstrated ductile response and experienced extended deformation, the PRR is much greater than 1 as expected. If the columns are considered to be in Condition i, as shown in yellow circular marker, the PRR is much closer to horizontal unit line and better estimations of plastic rotation are achieved.

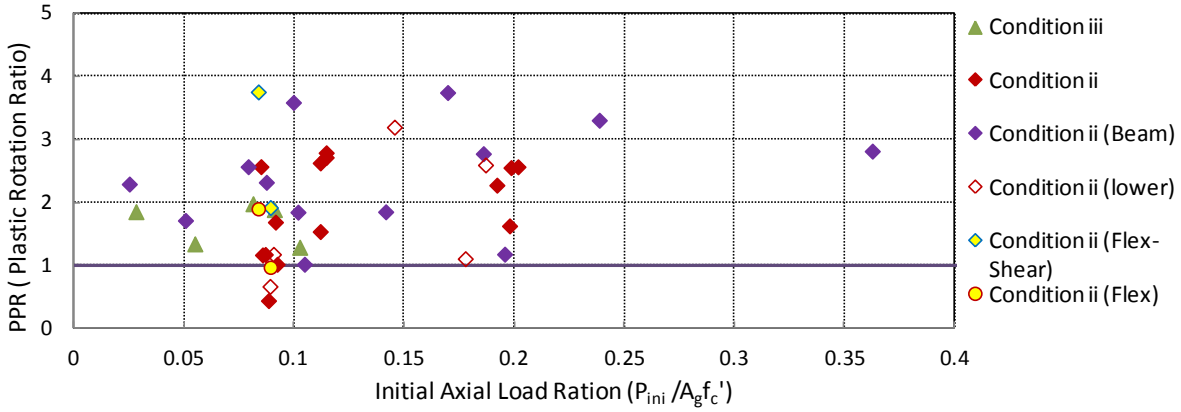

Figure 6.8 Plastic rotation ratio at significant loss of lateral resistant force

For columns in condition iii that are expected to experience shear failure prior to flexure yielding, ASCE/SEI 41 suggests that no plastic rotation could be relied upon the loss of lateral resistance force. Therefore, the plastic rotation ratio has to be replaced by total rotation ratio θ_l / θ_y in Figure 6.8, represented by triangular markers. Results indicated that ignoring all the plastic rotation is conservative for those shear-critical columns. However, the plastic rotation $\theta_l - \theta_y$ at the time of loss of significant lateral resistance for 6 shear-critical columns included in The Database is less than 1%, justifying the conservatism of recommendation of ASCE 41 for the sake of safety.

PRR for most flexure-critical columns is larger than 1, indicating ASCE/SEI 41 tends to provide conservative estimation of the plastic rotations at significant loss of lateral resistance for columns in condition ii. This conservatism is appropriate since axial capacity degradation is closely associated with the development of shear-failure plane. Almost all

columns in The Database were subjected to axial load ratio less than 0.25; hence caution should be taken when applying ASCE/SEI 41 to columns with higher axial load ratio.

6.4.3.2 Probability of Failure

From Figure 6.8, it is shown that significant scatter existed among the data of plastic rotation ratio, emphasizing the need to determine the level of safety provided by ASCE/SEI 41 provisions, rather than to analyze the mean value and coefficient variation of the data itself. Results of plastic rotation ratio could be represented by a lognormal cumulative distribution, commonly referred to as a fragility curve, as shown in Figure 6.9. The fragility curve is constructed based on the test data of flexure-shear-critical columns that experienced the shear failure during the tests (the data series in red diamond marker in Figure 6.8).

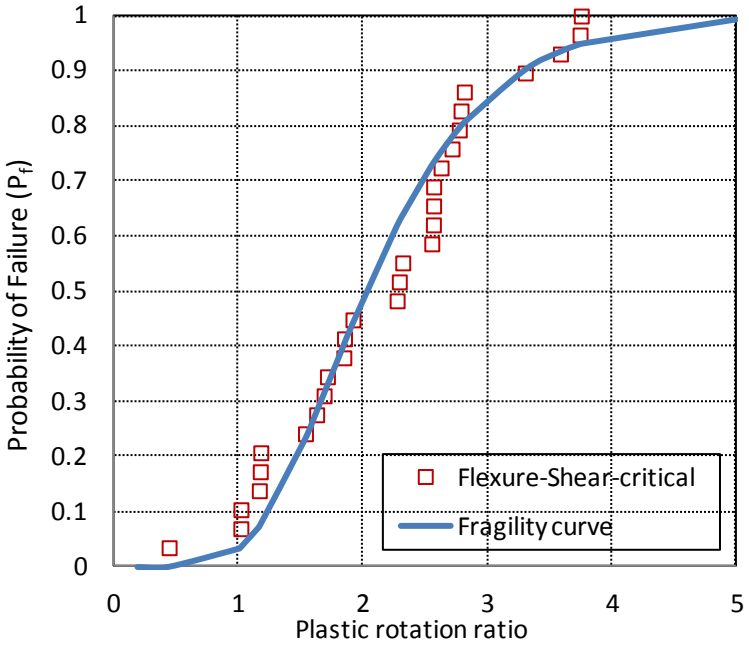

Figure 6.9 Lognomal fragility curve for plastic rotation at significant loss of lateral resistance

Based on Figure 6.9, there is 11% probability of failure for columns in "Condition ii" when experiencing plastic rotation demand equal to parameter *a* specified in ASCE/SEI 41.

The "failure" here refers to the point at which the column has lost more than 20% of its lateral resistance.

According to ASCE/SEI 41, applying the parameter *a* specified in the table shall achieve the probability of failure P_f less than 15% for columns vulnerable to shear failure, i.e. columns in condition ii and iii, while for flexure critical columns in condition i, the probability of failure P_f up to 35% is acceptable since flexure failure is less sudden and brittle. The resulting probability of failure at loss of significant lateral resistance for flexure-shear-critical columns in The Database is consistent with ASCE/SEI 41 targets.

6.4.4 Assessment of ASCE/SEI 41 Modeling Parameter b

6.4.4.1 Plastic Rotation Ratio at Loss of Axial Load Capacity

Modeling parameter *b* in ASCE/SEI 41 refers to plastic rotation at the time that column loses gravity load support. The ratio of measured plastic rotation at axial-load failure over the table value is plotted in Figure 6.10. The type of columns corresponding to each data series can be found in section 6.4.3.1 of this thesis.

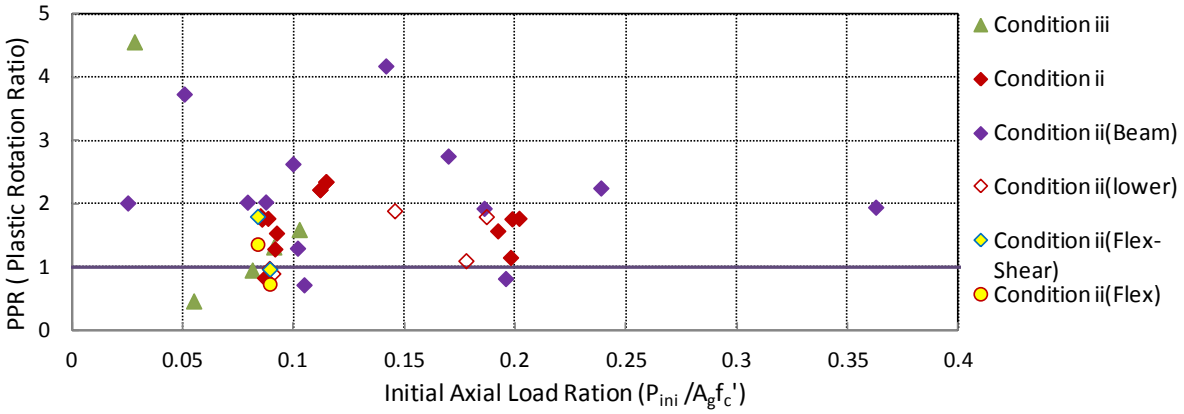

Figure 6.10 Plastic rotation ratio at loss of axial load support

Results show that PRR for most shear-critical columns is close to or below the unit horizontal line, indicating that the plastic rotation estimated by ASCE/SEI 41 can be unconservative for columns in Condition iii.

It is noticed that unlike other shear-critical columns, PPR is greater than 4 for column C2 in specimen S1 in NCREE 2007 Tests. It might be attributed to the fact that unlike other shear-critical columns in The Database that were part of portal frames, column C2 is the middle column in the two-bay planar frame and axial load could be redistributed to outside ductile columns after column axial-load failure, resulting in larger apparent deformation capacity (the column NCREE 2007-S1-C2 was subjected to tension instead of axial compression in the later stage of the tests). Interaction with other two ductile outside columns may greatly increase the drift capacity at axial-load failure for column C2.

ASCE/SEI 41 tends to provide conservative estimation of plastic rotation at loss of gravity load support for most of columns in "Condition ii". Two non-ductile columns (in Condition ii) C1 and C2 in specimen L of NCREE 2005 tests have exceptional high plastic rotation ratio equal to 3.7 and 4.2 respectively. With extended deformations in the positive direction were observed from the hysteretic response, yet those two columns experienced substantial damage after the failure of lap-sliced longitudinal reinforcements. The failure modes of the columns may be changed to the flexural failure, since the column could not transfer the moment and shear resistance after the failure of lap-spliced longitudinal reinforcement. The frame was weaker but the column would not experience shear failure.

6.4.4.2 Probability of Failure

Results of plastic rotation ratio could be represented by a lognormal cumulative distribution, commonly referred to as a fragility curve, as shown in Figure 6.11.

Since loss of gravity load support of certain columns could result in the collapse of structural system, higher level of safety should be achieved. Elwood et al. (2007) suggested that the probability of failure P_f should be less than 15% if columns experience a plastic rotation demand equal to the parameter b specified in ASCE/SEI 41. "Failure" here refers to the point that the column loses axial load support.

The fragility curve is constructed based on the test data of flexure-shear-critical columns that experienced axial-load failure during the tests (the data series in red diamond marker in Figure 6.10).

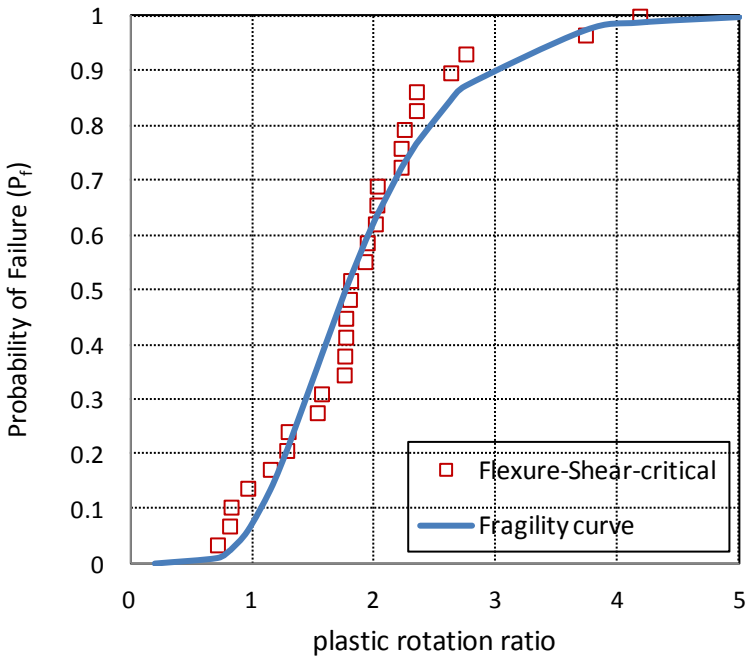

Figure 6.11 Lognomal fragility curve for plastic rotation at loss of axial-load support

Based on Figure 6.11, there is a 7.5% probability of failure for columns in "Condition ii" experiencing a plastic rotation demand equal to b specified in ASCE/SEI 41.

6.4.4.3 Comparison of Plastic Rotation at Shear Failure and Axial-Load Failure

Figure 6.12 compares the plastic rotation at loss of axial load capacity and at significant loss of lateral resistant force. Result of $\left(\theta_p\right)_{Axial} - \left(\theta_p\right)_{Shear}$ in Figure 6.12(a) is the drift "gap" that column exhibited between shear failure and the axial-load failure. The data of parameters $a - b$ in purple markers corresponds to the $\left(\theta_p\right)_{Axial} - \left(\theta_p\right)_{Shear}$ specified by ASCE/SEI 41 was found to be around 0.006 for most non-ductile columns. Because that the columns in The Database had similar transverse reinforcement ratio, axial load ratio as well as the shear stress level, the resulting parameters a and b are very close to each other. Measured plastic rotation in green markers is more scattered and many columns had $\left(\theta_p\right)_{Axial} - \left(\theta_p\right)_{Shear}$ close to zero, since these column lost 20% of its peak lateral strength at a point quite close to or even after axial-load failure.

Results in Figure 6.12(b) also show that the measured $\left(\theta_p\right)_{Axial} / \left(\theta_p\right)_{Shear}$ tends to be slightly higher than 1.0, while parameter b/a for most flexure-shear-critical columns was around 1.5.

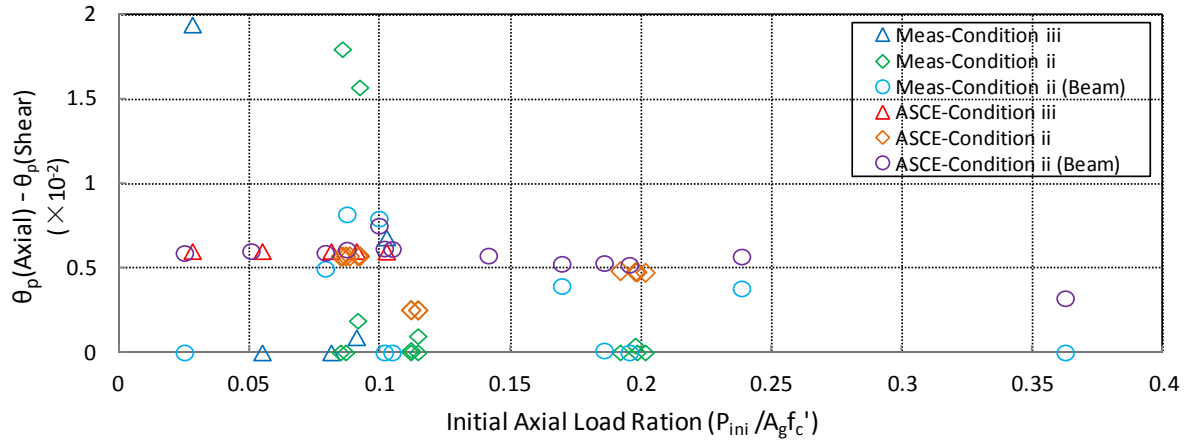

(a) Plastic rotation at axial-load failure minus the plastic rotation at shear failure

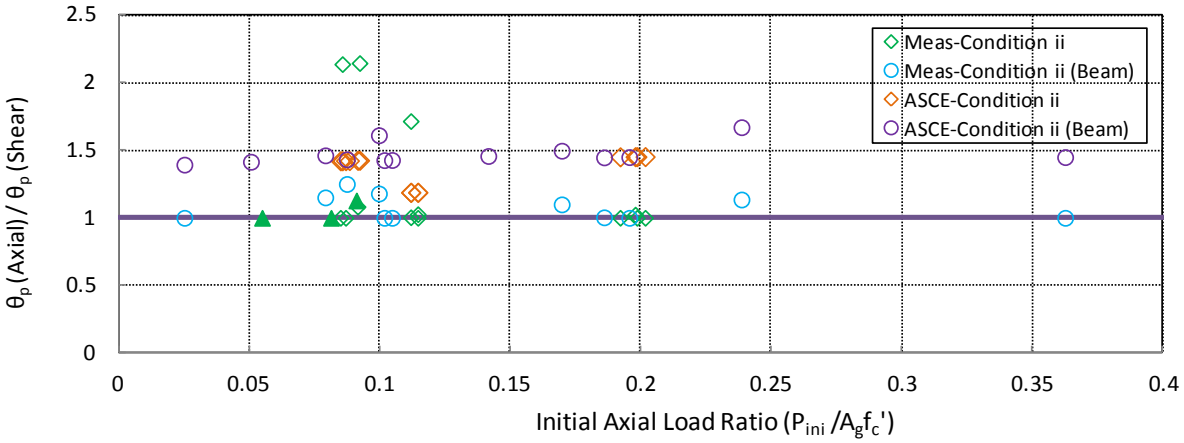

(b) Ratio of plastic rotation at axial-load failure over the plastic rotation at shear failure

Figure 6.12 Comparison of plastic rotation at axial-load failure and shear failure

It is observed that non-ductile columns in The Database experienced 20% of shear degradation at relatively large drift and many of them achieved same column drift at shear failure and axial-load failure. Since the shaking table tests usually last for a relatively short time, columns could only go through limited number of cycles during the tests and might not dissipate as much energy as the columns subjected to reversed-cyclic tests. Therefore gap between the measured drift at shear failure and at axial-load failure is quite small for columns subjected to shaking table tests. This also helps to explain the fact that while the drift models could capture the column drift capacity at axial-load failure fairly well, the measured drifts at shear failure tend to greatly exceeds the calculated drifts from available models.

6.4.5 Modeling Parameters for Columns in Condition i

Unlike the static cyclic tests conducted on single columns in past research, shaking table tests are often terminated at the collapse of whole frames or the end of strong input ground motion. Due to the early failure of non-ductile columns in the frames, the collapse of the structure induced the P-Delta failure of the flexure-critical columns in Condition i. The maximum plastic rotation measured during the tests is compared with the modeling parameter b in Figure 6.13 (in solid blue round marker). For flexure-critical columns belong to the frames that did not collapse are marked in blue hollow circle and the maximum plastic rotation could be considered as the lower bound of the drift capacity at axial-load failure.

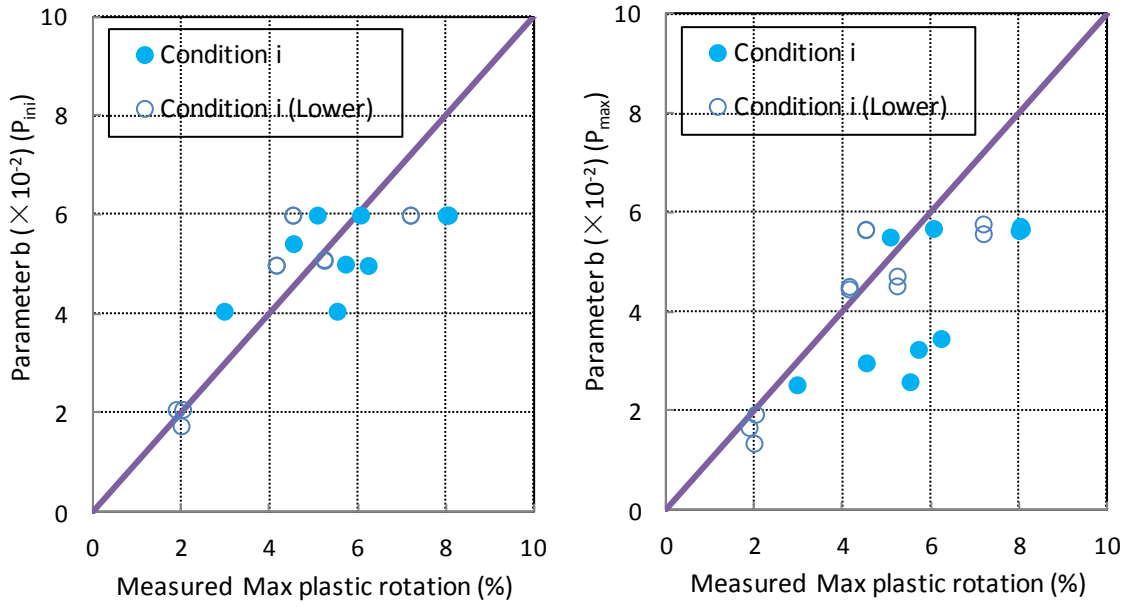

(a) Parameter b based on P_{ini} (b) Parameter b based on P_{max}

Figure 6.13 Evaluation of modeling parameter *b* for columns in Condition i

The modeling parameters for columns in Condition i is obtained by linearly interpolating the values specified in ASCE/SEI 41 based on the transverse reinforcement ratio and axial load ratio, thus the parameter b in Figure 6.13 (a) and (b) is relatively more sensitive to the axial load ratio than that for columns in other conditions.

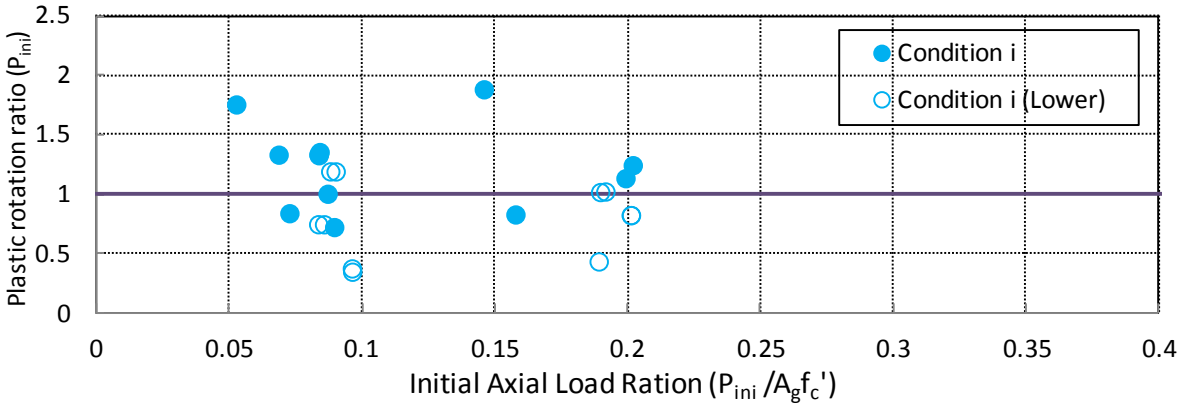

(a) PRR based on initial axial load P_{ini}

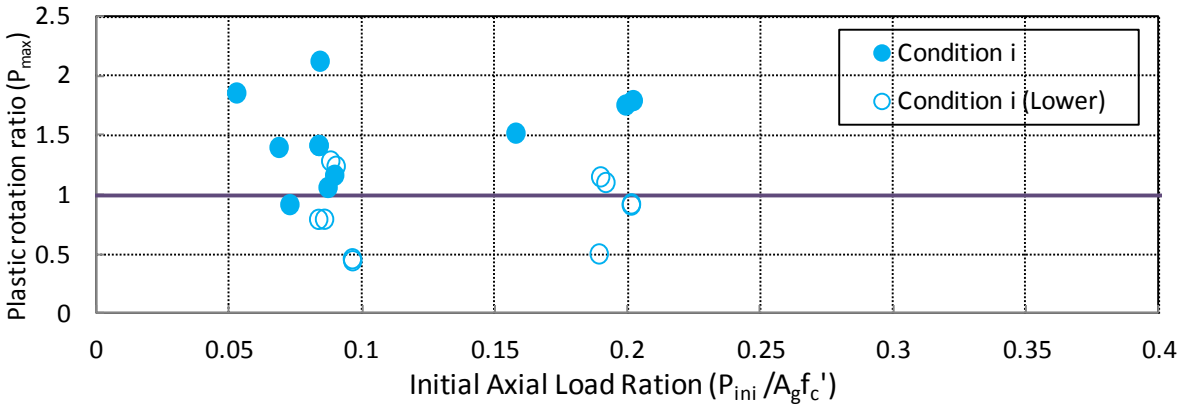

(a) PRR based on maximum axial load P_{max}

Figure 6.14 Plastic rotation ratio for columns in Condition i

The PRR (plastic rotation ratio) based on initial axial load P_{ini} and maximum axial load P_{max} is plotted in Figure 6.14. Results show that modeling parameter b based on initial axial load P_{ini} in Figure 6.14 (a) appears to represent the mean value of the plastic rotation at axial-load failure for flexure-critical columns and is pretty conservative for most columns in Condition i that experienced P-Delta failure during the tests.

The modeling parameter b based on P_{ini} is unconservative for the ductile columns C3 in Specimen S1 of NCREE 2007 Tests (PRR=0.73), ductile columns C1 (PRR=0.83) and D1 (PRR=0.84) in Ghannoum 2006 Tests. After the axial-load failure of non-ductile columns in the frame, flexure-critical column C1 in Ghannoum 2006 Tests and column C3 in Specimen

S1 of NCREE 2007 Tests picked up significant amount of axial load redistributed from the axially collapsed non-ductile columns. The modeling parameter b based on maximum axial load P_{max} in Figure 6.14 (b) is indeed a better reflection of the plastic drift capacity for those two columns (PPR equals to 1.51 and 1.16 based on P_{max}) respectively.

The PPR based on P_{max} for column D1 in Ghannoum 2006 is slightly lower than 1.0 (PRR=0.92). It is noticed that the test data for several columns are truncated, such as column D1 in Ghannoum 2006 Tests, since the column drift and shear force measured from the instruments are not reliable beyond certain point. The maximum drift obtained from the hysteretic response of columns may be lower than the actual column plastic drift.

6.5 Column Lateral Load-Deformation Backbones

6.5.1 Experimental Envelope of Effective Lateral Force

To assess the generalized load-deformation relationships recommended by ASCE/SEI 41 and better understand the column response, experimental envelopes and normalized envelopes are developed for non-ductile columns in The Database by following the procedure discussed in section 2.7 of this research.

Figure 6.15 to Figure 6.19 present the normalized experimental envelopes for non-ductile columns in several test programs (i.e. NCREE 2009 Tests, NCREE 2007 Tests, Elwood 2002 Tests and Shin 2005 Tests).

The dashed line in the figures shows the column response and shear degradation beyond the axial-load failure point (defined in section 5.1.3). The numbers in the bracket are the maximum axial load ratio measured during the tests for certain columns.

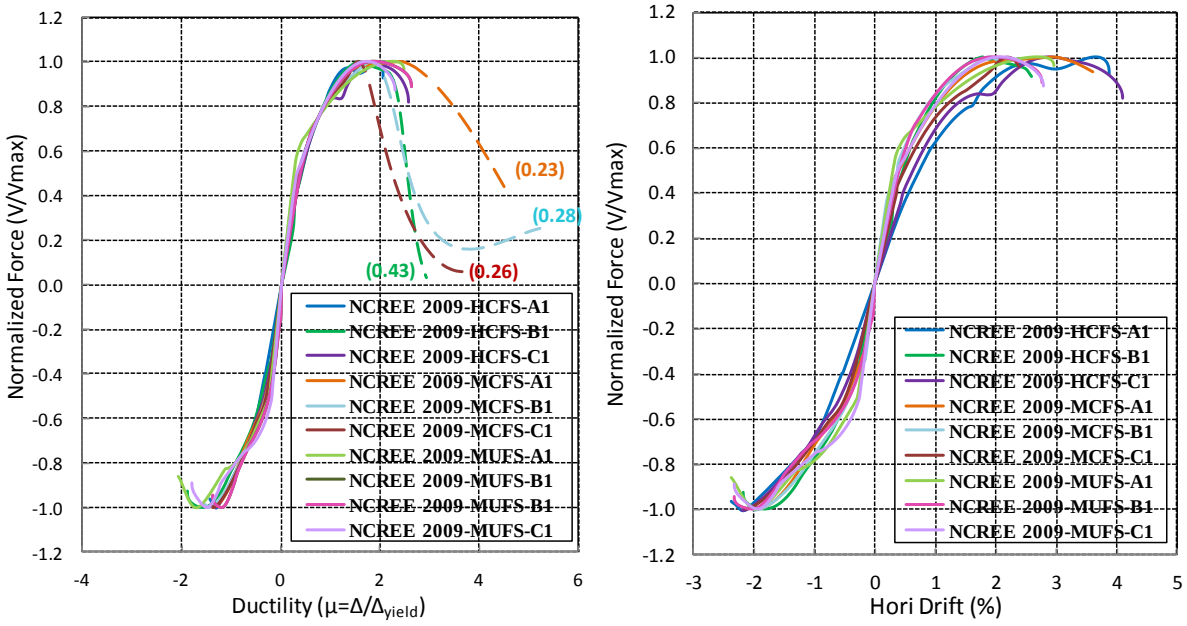

Note: the number in the bracket is the maximum axial load ratio measured during the test for each column; the dashed line is the column behavior beyond the axial-load failure point.

Figure 6.15 Normalized experimental envelopes for columns in NCREE 2009 Tests

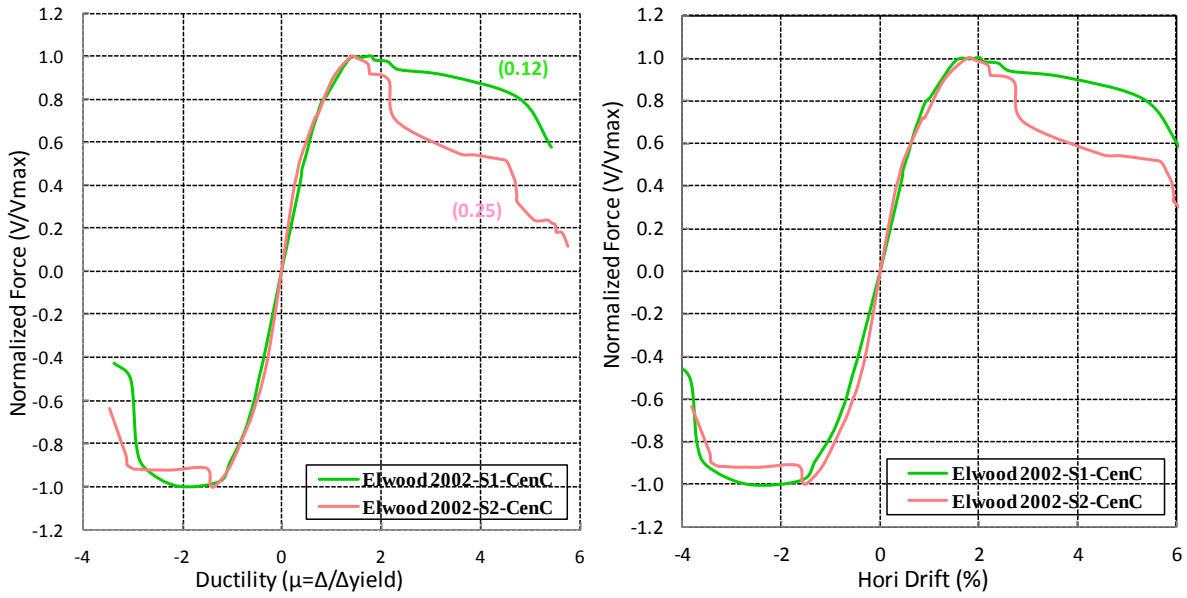

Note: the number in the bracket is the maximum axial load ratio measured during the test for each column; the dashed line is the column behavior beyond the axial-load failure point.

Figure 6.16 Normalized experimental envelope for Elwood 2002 Tests

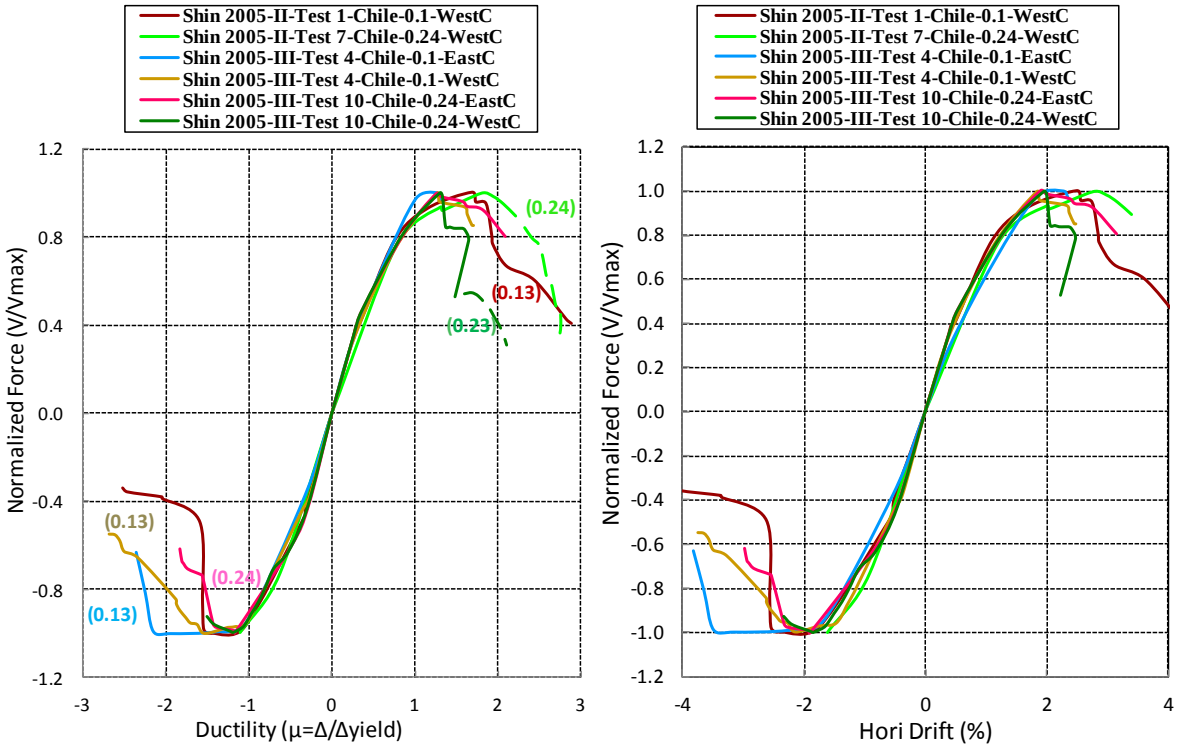

Figure 6.17 Normalized envelopes for columns subjected to Chile Earthquake in Shin 2005 Tests

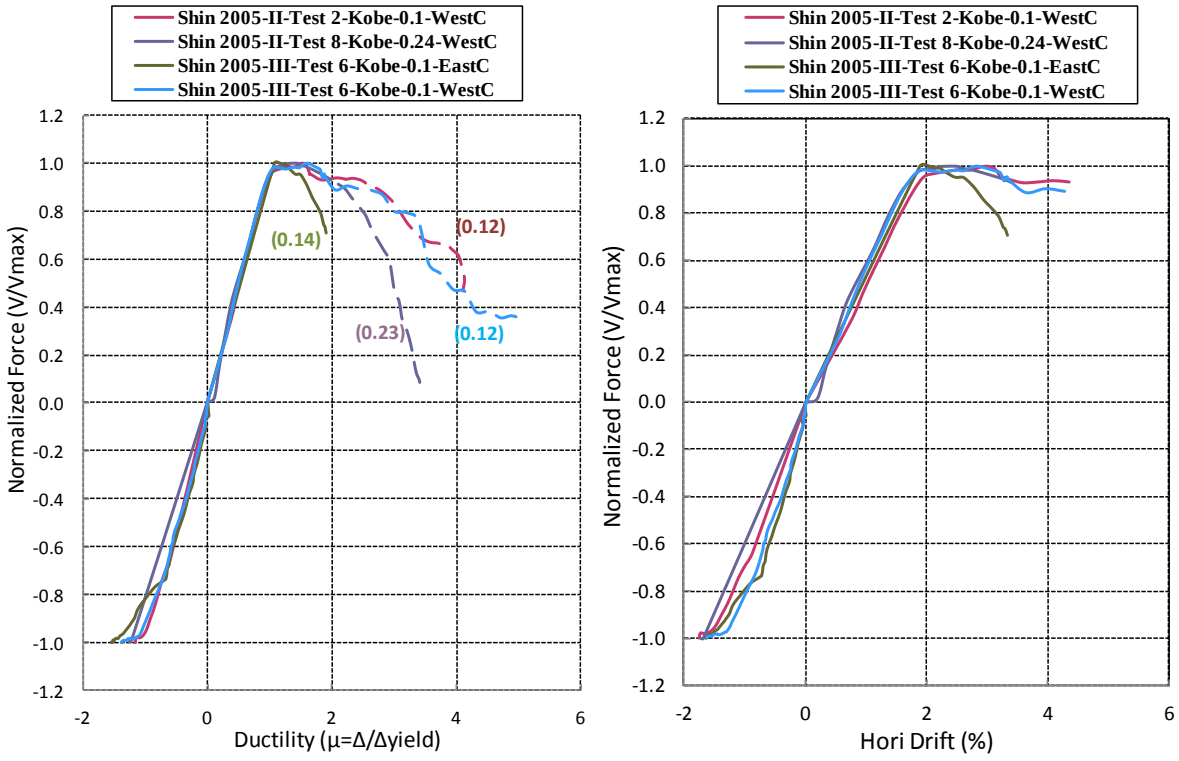

Figure 6.18 Normalized envelopes for columns subjected to Kobe Earthquake in Shin 2005 Tests

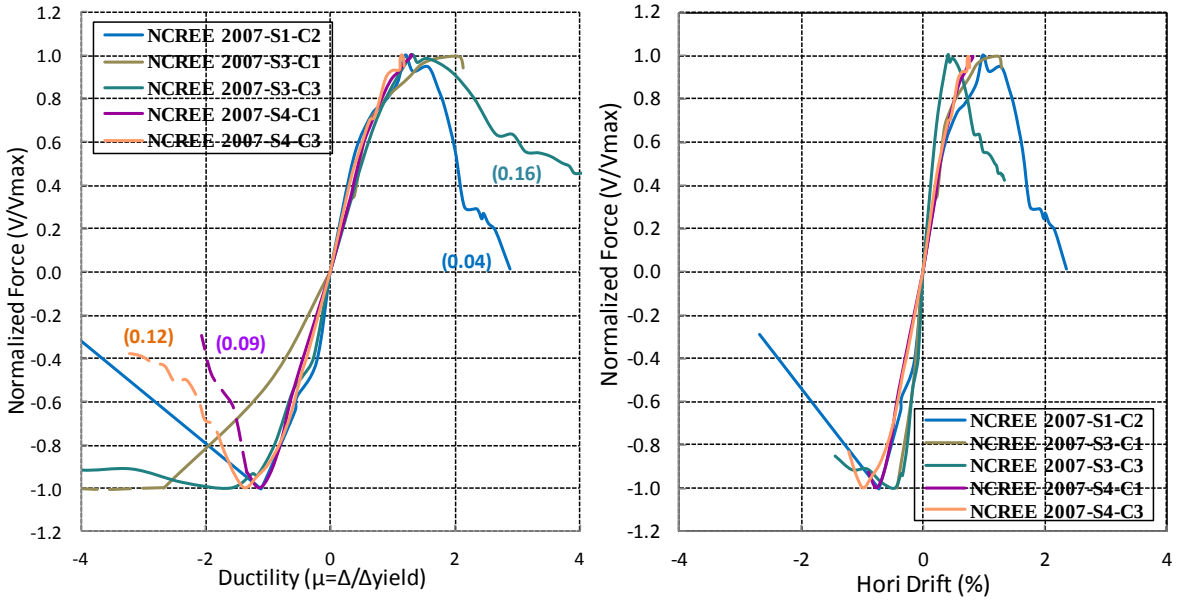

Note: the number in the bracket is the maximum axial load ratio measured during the test for each column; the dashed line is the column behavior beyond the axial-load failure point.

Figure 6.19 Normalized envelopes for shear-critical columns in NCREE 2007 Tests

Results in Figure 6.15 show that the columns in specimen HCFS subjected to higher axial load ratio demonstrated less deformation capacity than columns in specimen MCFS in the direction of column failure. In the other direction, columns showed very similar behavior.

Results in Figure 6.16 show that the column subjected to higher axial load (center column in S2) experienced more rapid and sever shear degradation than the column with lower axial load (the center column in S1). This trend is consistent with the response for flexure-shear critical columns shown in Figure 6.15 to Figure 6.19. The absolute value of the negative degrading slope increased as the column axial load ratio increased, indicating the shear degradation is more rapid and severe.

As shown in Figure 6.19, the middle column NCREE 2007-S1-C2 had relatively low maximum axial load ratio equal to 0.04 and was subjected to axial tension force instead of

compression at the later stage of the tests, possibly due to the axial load redistribution within the system after shear failure occurred. This shear-critical column lost lateral resistance very quickly and experienced sudden axial-load failure, suggesting that columns subjected to tension force are even more vulnerable to shear degradation and loss of axial load support.

From the normalized envelopes for non-ductile columns in The Database, it is observed that most non-ductile columns subjected to earthquake load achieved the maximum lateral force when ductility demand μ reached 1.5 and would suffer shear failure and axial-load failure before ductility demand μ reached 4.0.

A simplified normalized lateral load-deformation response for non-ductile columns could be constructed. With calculated shear strength and yield drift estimated by available models, a simplified lateral load-deformation relation could be established in preliminary structural analysis.

Figure 6.20 plots the normalized envelopes for non-ductile columns in The Database with the proposed simplified normalized backbone curve. The key points used to construct the simplified normalized lateral load-deformation for flexure-shear-critical columns connected with rigid beam are noted in Figure 6.20 (a). As shown in Figure 6.20 (b), the load-drift responses of flexure-shear-critical columns connected with relatively flexible beam are found to exhibit more deformation capacity due to the flexibility contributed by the beam compared with the proposed backbone which captures only the deformation capacity of the column. On the other hand, the load-drift responses of shear-critical columns shown in Figure 6.20 (c) exhibit lower deformation capacity compared with the simplified backbone for flexure-shear columns, demonstrating the limited deformation capacity of columns failing in pure shear.

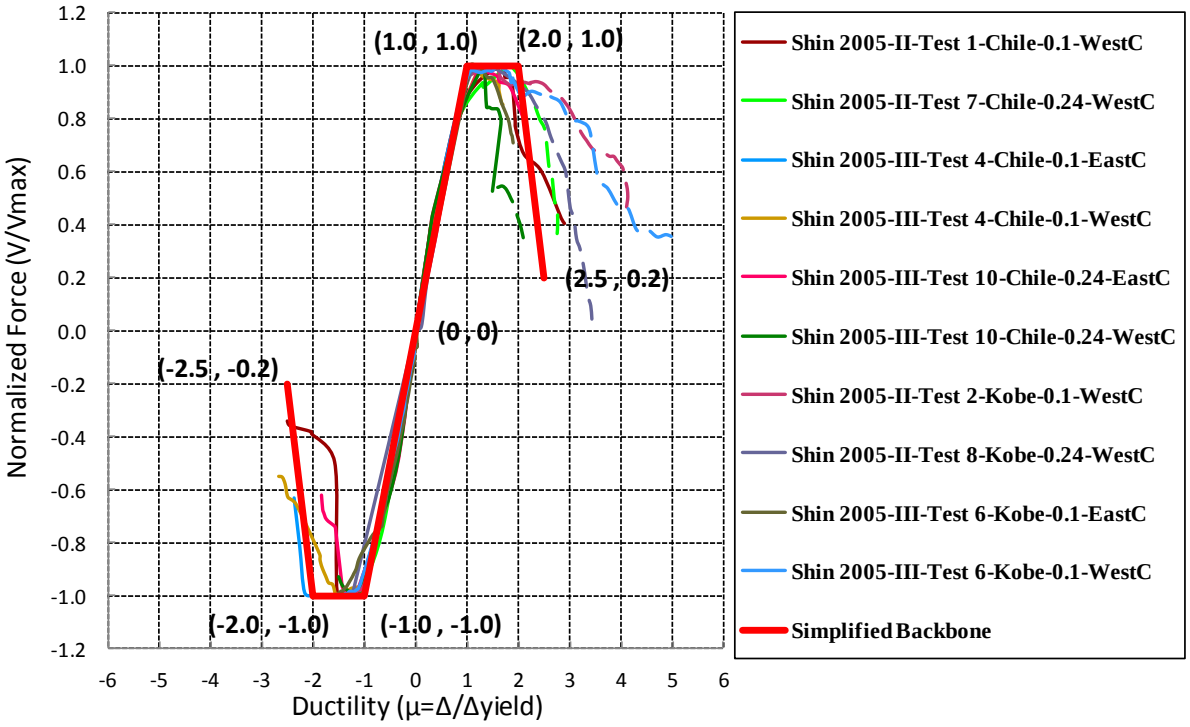

(a) Flexure-shear-critical columns connected with rigid beam

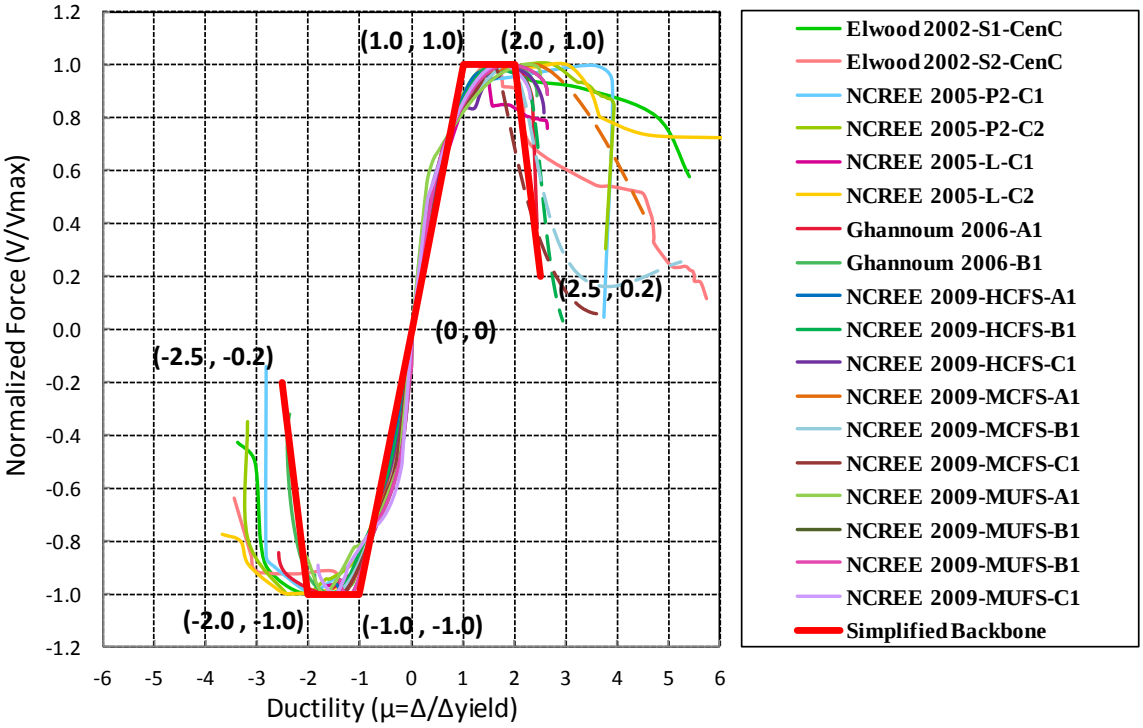

(b) Flexure-shear-critical columns connected with relatively flexible beam

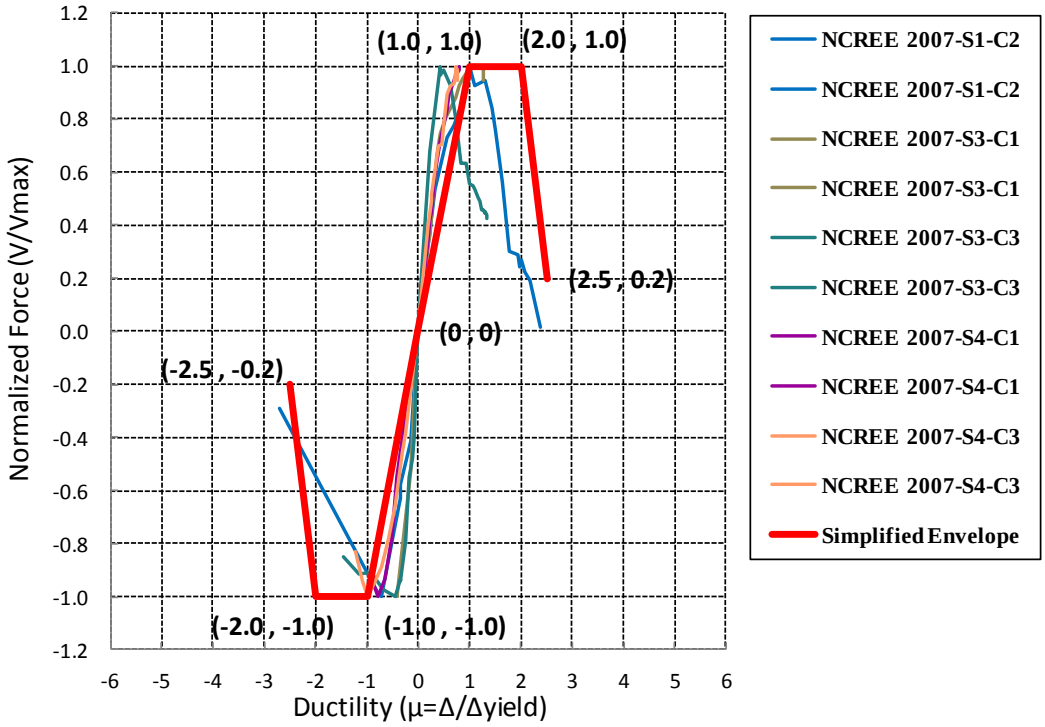

(c) Shear-critical columns

Figure 6.20 Normalized envelopes for non-ductile columns with proposed simplified envelopes

Figure 6.21 plots the normalized experimental envelope for non-ductile columns with column horizontal drift. It is observed in Figure 6.21 (a) that most flexure-shear critical columns achieve maximum lateral resistance when column drifts reach 1.2% and start to degrade when column drifts equal to 2.5%. A simplified backbone curve directly related to column drift is constructed in Figure 6.21 (a). The proposed backbone curve with the experimental envelopes for flexure-shear-critical columns connected with flexible beam and shear-critical columns are proposed in Figure 6.21 (b) and (c) respectively. Similar to the results shown in Figure 6.20 (b), columns connected with flexible beam exhibit more deformation due to the flexibility contributed by the beam. The shear-critical columns in Figure 6.21 (c) demonstrate very limited deformation compared with the simplified backbone curve.

The simplified envelope did not capture the load-drift relations for column NCREE 2005-L-C1 very well as shown in Figure 6.21 (b) (test series in the magenta line), possibly because the column response was changed to be dominated by flexural behaviour due to the failure of lap-spliced longitudinal reinforcement.

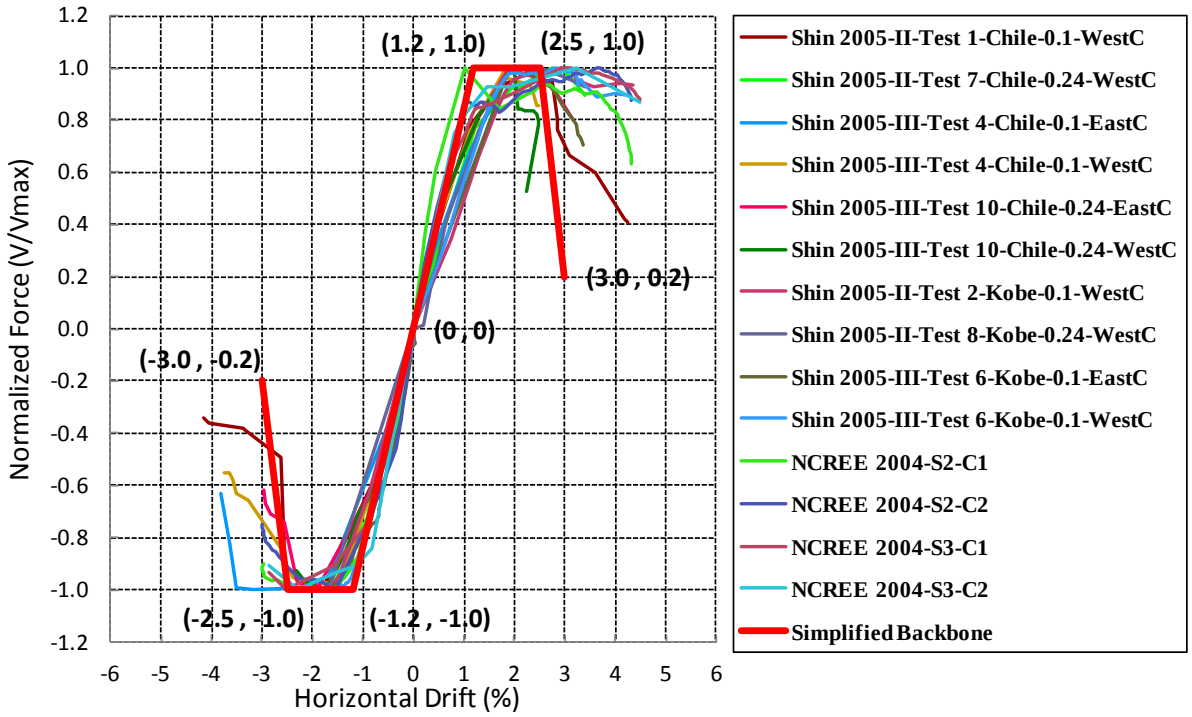

(a) Flexure-shear-critical columns connected with rigid beam

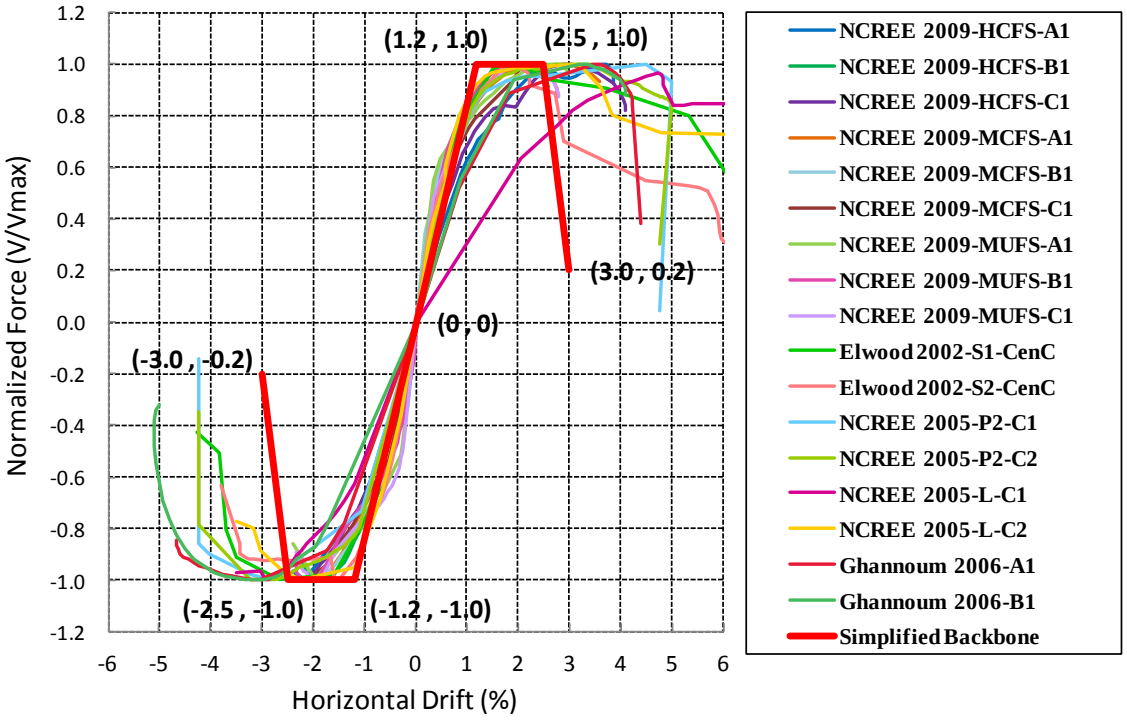

(b) Flexure-shear-critical columns connected with relatively flexible beam

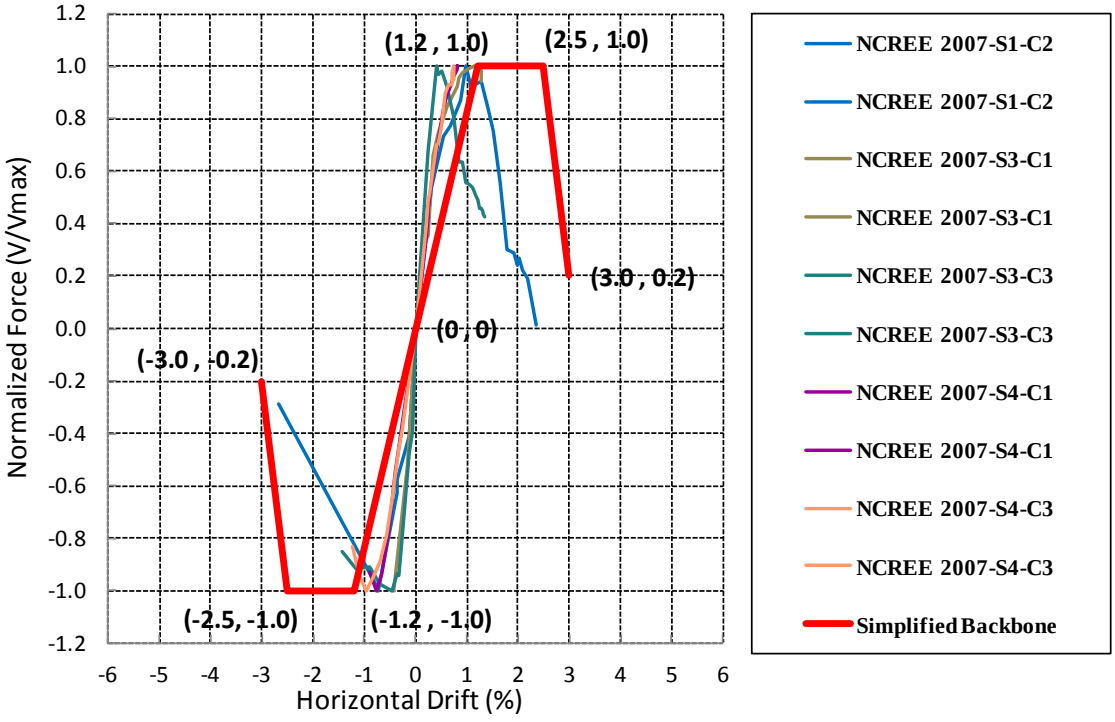

(b) Shear-critical columns

Figure 6.21 Envelope for non-ductile columns with normalized force and column horizontal drift

Figure 6.22 plots the experimental envelopes for non-ductile columns with normalized force and column plastic rotation. The column plastic rotation is calculated by subtracting the measured yield drift δ_y (discussed in section 3.2.5) from the total column drift.

As shown in Figure 6.22 (a), the proposed simplified backbone could represent the plastic rotation for columns connected with rigid beam fairly well, only slightly underestimating the plastic drift for two columns (column Shin 2005-III-Test 4-Chile-0.1-WestC and Shin 2005-III-Chile-0.24-WestC).

The plastic rotation for columns connected with flexible beams shown in Figure 6.22 (b) is generally lager than that of columns connected with rigid beam. Columns connected with relatively flexible beams in The Database are usually from multiple-bay multiple-storey frames and thus the column interactions and axial load redistribution mechanism may allow the columns to exhibit more extended plastic deformation after the column yielding.

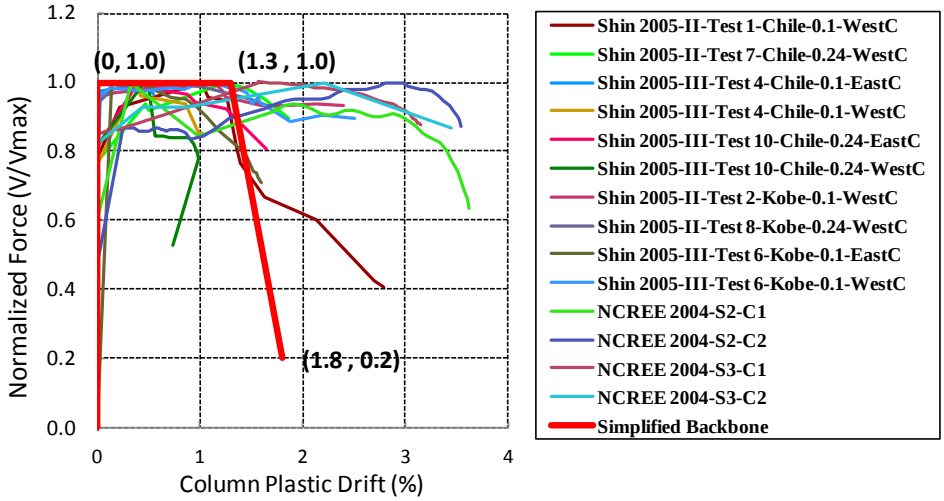

(a) Flexure-shear-critical columns connected with rigid beam

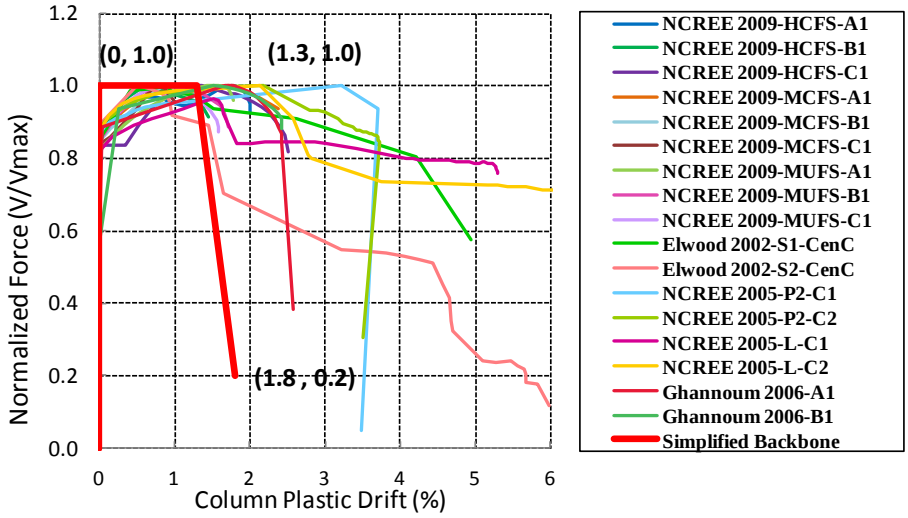

(b) Flexure-shear-critical connected with relatively flexible beam

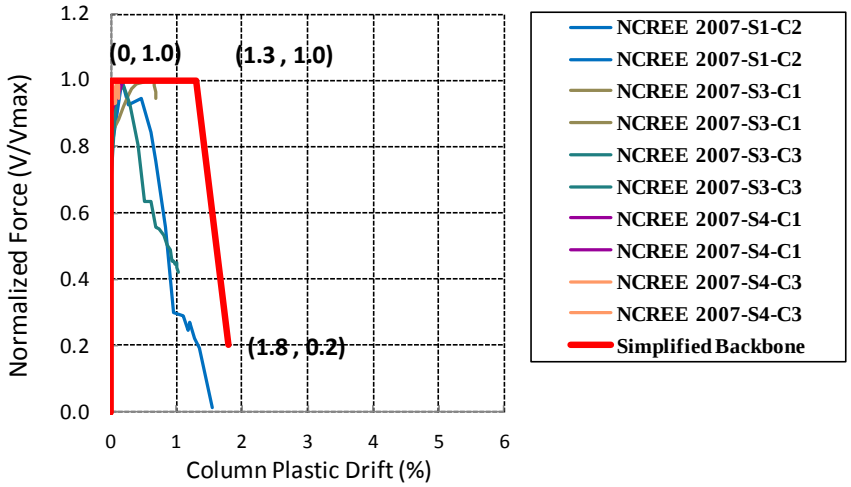

(c) Shear-critical columns

Figure 6.22 Envelope with normalized force and column plastic drift

6.5.2 ASCE/SEI Backbone Curve

The ASCE/SEI 41 backbone curves for non-ductile columns in The Database are constructed based on the plastic shear demand, measured maximum effective force as well as the effective stiffness ratio and modeling parameter a , b and c recommended by ASEC/SEI 41. For example the ASCE/SEI backbone curves for column Shin 2005-II-Test 1-Chile-0.1 are plotted in Figure 6.23.

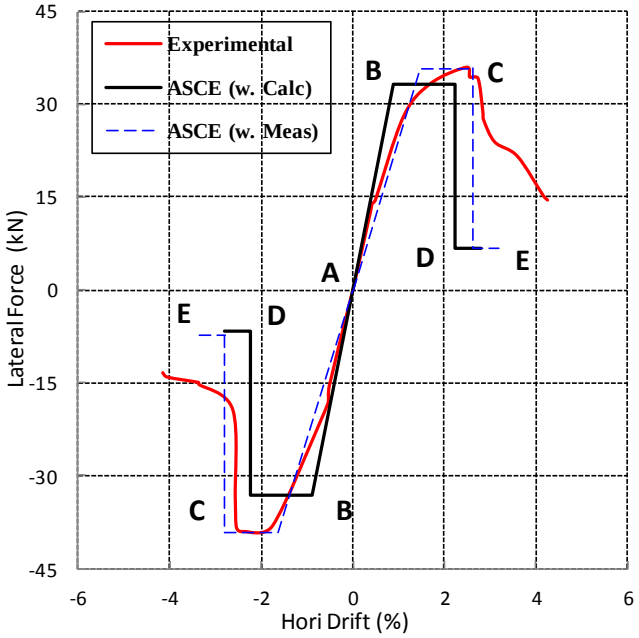

Figure 6.23 ASCE backbone cures for column Shin 2005-II-Test 1-Chile-0.1-WestC

The backbone curve "ASCE (w. Calc)" is constructed by following procedure:

The slope for the column initial response from A to B (the initial stiffness k_{eff}) in Figure 1.1 is derived from the ratio of modulus of gross section (EI_{eff}/EI_g) recommended by ASCE/SEI 41, assuming that the column has fixed-fixed end restraints.

1. The ordinate of the point B (the maximum lateral force in the backbone curve) for flexure-shear-critical column is the plastic shear demand V_p obtained from the moment-curvature analysis; for shear-critical column, the calculated shear strength

V_0' is used instead since the plastic shear demand V_p is expected to be larger than V_0'.

2. The column sustains the maximum lateral force up to the point C. The drift gap between the point B and C is the modeling parameter a obtained from the table in ASCE/SEI 41 based on the initial axial load ratio and calculated shear strength V_0'.
3. The lateral force then degrades to the point D, the residual force could be calculated by modeling parameter c in ASCE/SEI 41 based on the initial axial load ratio and calculated shear strength.
4. The column response is terminated at point E. The drift gap between point B and E is the modeling parameter b based on the initial axial load ratio and calculated shear strength.

The backbone curve "ASCE (w. Meas)" is constructed by following the similar procedure, except that:

1. The coordinate B is the measured yield drift from the TEST method discussed in section 3.2.4 and the ordinate is the measured maximum effective force in both positive and negative directions.
2. The modeling parameters a, b and c are obtained from the ASCE/SEI 41 based on the measured maximum axial load ratio and measured shear strength V_{Max}.

Figure 6.24 to Figure 6.30 plot the ASCE backbone curve with the experimental envelope for the non-ductile columns included in The Database. The dashed line represented the column behaviour beyond the axial-load failure point (defined in section 5.1.4).

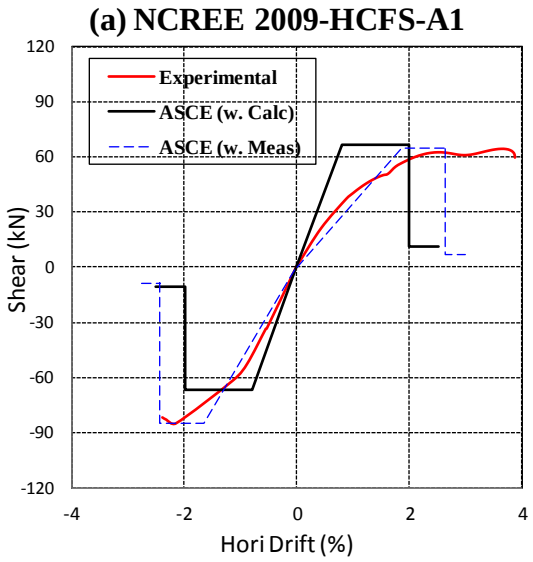
(a) NCREE 2009-HCFS-A1
Experimental
ASCE (w. Calc)
ASCE (w. Meas)
Shear (kN)
Hori Drift (%)

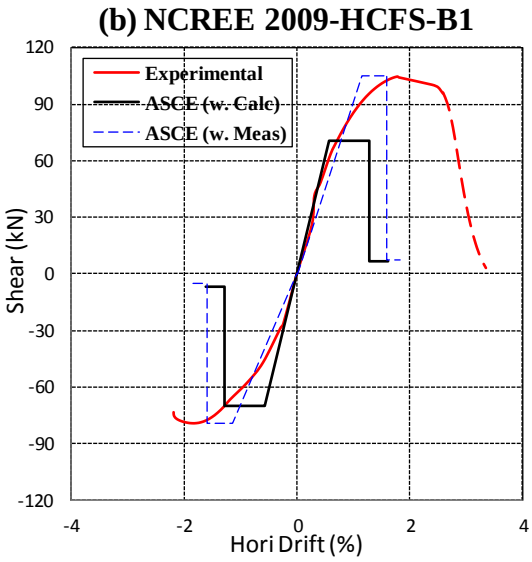
(b) NCREE 2009-HCFS-B1
Experimental
ASCE (w. Calc)
ASCE (w. Meas)
Shear (kN)
Hori Drift (%)

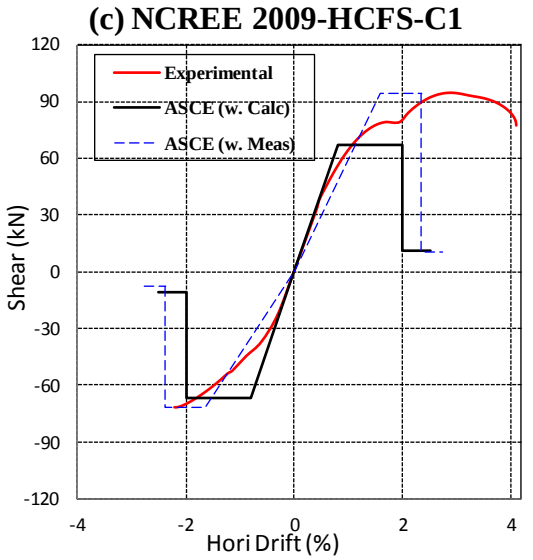
(c) NCREE 2009-HCFS-C1
Experimental
ASCE (w. Calc)
ASCE (w. Meas)
Shear (kN)
Hori Drift (%)

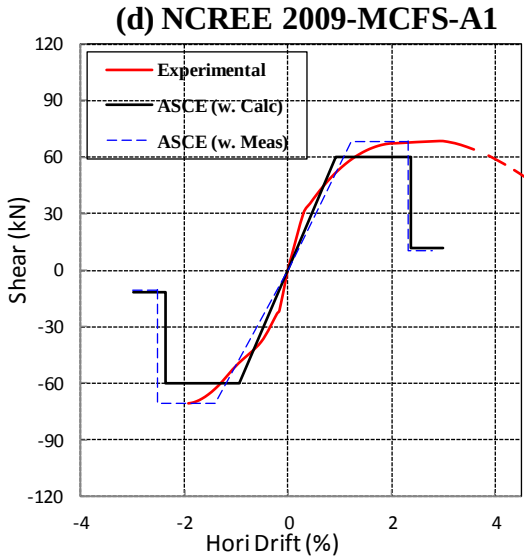
(d) NCREE 2009-MCFS-A1
Experimental
ASCE (w. Calc)
ASCE (w. Meas)
Shear (kN)
Hori Drift (%)

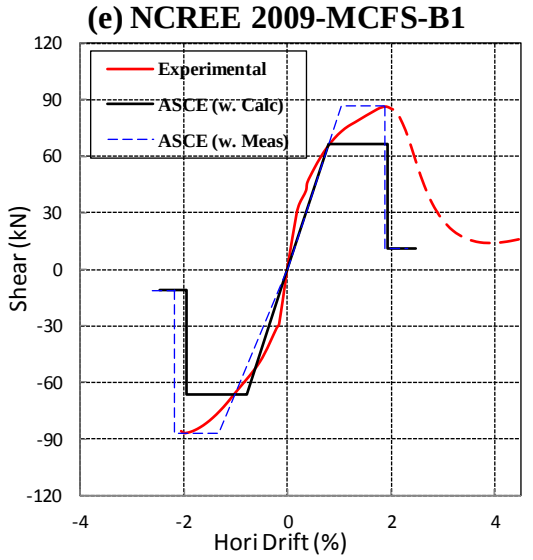
(e) NCREE 2009-MCFS-B1
Experimental
ASCE (w. Calc)
ASCE (w. Meas)
Shear (kN)
Hori Drift (%)

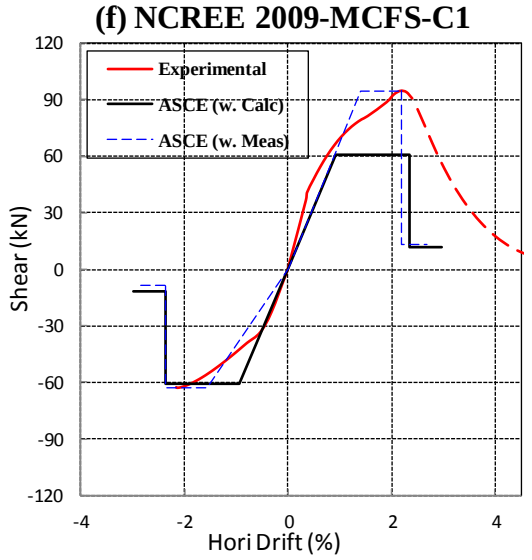
(f) NCREE 2009-MCFS-C1
Experimental
ASCE (w. Calc)
ASCE (w. Meas)
Shear (kN)
Hori Drift (%)

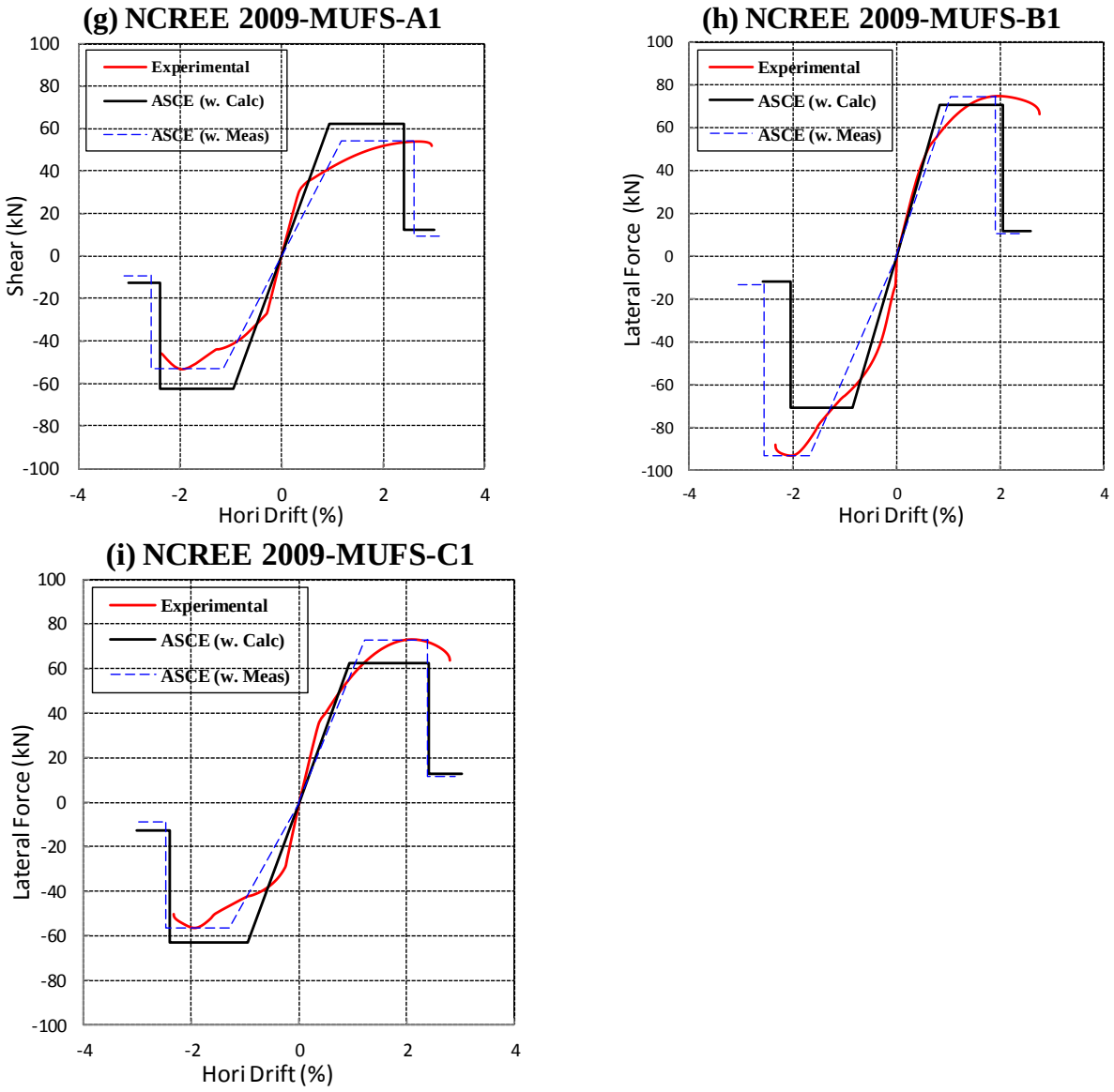

Note: The dashed line represents the column behavior beyond the axial-load failure point

Figure 6.24 ASCE/SEI 41 backbone curves for columns in NCREE 2009 Tests

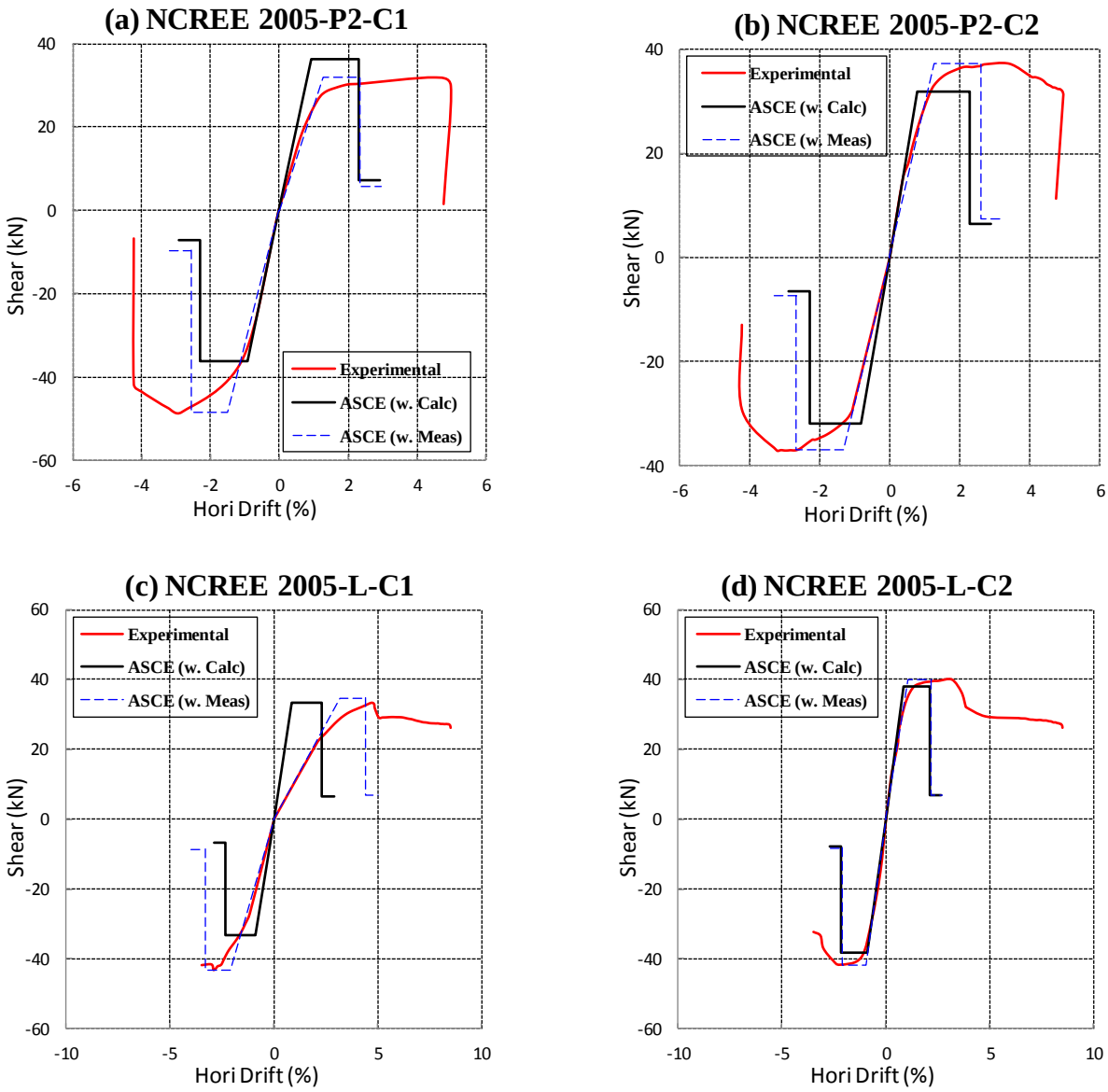

Figure 6.25 ASCE/SEI 41 backbone curves for columns in NCREE 2005 Tests

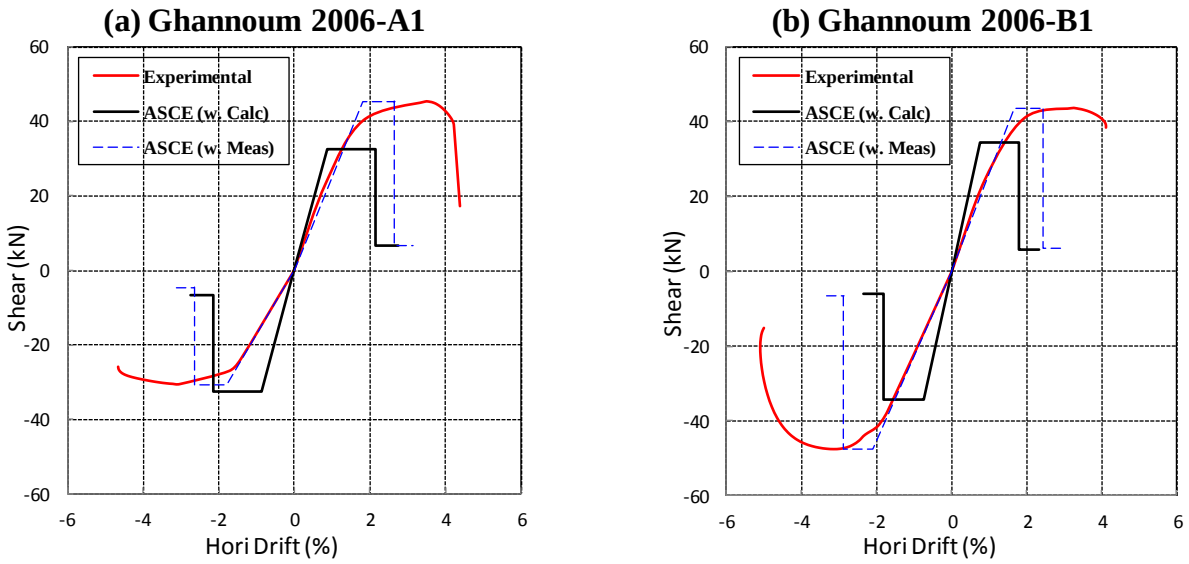

Figure 6.26 ASCE/SEI 41 backbone curves for columns in Ghannoum 2006 Tests

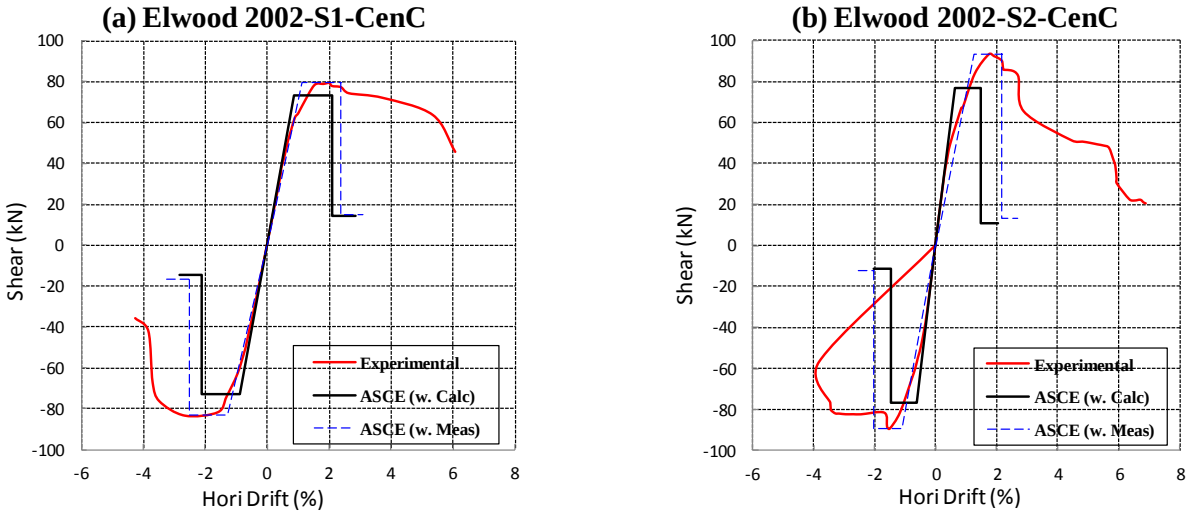

Figure 6.27 ASCE/SEI 41 backbone curves for columns in Elwood 2002 Tests

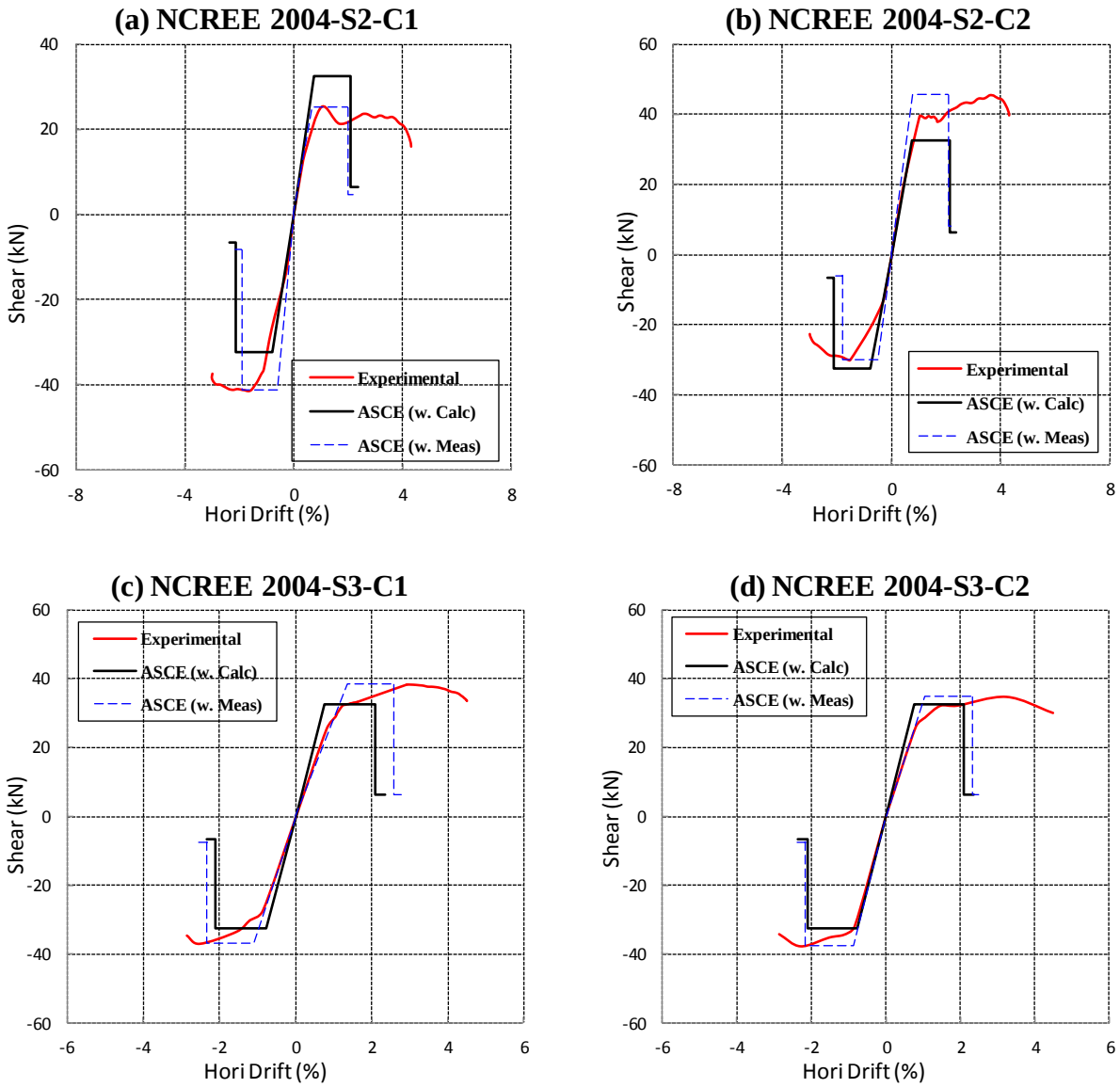

Figure 6.28 ASCE/SEI 41 backbone curves for columns in NCREE 2004 Tests

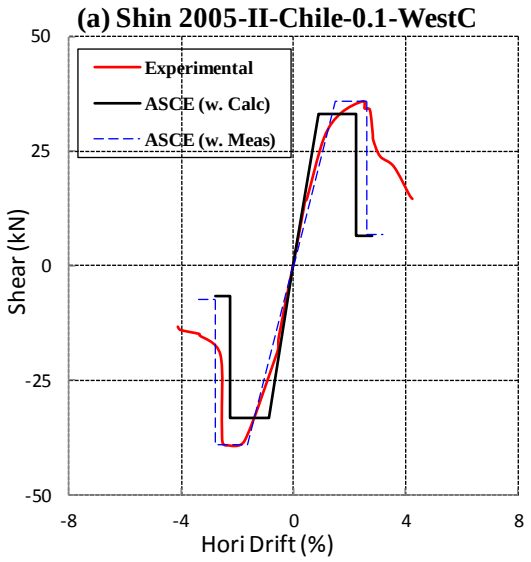
(a) Shin 2005-II-Chile-0.1-WestC
Experimental
ASCE (w. Calc)
ASCE (w. Meas)
Shear (kN)
Hori Drift (%)

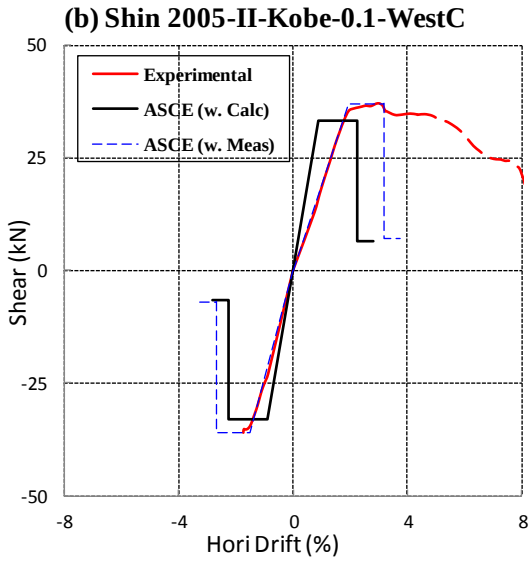
(b) Shin 2005-II-Kobe-0.1-WestC
Experimental
ASCE (w. Calc)
ASCE (w. Meas)
Shear (kN)
Hori Drift (%)

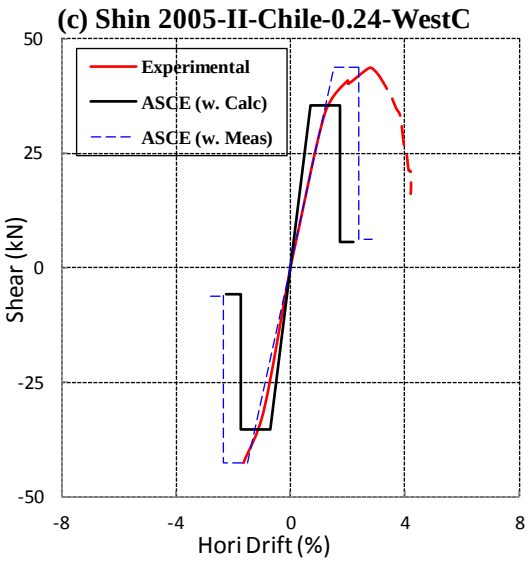
(c) Shin 2005-II-Chile-0.24-WestC
Experimental
ASCE (w. Calc)
ASCE (w. Meas)
Shear (kN)
Hori Drift (%)

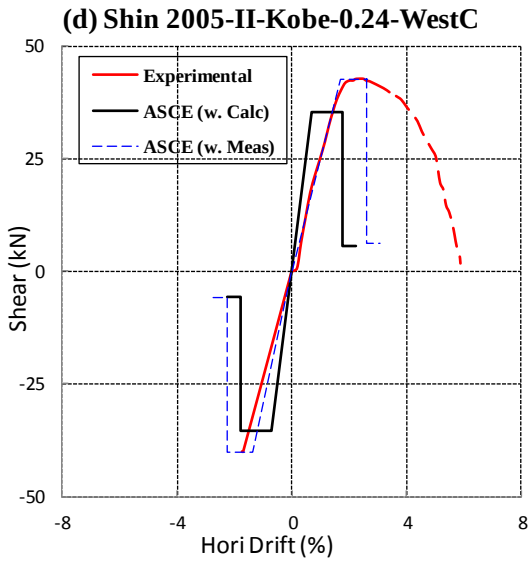
(d) Shin 2005-II-Kobe-0.24-WestC
Experimental
ASCE (w. Calc)
ASCE (w. Meas)
Shear (kN)
Hori Drift (%)

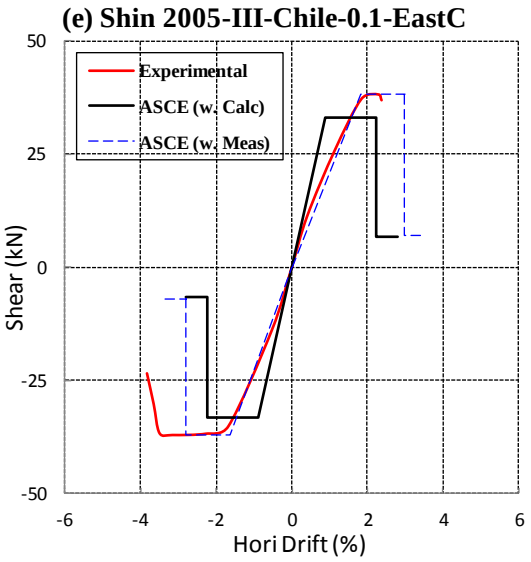
(e) Shin 2005-III-Chile-0.1-EastC
Experimental
ASCE (w. Calc)
ASCE (w. Meas)
Shear (kN)
Hori Drift (%)

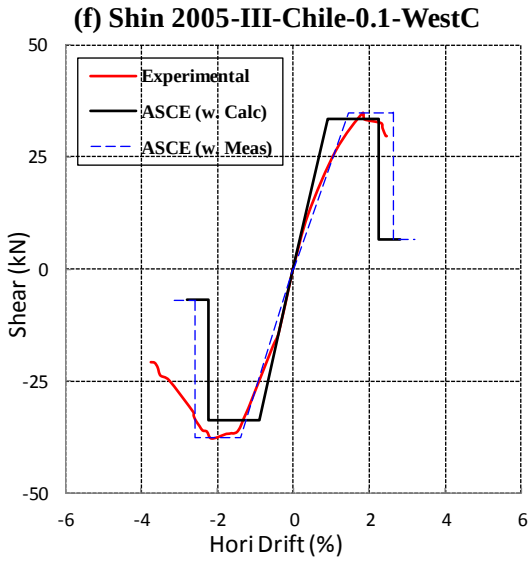
(f) Shin 2005-III-Chile-0.1-WestC
Experimental
ASCE (w. Calc)
ASCE (w. Meas)
Shear (kN)
Hori Drift (%)

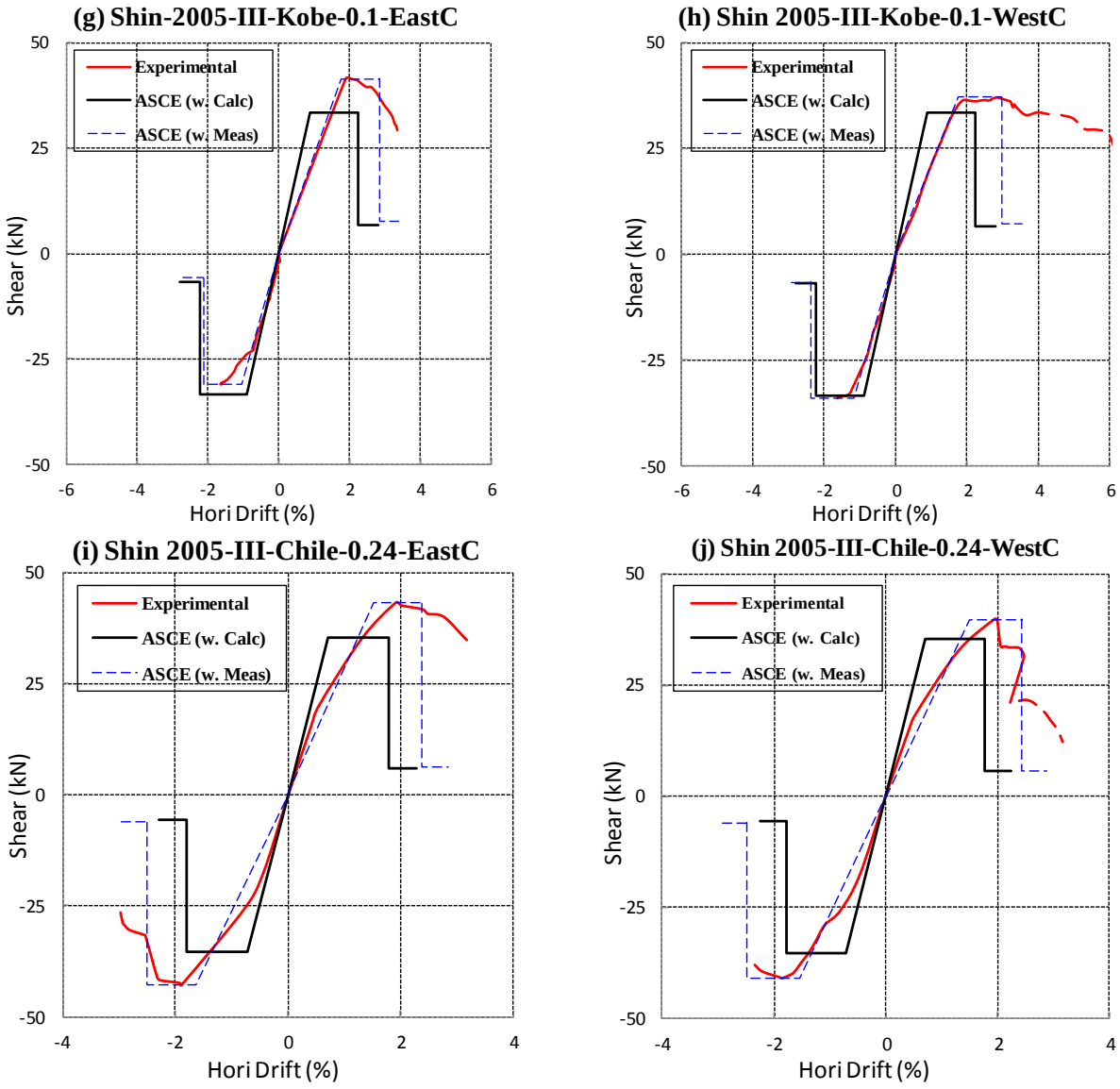

Note: The dashed line represents the column behavior beyond the axial-load failure point

Figure 6.29 ASCE/SEI 41 backbone curves for columns in Shin 2005 Tests

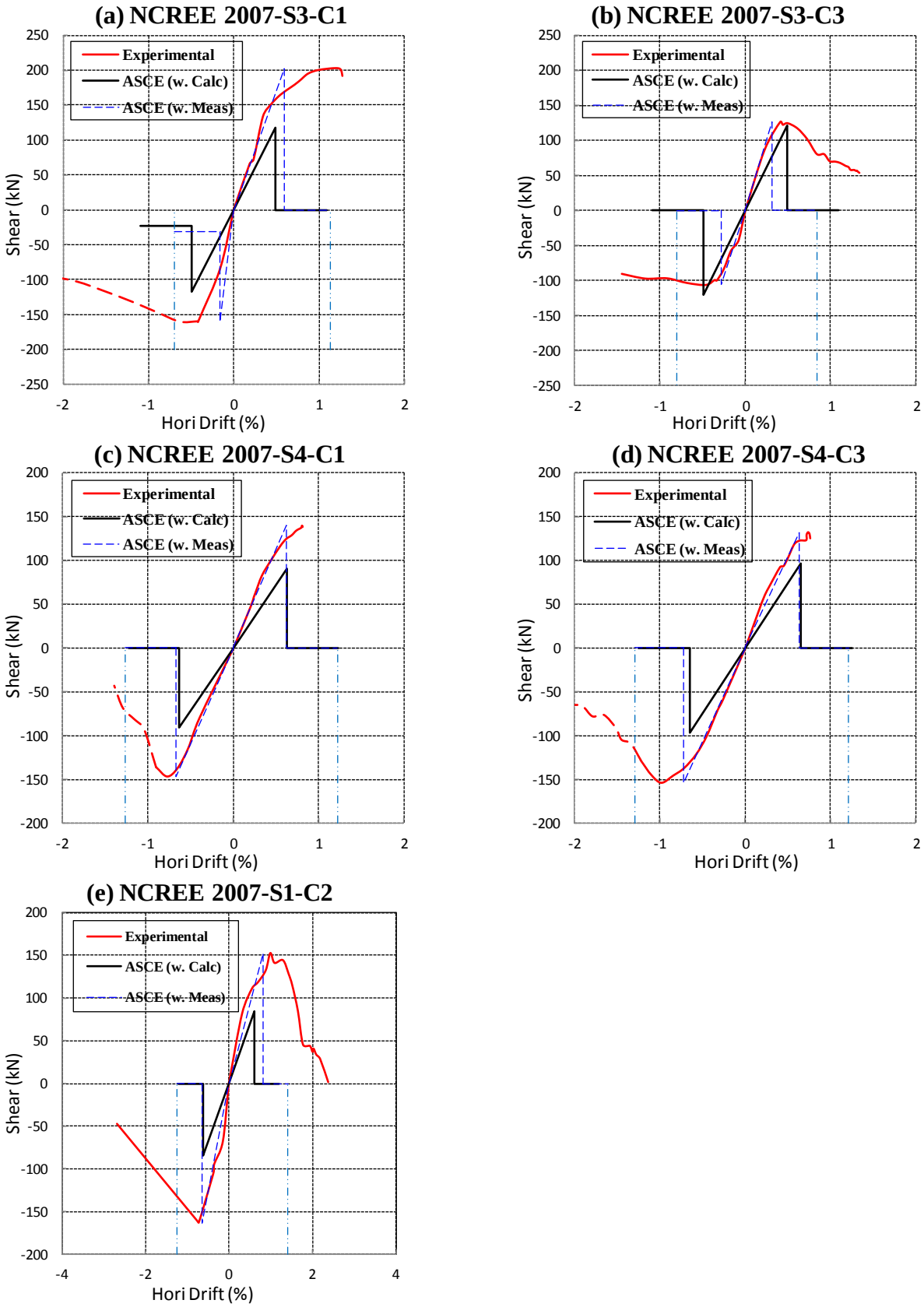

Figure 6.30 ASCE/SEI 41 backbone curves for columns in NCREE 2007 Tests

The ASEC/SEI 41 generally predicts stiffer initial response of non-ductile columns.

In NCREE 2009 Tests, outside columns A1 in the negative direction and columns C1 in the positive direction are subjected to higher axial load due to the overturning moment. It is observed in Figure 6.24 (a), (c), (d) and (f) that the maximum measured shear forces V_{Max} are very close to the V_p in the positive direction for columns A1 and in the negative direction for columns C1; while in the opposite direction, the higher axial load increased the maximum shear V_{Max} that exceeded the plastic shear demand V_p based on the initial axial load P_{ini}.

For columns in specimen MCFS shown in Figure 6.24 (a), (b) and (c), the modeling parameters predict the plastic rotation at shear failure fairly well but are a little bit unconservative for the plastic rotation at axial load failure.

For columns in specimen HCFS shown in Figure 6.24 (d), (e) and (f), the modeling parameters a and b seem to be very conservative. The beam to column strength ratio was relatively low for specimen HCFS of which columns were subjected to high axial load ratio and the extra flexibility contributed by the beam caused the total inter-story drift to be larger than the actual column deformation. Yavari (2011) suggested using the chord rotation (definition is introduced in section 2.4.2) instead to describe the column deformation. The chord rotation θ_t at the top of the columns in NCREE 2009 Tests could be estimated as 64% of the total rotation (inter-story drift ratio) based on the flexure rigidity of the columns and beams (Yavari, 2011).

$$\theta_t = 0.64\left(\Delta / L\right) = 0.64\theta_{total} \qquad \text{Equation 6.6}$$

If using the chord rotation instead, better agreement between the column behaviour and ASCE/SEI 41 modeling parameters could be achieved for columns in NCREE 2009 Tests.

Similarly, the deformation of columns connected with flexure beams shown in Figure 6.25, Figure 6.26 and Figure 6.27 is also greater than the actual column drift and modelling parameters appeared to be very conservative. Cautious should be taken when evaluating the drift capacities of these columns and the chord rotations or plastic rotation at column ends probably should be used instead.

Chapter 7: Conclusions and Future Work

7.1 Summaries

The Shaking Table Tests Column Database comprised of 59 reinforced concrete columns from seven test programs is compiled in this research. Key geometrical information, material properties and test data for each column are provided to facilitate the researchers to investigate the behavior of columns subjected to seismic load. Based on the test data of 36 non-ductile columns with light transverse reinforcement ($\rho_t \leq 0.007$), this research evaluates several available structural models for non-ductile columns that are typically used in old reinforced concrete structures, such as column effective stiffness models and the drift capacities models at shear failure and axial-load failure.

The provisions of current seismic rehabilitation standard ASCE/SEI 41 Supplement 1 regarding the concrete columns are also evaluated with The Database. The standard generally overestimates the column effective stiffness and could either underestimate or overestimate the shear strength. The modeling parameters provide fairly conservative estimate of the column drift capacities and satisfied the targeted probability of failure. Refinements of the shear strength model and criteria for column classification are suggested.

Columns are subjected to varying axial load during the shaking table tests. Especially for outside columns in a frame with multiple bays, the difference between axial load in the positive and negative direction could be very significant due to the overturning moment. When evaluating the models estimating column shear strength and drift capacities, the maximum axial load ratio is believed to better represent the column axial load level; while in estimation of column effective stiffness, it is appropriate use the initial axial load ratio.

It is noticed that the non-ductile columns included in The Database had very similar experimental setups and column detailing, such as transverse reinforcement ratio ρ_t, aspect ratio a / d and the ratio of transverse reinforcement spacing to column depth s / d. Most columns are subjected to axial load ratio $P / A_g f_c^{'}$ less than 0.25. Therefore the column data from The Database could be used to evaluate the available drift capacity models, but one should take cautious when developing new models based on this dataset.

7.2 Conclusions

7.2.1 Column Effective Stiffness

The measured column lateral stiffness k_{eff} is interpreted from lateral force-deformation relations by following TEST method, which regards the point that column achieves 75% of maximum lateral resistance V_{Max} as the first yield point. The PEER method is not selected, because it is difficult to identify the accurate first yield point from the section analysis with varying axial load and the lateral stiffness based on the selected first yield point for some columns (e.g. the first yield point with lateral resistance equal to $0.95V_{Max}$) could not reflect the column initial response well. Most columns in The Database have fixed-fixed ends and the column effective stiffness EI_{eff} could be calculated from lateral stiffness k_{eff}.

ASCE/SEI 41 recommends estimating the effective stiffness based on the axial load ratio and it is found that ASCE/SEI 41 tends to greatly overestimate the column stiffness. The ratio of measured stiffness to calculated stiffness has a mean value equal to 0.66 and coefficient of variation equal to 27.5%.

Elwood and Eberhard (2009) proposed a three-component model to calculate the column yield displacement by explicitly taking into account the deformation due to the flexure behavior, shear response and bar slip effects. Results show that around half of deformation are caused by flexure behavior and the deformation due to the bar slip effects could count for 50% of the total deformation. The shear response contributed less than 5% for shear-critical columns and was negligible for flexure and flexure-shear critical columns. The ratio of measured effective stiffness EI_{TEST} to the stiffness $EI_{Three-Comp}$ estimated by three-component model has a mean value of 1.09 and coefficient of variation of 24.8%.

The simplified three-component model calibrated by Elwood and Eberhard (2009) is evaluated with The Database. The resulted stiffness ratio is close to that of three-component model for most columns, with a mean value of 0.89 and coefficient of variation of 35.4%.

7.2.2 Drift Capacities at Shear Failure

The column drift at shear failure could be defined as the column drift at maximum shear force (Max V), maximum effective lateral force (Max V_{eff}) and 80% of maximum effective lateral force (80% Max V_{eff}). Most models are developed to estimate the column drift capacity at significant loss of lateral resistance, i.e. drift at 80% Max V_{eff}.

Compared with the cyclic test data for flexure-shear-critical columns that have similar axial load ratio and shear stress level, the measured drift at 80% Max V_{eff} generally exceeds the calculated drift from most available models, possibly due to the fact that the dynamic effect and the column interactions within the frame could increase the column drift capacity.

Pujol et al. (1999) model provided a conservative estimation of the column drift at 80% Max V_{eff} for flexure-shear critical columns.

The performance of Kato and Ohnishi (2002) model proposed to estimate the column plastic drift at 80% Max V_{eff} largely depends on the accuracy of estimated yield drift. When applying the measured yield drift, Kato and Ohnishi (2002) model could either overestimate or underestimate the column drift and there is larger scatter existing in the data. With calculated yield drift by three-component model, this model is likely to underestimate the column drift capacity for flexure-shear critical columns.

The calculated column drift from the probability model proposed by Zhu et al. (2006) and the empirical linear models developed by Elwood and Moehle (2005) generally fell in a flat banded region, because most non-ductile columns have similar transverse reinforcement ratio ρ_t and relatively low axial load ratio. Both models tend to greatly underestimate the column drift capacity.

Comparing the calculated plastic drift from Elwood and Moehle (2005) with the measured plastic drift, it is found that the flexure-shear-critical columns subjected to subduction earthquake (e.g. Chile earthquake) tend to have lower plastic drift capacity. An empirical plastic drift model is proposed to estimate the plastic drift at 80% Max V_{eff} for columns subjected to general type of earthquake and subduction earthquake. The proposed plastic drift model could reflect the trend of the measured plastic drift pretty well, yet large variability existed in the data.

All four models greatly overestimate the drift capacities of six short columns in NCREE 2007 Tests, indicating the shear failure mechanism of shear-critical columns may be

essentially different from flexure-shear-critical columns and the drift capacity should be calculated separately.

7.2.3 Drift Capacities at Axial-Load Failure

This research suggests defining the axial-load failure based on the column lengthening shortening, since it is closely related to the column damage (i.e. the sliding along the shear damaged plane). Though axial-load failure point represented the initiation of the condition that column lost support for gravity load, it is difficult to define the failure point directly based on axial load response. Past research also shows that column tends to loss gravity support when lateral force degraded to almost zero, yet using the shear degradation to define the axial load failure can be either impossible or erroneous.

Elwood and Moehle (2005) proposed a shear-friction model by relating the effective coefficient of friction μ with the measured column drift. The shear-friction model based on the maximum axial load ratio represented the mean value of the measured column drift at axial-load failure for the flexure-shear critical columns and described the variability in the data fairly well. If based on the initial axial load ratio, the model tends to overestimate the column drift capacity and the data is also more scattered.

Kato and Ohnishi (2002) model greatly overestimate the column drift capacity at axial-load failure and large variability existed in the data.

The ratio of measure column drift to calculated drift by Zhu et al. (2006) probability model which was developed based on shear-friction model had a mean value of 1.25 and coefficient of variation around 30%, consistent with the intent of the model to provide a median estimation of column drift capacity at axial-load failure.

The shear-friction model and Zhu et al. (2006) probability model are developed based on the limited amount static cyclic test data of non-ductile columns that have been tested up to the axial-load failure. However, both models are capable of representing the mean value of the measured column drift at axial-load failure for flexure-shear-critical columns included in The Database, indicating that the dynamic tests did not increase much of the ultimate column drift capacity and the shear-friction models could capture the failure mechanism properly. Yet the performance of the models depends on the estimation of the column axial load level and underestimation of column axial load may result in unconservative calculated column drift capacity.

7.2.4 Evaluation of ASCE/SEI 41

The current seismic rehabilitation standard ASCE/SEI 41 recommends calculating the column shear strength based on the Sezen (2004) model and reducing the contribution from concrete blocks for non-ductile columns with transverse reinforcement spacing larger than half of the cross-section depth ($s \geq d/2$).

Results show the reduction due to the ductility demand and large spacing transverse reinforcement could lead to a very conservative estimation of column strength. When following the ASCE/SEI 41 method to classify columns, the reduction on the shear strength should be ignored. It is also found that some flexure-shear critical columns were misclassified into Condition iii with the ratio of $V_P/V_0^{'}$ slightly higher than 1.0. Thus this research suggests modifying the criteria of columns in Condition ii as $0.6 < V_P/V_0^{'} \leq 1.1$ instead of $0.6 < V_P/V_0^{'} \leq 1.0$.

The modeling parameters of *a* and *b* for columns in Condition ii and Condition iii are evaluated with The Database. It is found that parameter *a* tends to underestimate the column plastic drift at significant loss of lateral strength and there is a11% probability of failure for columns in "Condition ii" subjected to plastic rotation demand equal to parameter *a* specified in ASCE/SEI 41. Parameter *b* also greatly underestimates the plastic drift capacity at axial load failure, with the probability of failure around 7.5%.

The maximum measured plastic drifts of flexure-critical columns are used to evaluate the modeling parameter *b* for columns in Condition i. Results show that the axial load ratio greatly influences the column plastic drift capacity and parameter *b* specified in ASCE/SEI 41 generally provides conservative estimate of the plastic drift capacity at axial-load failure.

7.3 Future Research

Inter-story drift ratio has been commonly used as the indicator of the column drift capacity in engineering practice. However, the inter-story column drift included the deformation contributed from the joint and beam response. The deformation measured over certain length (plastic hinge length) at column ends or the chord rotation should be reordered in future shaking table tests.

Evaluation of the available drift capacity models showed that large variability existed in the total column drift. The models based on the plastic drift or the plastic rotation at column ends should be developed to better describe the column drift capacity.

The drift capacity and lateral stiffness of columns in shaking table tests are likely to be higher than that of columns subjected to cyclic tests. High strain rate in longitudinal reinforcement is measured during the dynamic test and strain rate effect should be further

studied. Most strain gages installed in the specimen were damaged and not much reliable strain rate data was available. In future tests, the way that strain gages are installed and protected shall be improved.

The input ground motion casts great influence on the column behaviour, such as the number of cycles and drift capacity. Future dynamic tests with greater range of input ground motion could be conducted on the frame specimens and the effect of input ground motions on the structural behaviour should be further studied. Parameters representing the characteristics of ground motions, such as the PGA (peak ground acceleration), duration and number of cycles, probably could be introduced in estimation of the column drift capacity.

Most flexure-shear critical columns in The Database had similar geometrical properties, transverse confinements and axial load level, yet the drift capacity at shear failure and axial-load failure varied significantly. The displacement histories (the number of cycles that column went through), strain rate effect, energy dissipation, column interactions within the frame and the mechanism of axial load redistribution may also cast great influence on the column behaviour and drift capacities. Further research on the moment frame rehabilitation should pay more attention on those issues.

While Shear-Friction model represented the failure mechanism and column drift capacity at axial load failure fairly well, the shear critical columns expected to suffer pure shear failure may lose the gravity load support suddenly and faster. More tests should be done on shear critical columns to investigate the column behaviour and failure mechanism.

References

ASCE 2008. Seismic Rehabilitation of Existing Buildings. *ASCE/SEI 41, Supplement 1*. Reston,VA: American Society of Civil Engineers.

Berry, M. Parrish, M. & Eberhard, M. 2004. PEER Structural Performance Database User's Manual, Pacific Earthquake Engineering Research Center, University of California, Berkeley. [available at: www.ce.washington.edu/~peera1].

Camarillo, H. 2003. *Evaluation of Shear Strength Methodologies for Reinforced Concrete Columns.* Master, University of Washington, Seattle.

Elwood, K. 2003. *Shaking Table Tests and Analytical Studies on the Gravity Load Collapse of Reinforced Concrete Frames*. Ph.D. Dissertation, University of California, Berkeley.

Elwood, K., Eeri, M., Matamoros, A., Wallace, J., Lehman, D., Heintz, J., Mitchell, A., Moore, M., Valley, M. & Lowes, L. 2007. Update to ASCE/SEI 41 Concrete Provisions. *Earthquake Spectra*, 23, 493.

Elwood, K. J. & Eberhard, M. O. 2009. Effective Stiffness of Reinforced Concrete Columns. *ACI Structural Journal*, 106 (4), 476-484.

Elwood, K. J. & Moehle, J. P. 2005.Drift Capacity of Reinforced Concrete Columns with Light Transverse Reinforcement. *Earthquake Spectra*, 21, 71-89.

Ghannoum, W. M. 2007. *Experimental and Analytical Dynamic Collapse Study of a Reinforced Concrete Frame with Light Transverse Reinforcement*. Ph.D. Dissertation, University of California, Berkeley.

Kato, D. & Ohnishi, K. 2002. Axial Load Carrying Capacity of R/C Columns Under Lateral Load Reversals. *Third US-Japan Workshop on Performance Based Earthquake Engineering Methodology for Reinforced Concrete Building Structures, Seattle, WA, PEER Report*. Berkeley: Pacific Earthquake Engineering Research Center.

Kabeyasawa, T., Tasai, A. & Igarashi, S. 2002. An Economical and Efficient Method of Strengthening Reinforced Concrete Columns Against Axial Load Collapse during Major Earthquake. *Third US-Japan Workshop on Performance Based Earthquake Engineering Methodology for Reinforced Concrete Building Structures, Seattle, WA, PEER Report 2002/02*. Berkeley, Calif: Pacific Earthquake Engineering Research Center, University of California, pp. 399-41.

Kuo, W. W. 2008. Study on the collapse behavior of nonductile reinforced concrete frames subjected to earthquake loading. Ph.D. Dissertation, Department of Construction Engineering, National Taiwan University of Science and Technology, Taipei, Taiwan, 542pp.

Lynn, A.C. 2001. *Seismic evaluation of existing reinforced concrete building columns*. Ph.D. Dissertation, Department of civil and Environmental Engineering, University of California, Berkeley.

NBCC. 2005. "National building code of Canada". *Institute for Research in construction, Ottawa, Ontario, Canada*.

Pujol, S., Ramirez, J. A. & Sozen, M. A. 1999. Drift Capacity of Reinforced Concrete Columns Subjected to Cyclic Shear Reversals. *American Concrete Institute, Farmington Hills, Michigan,* SP-187, 255-274.

Sezen, H. 2002. Seismic response and modeling of reinforced concrete building columns, Ph.D. Dissertation, Department of Civil and Environmental Engineering, University of California, Berkeley.

Sezen, H. & Moehle, J. 2004. Shear strength model for lightly reinforced concrete columns. *ASCE Journal of Structural Engineering*, 130, 1692.

Shin, Y. B. 2007. *Dynamic Response of Ductile and Non-Ductile Reinforced Concrete Columns*. Ph.D. Dissertation, University of California, Berkeley.

Su, R.S. 2007. *Shake table tests on reinforced concrete short columns failed in shear*. Master thesis, Department of Construction Engineering, National Taiwan University of Science and Technology, Taipei, Taiwan.

Wu C.L., Yang Y.S. & Loh C.H. 2006. Dynamic Gravity Load Collapse of Non-ductile RC Frames I : Experimental Approach. *8th US National Conference on Earthquake Engineering - the 100th Anniversary Earthquake Conference Commemorating the 1906 San Francisco Earthquake, San Francisco, Moscone Center, April 18-22.*

Wu, C.L., Loh, C.H. & Yang, Y.S. 2006. *Shaking table tests on gravity load collapse of low-ductility RC frames under near-fault earthquake excitation.* Advances in Experimental Structural Engineering, Itoh and Aoki, Eds: 725-732.

Wu, C. L., Hwang, S. J., Yang, Y. S. & Su, R. S. 2007. *Shake Table Tests on Reinforced Concrete Short Columns Failing in Shear*. National Center for Research on Earthquake Engineering.

Wu, C. L., Kuo, W. W., Hwang, S. J., Yang, Y. S. & Loh, C. H. 2009. *Study on the Collapse Behavior of Nonductile Reinforced Concrete Frames Subjected to Earthquake Loadings*. National Center for Research on Earthquake Engineering.

Wu, C. L., Kuo, W. W., Yang, Y. S., Hwang, S. J., Elwood, K. J., Loh, C. H. & Moehle, J. P. 2009. Collapse of a Non-Ductile Concrete Frame: Shaking Table Tests. Earthquake Engineering & Structural Dynamics, 38, 205-244.

Yang Y.S., Wu C.L., Loh C.H., Lin C.H. & Chao S.H. 2006. Dynamic Gravity Load Collapse of Non-ductile RC Frames II : Computational Approach. *8th US National Conference on Earthquake Engineering - the 100th Anniversary Earthquake Conference Commemorating the 1906 San Francisco Earthquake, San Francisco, Moscone Center, April 18-22.*

Yavari, S., Elwood, K. J. & Wu, C. L. 2009. Collapse of a non-ductile concrete frame: Evaluation of analytical models. *Earthquake Engineering & Structural Dynamics*, 38, 225-241.

Appendices

Appendix A Properties of the Shaking Table Tests Column Database

Column Information				Geometry				Long. Rein.				Trans. Rein.					Classification		
	Specimen	Column	Scale	D	b	L	f_c'	d_l	c	f_{yl}	ρ_l	d_t	Tie Type	s	f_{yt}	ρ_t	V_p	V_0'	Failure Type
				(mm)	(mm)	(mm)	(Mpa)	(mm)		(Mpa)		(mm)		(mm)	(Mpa)	(%)	(kN)	(kN)	
NCREE 2009 Tests																			
1	MCFS	A1	1/2.25	200	200	1400	34.0	12.7	17	439.0	2.53%	5	r90	120	469.0	0.16%	61.91	59.79	FS
2	MCFS	B1	1/2.25	200	200	1400	34.0	12.7	17	439.0	2.53%	5	r90	120	469.0	0.16%	68.63	66.95	FS
3	MCFS	C1	1/2.25	200	200	1400	34.0	12.7	17	439.0	2.53%	5	r90	120	469.0	0.16%	61.34	59.28	FS
4	HCFS	A1	1/2.25	200	200	1400	34.4	12.7	17	439.0	2.53%	5	r90	120	469.0	0.16%	68.57	66.82	FS
5	HCFS	B1	1/2.25	200	200	1400	34.4	12.7	17	439.0	2.53%	5	r90	120	469.0	0.16%	72.71	78.23	F
6	HCFS	C1	1/2.25	200	200	1400	34.4	12.7	17	439.0	2.53%	5	r90	120	469.0	0.16%	68.23	75.78	F
7	MUF	A1	1/2.25	200	200	1400	35.8	12.7	17	467.0	2.53%	5	r135	40	475.0	0.49%	60.58	119.45	F
8	MUF	B1	1/2.25	200	200	1400	35.8	12.7	17	467.0	2.53%	5	r135	40	475.0	0.49%	69.17	118.03	FS
9	MUF	C1	1/2.25	200	200	1400	35.8	12.7	17	467.0	2.53%	5	r135	40	475.0	0.49%	60.68	120.85	FS
10	MUFS	A1	1/2.25	200	200	1400	36.5	12.7	17	467.0	2.53%	5	r90	120	475.0	0.16%	60.08	54.05	FS
11	MUFS	B1	1/2.25	200	200	1400	36.5	12.7	17	467.0	2.53%	5	r90	120	475.0	0.16%	69.38	72.83	FS
12	MUFS	C1	1/2.25	200	200	1400	36.5	12.7	17	467.0	2.53%	5	r90	120	475.0	0.16%	60.40	69.42	S
NCREE 2007 Tests																			
13	S1	C1	1/2	250	250	1000	29.9	12.7	16	436.4	1.62%	4	r135	50	643.3	0.30%	114.93	189.68	FS
14	S1	C2	1/2	250	250	1000	29.9	12.7	16	436.4	3.24%	4	r90	150	643.3	0.07%	170.74	88.21	S
15	S1	C3	1/2	250	250	1000	29.9	12.7	16	436.4	1.62%	4	r135	50	643.3	0.30%	116.60	190.99	FS
16	S3	C1	1/2	250	250	750	29.9	12.7	16	436.4	3.24%	4	r90	150	643.3	0.07%	246.86	136.80	S

Column Information				Geometry				Long. Rein.				Trans. Rein.					Classification		
	Specimen	Column	Scale	D	b	L	f_c'	d_l	c	f_{yl}	ρ_l	d_t	Tie Type	s	f_{yt}	ρ_t	V_p	V_0'	Failure Type
				(mm)	(mm)	(mm)	(Mpa)	(mm)		(Mpa)		(mm)		(mm)	(Mpa)	(%)	(kN)	(kN)	
17	S3	C2	1/2	250	250	750	29.9	12.7	16	436.4	3.24%	4	r90	150	643.3	0.07%	249.90	140.29	S
18	S4	C1	1/2	250	250	1000	29.9	12.7	16	436.4	3.24%	4	r90	150	643.3	0.07%	177.36	99.69	S
19	S4	C2	1/2	250	250	1000	29.9	12.7	16	436.4	3.24%	4	r90	150	643.3	0.07%	183.18	106.21	S
NCREE 2005 Tests																			
20	P2	C1	1/3	150	150	1000	33.8	9.53	14	470.9	2.53%	3.2	r90	100	548.1	0.16%	33.85	36.33	F
21	P2	C2	1/3	150	150	1000	33.8	9.53	14	470.9	2.53%	3.2	r90	100	548.1	0.16%	31.98	32.44	F
22	P2	C3	1/3	150	150	1000	33.8	6	12	231.7	1.39%	5	r135	33	661.9	1.19%	21.16	176.12	FS
23	P2	C4	1/3	150	150	1000	33.8	6	12	231.7	1.39%	5	r135	33	661.9	1.19%	13.90	171.04	FS
24	L	C1	1/3	150	150	1000	32.3	9.53	14	470.9	2.53%	3.2	r90	100	548.1	0.16%	33.64	34.06	F
25	L	C2	1/3	150	150	1000	32.3	9.53	14	470.9	2.53%	3.2	r90	100	548.1	0.16%	39.15	38.84	F
26	L	C3	1/3	150	150	1000	32.3	6	12	231.7	1.39%	5	r135	33	661.9	1.19%	16.18	172.81	FS
27	L	C4	1/3	150	150	1000	32.3	6	12	231.7	1.39%	5	r135	33	661.9	1.19%	15.00	171.97	FS
NCREE 2004 Tests																			
28	S2	C1	1/2	200	200	1730	31.8	9.53	9.5	385.9	1.43%	4	r90	125	385.9	0.10%	30.62	39.21	FS
29	S2	C2	1/2	200	200	1730	31.8	9.53	9.5	385.9	1.43%	4	r90	125	385.9	0.10%	30.66	39.24	FS
30	S3	C1	1/2	200	200	1730	31.8	9.53	9.5	385.9	1.43%	4	r90	125	385.9	0.10%	30.88	39.41	FS
31	S3	C2	1/2	200	200	1730	31.8	9.53	9.5	385.9	1.43%	4	r90	125	385.9	0.10%	30.88	39.40	FS
Ghannoum 2006 Tests																			
32	S1	A1	1/3	152	152	991	24.6	9.53	17	441.3	2.45%	3.18	r90	102	655.0	0.15%	32.51	36.35	F
33	S1	B1	1/3	152	152	991	24.6	9.53	17	441.3	2.45%	3.18	r90	102	655.0	0.15%	34.88	39.93	F
34	S1	C1	1/3	152	152	991	24.6	6.35	17	482.6	1.09%	4.76	r135	31.8	556.3	1.10%	23.04	143.63	FS
35	S1	D1	1/3	152	152	991	24.6	6.35	17	482.6	1.09%	4.76	r135	31.8	556.3	1.10%	19.19	140.03	FS

Column Information				Geometry				Long. Rein.				Trans. Rein.					Classification		
	Specimen	Column	Scale	D	b	L	f_c'	d_l	c	f_{yl}	ρ_l	d_t	Tie Type	s	f_{yt}	ρ_t	V_p	V_0'	Failure Type
				(mm)	(mm)	(mm)	(Mpa)	(mm)		(Mpa)		(mm)		(mm)	(Mpa)	(%)	(kN)	(kN)	
Elwood 2002 Tests																			
36	S1	CenC	1/2	229	229	1473	24.6	12.7	25	479.3	2.48%	4.76	d90	152	689.7	0.18%	73.07	91.30	F
37	S2	CenC	1/2	229	229	1473	23.9	12.7	25	479.3	2.48%	4.76	d90	152	689.7	0.18%	77.66	104.04	F
Shin 2005 Tests																			
38	Setup I	EastC	1/3	152	152	991	25.6	9.53	12.2	444.1	2.46%	4.76	r135	38.1	549.0	0.92%	30.93	113.13	F
39	Setup I	WestC	1/3	152	152	991	25.6	9.53	12.2	444.1	2.46%	4.76	r135	38.1	549.0	0.92%	30.87	113.03	F
40	Setup I	EastC	1/3	152	152	991	25.6	9.53	12.2	444.1	2.46%	4.76	r135	38.1	549.0	0.92%	30.98	113.23	F
41	Setup I	WestC	1/3	152	152	991	25.6	9.53	12.2	444.1	2.46%	4.76	r135	38.1	549.0	0.92%	31.03	113.32	F
42	Setup I	EastC	1/3	152	152	991	25.6	9.53	12.2	444.1	2.46%	4.76	r135	38.1	549.0	0.92%	33.57	117.62	F
43	Setup I	WestC	1/3	152	152	991	25.6	9.53	12.2	444.1	2.46%	4.76	r135	38.1	549.0	0.92%	33.37	117.29	F
44	Setup I	EastC	1/3	152	152	991	25.6	9.53	12.2	444.1	2.46%	4.76	r135	38.1	549.0	0.92%	33.33	117.22	F
45	Setup I	WestC	1/3	152	152	991	25.6	9.53	12.2	444.1	2.46%	4.76	r135	38.1	549.0	0.92%	33.37	117.29	FS
46	Setup II	EastC	1/3	152	152	991	25.6	9.53	12.2	444.1	2.46%	4.76	r135	38.1	549.0	0.92%	31.54	113.19	F
47	Setup II	WestC	1/3	152	152	991	25.6	9.53	13.8	444.1	2.46%	3.17	r90	102	554.5	0.15%	31.76	32.99	FS
48	Setup II	EastC	1/3	152	152	991	25.6	9.53	12.2	444.1	2.46%	4.76	r135	38.1	549.0	0.92%	30.88	113.04	F
49	Setup II	WestC	1/3	152	152	991	25.6	9.53	13.8	444.1	2.46%	3.17	r90	102	554.5	0.15%	31.73	32.96	FS
50	Setup II	EastC	1/3	152	152	991	25.6	9.53	12.2	444.1	2.46%	4.76	r135	38.1	549.0	0.92%	33.59	117.65	F
51	Setup II	WestC	1/3	152	152	991	25.6	9.53	13.8	444.1	2.46%	3.17	r90	102	554.5	0.15%	34.50	37.56	FS
52	Setup II	EastC	1/3	152	152	991	25.6	9.53	12.2	444.1	2.46%	4.76	r135	38.1	549.0	0.92%	33.53	117.55	FS
53	Setup II	WestC	1/3	152	152	991	25.6	9.53	13.8	444.1	2.46%	3.17	r90	102	554.5	0.15%	34.43	37.45	FS
54	Setup III	EastC	1/3	152	152	991	25.6	9.53	13.8	444.1	2.46%	3.17	r90	102	554.5	0.15%	31.81	33.05	FS
55	Setup III	WestC	1/3	152	152	991	25.6	9.53	13.8	444.1	2.46%	3.17	r90	102	554.5	0.15%	32.00	33.29	FS

Column Information				Geometry				Long. Rein.				Trans. Rein.					Classification		
	Specimen	Column	Scale	D	b	L	f_c'	d_l	c	f_{yl}	ρ_l	d_t	Tie Type	s	f_{yt}	ρ_t	V_p	V_0'	Failure Type
				(mm)	(mm)	(mm)	(Mpa)	(mm)		(Mpa)		(mm)		(mm)	(Mpa)	(%)	(kN)	(kN)	
56	Setup III	EastC	1/3	152	152	991	25.6	9.53	13.8	444.1	2.46%	3.17	r90	102	554.5	0.15%	31.98	33.25	FS
57	Setup III	WestC	1/3	152	152	991	25.6	9.53	13.8	444.1	2.46%	3.17	r90	102	554.5	0.15%	31.86	33.12	FS
58	Setup III	EastC	1/3	152	152	991	25.6	9.53	13.8	444.1	2.46%	3.17	r90	102	554.5	0.15%	34.29	37.22	FS
59	Setup III	WestC	1/3	152	152	991	25.6	9.53	13.8	444.1	2.46%	3.17	r90	102	554.5	0.15%	34.29	37.42	FS

Note: D = height of column section; b = width of column section; L= clear height of the column; f_c'= concrete compressive stress at test day; d_l = the diameter of longitudinal reinforcement; c = clear cover (measured from the outer face of the concrete to outer face of longitudinal reinforcement); f_{yt} = yield stress of longitudinal reinforcement; ρ_l = longitudinal reinforcement ratio; d_t = the diameter of transverse reinforcement; Tie Type = the type of the transverse reinforcement, "r135" means rectangular-shaped hoops with 135-degree hooks and "d90" means diamond-shaped transverse reinforcement with 90-degree hooks; s = spacing of transverse reinforcement; f_{yl} = yield stress of transverse reinforcement; ρ_t = volumetric ratio of transverse reinforcement; V_p = plastic shear demand obtained from section analysis; V_0'= the calculated shear strength from ASCE/SEI 41(discussed in section 6.2.3).

Appendix B Information of Test Series in Shaking Table Tests Column Database

ID	Column Name	Prestressed Force*	Test Series	Initial axial load	Initial axial load ratio	Max axial load ratio	Min axial load ratio	PGA	Shear demand	Max Hori. Drift
				P_{ini}	$P_{ini}/A_g f_c'$	$P_{max}/A_g f_c'$	$P_{min}/A_g f_c'$		V_{max}	δ_{max}
				(kN)				(g)	(kN)	(%)
1	NCREE 2009-MCFS-A1	N	Test 1	138.4	0.102	0.229	0.021	0.82	70.3	2.26
			Test 2	138.3	0.102	0.215	0.003	0.88	68.5	5.50
2	NCREE 2009-MCFS-B1	N	Test 1	266.1	0.196	0.277	0.005	0.88	86.7	5.38
			Test 2	266.1	0.196	0.266	0.169	0.82	86.7	2.15
3	NCREE 2009-MCFS-C1	N	Test 1	142.4	0.105	0.234	0.027	0.82	85.1	2.15
			Test 2	142.3	0.105	0.259	-0.005	0.88	94.8	5.38
4	NCREE 2009-HCFS-A1	Y	Test 1	257.3	0.187	0.308	0.098	0.86	85.0	2.19
			Test 2	257.3	0.187	0.345	0.080	0.88	83.0	3.87
5	NCREE 2009-HCFS-B1	Y	Test 1	499.0	0.363	0.401	0.342	0.86	105.0	2.18
			Test 2	498.9	0.363	0.429	-0.020	0.88	100.6	3.61
6	NCREE 2009-HCFS-C1	Y	Test 1	255.9	0.186	0.304	0.105	0.86	78.9	2.26
			Test 2	256.0	0.186	0.323	0.069	0.88	94.2	4.10
7	NCREE 2009-MUFS-A1	N	Test 1	130.0	0.089	0.162	0.028	0.82	54.2	2.96
			Test 2	130.2	0.089	0.158	0.051	1.02	43.5	2.92
8	NCREE 2009-MUFS-B1	N	Test 1	259.5	0.178	0.247	0.136	0.82	93.0	2.75
			Test 2	259.5	0.178	0.233	-0.020	1.02	69.3	2.62
9	NCREE 2009-MUFS-C1	N	Test 1	132.3	0.091	0.202	0.016	0.82	73.1	2.80
			Test 2	132.3	0.091	0.190	0.021	1.02	61.5	2.71
10	NCREE 2009-MUF-A1	N	Test 1	137.4	0.096	0.207	0.039	0.76	62.2	2.95
			Test 2	137.3	0.096	0.199	0.046	0.96	53.2	2.97

ID	Column Name	Prestressed Force*	Test Series	Initial axial load	Initial axial load ratio	Max axial load ratio	Min axial load ratio	PGA	Shear demand	Max Hori. Drift
		N		P_{ini}	$P_{ini}/A_g f_c'$	$P_{max}/A_g f_c'$	$P_{min}/A_g f_c'$		V_{max}	δ_{max}
		N		(kN)				(g)	(kN)	(%)
11	NCREE 2009-MUF-B1	N	Test 1	270.4	0.189	0.220	0.148	0.76	77.6	2.78
			Test 2	270.4	0.189	0.254	0.166	0.96	75.7	2.80
12	NCREE 2009-MUF-C1	N	Test 1	137.5	0.096	0.226	0.037	0.76	74.4	2.79
			Test 2	137.7	0.096	0.208	0.036	0.96	64.7	2.82
13	NCREE 2007-S1-C1	N	Test 1	156.6	0.084	0.313	0.042	0.95	150.8	3.38
			Test 2	345.2	0.185	0.303	0.158	0.58	143.0	5.93
14	NCREE 2007-S1-C2	N	Test 1	52.7	0.028	0.039	-0.311	0.95	162.9	3.35
			Test 2	-319.8	-0.171	-0.168	-0.319	0.56	19.1	4.18
15	NCREE 2007-S1-C3	N	Test 1	166.8	0.089	0.322	0.035	0.95	149.3	3.37
			Test 2	360.0	0.193	0.296	0.174	0.56	119.8	3.27
16	NCREE 2007-S3-C1	N		170.2	0.091	0.150	0.045	1.20	203.0	1.28
17	NCREE 2007-S3-C3	N		191.7	0.103	0.165	0.018	1.20	126.5	1.44
18	NCREE 2007-S4-C1	N		102.7	0.055	0.091	0.007	1.15	147.1	0.91
19	NCREE 2007-S4-C3	N		152.1	0.081	0.118	0.005	1.15	154.2	1.22
20	NCREE 2005-P2-C1	N		68.3	0.090	0.150	0.020	1.60	48.3	4.98
21	NCREE 2005-P2-C2	N		19.7	0.026	0.111	-0.035	1.53	37.2	4.98
22	NCREE 2005-P2-C3	N		110.7	0.146	0.428	0.051	1.60	41.1	11.00
23	NCREE 2005-P2-C4	N		39.8	0.052	0.132	-0.111	1.60	28.3	11.00
24	NCREE 2005-L-C1	N		36.8	0.051	0.111	0.028	1.66	43.2	8.50
25	NCREE 2005-L-C2	N		102.9	0.142	0.161	0.034	1.66	41.7	8.50
26	NCREE 2005-L-C3	N		60.6	0.083	0.135	0.051	1.66	25.8	8.50

ID	Column Name	Prestressed Force*	Test Series	Initial axial load	Initial axial load ratio	Max axial load ratio	Min axial load ratio	PGA	Shear demand	Max Hori. Drift
				P_{ini}	$P_{ini}/A_g f_c'$	$P_{max}/A_g f_c'$	$P_{min}/A_g f_c'$		V_{max}	δ_{max}
				(kN)				(g)	(kN)	(%)
27	NCREE 2005-L-C4	N		49.7	0.068	0.127	0.035	1.66	29.9	8.50
28	NCREE 2004-S2-C1	N		142.4	0.112	0.148	0.062	0.17	41.4	4.31
29	NCREE 2004-S2-C2	N		142.4	0.112	0.150	0.064	0.17	45.6	4.31
30	NCREE 2004-S3-C1	N		145.9	0.115	0.180	0.089	0.63	38.4	4.49
31	NCREE 2004-S3-C2	N		145.9	0.115	0.145	0.084	0.63	37.7	4.49
32	Ghannoum 2006-A1	N	DT 1	45.3	0.079	0.209	-0.036	N.A.	45.5	4.66
			DT 2	63.7	0.111	0.224	0.047	N.A.	35.5	4.17
			DT 3	75.3	0.132	0.168	0.090	N.A.	14.2	1.88
			HY	46.3	0.081	0.128	0.038	N.A.	18.8	0.58
33	Ghannoum 2006-B1	N	DT 1	97.1	0.170	0.246	0.034	N.A.	47.4	5.11
			DT 2	50.3	0.088	0.128	-0.016	N.A.	11.4	4.46
			DT 3	26.1	0.046	0.055	0.012	N.A.	9.3	2.19
			HY	96.9	0.169	0.182	0.154	N.A.	19.6	0.59
34	Ghannoum 2006-C1	N	DT 1	90.0	0.157	0.265	0.098	N.A.	33.7	5.41
			DT 2	130.2	0.228	0.352	0.166	N.A.	31.1	4.72
			DT 3	148.5	0.260	0.402	0.198	N.A.	31.0	5.05
			HY	90.6	0.158	0.168	0.143	N.A.	17.4	0.62
35	Ghannoum 2006-D1	N	DT 1	41.4	0.072	0.148	-0.025	N.A.	30.9	5.58
			DT 2	30.3	0.053	0.137	-0.030	N.A.	19.0	5.09
			DT 3	27.1	0.047	0.091	-0.036	N.A.	14.1	4.28
			HY	41.5	0.073	0.114	0.034	N.A.	14.6	0.51

ID	Column Name	Prestressed Force*	Test Series	Initial axial load	Initial axial load ratio	Max axial load ratio	Min axial load ratio	PGA	Shear demand	Max Hori. Drift
				P_{ini}	$P_{ini}/A_g f_c'$	$P_{max}/A_g f_c'$	$P_{min}/A_g f_c'$		V_{max}	δ_{max}
				(kN)				(g)	(kN)	(%)
36	Elwood 2002-S1-CenC	Y		127.9	0.100	0.122	-0.006	0.79	83.2	6.07
37	Elwood 2002-S2-CenC	Y		298.4	0.239	0.251	0.033	0.73	93.6	7.24
38	Shin 2005-I-Test 3-Chile-0.1-EastC	N	Test 3	50.8	0.085	0.134	0.021	1.13	42.1	5.39
39	Shin 2005-I-Test 3-Chile-0.1-WestC	N	Test 3	49.5	0.083	0.133	0.037	1.13	39.7	5.39
40	Shin 2005-I-Test 5-Kobe-0.1-EastC	N	Test 5	52.2	0.088	0.141	0.063	0.90	43.3	8.07
41	Shin 2005-I-Test 5-Kobe-0.1-WestC	N	Test 5	53.4	0.090	0.122	0.046	0.90	37.7	8.07
42	Shin 2005-I-Test 9-Chile-0.24-EastC	Y	Test 9	119.4	0.201	0.248	0.148	1.06	44.9	4.84
43	Shin 2005-I-Test 9-Chile-0.24-WestC	Y	Test 9	119.4	0.201	0.253	0.148	1.06	42.7	4.84
44	Shin 2005-I-Test 11-Kobe-0.24-EastC	Y	Test 11	112.5	0.189	0.247	0.151	0.87	47.4	5.95
45	Shin 2005-I-Test 11-Kobe-0.24-WestC	Y	Test 11	113.7	0.191	0.227	0.153	0.87	43.4	5.95
46	Shin 2005-II-Test 1-Chile-0.1-EastC	N	Test 1	51.6	0.087	0.131	0.044	1.22	41.9	6.94
47	Shin 2005-II-Test 1-Chile-0.1-WestC	N	Test 1	50.9	0.086	0.126	0.044	1.01	39.1	4.26
48	Shin 2005-II-Test 2-Kobe-0.1-EastC	N	Test 2	49.5	0.083	0.132	0.046	0.89	43.9	8.93

ID	Column Name	Prestressed Force*	Test Series	Initial axial load	Initial axial load ratio	Max axial load ratio	Min axial load ratio	PGA	Shear demand	Max Hori. Drift
				P_{ini}	$P_{ini}/A_g f_c'$	$P_{max}/A_g f_c'$	$P_{min}/A_g f_c'$		V_{max}	δ_{max}
				(kN)				(g)	(kN)	(%)
49	Shin 2005-II-Test 2-Kobe-0.1-WestC	N	Test 2	50.5	0.085	0.120	0.034	0.89	37.1	4.36
50	Shin 2005-II-Test 7-Chile-0.24-EastC	Y	Test 7	119.8	0.202	0.353	0.071	1.18	47.0	6.93
51	Shin 2005-II-Test 7-Chile-0.24-WestC	Y	Test 7	119.9	0.202	0.242	0.137	0.83	43.7	3.40
52	Shin 2005-II-Test 8-Kobe-0.24-EastC	Y	Test 8	118.2	0.199	0.375	0.027	0.96	46.9	6.42
53	Shin 2005-II-Test 8-Kobe-0.24-WestC	Y	Test 8	118.0	0.199	0.228	0.144	0.96	42.6	3.41
54	Shin 2005-III-Test 4-Chile-0.1-EastC	N	Test 4	51.7	0.087	0.132	0.046	0.81	38.2	3.83
55	Shin 2005-III-Test 4-Chile-0.1-WestC	N	Test 4	54.9	0.092	0.132	0.053	0.81	37.6	3.83
56	Shin 2005-III-Test 6-Kobe-0.1-EastC	N	Test 6	54.4	0.092	0.139	0.061	1.00	41.4	3.35
57	Shin 2005-III-Test 6-Kobe-0.1-WestC	N	Test 6	52.5	0.088	0.118	0.033	1.00	37.2	4.28
58	Shin 2005-III-Test 10-Chile-0.24-EastC	Y	Test 10	114.2	0.192	0.238	0.148	0.87	43.2	3.16
59	Shin 2005-III-Test 10-Chile-0.24-WestC	Y	Test 10	117.6	0.198	0.234	0.155	0.87	40.9	2.48

*In order to achieve high column axial load level in shaking table tests, prestressed force (e.g. by using pneumatic jack) might be applied to increase the column axial load on top of the lead weight packets. “Y” means that prestressed force is applied during the tests and “N” means the opposite.